

AD_____

Award Number: W81XWH-07-1-0306

TITLE: PROSPECT: Profiling of Resistance Patterns & Oncogenic Signaling Pathways
in Evaluation of Cancers of the Thorax and Therapeutic Target Identification

PRINCIPAL INVESTIGATOR: Waun Ki Hong, M.D.

CONTRACTING ORGANIZATION: University of Texas M. D. Anderson Cancer Center
Houston, TX 77030

REPORT DATE: June 2012

TYPE OF REPORT: Final

PREPARED FOR: U.S. Army Medical Research and Materiel Command
Fort Detrick, Maryland 21702-5012

DISTRIBUTION STATEMENT: Approved for Public Release;
Distribution Unlimited

The views, opinions and/or findings contained in this report are those of the author(s) and should not be construed as an official Department of the Army position, policy or decision unless so designated by other documentation.

REPORT DOCUMENTATION PAGE				<i>Form Approved</i> OMB No. 0704-0188	
Public reporting burden for this collection of information is estimated to average 1 hour per response, including the time for reviewing instructions, searching existing data sources, gathering and maintaining the data needed, and completing and reviewing this collection of information. Send comments regarding this burden estimate or any other aspect of this collection of information, including suggestions for reducing this burden to Department of Defense, Washington Headquarters Services, Directorate for Information Operations and Reports (0704-0188), 1215 Jefferson Davis Highway, Suite 1204, Arlington, VA 22202-4302. Respondents should be aware that notwithstanding any other provision of law, no person shall be subject to any penalty for failing to comply with a collection of information if it does not display a currently valid OMB control number. PLEASE DO NOT RETURN YOUR FORM TO THE ABOVE ADDRESS.					
1. REPORT DATE June 2012		2. REPORT TYPE Final		3. DATES COVERED 1 June 2007 – 31 May 2012	
4. TITLE AND SUBTITLE PROSPECT: Profiling of Resistance Patterns & Oncogenic Signaling Pathways in Evaluation of Cancers of the Thorax and Therapeutic Target Identification				5a. CONTRACT NUMBER	
				5b. GRANT NUMBER W81XWH-07-1-0306	
				5c. PROGRAM ELEMENT NUMBER	
6. AUTHOR(S) Waun Ki Hong, M.D. E-Mail: whong@mdanderson.org				5d. PROJECT NUMBER	
				5e. TASK NUMBER	
				5f. WORK UNIT NUMBER	
7. PERFORMING ORGANIZATION NAME(S) AND ADDRESS(ES) University of Texas M. D. Anderson Cancer Center Houston, TX 77030				8. PERFORMING ORGANIZATION REPORT NUMBER	
9. SPONSORING / MONITORING AGENCY NAME(S) AND ADDRESS(ES) U.S. Army Medical Research and Materiel Command Fort Detrick, Maryland 21702-5012				10. SPONSOR/MONITOR'S ACRONYM(S)	
				11. SPONSOR/MONITOR'S REPORT NUMBER(S)	
12. DISTRIBUTION / AVAILABILITY STATEMENT Approved for Public Release; Distribution Unlimited					
13. SUPPLEMENTARY NOTES					
14. ABSTRACT We will develop a high throughput therapeutic-target focused (TTF) profiling platform and will combine this with tumor genome wide mRNA profiling and with serum or plasma profiling of phosphopeptides and DNA. We will use these molecular profiles to help define how various molecular factors alone and in combination relate to resistance to therapy, to prognosis, and to metastatic patterns at relapse. Using tumor and blood samples from non-small cell lung cancer (NSCLC) patients as well as NSCLC cell lines with defined chemotherapy resistance patterns, we will examine how molecular profiles may confer resistance and will identify new, potential therapeutic targets. The PROSPECT approach will be novel in that we will assess tumors from NSCLC patients undergoing surgical resection after having received neoadjuvant therapy as a model of resistance. Tumor surviving neoadjuvant therapy would be expected to be enriched for resistant cells. We will define what combinations of targeted therapies are most effective against resistant cell lines with similar molecular profiles, and this will drive later clinical trials (beyond the scope of this Program). Similar studies will be conducted in patients with mesotheliomas undergoing surgical resection of tumor after neoadjuvant therapy with the new Src inhibitor dasatinib.					
15. SUBJECT TERMS Lung cancer, biomarker, targeted therapy, Dasatinib, Quantum Dot					
16. SECURITY CLASSIFICATION OF:			17. LIMITATION OF ABSTRACT UU	18. NUMBER OF PAGES FJl	19a. NAME OF RESPONSIBLE PERSON USAMRMC
a. REPORT U	b. ABSTRACT U	c. THIS PAGE U			19b. TELEPHONE NUMBER (include area code)

Waun Ki Hong, M.D., D.M.Sc. (Hon.)
Vice-Provost, Clinical Research
Head, Division of Cancer Medicine, Box 421
Samsung Distinguished University Chair in Cancer Medicine
Professor, Department of
Thoracic/Head & Neck Medical Oncology
Telephone (713) 792-7770
Fax (713) 792-4654

July 27, 2012

Rebecca Fisher
Science Officer (General Dynamics)
CDMRP, U.S. AMRMC
1077 Patchel Street
Fort Detrick, MD 21702

RE: The 2012 FINAL Report of PROSPECT GRANT (W81XWH-05-2-0027)

Dear Dr. Kinnard:

Provided is our 2012 FINAL report of the DOD-funded research program PROSPECT (*Profiling of Resistance Patterns and Oncogenic Signaling Pathways in Evaluation of Cancer of the Thorax and Therapeutic Target Identification*), covering the period from July 1, 2011 to June 30, 2012.

We are extremely proud of the work accomplished through this DOD-sponsored program, particularly the molecular analyses that are providing high-potential leads for future clinical trials.

Please do not hesitate to contact me if you have any questions regarding this final report.

With highest regards,



Waun Ki Hong, M.D.
Principal Investigator

TABLE OF CONTENTS

INTRODUCTION	4
PROGRESS REPORT (BODY)	4
<i>Project 1</i>	4
<i>Project 2</i>	9
<i>Project 3</i>	12
<i>Project 4</i>	25
<i>Project 5</i>	29
<i>Pathology Core</i>	34
<i>Biostatistics Core</i>	36
KEY RESEARCH ACCOMPLISHMENTS	38
PERSONNEL	40
REPORTABLE OUTCOMES	40
CONCLUSIONS	43
APPENDICES	45

Appendix A - Personnel

Appendix B - Abstracts and Publications

INTRODUCTION

Lung cancer is the leading cause of cancer death in the world. Non-small cell lung cancer (NSCLC) accounts for 85% of all lung cancer cases. Only 15% of patients diagnosed with lung cancer survive five years from diagnosis. Therapy for advanced disease increases average life expectancy by only a few months, and slightly improves quality of life. Similarly, adjuvant chemotherapy for resected disease has only a modest impact on survival rates. More effective therapy is needed. We believe that applying state-of-the-art molecular tools to carefully conducted clinical trials will lead to the identification of molecular mechanisms that contribute to lung cancer therapeutic resistance and that drive prognosis, and that this in turn will lead to the development of drugs with novel biological and therapeutic functions. Therefore, we have undertaken a translational research program named **PROSPECT: Profiling of Resistance Patterns & Oncogenic Signaling Pathways in Evaluation of Cancers of the Thorax and Therapeutic Target Identification**. The goal of PROSPECT is to use therapeutic target-focused (TTF) profiling along with genome-wide mRNA and serum phosphopeptide profiling to identify and evaluate molecular targets and pathways that contribute to therapeutic sensitivity or resistance, prognosis, and recurrence patterns, and to use this information to guide formulation of new rational therapeutic strategies for NSCLC and mesotheliomas. In the Program, we have 5 research projects and 3 Cores to address 3 central issues: therapeutic resistance, prognosis and new therapeutic targets and strategies.

FINAL REPORT:

Project 1: Therapeutic target-focused (TTF) profiling for the identification of molecular targets and pathways that contribute to drug sensitivity or resistance *in vitro* and the development of rational treatment strategies for NSCLC.

(Leader: Dr. John Heymach; Co-Leader: Dr. John Minna)

Hypotheses:

We hypothesize that a broad, systematic molecular profiling of NSCLC cell lines, using both TTF and global approaches, will lead to the following results:

1. The identification of new potential therapeutic targets for NSCLC.
2. The development of predictive markers for *in vitro* sensitivity to targeted agents, which will form the starting point for the development of a predictive model of *in vivo* sensitivity using clinical specimens as described in Aim 3.
3. Insights into the molecular mechanism underlying therapeutic resistance and into the relationship of resistance mechanisms to factors innately affecting tumor growth rate and prognosis.
4. Identification of readily translatable therapeutic strategies to combat these resistance mechanisms.

Specific Aims:

In this project, we will develop and validate a novel therapeutic target-focused (TTF) profiling platform at MD Anderson Cancer Center. The platform will provide a high throughput, quantitative, scalable, and highly sensitive set of assays to assess activation of key signaling pathways (e.g., PI3K/AKT, STAT, RAS-RAF-ERK) as well as other potential therapeutic targets such as receptor tyrosine kinases (RTKs). It will be coupled with global profiling of gene expression using Affymetrix 2.0 array. These molecular profiles will then be coupled with information from a broad drug and therapeutic target siRNA (DATS) screen to develop markers for predicting drug sensitivity *in vitro* based on molecular profiles, elucidate the molecular determinants of sensitivity or resistance to a given therapeutic agent, and identify potential

therapeutic targets for tumor cells resistant to a given agent. This project lays the foundation for Project 3, where the same TTF and global profiling approaches will be used to characterize clinical tumor specimens and investigate molecular markers identified in this project, for Project 4, in which the profiles and therapeutic targets for mesothelioma will be explored, and for Project 2, in which the profiles will be correlated with patient prognosis and metastatic patterns. The specific aims of this project are as follows:

Specific Aim 1: To develop a TTF profile for assessing critical signaling pathways and potential therapeutic targets, and to apply TTF and gene expression profiling to NSCLC and mesothelioma cell lines.

- 1.1. Development and technical validation of a TTF profile using reverse phase lysate arrays (RPPA) and multiplexed bead array technology.
- 1.2. Application of TTF profiling to a cell line panel representing malignant (NSCLC and mesothelioma) and non-malignant (endothelial and stromal cells, normal bronchial epithelium) cell types.
- 1.3. Gene expression profiling of the cell line panel using Affymetrix microarrays.
- 1.4. Correlation of TTF and gene expression profiles from the cell line panel to determine gene expression signatures that correlate with activation of individual proteins (e.g., EGFR activation) and critical signaling pathways (e.g., RAS pathway activation).

Specific Aim 2: To determine the sensitivity of the cell line panel to the selected drug and therapeutic target siRNA (DATS) screen.

- 2.1. Screening of the cell line panel for sensitivity to a panel of 20-25 targeted agents and standard chemotherapy agents.
- 2.2. Screening of the cell line panel using siRNA representing potential therapeutic targets, including molecules targeted by specific agents in Aim 2.1 (e.g., EGFR, IGFR-1, etc.) and potential therapeutic targets for which drugs are not currently available (e.g., RTKs for which drugs are currently in development).
- 2.3. Comparison of *in vitro* and *in vivo* profiles (TTF and global) and drug sensitivity in selected NSCLC cell lines and xenografts grown from the same lines.

Specific Aim 3: Development of markers for predicting drug and targeted siRNA sensitivity *in vitro* based on TTF and molecular profiles, and identification of candidate therapeutic targets in chemotherapy-resistant lines.

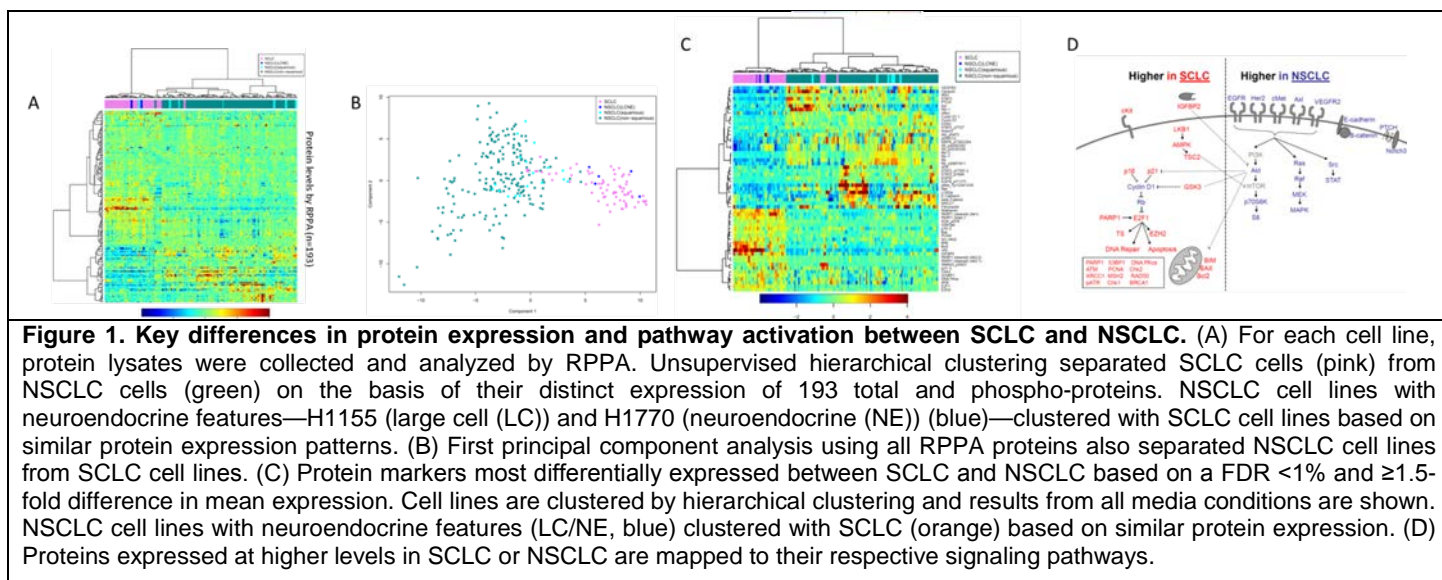
Summary of Research Findings

The overall goals of this project were to systematically investigate signaling pathways and potential therapeutic targets using NSCLC cell lines and tumors; and, by correlating these molecular profiles with drug sensitivity phenotypes, to develop markers for predicting response and resistance and to develop strategies for overcoming resistance.

We have made substantial progress towards these goals in the past year through completion of our aims, with several discoveries of potentially high impact, reflected in part by publications in journals such as the Cancer Discovery, Clinical Cancer Research, and Journal of the National Cancer Institute.

Major advances achieved this year included: 1) Identification of fundamental differences in the patterns of pathway activation in Small Cell Lung Cancer (SCLC) and NSCLC, and identification of potential therapeutic targets for SCLC including PARP1 and EZH2; 2) Development of a

robust EMT signature that predicts resistance to erlotinib as well as to PI3K/Akt inhibitors, and application of this signature to the DoD-sponsored BATTLE trial; 3) Discovery that *LKB1*- and *KRAS*-mutant NSCLC demonstrate increased resistance to PI3K/Akt inhibitors and that *LKB1*-mutant NSCLC exhibits increased activation of the IGF1R signaling pathway. These accomplishments are described in more detail below.

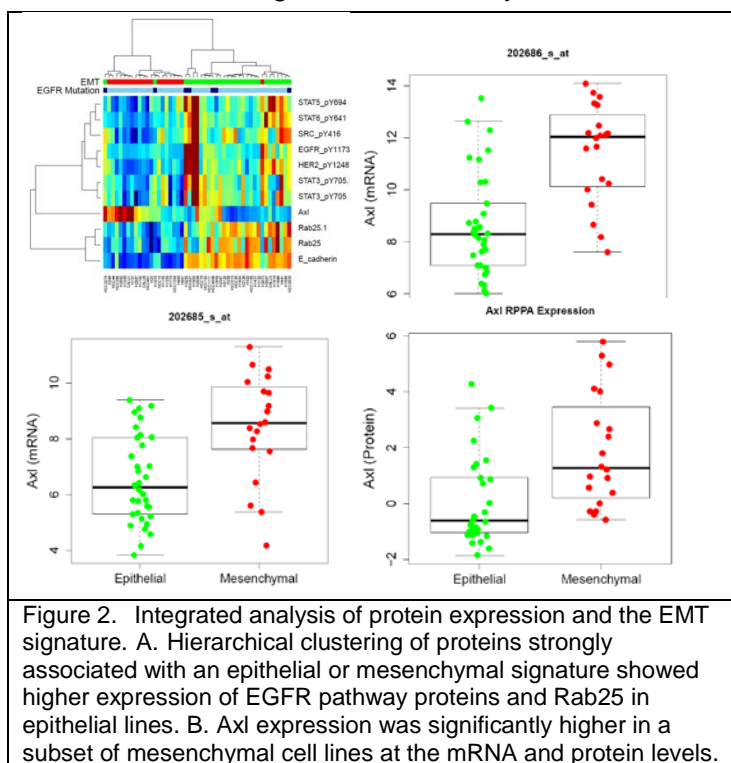


Using systematic molecular and proteomic profiling of NSCLC cell lines, we have successfully identified numerous expression signatures that correlate with in vitro and in vivo drug sensitivity. We have applied these signatures to the analysis of patient samples and correlated the results with outcome and survival. Reverse phase proteomic array (RPPA) is an emerging approach to quantify the levels and activation status of multiple phospho- and total proteins in NSCLC cell lines and patient samples in a comprehensive, convenient, and sensitive manner. From this profiling, we have made significant progress on a number of projects. Using the integrative proteomic and transcriptomic analysis described in Aim 1, we investigated differences contributing to the distinct clinical behavior of SCLC and NSCLC. SCLC exhibited lower levels of several receptor tyrosine kinases and decreased activation of PI3K and Ras/MEK pathways, but had significantly increased levels of E2F-1-regulated factors including EZH2, thymidylate synthase, apoptosis mediators, and DNA repair proteins. Additionally, poly (ADP-ribose) polymerase 1 (PARP1), a DNA repair protein and E2F1 co-activator, was highly expressed at the mRNA and protein levels in SCLC. Therefore, we investigated the effects of PARP inhibitors in SCLC cell lines (**Figure 1**). SCLC cell lines were significantly more sensitive to PARP inhibitors than NSCLC, and PARP inhibition downregulated key components of the DNA repair machinery and enhanced the efficacy of chemotherapy. By systematically profiling SCLC with a focus on therapeutically relevant signaling pathways, we identified several potential therapeutic targets for SCLC. Based on these data, we are currently opening a multi-site Phase II clinical trial testing temozolomide ± a PARP inhibitor, ABT-888 (Byers et al., *Cancer Discovery*, in press).

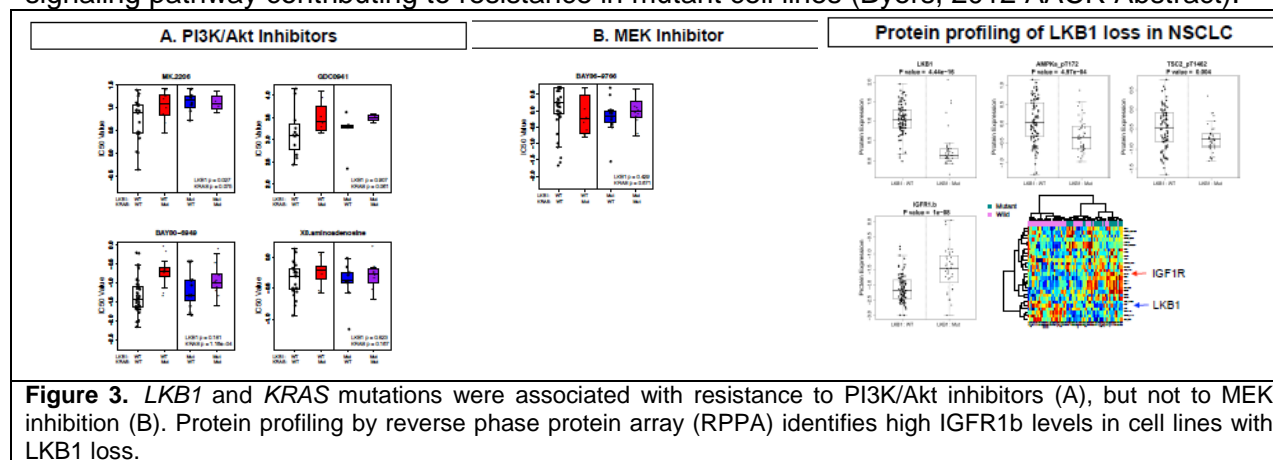
Using a similar approach, we conducted an integrated gene expression, proteomic and drug response analysis in cell lines and tumors from NSCLC patients. Although some molecular markers such as *EGFR* mutations and *ALK* gene fusions have been identified in NSCLC and can be used to select patient therapy, there are still no validated predictive biomarkers for the majority of NSCLC patients. In this study, we investigated whether epithelial-mesenchymal

transition (EMT) influenced sensitivity to established (ex., EGFR inhibitors) and emerging (ex., PI3K inhibitors) targeted drugs in lung cancer cell lines and patient tumors. A 76-gene EMT signature was developed and validated using gene expression profiles from four microarray platforms of NSCLC cell lines and patients treated in the BATTLE study, and potential therapeutic targets associated with EMT were identified (**Figure 2**). Using the 76-gene signature, we determined that mesenchymal cells demonstrated significantly greater resistance to EGFR and PI3K/Akt pathway inhibitors, independent of EGFR mutation status. Mesenchymal cells expressed increased levels of the receptor tyrosine kinase Axl and showed a trend towards greater sensitivity to the Axl inhibitor SGI7079. Furthermore, the combination of SGI7079 with erlotinib reversed erlotinib resistance in mesenchymal lines expressing Axl. In NSCLC patients, the EMT signature predicted 8-week disease control in patients receiving erlotinib, but not other therapies (Byers et al., *Clinical Cancer Research*, in revision). Our data suggest that a robust gene expression signature can identify mesenchymal NSCLC cancers that are likely to be resistant to certain targeted therapies such as EGFR and PI3K/Akt inhibitors, and reveals potential therapeutic strategies for targeting them. The receptor tyrosine kinase Axl, shown here for the first time as a novel EMT marker in NSCLC, has shown early potential as a therapeutic target in other epithelial cancers and should be further investigated in mesenchymal NSCLC.

We have also demonstrated that performing RPPA profiling on a large panel of NSCLC cell lines (~75 cell lines) with known mutational status provides information on drug sensitivity and signaling response. *LKB1* and *KRAS* are the most commonly mutated genes in non-small cell lung cancer (NSCLC), each present in up to 35% of patient tumors. *KRAS* mutations have been associated with resistance to EGFR tyrosine kinase inhibitors, but it is not established to what extent *KRAS* or *LKB1* mutations may predict response to other systemic treatments, including PI3K/Akt and MEK inhibitors. We determined IC₅₀ values for cytotoxic chemotherapies and targeted drugs in the panel of NSCLC cell lines. Cells lines with and without mutations were compared by t-test and linear mixed model to determine the effect of single and double mutations (**Figure 3**). Protein expression in cell lines was then measured by RPPA. *LKB1* mutations strongly predicted resistance to Akt inhibition by MK2206 ($p < 0.05$), but not to PI3K inhibitors BAY80-6949, GDC0941, or 8-amino-adenosine. In contrast, *KRAS* mutations were strongly associated with resistance to PI3K inhibitors BAY80-6949 and GDC0941 and to Akt inhibition by MK2206. Conversely, there was a trend towards greater sensitivity in the *KRAS*-mutated cells to the MEK inhibitor BAY86-9766. Resistance to PI3K inhibition in *KRAS*-mutated lines was largely abrogated by the combination of BAY80-6949 and BAY86-9766. Coexisting *LKB1* and *KRAS* mutations were present in 18% of cell lines, but were not significantly more resistant to PI3K/Akt inhibitors, nor did they predict greater MEK inhibitor sensitivity. There was no association between *KRAS* or *LKB1* mutations and response to cytotoxic chemotherapies, including docetaxel, pemetrexed, or platinum



doublets. At the protein level, *LKB1*-mutant cell lines had significantly higher expression of IGF1R ($p < 0.0001$ by t-test), compared to wild-type cell lines, which may represent an alternative signaling pathway contributing to resistance in mutant cell lines (Byers, 2012 AACR Abstract).



Key Research Accomplishments

- Identified fundamental differences distinguishing SCLC and NSCLC by RPPA profiling, including the possible therapeutic target PARP1.
- Established a robust, cross-platform EMT signature capable of classifying NSCLC cell lines and patient tumors as epithelial-like or mesenchymal-like. The mesenchymal phenotype is a negative predictor of response to erlotinib and PI3K/Akt pathway inhibitors. We also identified Axl as a novel marker of EMT and potential therapeutic target for NSCLC.
- Determined that *LKB1* and *KRAS* mutations are associated with resistance to PI3K/Akt inhibitors. The combination of PI3K+MEK inhibitors largely overcomes resistance of mutated lines to single-agent PI3K inhibition. RPPA analysis revealed that IGF1R is upregulated in *LKB1* mutated cell lines.

Conclusions

Using comprehensive gene expression and proteomic profiling, we have demonstrated that we can systematically profile lung cancer cell lines to identify molecular markers and signaling changes associated with mutation status and drug response. The resulting profiles can be correlated with patient tissue data for association with clinical outcome. These techniques have led to the development of novel therapeutic targets in SCLC (PARP1), mesenchymal NSCLC (Axl), and *LKB1* mutated NSCLC (IGF1R). Clinical trials based on all three of these observations are currently being planned.

Project 2: Tumor molecular profiles in patients with operable non-small cell lung cancer (NSCLC): impact on stage, prognosis, and relapse pattern.

(Leaders: Drs. David Stewart, Jack Roth; Co-Leaders: Drs. Roy Herbst, Edward Kim, Katherine Pisters, Stephen Swisher)

Hypotheses:

We hypothesize that:

1. In tumors from patients with NSCLC, patterns of co-expression of molecules that modulate cell proliferation, survival, angiogenesis, invasion, metastasis and apoptosis will substantially influence tumor stage and size at the time of diagnosis, and will largely define patient prognosis.
2. Impact of adjuvant and neoadjuvant therapies on disease-free, progression-free, and overall survival will vary across prognostically distinct groups.
3. Specific molecular signatures in primary tumors will predict both metastatic patterns at relapse and molecular profiles of recurrent tumors, and this could help guide adjuvant strategies and therapeutic strategies at relapse.

Specific Aims:

Aim 1: To define characteristic TTF/gene expression profiles of prognostically distinct subpopulations of patients with resectable NSCLC, and to assess the extent to which these molecular profiles correlate with tumor stage and/or size.

The main goal of this aim is to use 150 archival NSCLC tumor samples from our tissue bank (with corresponding clinical data) and to prospectively collect tumor samples, blood samples, and clinical data from 300 additional patients undergoing surgical resection of NSCLC. The tissue and blood samples will be used by Project 3 and the Pathology Core to generate comprehensive TTF/gene expression molecular profiles using methods developed in Project 1. We will construct Kaplan-Meier estimated survival curves for disease-free survival, progression-free-survival, and overall survival, and will use Cox proportional hazards models and recursive partitioning methods to identify important biomarkers and prognostically distinct subpopulations. We will also correlate TTF/gene expression molecular profiles with initial tumor size and stage. In addition, we will explore the feasibility of using nonlinear regression analyses of semilog plots of % disease-free survival, % progression-free survival, and % overall survival vs time to facilitate identification of prognostically distinct subpopulations with characteristic TTF/gene expression molecular profiles.

Aim 2: To assess the impact of adjuvant and neoadjuvant chemotherapy on disease-free survival, progression-free survival, and overall survival in prognostically distinct subgroups, and to provide tumor, blood and clinical data to Project 3 for an assessment of factors contributing to resistance to chemotherapy and to Project 5 for assessment of profiling of EGFR and related molecules by new quantum dot technologies.

Of the 450 patients included in the project, we will assess 100 new prospectively recruited patients who will receive neoadjuvant therapy, 100 patients who will receive postoperative adjuvant therapy (including approximately 20 tumor bank patients and 80 new patients), and 250 patients who did not receive adjuvant or neoadjuvant therapy (including approximately 130 tumor bank patients and 120 new patients). We will collect patient clinical data on all 450 patients and will collect blood samples on the 300 new, prospectively recruited patients. Tumor and blood samples and clinical data will be provided to Project 3 for studies of therapeutic

resistance and to Project 5 for assessment of profiling of epidermal growth factor receptor (EGFR) and related molecules by new quantum dot technologies, while in Project 2 we will assess impact of adjuvant and neoadjuvant therapy on outcome in each prognostic group.

Aim 3: To correlate TTF/gene expression molecular profiles in the primary tumor with metastatic patterns and with tumor molecular profiles at relapse.

For patients who relapse, we will define metastatic sites at relapse, obtain tumor tissues from selected patients who undergo biopsies to confirm relapse, and define TTF/gene expression molecular profiles in the patients' original primary tumor specimens that predict sites of later relapse (and in particular that predict relapse in brain). We will also assess whether tumor at relapse is enriched for particular molecular characteristics that may promote metastasis when compared to the primary tumor, and will assess the extent to which TTF/gene expression molecular profile at diagnosis may help guide choice of therapies at relapse.

Summary of Research Findings

During this fifth and final year of research, we continued to collect extensive clinical follow-up data on 272 patients with NSCLC who had previously undergone tumor resection and for whom we have completed extensive molecular profiling on high quality fresh-frozen and formaldehyde-fixed paraffin-embedded (FFPE) tumor samples in our lung cancer tissue bank. Clinical data collected include: follow-up duration; survival status at last follow-up; contribution of lung cancer to patient's death (for those who have died) in order to assess cause-specific survival; follow-up duration for detection of relapse, date of first detection of relapse for each individual organ system (e.g., lung, brain, liver, bone, etc), number of hematogeneous metastases at time of development of hematogeneous metastases; and date of first detection of a new primary lung cancer. We have completed extensive molecular analyses of these 272 tumor specimens (gene expression profiles, microRNA profiling, mutation analyses, etc.) in collaboration with Project 3, and results are outlined in more detail in the reports from Project 3 and the Pathology Core. In multivariate analyses, final bioinformatic analyses will correlate molecular profiles and clinical and histopathologic characteristics with survival time, cause-specific survival, time to any relapse, time to development of a new primary lung cancer, and time to development of relapse in each specific site. Since a high proportion of deaths were from causes other than lung cancer, the most relevant comparisons of tumor molecular profiles will be with variables such as time to relapse, organ-specific relapse, and cause-specific survival, rather than with overall survival.

We have also prospectively collected fresh-frozen and FFPE tumor tissues on 401 patients with NSCLC who have undergone tumor resection, and we banked blood samples on 345 of these cases. The same detailed clinical data have been collected as described above for our tissue bank cases, including survival, cause-specific survival, time to relapse at any site, time to relapse in each specific organ site, number of hematogeneous metastases at time of distant relapse, and time to development of a new primary lung cancer. Data from these prospective cases will be used to validate the risk models generated for our Tissue Bank cases.

The same clinical/survival/relapse data have been collected on a separate group of 312 patients for whom we have FFPE tumor tissue in our tumor bank, and have done extensive immunohistochemistry/tissue microarray assessments of expression of more than 100 proteins. These data will be used to further validate and refine our models.

We also have detailed information on neoadjuvant and adjuvant chemotherapy received by patients, and multivariate modeling will be used to assess interactions between outcome, molecular risk factors, and adjuvant/neoadjuvant therapies. As platinum is known to remain in

tissues for several months after last drug exposure, we have measured platinum concentrations in resected tumor specimens from 44 patients who had received neoadjuvant chemotherapy with cisplatin or carboplatin. We found that the percentage of tumor shrinkage with chemotherapy correlated strongly with tumor platinum concentrations for both cisplatin and carboplatin and for each of adenocarcinomas, squamous cell carcinomas and for patients with either large cell carcinoma or NSCLC not otherwise specified. Despite marked differences in doses between cisplatin and carboplatin, platinum concentrations in tissues were similar, reflecting the reduced rate of uptake of carboplatin into tissues as compared to cisplatin. In addition, tumor platinum concentrations increased only minimally with increasing number of cycles of platinum, suggesting that uptake is limited by down-regulation of uptake mechanisms after initial exposure. A manuscript has been accepted for publication pending minor revisions (Kim et al., J Clin Oncol).

In further assessments of patients who received neoadjuvant chemotherapy, we found in multivariate analysis that the percentage of residual viable tumor cells in the post-neoadjuvant resected tumor correlated inversely with overall survival and disease-free survival ($p=0.005$) (Pataer et al., J Thor Oncol 2012). There was no association of percentage of viable tumor cells with survival or disease-free survival in patients who did not receive neoadjuvant chemotherapy.

Key Research Accomplishments

- Obtained data on relapse patterns, overall survival and cause-specific survival in 985 patients with resected NSCLC.
- Derived detailed molecular profiles on tumors of 272 of these patients, and tissue microarray data on another 315 patients.
- Have banked high quality FFPE and fresh frozen tumor samples available for assessment from another 401 patients.
- Demonstrated that tumor shrinkage after platinum-based neoadjuvant chemotherapy is proportional to tumor platinum concentration and that uptake of platinum into tumor may be down-regulated after initial tumor exposure to drug.
- Demonstrated that overall survival and progression-free survival after neoadjuvant chemotherapy is inversely proportional to percentage of tumor cells that remain viable after neoadjuvant therapy.

Conclusions

In summary, we have collected very detailed information on relapse patterns, overall survival and cause-specific survival in 985 patients with resected NSCLC, have detailed molecular profiles on tumors of 272 of these patients, have detailed tissue microarray data on another 315 patients, and have high quality FFPE and fresh frozen tumor samples available for assessment in a further 401 of these patients. Construction of risk models for relapse at any site, relapse at specific sites, development of new lung primary cancers, overall survival and cause-specific survival is pending. We have demonstrated that tumor shrinkage after platinum-based neoadjuvant chemotherapy is proportional to tumor platinum concentration and that uptake of platinum into tumor may be down-regulated after initial tumor exposure to drug. Overall survival and progression-free survival after neoadjuvant chemotherapy is inversely proportional to percentage of tumor cells that remain viable after neoadjuvant therapy.

Project 3: Molecular Profiling of Non-Small Cell Lung Cancer Tissue Specimens and Serum and Plasma Samples: Correlation with Patient Response and Tumor Resistance to Chemotherapy.

(Leader: Dr. Ignacio Wistuba; Co-Leaders: Lin Ji and John Minna)

Hypothesis:

In Project 3, we hypothesize that systematic molecular profiling of surgically resected non-small cell lung cancer (NSCLC) tissue specimens using therapeutic target-focused (TTF) and mRNA approaches, along with serum phosphopeptide screening and plasma DNA analysis, will lead to the following results:

1. Validation in patients' tissue specimens of molecular signatures obtained from NSCLC cell lines that are associated with *in vitro* and *in vivo* (xenograft) resistance of NSCLC cell lines to chemotherapeutic and targeted agents.
2. Identification of molecular profiling signatures associated with NSCLC sensitivity or resistance to chemotherapeutic agents that can identify NSCLC patients most likely to respond to a given targeted therapeutic agent.
3. Development and validation of serum phosphopeptide profiles and plasma DNA markers associated with NSCLC patient response and tumor resistance to chemotherapeutic agents.

Objectives:

The greatest obstacle to creating effective treatments for lung cancer is the development of resistance to both chemotherapeutic and targeted agents. In this highly integrated and translational program project, we tackle one of the most clinically significant problems in lung cancer: the prediction of patient response to therapy, especially in the context of tumor resistance to current standard chemotherapies. The main objectives of this project are as follows:

- a) To profile surgically resected tumor tissue specimens obtained from NSCLC patients to validate molecular signatures found in the TTF and mRNA profiles developed in Project 1. These profiles will be compared with molecular signatures obtained from NSCLC cell lines that are associated with *in vitro* and *in vivo* (xenograft) resistance to chemotherapeutic and targeted agents.
- b) By comparing NSCLC tumor specimens (collected in Project 2) from patients who have received preoperative chemotherapy and from those who have not, to validate TTF and mRNA signatures that are found in Project 1 to be associated with resistance to therapy and with the activation of resistance-associated molecular pathways or that are found in Project 1 to be potentially exploitable as new therapeutic targets.
- c) To identify serum and plasma biomarkers as surrogate markers to predict the response of NSCLC patients to neoadjuvant chemotherapy and to predict patient outcome.
- d) To provide tissue- and serum-based molecular profile signatures or markers to Project 2 that can predict the clinical outcome of NSCLC patients who had undergone surgical resection with curative intent, with or without neoadjuvant therapy.

This interdisciplinary research proposal for profiling cell lines, tumor tissue, and serum samples from patients with NSCLC requires extensive histopathological, molecular, and

immunohistochemical studies, which will be coordinated and/or performed by the Pathology Core (see Pathology Core's report).

Specific Aims:

Aim 1: To validate, in retrospectively collected NSCLC tumor tissue specimens, the TTF and mRNA profiles predictive of the *in vitro* and *in vivo* (xenograft) resistance of NSCLC cell lines to chemotherapeutic and targeted agents.

Summary of proposal: We will select 150 surgically resected NSCLC tumor specimens from The University of Texas Lung SPORE (UT-SPORE) Tissue Bank for TTF and mRNA profiling. Using those 150 frozen archival NSCLC tumor tissues, we will perform reverse-phase protein array (RPPA), multiplex bead-based protein analysis (MBPA) and Affymetrix U133 Plus 2.0 array to validate the molecular signatures developed in Project 1. Then, we will compare the profile signatures obtained from the NSCLC tumor specimens with the signatures obtained from NSCLC cell lines in Project 1 that predict the *in vitro* and *in vivo* resistance to chemotherapeutic and targeted agents. Finally, using formalin-fixed and paraffin-embedded tissue specimens, we will validate the expression of proteins abnormally represented in the molecular profiling analyses of NSCLC tumor specimens by using tissue microarrays (TMAs) and semiquantitative immunohistochemical (IHC) methods.

Summary of Research Findings

During this no-cost extension (5th) and final year of research, in collaboration with the Pathology Core (I. Wistuba) and the Biostatistics/Bioinformatics Core (J. Lee and K. Coombes), we have completed the analysis of the molecular profiling data of NSCLC specimens and, in collaboration with Project 4 and the Biostatistics Core, a comprehensive molecular profiling of malignant pleural mesothelioma (MPM) tumor and cell lines, all (NSCLC and MPM) with annotated clinico-pathological information, and achieved the following milestones:

- 1) Published 3 papers (see below) describing novel clinically relevant pathological and molecular markers in NSCLC:
 - Using FFPE lung tumor tissues, we identified a set of genes whose expression level provides prognostic information across different profiling platforms and studies, which may be applied in clinical settings (Yang et al., Clin Can Res, 2011).
 - We identified that high levels of Folate Receptor- α in lung adenocarcinomas is associated with EGFR mutations and represents a potential novel target for this tumor type (Nunez et al, JTO, 2012).
 - We demonstrated, in collaboration with other investigators (Vancouver, Canada), that adenocarcinomas and squamous cell carcinomas of the lung develop through distinct pathogenetic pathways that have significant implication in our approach to the clinical management of NSCLC (Lockwood, PLoSOne, 2012).
- 2) Submitted 2 papers (see below) characterizing clinical relevant molecular profiles in NSCLC and MPM:
 - We found that MPM tumors show significant deregulation of the Mitotic Spindle Assembly Check-point pathway genes and can be classified into three newly discovered molecular subgroups of prognostic, diagnostic and therapeutic importance (Suraokar et al., submitted to Cancer Res).
 - We integrated, for the first time, genetic alteration data, genome-wide siRNA functional data, and mRNA expression data to identify a functional gene set that predicts clinical

benefit of surgically resected lung adenocarcinomas (Tang et al., submitted to J Clin Oncol).

- 3) Tested our newly developed strategy for gene (mRNA) signature validation using the high-throughput Quantitative Nuclease Protection Assay (qNPA™) and Fluidigm™ microfluidic quantitative dynamic array (Erickson et al., AACR abstract, 2012).
- 4) Identified a series of molecular pathways and markers, using gene profiling, as potential novel targets in NSCLC (EZH2, miR-101 and ETS2) and MPM (GPC5A, Twist1) (Behrens et al., Riquelme et al., Kabbout et al., Fujimoto et al., and Suraokar et al., AACR abstracts, 2012).

The detailed progress update of the studies in items #3 and #4 is as follows:

Nanoscale high-throughput quantitative RT-PCR for the characterization of targeted-therapy-related molecular biomarkers from recurrent and non-recurrent NSCLC tissues.

Currently, there are no effective biomarkers to predict targeted therapy outcomes for patients whose cancers recur versus those that do not. Technology limitations have prevented extensive qRT-PCR biomarker analysis on small tumor tissue samples. Clinical sample size limitations are inherent due to the extremely small core needle biopsies (CNB) and fine needle aspirates (FNA) that are available in these cases. Identifying technology that can reliably analyze, in a quantitative manner, molecular biomarker signatures of 200-300 genes from CNB and FNA will allow for comparative analysis of patients' untreated tumors with treated follow-up tissue samples. We hypothesize that RNA amplification coupled with nanoscale high-throughput (HT) qRT-PCR, will allow analysis of 320 gene expression patterns from 10ng RNA from frozen NSCLC tissues. We believe primary NSCLC tumors that recur have a different pattern of molecular abnormalities than NSCLCs from non-recurrent (< 5 years) tumors, possibly accounting for the lack of response to targeted therapy in some patients. RNA from 40 frozen adenocarcinoma (ADC) NSCLC tumor and matched normal cases with annotated clinicopathologic data was extracted, isolated, and their quantity/quality measured. A total of 10ng from each sample was pre-amplified by WT-Ovation Pico protocol (NuGEN). Nanoscale high-throughput OpenArray quantitative RT-PCR (Life Technologies) with SYBR chemistry and DLD platform TaqMan chemistry was used to analyze 206 and 94 genes of interest, respectively, and 18 endogenous controls (EC). EC geometric mean was used for data normalization. Two-sample t-test was applied as a test statistic for identifying differentially expressed genes with respect to recurrence, clinical stage, race and gender. Statistical significant level was set as $p \leq 0.05$. Statistical analysis was conducted using R packages. WT-Ovation Pico protocol successfully amplified all 10ng samples (mean = 235.2ng/ul, 1.94 260/280). OpenArray qRT-PCR successfully produced quantitative gene expression measurements as assessed by technical replicates (SD, median = 0.14; range = 0.00 to 12.70; $R=0.931$) and sample-to-sample correlation from chip to chip for each gene (Spearman Rho median = 0.3; range = -0.44 to 0.82). Fourteen genes (**Figure 1**) included in the SYBR subset

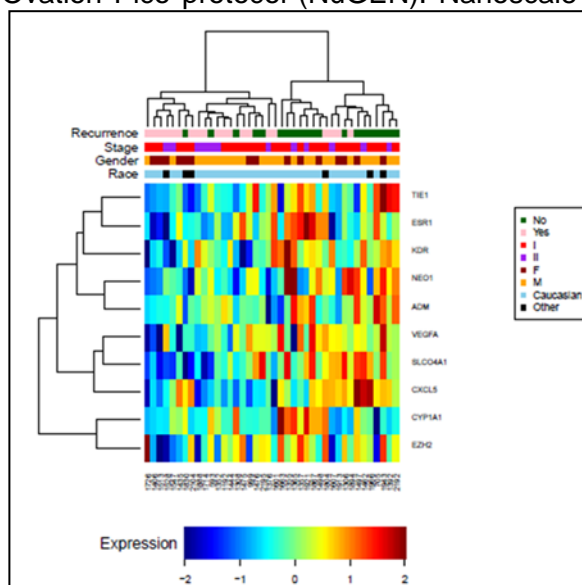
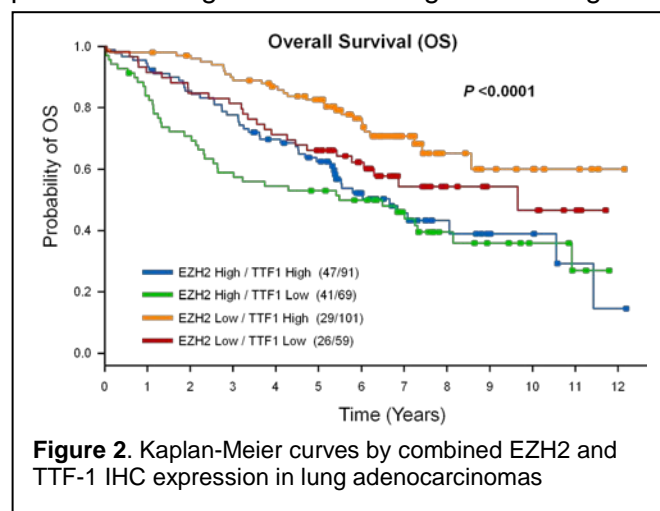


Figure 1. Top 10 genes identified as dysregulated in recurrent vs. non-recurrent lung adenocarcinomas assessed from the 206 SYBR gene set.

(*KDR*↓, *SLCO4A1*↓, *ESR1*↓, *TIE1*↓, *EZH2*↓, *VEGFA*↓, *ADM*↓, *CYP1A1*↓, *NEO1*↓, *CXCL5*↓, *FGFR2*↓, *HMBS*↓, *ID1*↑, *NRP2*↓) and 3 genes included in the TaqMan subset (*DDX20*↑, *CIDEA*↓, *PERP*↓) were significantly dysregulated in recurrent vs. non-recurrent ADC NSCLCs. We found that amplification coupled with nanoscale HT qRT-PCR allowed for 320 quantitative gene expression measurements from 10ng RNA from NSCLC tissue. We identified 17 genes with significantly dysregulated expression in recurrent vs. non-recurrent ADC NSCLCs (Erickson et al., AACR Annual Meeting 2012, and manuscript in preparation).

Analysis of EZH2 and TTF-1 Protein Expression Identifies a Subset of Lung Adenocarcinomas with Better Prognosis. Lung adenocarcinoma is a heterogeneous tumor with multiple phenotypes that have been associated with prognosis. Recently, we reported that in surgically resected adenocarcinomas, the presence of a solid histologic pattern is associated with poor prognosis. To characterize molecular targets and identify novel prognostic markers in lung adenocarcinoma, we examined by immunohistochemistry (IHC) and tissue microarrays (TMAs) the expression of 75 proteins in archival tumor tissues obtained from 204 surgically resected tumors. We selected two top markers, EZH2 (enhancer of zeste homolog 2) and TTF-1 (thyroid transcription factor-1) that had significant correlation with solid and bronchioloalveolar patterns, respectively, for more detailed clinico-pathologic analyses, including patients' outcome. EZH2 is part of a protein complex that promotes cancer development by epigenetically silencing tumor suppressor genes. TTF-1 is a transcription factor considered a potential lineage-survival oncogene in lung cancer. For EZH2 and TTF-1 IHC expression



analysis, we examined 320 surgically resected lung adenocarcinomas, stages I-III, with median follow-up of 6.7 years. *EGFR* and *KRAS* mutation data were available in most cases. High nuclear EZH2 expression in tumor cells correlated with younger patient age ($P<0.0001$), smoking history ($P<0.0001$), higher TNM stage ($P=0.02$), and lack of *EGFR* mutation ($P=0.001$). High nuclear TTF-1 expression correlated with female sex ($P=0.002$), smaller tumor size ($P=0.001$), lower TNM stage ($P=0.02$), and *EGFR* mutation ($P=0.007$). EZH2 and TTF-1 expression did not correlate with *KRAS* mutation status; however, we found that their expression

levels were significantly higher ($P=0.022$ and $P=0.005$, respectively) in tumors with *KRAS* CYS substitution compared with other amino acid changes. Univariate and multivariate (adjusting by other clinical prognostic factors) analyses were used to correlate EZH2 and TTF-1 expression with recurrence-free survival (RFS) and overall survival (OS). In the multivariate analysis, high EZH2 expression (≤ 42 , median score) was associated with worse RFS ($P=0.034$; HR 1.52) and OS ($P=0.0002$; HR 1.94), and high TTF-1 expression (>120 score) correlated with better OS ($P=0.004$; HR 0.62). We identified a subset (32%) of tumors with low-EZH2/high-TTF-1 that demonstrated better outcome in multivariate analysis, compared with other tumors, including RFS ($P=0.004$; HR 0.51) and OS ($P=0.0007$; HR 0.49) (**Figure 2**). These tumors were more frequent in patients with female sex ($P=0.003$), never-smoking history ($P=0.004$), smaller tumor size ($P=0.018$), lower TNM stage ($P=0.024$), and *EGFR* mutation ($P=0.0001$). Our findings indicate that the combined analysis of the EZH2 and TTF-1 expression identifies a subset of lung adenocarcinoma patients with better outcome after surgical resection with curative intent (Behrens et al., AACR Annual Meeting 2012, and manuscript in preparation).

EZH2 high-expression and miR-101 low-expression are associated with chemoresistance and shorter survival in patients with lung adenocarcinoma who received adjuvant chemotherapy.

EZH2 is implicated in neoplastic transformation, tumor progression, and drug resistance to chemotherapy. EZH2 overexpression has been described in NSCLC. Recently, it was demonstrated that miR-101 negatively regulates the expression of EZH2. In this study, we investigated the effect of EZH2 gene/protein and miR-101 expressions in the outcome of lung adenocarcinoma patients treated with surgery and adjuvant chemotherapy, and studied in vitro mechanisms associated with the role of EZH2/miR-101 abnormalities in lung adenocarcinoma chemoresistance. We analyzed EZH2 and miR-101 expression in RNA extracted from 151 lung adenocarcinoma tumors obtained from patients treated with surgery and with (n=57) or without (n=94) platinum adjuvant therapy, and compared those data with patients' survival (median follow-up 5.6 years). EZH2 and miR-101 expressions were tested using Illumina mRNA arrays W6-6 V.3 and Agilent V3 human microRNA, respectively. To investigate the role of EZH2 overexpression in resistance to cisplatin and cell migration, we knocked down EZH2 expression in adenocarcinoma cell lines using small interfering RNA (siRNA). Cisplatin sensitivity (IC₅₀) was determined by MTS assay. Cell migration was measured using Boyden chambers. We found an inverse correlation in the expression of EZH2 and miR-101 in tumor samples. Interestingly, EZH2 high-expression (P=0.007) and miR101 (P=0.01) low-expression were significantly associated with worse overall survival in lung adenocarcinoma patients who received platinum adjuvant therapy, but not in patients who did not receive such therapy. Similar results (P=0.008) were observed when combined EZH2^{High}/miR-101^{Low} expression was examined. From a panel of 21 adenocarcinoma cell lines with known EZH2 gene/protein expression, we selected 4 cell lines: 2 with high EZH2 (H1993 and HCC1171), and 2 with low EZH2 (HCC461 and HCC193). Knockdown of EZH2 using siRNA reduced cell migration of H1993 and HCC1171 cells (3.7-fold decrease and 1.7-fold, respectively, P<0.05), but not of HCC193 and HCC461 cells (**Figure 3**). Knockdown of EZH2 significantly decreased (P<0.05) the viability of cell lines H1993 and HCC1171 when treated with cisplatin by MTS assay, but not viability of HCC193 and HCC46 cells. Our findings suggest that EZH2 overexpression may promote a more malignant phenotype of lung adenocarcinoma cell lines, including increased chemoresistance and cell migration capabilities. Expression of EZH2 and miR-101 may represent a predictive marker of worse outcome of lung adenocarcinoma patients treated with surgery and adjuvant platinum chemotherapy. In addition, EZH2 could be a potential novel target to overcome drug resistance in lung cancer (Riquelme et al., AACR Annual Meeting 2012, and manuscript in preparation).

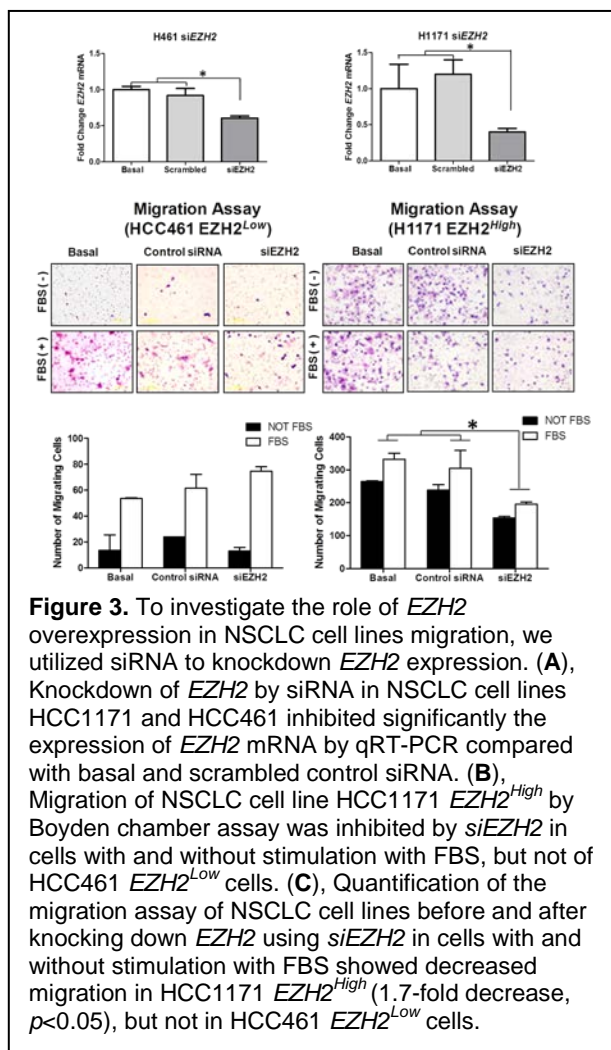


Figure 3. To investigate the role of *EZH2* overexpression in NSCLC cell lines migration, we utilized siRNA to knockdown *EZH2* expression. (A), Knockdown of *EZH2* by siRNA in NSCLC cell lines HCC1171 and HCC461 inhibited significantly the expression of *EZH2* mRNA by qRT-PCR compared with basal and scrambled control siRNA. (B), Migration of NSCLC cell line HCC1171 *EZH2*^{High} by Boyden chamber assay was inhibited by *siEZH2* in cells with and without stimulation with FBS, but not of HCC461 *EZH2*^{Low} cells. (C), Quantification of the migration assay of NSCLC cell lines before and after knocking down *EZH2* using *siEZH2* in cells with and without stimulation with FBS showed decreased migration in HCC1171 *EZH2*^{High} (1.7-fold decrease, p<0.05), but not in HCC461 *EZH2*^{Low} cells.

Tumor suppressor effects of the ETS2 canonical transcriptional factor in human non-small cell lung cancer pathogenesis.

Although v-ets erythroblastosis virus E26 oncogene homolog 2 (ETS2) is a transcription factor that regulates various cancer-associated cellular and developmental processes including proliferation and migration, its function in lung carcinogenesis is still unknown. In this study, we sought to examine the role of the ETS2 canonical transcription factor in NSCLC pathogenesis. We first examined ETS2 mRNA expression in lung adenocarcinomas (n=80) and normal lung (n=30), which we had profiled using microarrays and, in seven matched adenocarcinoma and normal lung pairs, analyzed using next-generation sequencing (NGS) technology. Both array and sequencing datasets revealed that ETS2 mRNA was significantly lower in lung adenocarcinomas relative to normal lung ($p<0.001$), which was confirmed by quantitative PCR analysis. Moreover, in the microarray dataset, ETS2 mRNA expression was significantly inversely correlated with that of the proliferation marker KI67 ($R=-0.59$, $p<0.001$). In addition, in silico analysis of

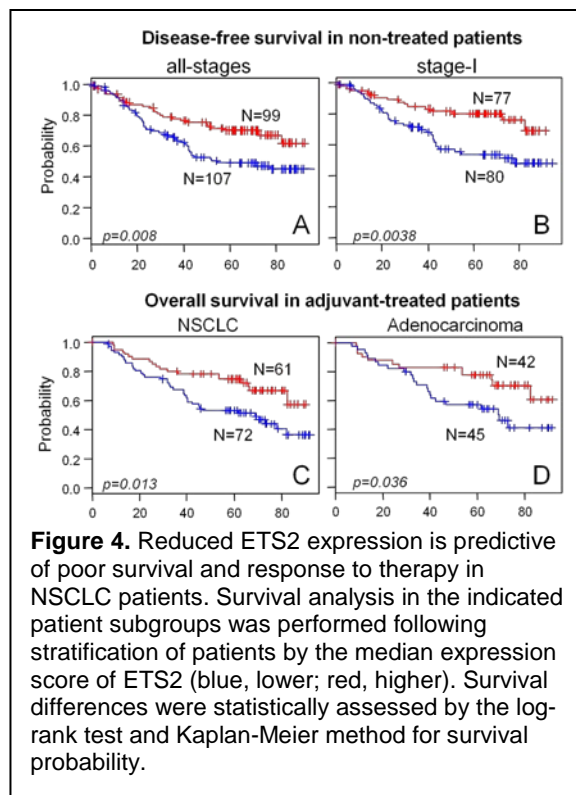


Figure 4. Reduced ETS2 expression is predictive of poor survival and response to therapy in NSCLC patients. Survival analysis in the indicated patient subgroups was performed following stratification of patients by the median expression score of ETS2 (blue, lower; red, higher). Survival differences were statistically assessed by the log-rank test and Kaplan-Meier method for survival probability.

publicly available datasets also demonstrated that ETS2 mRNA was lower in NSCLC compared to normal lung (all $p<0.001$). We next assessed ETS2 immunohistochemical protein expression using tissue microarrays comprised of 342 formalin-fixed paraffin-embedded (FFPE) NSCLC (adenocarcinoma, n=226; SCC, n=116) tissue specimens. There were no statistically significant differences in ETS2 protein expression by histology, stage or age. We next assessed the association of ETS2 protein expression with clinical outcome. Non-treated all-stage (n=206) or stage-I (n=157) patients with relatively lower ETS2 protein expression exhibited significantly shortened disease-free survival compared to patients with higher expression ($p=0.008$ and $p=0.004$ of the log-rank test, respectively) (**Figure 4**). In addition, patients with relatively lower ETS2 expression exhibited significantly poorer response to adjuvant therapy compared to patients with higher ETS2 expression ($p=0.01$). We then probed the effect of modulating ETS2 expression in NSCLC cells. Knockdown of ETS2 expression by RNA interference significantly increased anchorage-dependent colony formation ($p=0.004$) as well as significantly augmented cellular migration and invasion ($p=0.02$ and $p=0.01$, respectively) compared to cells transfected with scrambled siRNA (**Figure 5**). Our

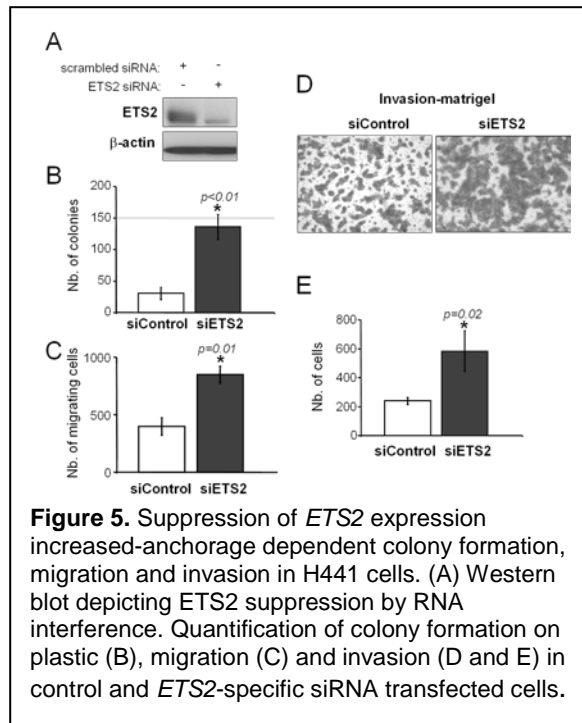


Figure 5. Suppression of ETS2 expression increased-anchorage dependent colony formation, migration and invasion in H461 cells. (A) Western blot depicting ETS2 suppression by RNA interference. Quantification of colony formation on plastic (B), migration (C) and invasion (D and E) in control and ETS2-specific siRNA transfected cells.

findings provide evidence that ETS2 may function as a tumor suppressor gene in NSCLC that may aid clinically in identification of aggressive tumors and biologically in increasing our understanding of the pathogenesis of this malignancy (Kabbout et al., AACR Annual Meeting 2012, and manuscript in preparation).

Expression patterns of the G protein-coupled receptor, GPRC5A, in human MPM.

The G protein-coupled receptor family C group 5 member A (hGPRC5A, mGprc5a) was previously shown to function as a lung-specific tumor suppressor gene evidenced by the development of lung adenomas and adenocarcinomas in mice with knockout of both alleles of this gene. Moreover, we have demonstrated that the IHC expression of GPRC5A protein was significantly lower in NSCLC resected specimens compared to normal bronchial epithelia from healthy individuals. The latter findings prompted us to examine the expression patterns of GPRC5A in MPM because, like NSCLC, this malignancy develops in the thoracic cavity. Analysis of two publicly available MPM microarray datasets revealed that GPRC5A mRNA expression is significantly higher in MPMs compared to matched normal pleura (5.5 fold higher, $p=0.002$; 6.57 fold higher, $p=0.04$). GPRC5A immunohistochemical protein expression was semi-quantitatively assessed in formalin-fixed and paraffin-embedded (FFPE) MPM surgical specimens ($n=73$) comprised of 41 epitheloid, 14 biphasic and 18 sarcomatoid type MPMs. GPRC5A protein expression was also assessed in a subset of the MPM specimens ($n=51$) that were reconstructed as high-density spiral tissue microarrays (TMA) developed by J. Fukuoka and colleagues (Sakura-Finetek, Tokyo, Japan) comprised of 35 epitheloid, 9 biphasic and 7 sarcomatoid type MPMs (**Figure 6**). ANOVA analysis demonstrated significant differences in GPRC5A immunohistochemical expression among MPMs based on the histological subtype ($p<10^{-6}$) with relative highest expression in the epitheloid tumors (mean, 98.04 ± 54.55 ; min, 0; max, 200), intermediate expression in biphasic-type tumors (mean, 53.57 ± 38.55 ; min, 0; max, 140) and lowest expression in sarcomatoid-type MPMs (mean, 24.44 ± 21.48 ; min, 0; max, 70). The patterns of GPRC5A expression based on histological type of surgical MPM specimens were corroborated using spiral TMA technology, with relative highest expression in the epitheloid tumors and lowest expression in sarcomatoid-type MPMs. Importantly, GPRC5A immunohistochemical protein expression was positively significantly correlated between the surgical and spiral TMA specimens ($R=0.71$, $p<10^{-6}$). We then sought to examine the association of GPRC5A expression with overall survival in MPM. GPRC5A expression was not associated with overall survival when all histological-type MPMs were included. Interestingly, patients with non-epitheloid type MPMs with relatively higher GPRC5A expression exhibited significantly worse overall survival compared to MPM patients with similar histology and lower expression ($p=0.02$ of the log-rank test). These findings suggest that, unlike what was observed in murine and human NSCLC, GPRC5A may function as an oncogene in MPMs and warrant further studies to probe the function of this receptor in mesotheliomas (Fujimoto et al., AACR Annual Meeting 2012).

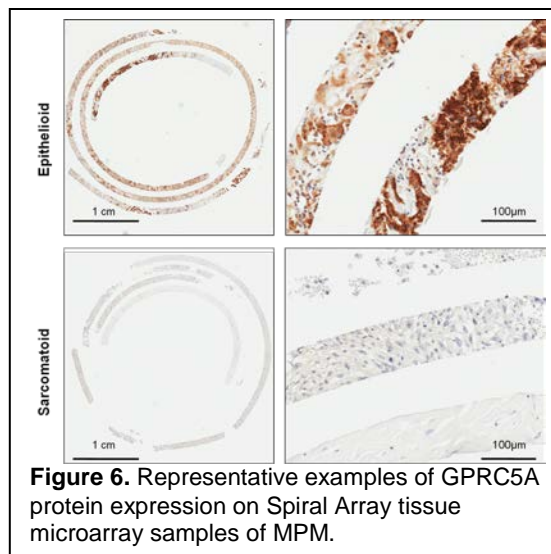
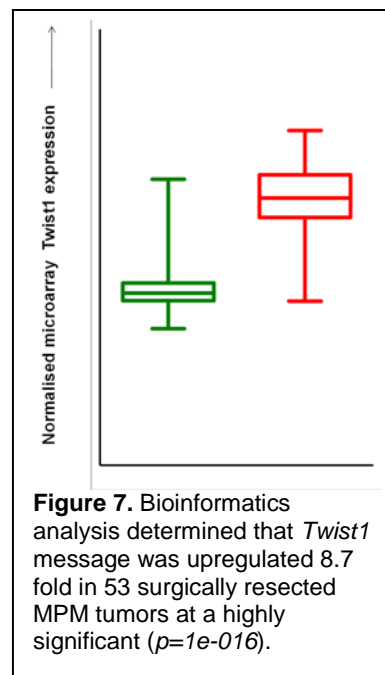


Figure 6. Representative examples of GPRC5A protein expression on Spiral Array tissue microarray samples of MPM.

Exploring the role of Twist 1 in the pathogenesis of MPM. MPM is caused by lethal neoplastic growth of the pleura surrounding lungs. It is resistant to most standard anti-cancer treatment regimens and needs discovery of newer therapeutic approaches. MPM is characterized by massive loco-regional invasion of the malignant pleural cells into the lung

parenchyma. Twist1 is a transcription factor that promotes invasion and metastasis of tumor cells, increases chemotherapeutic resistance and is involved in the pathobiology of many cancers. Also, recent studies have highlighted the potential of Twist1 as a therapeutic target in cancer; however, there is no report investigating its function in mesothelioma. We extracted total RNA from 53 frozen resected tumor tissue specimens, comprised of 35 epithelioid, 12 biphasic and 6 sarcomatoid case histotypes, along with paired normal tissue (**Figure 7**). The RNA was labeled and hybridized to Affymetrix U133 plus 2.0 microarray to obtain transcriptomic profiles. Bioinformatic analysis of the microarray data using a 2-sample t-test was applied, on a probe-by-probe basis followed by Beta-uniform Mixture for multiple comparisons, to determine the differences between tumor vs normal specimens. The microarray results were validated by quantitative reverse transcriptase polymerase chain reaction (qRT-PCR) using Taqman assays on the ABI 7300 platform. For all qRT-PCR experiments, the twist1 transcript levels were determined relative to endogenous GAPDH as control using $\Delta\Delta CT$ calculation. We performed Western blot analysis on a panel of 16 mesothelioma cell lines including Met-5A (SV-40 immortalized) and HCT-4012 (telomerase immortalized) pleural mesothelial control cell lines. The bioinformatic analysis of microarray data showed that Twist1 transcript level was 8.7-fold higher in tumors ($p = 1.1e-16$) compared to paired normal specimens. Using qRT-PCR, we compared Twist1 transcript levels in 12 pairs of tumor vs paired normal tissue specimens and found that Twist1 was upregulated to more than 10-fold in MPM tumors ($p = 1e-4$). Western blot showed that 10 MPM cancer cell lines had higher expression of Twist1 protein compared to Met-5A and HCT-4012 cell lines. The highest expression was seen in 2 of the sarcomatoid cell lines - RS5 and DM3 - suggesting a correlation with metastatic phenotype, since sarcomatoid tumors are highly metastatic in nature. Our preliminary findings suggest that Twist1 is upregulated in MPM tumors and cell lines, and may play a role in the development of MPM. Further studies are needed to investigate its role in the process of tumorigenesis and metastasis (Suraokar et al., AACR Annual Meeting 2012).



Aim 2: To develop TTF and mRNA signatures of NSCLC resistance to chemotherapy, and identify chemoresistance-associated targets/pathways as new therapeutic targets.

Summary of proposal: Whereas Aim 1 focuses on the identification in archived tumor specimens of TTF and mRNA molecular profiles detected in NSCLC cell lines, the main focus of Aim 2 is to determine whether the molecular signatures in the tumor specimens correlate with patient response to neoadjuvant chemotherapy. From the clinical trial in Project 2, we will use specimens from 100 NSCLC patients who received neoadjuvant therapy and had surgical resection with curative intent (cases) and from 200 NSCLC patients who had surgical resection but did not receive neoadjuvant therapy (controls) to perform RPPA, MBA, and Affymetrix U133 Plus 2.0 array analyses. Then, we will compare the TTF and mRNA profile signatures obtained from these NSCLC tumor specimens with signatures obtained in Project 1 to predict the in vitro and in vivo resistance of NSCLC cell lines to therapy. Those data will be provided to Project 2 for correlation with clinical characteristics, including prognosis and metastasis. Finally, using formalin-fixed and paraffin-embedded tissue specimens, we will validate the expression of proteins abnormally represented in the molecular profiling analyses in NSCLC tumor specimens from all patients enrolled in Project 2 by using TMAs and semiquantitative IHC methods.

Summary of Research Findings

During the no-cost extension (5th) year of research, in collaboration with the Pathology Core (I. Wistuba) and the Biostatistics/Bioinformatics Core (J. Lee and K. Coombes), we completed the analysis of the molecular profiling data of surgically resected NSCLC specimens obtained from patients who have received neoadjuvant chemotherapy. Our progress included the following:

- 1) Published 2 papers (see below) describing novel clinical relevant pathological and molecular markers associated to chemotherapy response in NSCLC:
 - We showed for the first time that tumor cell KDR copy number gains (CNGs) promote a more malignant phenotype, including increased chemoresistance and angiogenesis, and that KDR CNGs may be a useful biomarker for identifying patients at high risk for recurrence after adjuvant therapy (Yang et al., Cancer Res, 2011).
 - We demonstrated that the histopathologic assessment of resected specimens after neoadjuvant chemotherapy could potentially have a role in addition to pathologic stage in assessing prognosis, chemotherapy response, and the need for additional adjuvant therapies (Pataer et al., JTO, 2012).
- 2) Completed the mRNA profiling analysis of 63 NSCLC tumors banked in the Pathology Core and completed the bioinformatics mRNA profiling analysis of 89 frozen tumor samples as reported in the AACR Annual Meeting 2012 (Dalvi et al., AACR abstract 2012).

The detailed progress update of the studies listed in item #2 is as follows:

Developing a molecular understanding of NSCLC resistance to platin-taxane chemotherapy. While chemotherapy has improved lung cancer patient survival, relapse rates after neoadjuvant or adjuvant chemotherapy (minimal residual disease settings) are high. This could be due to cancer cells acquiring resistance to therapy or selective survival of pre-existing resistant cells. The molecular basis for primary or acquired resistance to standard platinum doublet chemotherapies are unknown and their elucidation is necessary for developing curative therapy that can be personalized for each patient. Three complementary approaches were used to explore mechanisms underlying NSCLC resistance to platin-taxane chemotherapy:

- A) NSCLC lines were exposed in vitro to cycles of paclitaxel + carboplatin to mimic clinical treatment, and resistance was validated with cell viability and colony formation assays. Genome-wide mRNA expression profiles of resistant and parental lines were compared using Illumina arrays and qRT-PCR.
- B) A large dataset of clinically and molecularly annotated NSCLC tumor specimens obtained after no chemotherapy or neoadjuvant platin-taxane chemotherapy were subjected to mRNA microarray analysis.
- C) Lung cancer xenografts were treated with chemotherapy in vivo in mice and profiled for mRNA expression.

Biostatistical and bioinformatics approaches were used to identify genes that are differentially expressed in resistant cells in these three settings, and their function studied using over-expression or shRNA-mediated knockdown. NSCLC lines H1299 and H1355 were treated in vitro with paclitaxel + carboplatin and showed progressive increases in resistance to chemotherapy (after 5 to 15 cycles) ultimately achieving 30- (H1299) or 60-fold (H1355) differences compared to parental cells. In addition, multiple single cell clones also demonstrated chemotherapy resistance. Resistant NSCLC strains were also resistant to platin+docetaxel and

also to platin+pemetrexed combinations. Expression profiles revealed upregulation of ABCB1/MDR1, down regulation of epithelial-specific genes suggesting EMT), differences in expression of epigenetic modulators and cancer testis family of GAGE genes and many of these genes had expression correlated with recurrence after neoadjuvant chemotherapy and with poor survival. Resistance was only partially reversed by verapamil, indicating that it is only partially explained by MDR mechanisms. Mechanistic studies of genes identified by these three approaches provide opportunities for overcoming chemotherapy resistance and developing novel therapies for NSCLC (Dalvi et al., AACR Annual Meeting 2012, and manuscript in preparation).

Aim 3: To identify surrogate serum phosphopeptide profiles and plasma DNA markers associated with NSCLC tumor resistance and patient response to neoadjuvant chemotherapy.

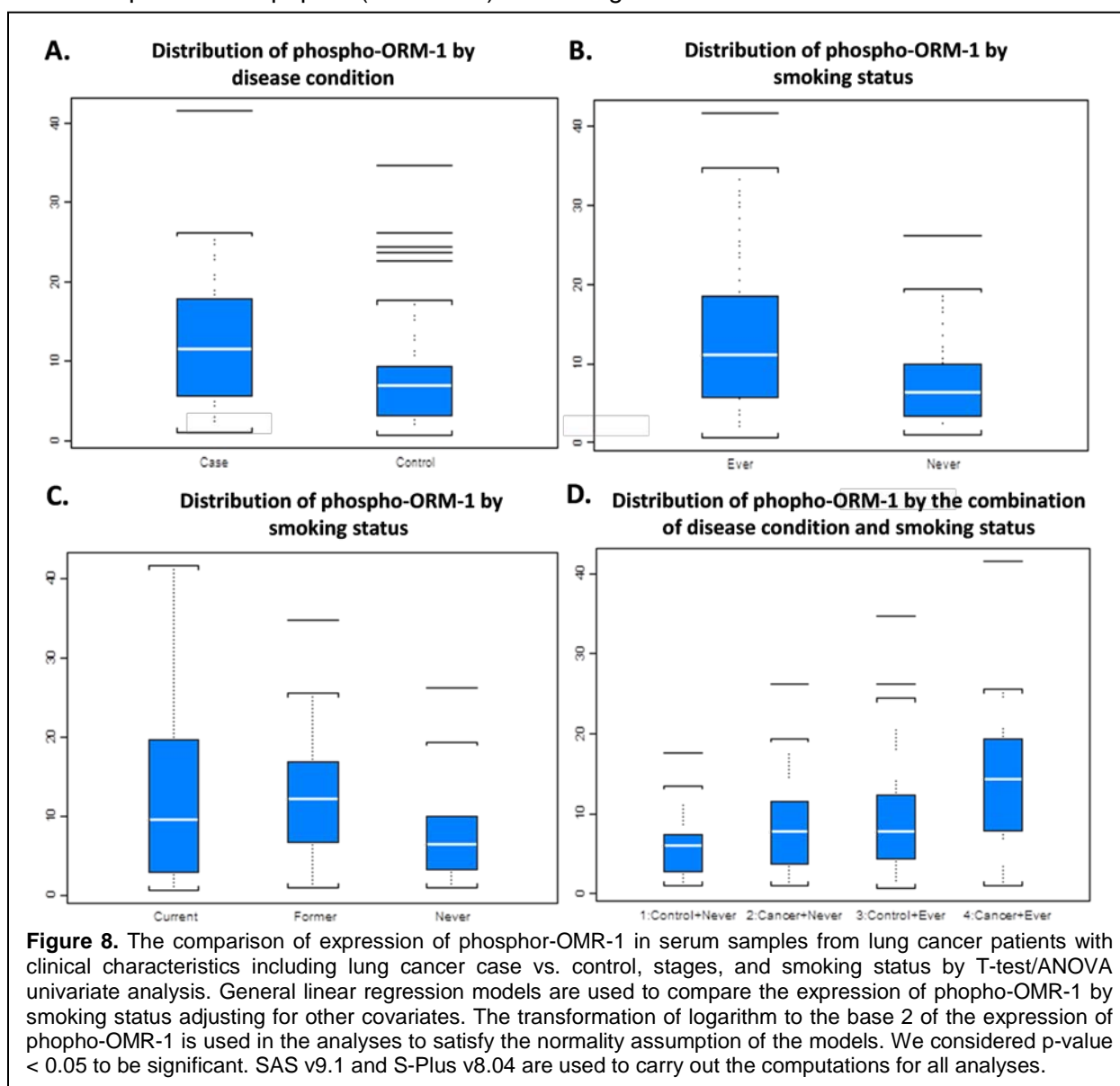
Summary of proposal: We will identify serum samples from the UT-SPORE Tissue Bank that match the NSCLC tumor resection specimens examined in Aim 1. We will use these serum samples for phosphopeptide profiling and peptide mapping by ProteinChip array-based surface-enhanced laser-desorption/ionization (SELDI) mass spectrometry (MS) and laser desorption/ionization (LDI) mass spectrometry (MS)/MS to compare serum phosphopeptides with TTF and mRNA profiles. The phosphopeptide MS profiles from retrospective specimens will later be used as references and controls for the prospective serum proteomic analysis. As in Aim 2, we will use serum samples collected prospectively in Project 2 from 100 NSCLC cases undergoing neoadjuvant chemotherapy and 200 NSCLC controls undergoing surgery without neoadjuvant chemotherapy, and, when relevant, at the time of relapse. Using these serum specimens, we will perform phosphopeptide profiling on ProteinChip arrays by SELDI-MS to measure the temporal changes in serum phosphopeptides before and after the therapeutic intervention. We will use LDI-QSTAR-MS/MS and liquid chromatography (LC)-MS/MS to identify specific serum phosphopeptides that are determined by SELDI-MS to be relevant to targeted therapeutic response and acquired resistance in lung cancer patients. In addition, we will compare serum phosphopeptide profiles with TTF (RPPA and MBA) profiles, mRNA profiles, and TMAs and IHC analysis developed in Project 1 and in Aims 1 and 2 of this project. This comparison will identify TTF serologic molecular signatures and elucidate the biologic pathways potentially associated with patient response and tumor resistance to targeted therapeutic agents. Finally, in collaboration with Project 2, we will perform correlation analysis of these NSCLC serum phosphopeptide profile signatures with patients' clinical characteristics to predict lung cancer, cancer progression, cancer stages, and overall survival rate; to characterize serum phosphopeptide proteomic patterns and signatures in correlation to tumor recurrence, clinical response to adjuvant chemotherapeutic and targeted agents, and development of resistance; and to identify serum phosphopeptide markers as surrogate predictors of patient outcome.

Moreover, in Aim 3 we will quantify total circulating plasma DNA and methylation-specific DNA in all 300 patients with NSCLC enrolled in the Project 2 clinical trial. The circulating DNA levels will be correlated with patients' clinicopathologic characteristics. Any changes in these levels during chemotherapy and after surgery will be correlated with patient response to neoadjuvant therapy and patient outcome after surgery. The correlation between circulating methylated DNA levels and tumor DNA methylation will also be examined in a selected panel of patients.

Summary of Research Findings

During the no-cost extension (5th) year of research, we completed the goals proposed in this aim, and achieved the following milestones:

- We developed a novel ProteinChip array and mass spectrometry-based high-throughput serum phospho-peptide profiling and identification platform.
- We identified a novel serum phospho-MOR-1 peptide marker that is significantly upregulated in lung cancer patients and in smokers.
- We demonstrated the role of OMR-1 in nAChR-mediated signaling pathway in tobacco-related lung cancer pathogenesis.
- We published 2 papers (*see below*) describing our results.



The detailed progress update of the studies is as follows:

As shown in **Figure 8**, we found that lung cancer patients had higher level of phospho-ORM-1 than controls (p-Value=0.006) in smokers as well as in non-smokers. Smokers had higher level of phospho-ORM-1 than non-smokers (p-value=0.0006). Former smokers had the highest level of phospho-ORM-1 while non-smokers had the lowest (p-Value=0.0387). At a significant level of

0.05, the difference of phopho-ORM-1 between current smokers and non-smokers is significant (p-value = 0.0443), as is the difference of phopho-ORM-1 between former smokers and non-smokers (p-value = 0.0043). However, the difference of phopho-ORM-1 between current smokers and former smokers is not significant. The expression of phopho-ORM-1 is positively correlated with age (p-value=.022) and with packs per year among smokers (p-value=.002). Lung cancer patients, smoking status, and age remain significant in a multivariate model of phopho-ORM-1.

A computer-aided structural and function analysis predicted the potential association of ORM-1 to the nicotinic acetyl choline receptor (nAChRs) and to be a substrate of EGFR and other protein tyrosine kinases (PTKs). We analyzed the interaction of ORM-1 with nAChR family proteins under physiological conditions in NSCLC cell lines by a novel Duolink-in-cell-co-IP (Olink) assay (Olink Bioscience, Uppsala, Sweden). We demonstrated the direct interaction

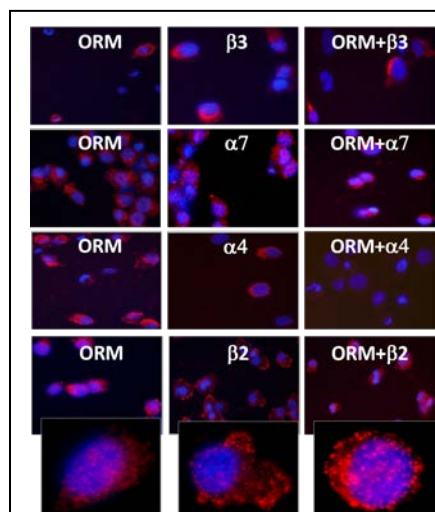


Figure 9. Interaction of ORM-1 with nAChR subunits in H1299 cells by Duolink-in-cell-co-IP assay.

of ORM-1 with nAChR subunits $\beta 2$, $\beta 3$, and $\alpha 7$ but not $\alpha 4$ (**Figure 9**), suggesting an important role of phosphor-ORM-1 in nAChR-mediated lung cancer pathogenesis in association with tobacco smoking. We also screened a panel of more than 80 PTKs for their potential phosphorylation activities on ORM-1 peptides and found several PTKs including EGFR can significantly using the predicted ORM-1 peptide as a substrate and phosphorylate the predicted tyrosine residual (**Figure 10**). We also confirmed EGFR-mediated ORM-1 peptide phosphorylation by an in vitro kinase phosphorylation assay (**Figure 11**). These findings warrant further investigation of the roles of these important PTKs, such as EGFR, in regulation of ORM-1 activity and the serum phosphor-ORM-1-mediated interaction with nAChR family proteins in lung cancer pathogenesis.

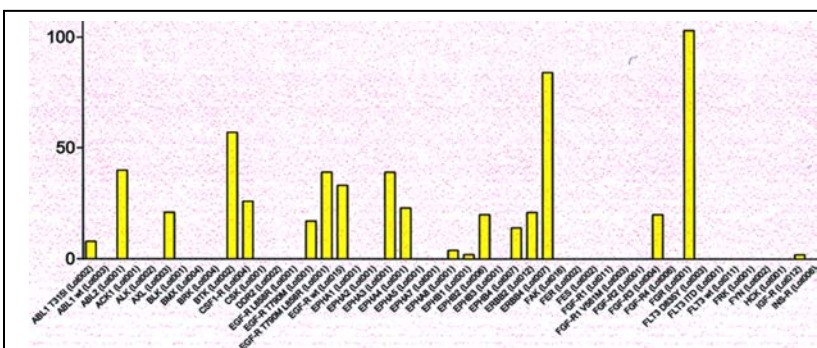


Figure 10. Phosphorylation of tyrosine on ORM-1 peptide substrate by protein tyrosine kinases by tyrosine kinase array screening.

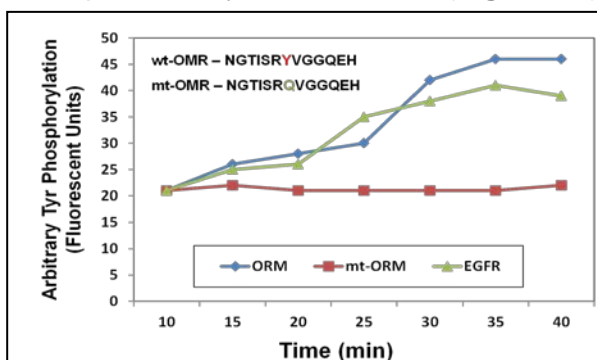


Figure 11. Tyrosine phosphorylation of ORM-1 peptide by EGFR using Delfia kinase assay.

Key Research Accomplishments

- Published 3 papers and submitted 2 manuscripts describing novel clinical relevant molecular markers (mRNA signatures, $FR\alpha$, KDR CNG, etc) associated to prognosis in surgically resected NSCLCs and MPMs.

- Developed and tested a strategy for gene (mRNA) signature validation using high-throughput Quantitative Nuclease Protection Assay (qNPA™) and Fluidigm™ microfluidic quantitative dynamic array.
- Identified a series of molecular pathways and markers, using gene profiling, as potential novel markers associated to development and chemotherapy in NSCLC (EZH2, miR-101 and ETS2) and MPM (GPRC5A).
- Developed a molecular understanding of NSCLC resistance to platin-taxane chemotherapy using tumor tissues and cell lines.
- Developed a novel ProteinChip array and mass spectrometry based high-through-put serum phosphor-peptide profiling and identification platform, and identified a novel serum phosphor-MOR-1 peptide marker that is significantly upregulated in lung cancer patients and in smokers. These data were published in 2 papers.

Conclusions

During the last year, the PROSPECT Project 3 investigators completed the goals established for all three Aims. We identified and characterized a number of novel clinical relevant molecular markers associated to the prognosis in surgically resected NSCLCs and MPMs. We developed and tested a strategy for gene (mRNA) signature validation using high-throughput Quantitative Nuclease Protection Assay (qNPA™) and Fluidigm™ microfluidic quantitative dynamic array. We developed a molecular understanding of NSCLC resistance to platin-taxane chemotherapy using neo-adjuvant-treated tumors tissues and cell lines. We identified the role of the Phospho-ORM-1 peptide as a novel nAChR-associated protein in lung cancer pathogenesis and smoking-associated carcinogenesis, and as a potential serum marker and target for lung cancer detection and treatment.

Project 4: Target Modulation Following Induction Treatment with Dasatinib in Patients with Malignant Pleural Mesothelioma (MPM) and Identification of New Therapeutic Targets/Strategies for MPM

(Leaders: Drs. Anne Tsao, Reza Mehran)

Hypothesis:

We hypothesize that dasatinib, a broad spectrum ATP-competitive inhibitor for oncogenic tyrosine kinases (BCR-ABL, SRC, c-Kit, PDGFR, and ephrin receptor kinases), may be a new therapeutic agent in malignant pleural mesothelioma (MPM). We also believe that conducting therapeutic target-focused (TTF) molecular and gene profiling (Affymetrix arrays) will lead to development of other novel therapies for MPM.

Specific Aims:

Aim 1: Conduct a phase I clinical trial with the primary endpoint of biomarker modulation using dasatinib as induction therapy in patients with resectable MPM.

Trial design: Untreated MPM patients undergo extended surgical staging (ESS) with multiple biopsies to account for tumor heterogeneity. If deemed a surgical candidate for either P/D or EPP, patients receive 4 weeks of oral dasatinib (70 mg BID) followed by pleurectomy/decortication (P/D) or extrapleural pneumonectomy (EPP). If a radiographic response is seen, an additional 2 years of dasatinib maintenance after adjuvant radiotherapy and chemotherapy is given. Serum/blood/platelets/pleural effusion specimens are collected for exploratory analysis of peripheral surrogate biomarkers. The primary endpoint is biomarker modulation of Src Tyr419 immunohistochemistry (IHC) in tumor tissue. Secondary endpoints include response, survival, safety/toxicity, and biomarker modulation.

- 1a. Determine the effects of dasatinib induction therapy on selected tumor biomarkers (activated Src, PDGFR, VEGFR) pre- and post-induction therapy.
- 1b. Determine the modulatory effects of dasatinib on selected biomarkers of survival and apoptosis (PI3K/AKT, bcl-xL, caspases), proliferation (IGFR, Ki-67), angiogenesis (IL-8, bFGF, TNF- α), epithelial-mesenchymal transition (TNF- β , E-cadherin, c-Kit/Slug) and invasion/migration (Ephrin, MMP) in tumor specimens pre- and post- induction therapy.
- 1c. Determine the effects of induction dasatinib therapy on tumor mean vessel density, cell apoptosis, and the proliferation index.
- 1d. Determine the modulatory effects of dasatinib on serum, platelet, and pleural effusion markers of survival (PI3K/AKT, bcl-xL, caspases), proliferation (IGFR, Src), angiogenesis (soluble VEGFR, VEGF, PDGF, IL-8, bFGF, TNF- α), and invasion/migration (Ephrin, MMP).
- 1e. Determine the drug concentration of dasatinib in tumor and serum.
- 1f. Assess the effects of dasatinib and cytoreductive surgery on the serum mesothelin-related peptide (SMRP) level.
- 1g. Assess the safety and toxicity profile of induction dasatinib in patients with resectable MPM.

Aim 2: Conduct radiographic correlates of tumor response and clinical outcome with positron-emission technology-computer tomography (PET-CT).

Aim 3: Explore and develop new therapeutic targets and treatment strategies for MPM in tumor specimens collected from Specific Aim1 and in MPM cell lines.

- 3a. Determine key signaling pathways involved in tumor resistance or sensitivity to dasatinib using therapeutic target-focused (TTF) molecular and global gene expression profiling on MPM tumor specimens pre- and post- induction dasatinib therapy.
- 3b. Determine the sensitivity of a panel of MPM cell lines to targeted agents tested in Project 1 via TTF profiling and DATs (drug and therapeutic target siRNA).

Summary of Research Findings

Preliminary Results. Over 60 patients were screened for the trial (4/08 – 5/12); 24 patients were successfully enrolled and completed ESS, neoadjuvant dasatinib, and P/D or EPP. Of the 24 patients (20 men; 4 women), 22 had epithelioid and 2 had biphasic histology. The neoadjuvant dasatinib treatment's main side effects were grade 1-2 anemia, nausea, vomiting, anorexia, fatigue, and anxiety. Grade 3 toxicities included fluid retention, infection (pneumonia), and hypoxia. There were no grade 4-5 toxicities. Post-surgical grade 3 toxicity included anemia, arrhythmia, HTN, and pleural effusion; there was 1 grade 4 episode of hyperglycemia. **To date, neoadjuvant dasatinib did not add significant toxicity to MPM surgical resection.**

After 4 weeks of neoadjuvant oral dasatinib therapy, in the initial analysis of IHC Src Tyr⁴¹⁹ in 13 patients (see **Figure 1**), higher baseline levels of p-Src Tyr⁴¹⁹ predicted for an improved TTP with dasatinib therapy ($p=0.008$). Also, patients who had significant modulation of p-Src Tyr⁴¹⁹ after dasatinib therapy had improved TTP ($p=0.005$) (see **Figure 2**).

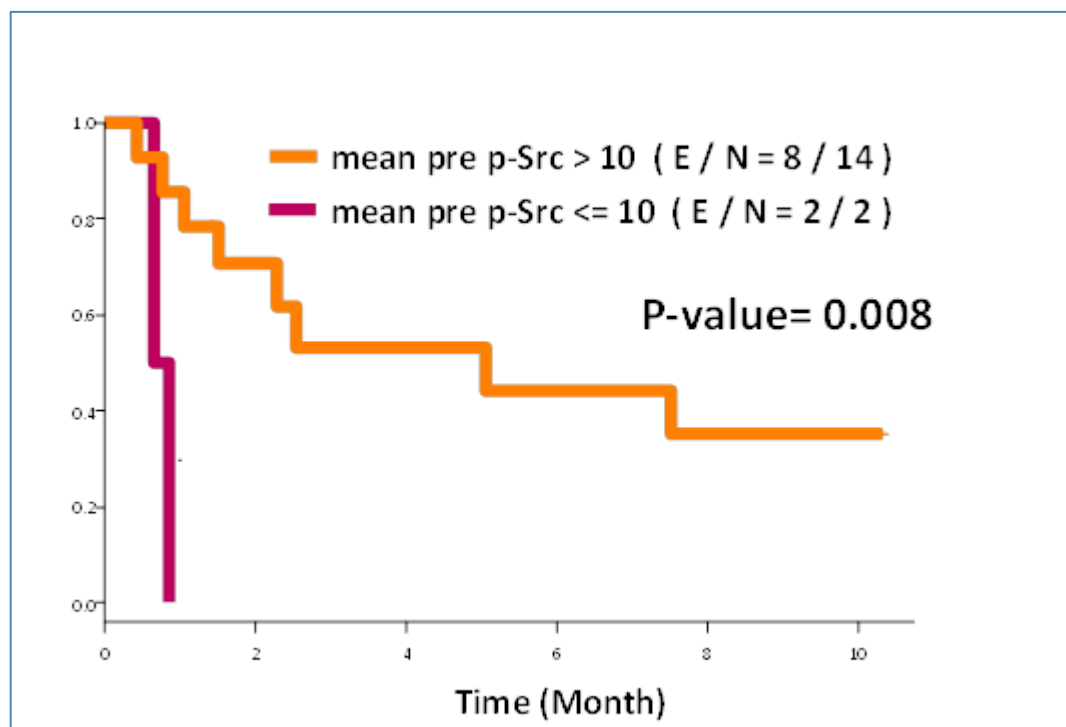


Figure 1: Baseline levels of IHC p-Src Tyr⁴¹⁹ by time to progression

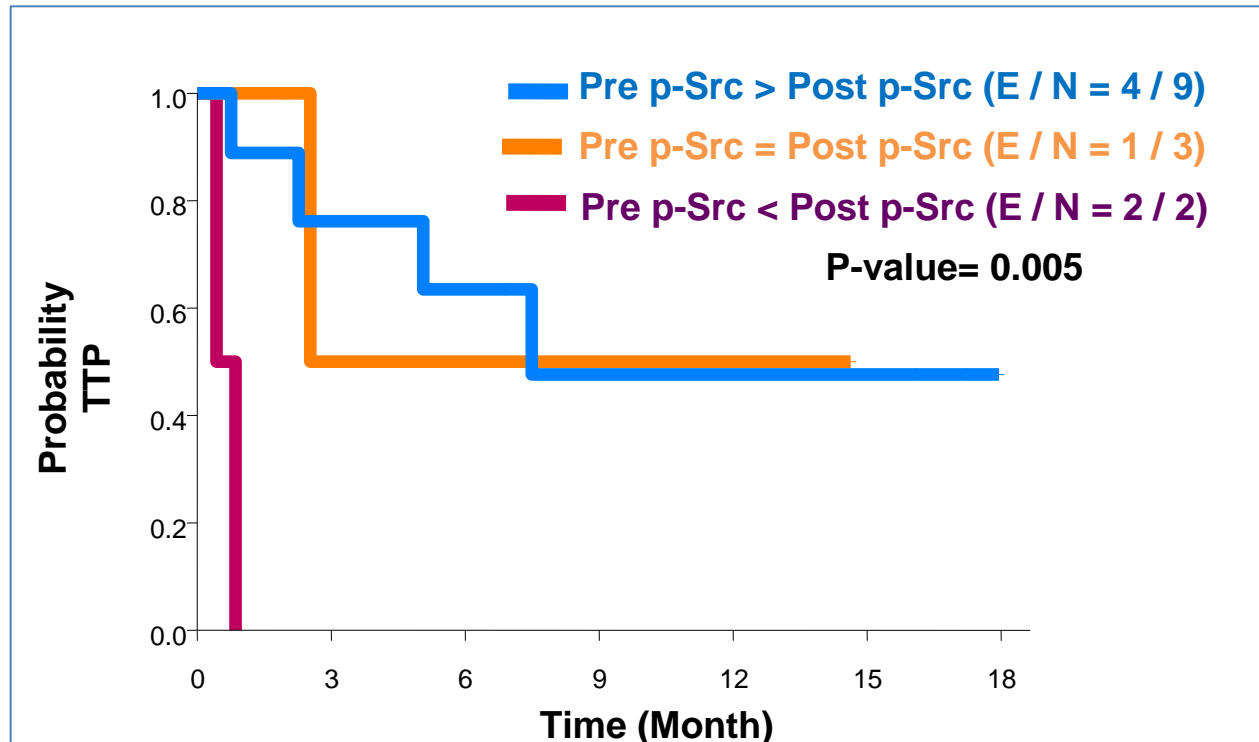
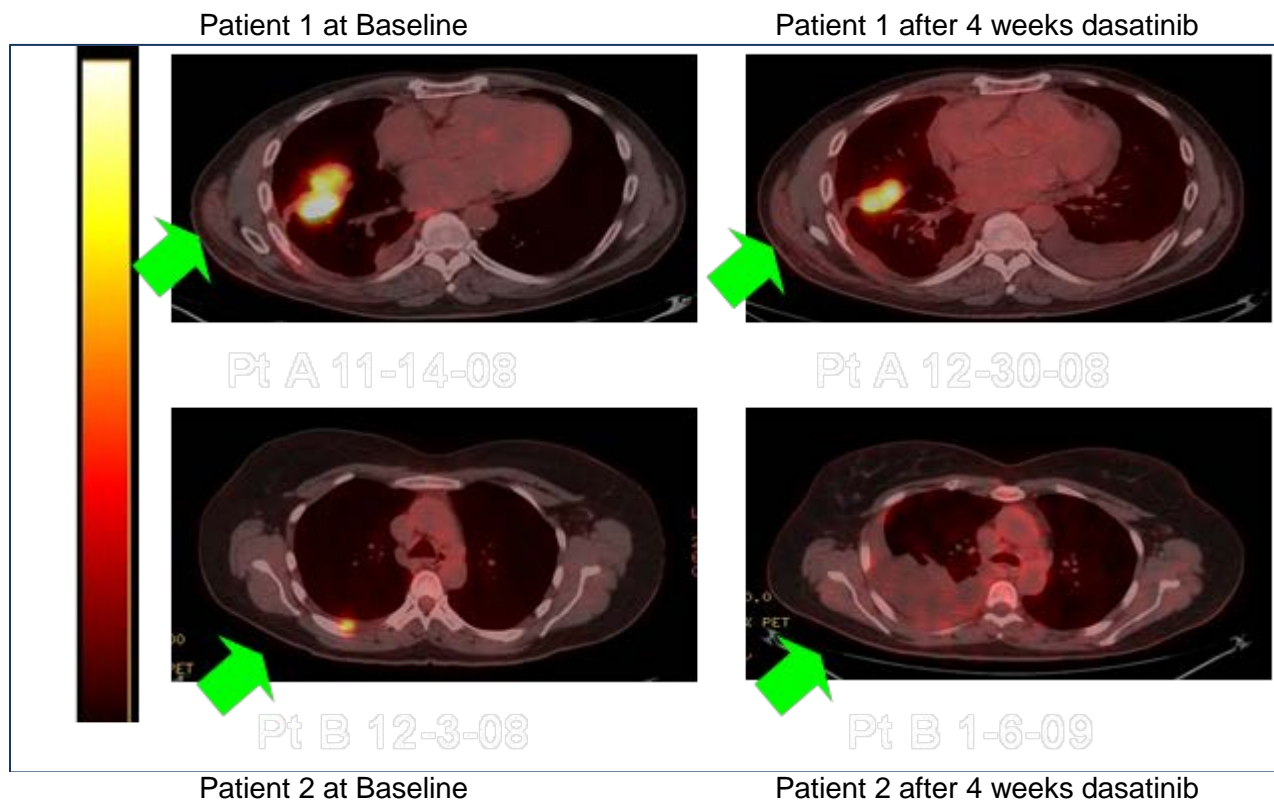


Figure 2: Modulation of p-Src Tyr⁴¹⁹ calculated from before (pre-) and after (post-) neoadjuvant dasatinib therapy.



Key Research Accomplishments

We have demonstrated the following:

- There is a subpopulation of MPM patients that may derive clinical benefit from oral dasatinib therapy.
- MPM is a very heterogeneous tumor. Molecular profiling will be necessary to ultimately optimize targeted therapy in this disease.
- There is preliminary evidence that higher baseline levels of p-Src Tyr⁴¹⁹ are predictive for improved PFS with dasatinib.
- Initial evidence suggests that modulation of p-SrcTyr⁴¹⁹ is also a reasonable pharmacodynamic marker for dasatinib treatment.
- The approach to this novel clinical was proven feasible and has the potential to advance the field of MPM in personalized medicine.

Future plans include correlating outcome and tumor p-Src Tyr⁴¹⁹ to peripheral surrogate markers in blood/serum/platelets and pleural effusion and to analyze pathways of resistance in MPM tumors.

Conclusions

There is preliminary evidence that a subgroup of MPM patients gain clinical benefit from dasatinib therapy and that baseline p-Src Tyr⁴¹⁹ levels in MPM tumor tissue may be predictive of TTP. This is the first targeted therapy neoadjuvant trial to potentially identify a predictive biomarker in MPM. We have just completed accrual to the trial and are awaiting the final translational research studies. We will plan on completing these IHC and FISH studies (outside of the scope of this application) by September of this year and having a draft manuscript by the end of this year. Future plans include correlating outcome and tumor p-Src Tyr⁴¹⁹ to peripheral surrogate markers in blood/serum/platelets and pleural effusion and to analyze pathways of resistance in MPM tumors.

Project 5: Development of a Novel Multi-Biomarker System Using Quantum Dot Technology for Assessments of Prognosis of NSCLC and Prediction of Outcome of EGFR-Targeted Therapy

(Leader: Dr. Zhuo (Georgia) Chen; Co-Leaders: Drs. Fadlo Khuri, Dong Shin, Ruth O'Regan, Shi-Yong Sun)

Quantum dots (QDs) provide sharper fluorescent signals than organic dyes and can detect multi-biomarkers simultaneously in the same material, allowing quantification and correlation of molecular signature with cellular response to targeted therapies.

Hypothesis:

A multi-biomarker system using quantum dot (QD) technology will enhance accuracy in assessment of prognosis of non-small cell lung cancer (NSCLC) and prediction of outcome of epidermal growth factor receptor (EGFR)-targeted therapy.

Specific Aims:

Specific Aim 1: Development of QD-Abs and imaging systems for detection and quantification of multi-biomarkers (MBM) using lung cancer cell lines.

Summary of Research Findings

This aim was completed as reported in the previous annual report.

Specific Aim 2: Verification of QD-Abs for detection and quantification of MBM by comparison with conventional IHC using paraffin-embedded tissues and evaluation of their prognostic value in NSCLC.

Summary of Research Findings

Most of studies in this aim were completed as reported in the previous annual report. Evaluation of their prognostic value in NSCLC will be continued outside of the scope of this application.

Specific Aim 3: Correlation of the MBM detected by QD-Abs with outcomes of chemotherapies and EGFR- targeted therapy using resectable NSCLC tissues.

Summary of Research Findings

Similar to the studies in Specific Aim 2, correlation of the MBM with outcome to chemotherapies is ongoing. The study of correlation of the MBM with EGFR-targeted therapy will be initiated when sufficient tissue samples from patients treated with EGFR-targeting therapy are acquired.

Marker Name	Cell Lines		
Amelogenin	X,Y	X,Y	X,Y
CSF1PO	12	12	12
D13S317	12	12	12
D16S539	13	13	13
D5S818	11	11	11
D7S820	9	9	9
TH01	7	7	7
TPOX	9,11	9,11	9,11
vWA	18	18	18

Table 1. Satellite tandem repeat (STR) analysis confirmed the same genomic background of 801BL as 801C and 801D cell lines.

In the last budget year, we performed two additional studies.

(1) Validation of the lung metastasis model. As reported last year, we established a lung metastasis mouse model and completed proteomic studies and completed further validations

for this model. First, we confirmed that the highly metastatic derivative (801BL) has the same genetic origin with the poor metastatic parental cell line (801D) and non-metastatic cell line (801C) from the same patient (**Table 1**). We also compared the invasion capability of 801BL with 801C and found that the invasive capability of the highly metastatic 801BL cells increased by 3.47 ± 0.44 fold as compared to the non-metastatic counterpart 801C cells ($p < 0.001$) (**Figure 1**).

Proteins from each of the altered biological pathways found in the proteomics study (see previous annual report) were confirmed by immunoblotting analyses (**Figure 2**). Altered proteins in the highly metastatic cell line 801BL include LDHA, Ezrin, RAB-2A, Vinculin, and TGM2, which deserve further study.

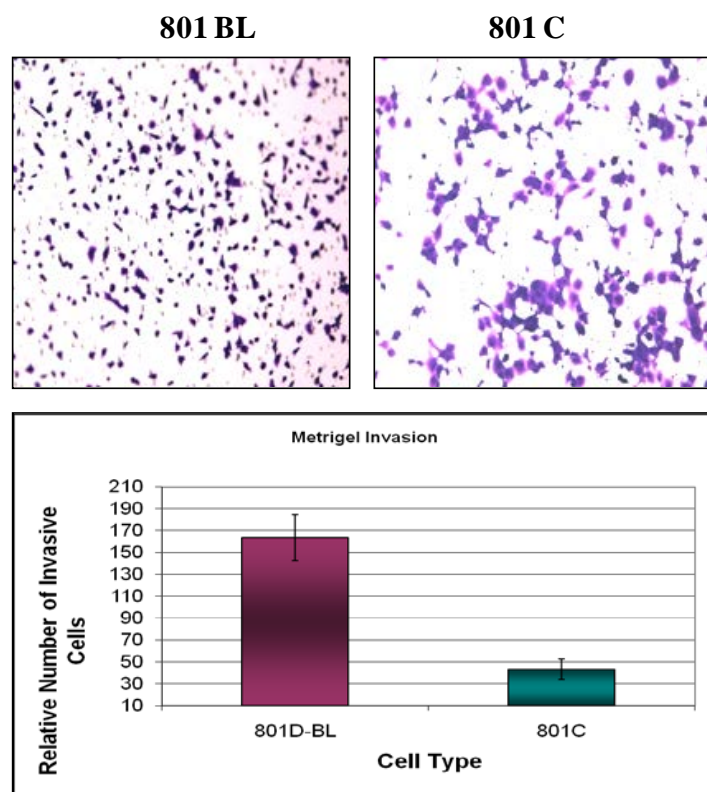


Fig. 1. 801BL cells are more invasive than 801C cells

801C and 801BL cells were seeded in the number of 3×10^4 per chamber, respectively. Matrigel invasion assay was performed for 36 h. The invasive cells were counted as a sum of 10 high power fields ($\times 200$) in the central membrane under the microscope. The invasive capability of 801BL cells increased by 3.47 ± 0.44 fold comparing to the non-metastatic counterpart 801C cells ($p < 0.001$). Matrigel invasion assay for each cell line was repeated 3 times.

Microsatellite Marker Analysis for Human Cell Lines. To confirm the cell originality, a PCR-based microsatellite marker analysis was performed in the Radil Lab in Missouri University. **Table 1** shows that the satellite tandem repeat (STR) analysis confirmed the same genomic background of the newly established metastatic cell line 801BL as the non-metastatic counterpart 801C and low-metastatic counterpart 801D cell lines.

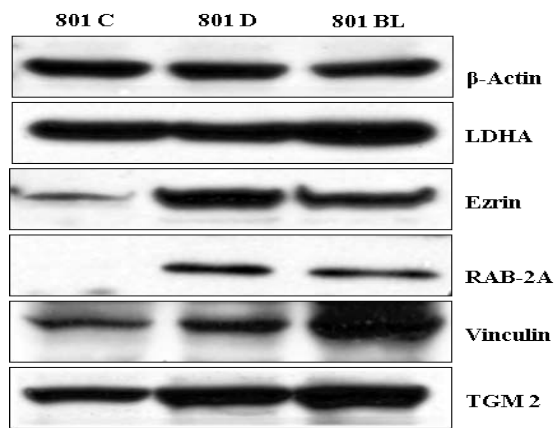


Fig. 2. Proteomics analysis findings were confirmed by Western blot assay. Several proteins from each of altered biological pathways found in proteomics study were chosen for immunoblotting analyses. Alterations of proteins LDHA, Ezrin, RAB-2A, Vinculin, and TGM2 were confirmed by Western blot study.

(2) Study of expression of ribonucleotide reductase subunit M2 and its correlation with Bcl2 in non-small cell lung cancer using quantum dot (QD)-based immunofluorescence IHF. Ribonucleotide reductase subunit M2 (RRM2) is an essential regulator of DNA replication that plays an active role in tumor progression. Using QD-IHF, we revealed the co-localization of Bcl-2 and RRM2 and a significantly positive correlation between their expressions in tumor tissues from NSCLC patients (N = 50, **Figure 3**).

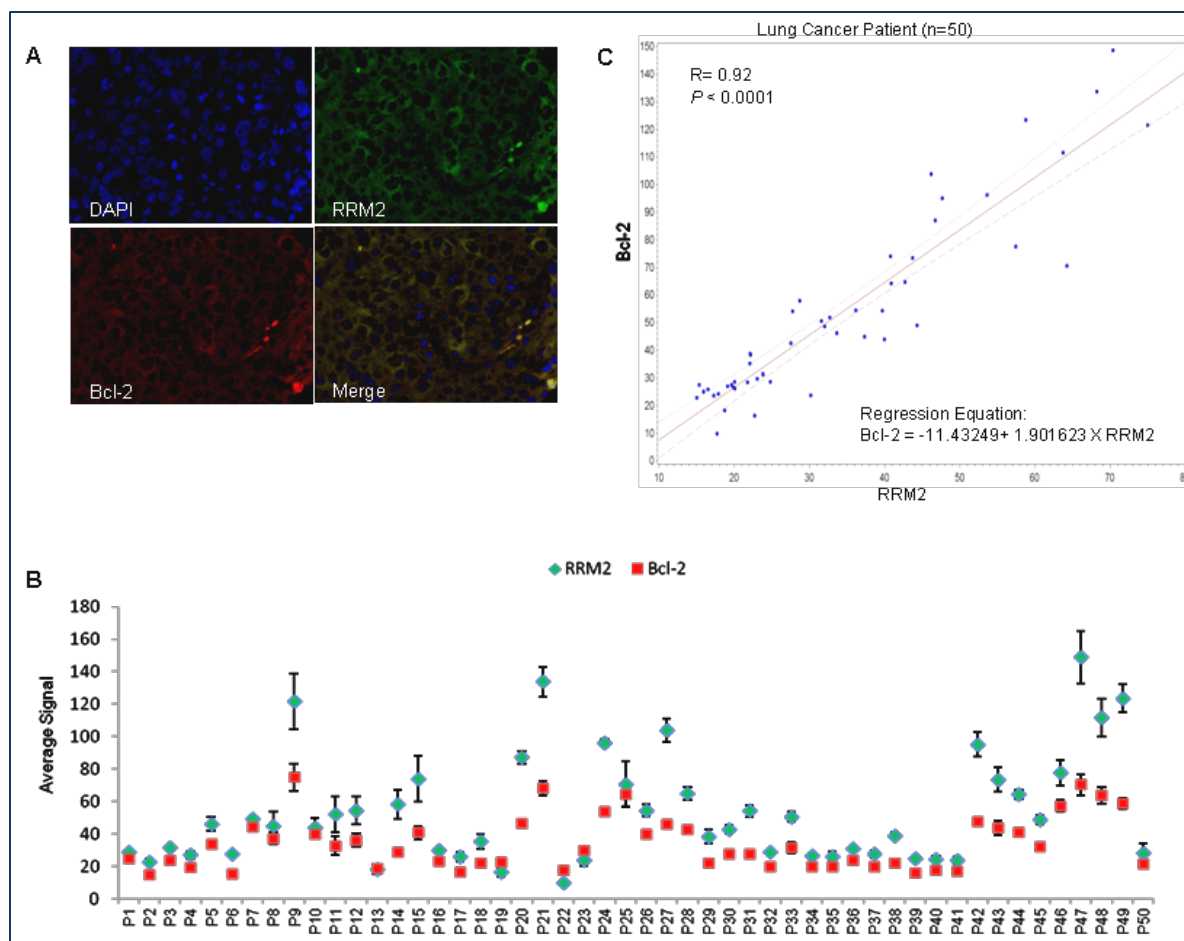


Fig. 3. RRM2 and Bcl-2 proteins were co-localized and their expression was positively correlated in tumor tissues from HNSCC and NSCLC patients. (A) Staining of RRM2 and Bcl-2 in paraffin-embedded formalin-fixed NSCLC tissue sections using primary antibodies with QD-secondary antibody conjugates. A representative QD-image is shown (400X magnification). (B) Quantification of QD-signals. Average signals of RRM2 and Bcl-2 expression in NSCLC patient sample were plotted. (C) Spearman's correlation coefficient was estimated between Bcl-2 and RRM2 in NSCLC tissues. A linear regression was used to plot their relationship with 95% confidence interval bound.

A mechanism study using NSCLC and head and neck cancer cell lines has showed that RRM2 regulates Bcl-2 at the post-translational level (data not shown). Our data provide strong support to this observation in actual patients' samples.

Key Research Accomplishments

- Our proteomics study showed a different protein profile between the newly established metastatic cell line and its non-metastatic counterpart. Differences in the invasive capability and differential expression of several metastasis-related proteins in these two cell lines have been confirmed.
- The genetic origin of the highly metastatic and non-metastatic cell lines has been confirmed. Since the two cell lines have the same genetic background, they can provide a powerful tool in understanding the mechanism of lung metastasis and good model for development of new therapeutic agents for treatment of lung metastasis.

- Our study presents a positive correlation between RRM2 and Bcl-2 in tumor tissues from NSCLC patients. This novel finding adds to emerging knowledge of the regulatory effects of RRM2 on apoptosis induction by modulation of Bcl-2.

Conclusions

In addition to the preparation of publications summarizing the studies on CXCR4/E-cadherin and EGFR/ β -catenin, we further characterized the new lung metastasis model. This model is currently being used by our group and our colleagues in a study of anti-lung-cancer agents and will provide a unique tool for further understanding lung metastasis and its microenvironment. In addition, QD-based technology developed through this grant support has been used in several collaborative projects. As one example, we identified a significantly positive correlation between RRM2 and Bcl-2 expression in tumor tissues from NSCLC patients. This imaging technique allows quantification of multiple biomarkers at the per-cell level, providing evidence to support the underlying biological significance of co-localized proteins.

Pathology Core

(Director: Dr. Ignacio Wistuba)

The Pathology Core is an essential component of the PROSPECT program, and plays an important role by collecting, processing and distributing tissue and serum specimens obtained from clinical trials for non-small cell lung carcinoma (NSCLC) (Project 2) and malignant pleural mesothelioma (MPM; Project 4) for molecular profiles and biomarker analysis.

Our objectives are as follows:

1. Develop and maintain a repository of tissue and serum specimens from patients with NSCLC and MPM.
2. Process NSCLC cell lines and tissue specimens for histopathologic and molecular analyses.
3. Perform and evaluate immunohistochemical (IHC) analysis in human tumor tissue specimens and mouse xenograft tissues.

Objective 1. Develop and maintain repository of tissue and serum specimens from patients with NSCLC and malignant pleural mesothelioma (MPM).

Summary of Research Findings

This objective was achieved during the first 4 years of the grant, and reported last year. During the no-cost extension (5th) year, we have maintained the samples in the MD Anderson Thoracic Tissue Bank, and completed the collection of clinico-pathological data of the tumor specimens in collaboration with Project 2 (D. Stewart).

In addition, during the last year, we completed the collection of the MPM tumor tissue specimens of the dasatinib neo-adjuvant clinical trial in collaboration with Project 4 (A. Tsao). In summary, the Pathology Core has collected, banked, and characterized MPM tumor tissue from 40 patients enrolled in the dasatinib clinical trial who underwent to video-assisted thoracoscopy (VAT) and extrapleural pneumonectomy (EPP). A total of 395 (211 baseline [VAT] and 184 at surgery [EPP]) fresh frozen and formalin-fixed tumor tissue specimens from 40 patients have been obtained, processed, and histologically characterized by the Pathology Core.

Objective 2. Process NSCLC cell lines and tissue specimens for histopathological and molecular analyses.

Summary of Research Findings

This objective was achieved during the first 4 years of the grant, and reported last year. During the no-cost extension (5th) year, we have maintained the NSCLC cell line repository in the MD Anderson Thoracic Tissue Bank. We also have participated in the molecular profiling data analysis of tumor and cell lines specimens, and in the preparation of manuscripts and abstract to report the research findings (see below).

Objective 3. Perform and evaluate immunohistochemical (IHC) analysis in human tumor tissue specimens and mouse xenograft tumor specimens.

Summary of Research Findings

Most of this objective was achieved during the first 4 years of the grant, and reported last year. During the no-cost extension (5th) year, we have maintained the NSCLC and MPM tissue

microarray (TMA) specimens developed in the previous years, which are available for future research projects. Additionally, we completed the examination of the expression of total Src and p-Src (Tyr 416) in the tissue samples obtained from patients enrolled in the dasatinib clinical trial for Project 4 (A. Tsao). During the non-cost extension (5th) year, we have participated in the data analysis and publication of 6 papers in peer-reviewed journals, the submission of 4 manuscripts, and in the presentation of 8 abstracts in scientific meetings.

Key Research Accomplishments

- Maintained the prospectively collected frozen tissue specimens from 565 NSCLC and 43 MPM cases, with annotated clinical and pathological data.
- Maintained a NSCLC and MPM cell line repository for distribution for molecular profiling in collaboration with PROSPECT Projects 1 and 4.
- Distributed nucleic acids (DNA and RNA) and tissue for protein analyses from large series of NSCLC and MPM tumor specimens with annotated clinico-pathological information for molecular profiling.
- Collected, processed, and analyzed nearly 400 MPM tumor tissue specimens from patients enrolled in the neo-adjuvant dasatinib clinical trial in collaboration with Project 4.
- Contributed to the publication of 6 papers and submission of 4 manuscripts in peer-reviewed journals, and 8 abstracts presentations in scientific meetings.

Conclusions

During the last year, the PROSPECT Pathology Core completed the goals established for all three Objectives. The Pathology Core has played an important role in the processing of NSCLC and MPM tissue and cell line specimens for comprehensive molecular profiling, and in the characterization of tissue specimens on the expression of protein expression by immunohistochemistry. The Pathology Core contributed to the publication of 6 papers and submission of 4 manuscripts in peer-reviewed journals, and 8 abstracts presentations in scientific meetings.

Biostatistics/Bioinformatics Core

(Director: Dr. J. Jack Lee; Co-Director: Kevin Coombes)

In close collaboration with the Pathology Core and each of the five main projects, the Biostatistics and Data Management Core (BDMC) for the Department of Defense (DoD) PROSPECT lung cancer research program is a comprehensive, multi-lateral resource for designing clinical and basic science experiments; developing and applying innovative statistical methodology, data acquisition and management, and statistical analysis; and publishing translational research generated by this research proposal. We deliver planned and tailored statistical analyses for rapid communication of project results among project investigators, and by collaborating with all project investigators to facilitate the timely publication of scientific results.

The main objectives of the Biostatistics and Data Management Core are to:

1. Provide the statistical design, sample size, and power calculations for each project.
2. Develop a secure, internet-driven, Web-based database application to integrate data generated by the five proposed projects and the Pathology Core of the PROSPECT research project.
3. Develop a comprehensive, Web-based database management system for tissue specimen tracking and distribution and for a central repository of all biomarker data.
4. Provide all statistical data analyses, including descriptive analysis, hypothesis testing, estimation, and modeling of prospectively generated data.
5. Provide prospective collection, entry, quality control, and integration of data for the basic science, pre-clinical, and clinical studies in the PROSPECT grant.
6. Provide study monitoring and conduct of the neoadjuvant clinical trial that ensures patient safety by timely reporting of toxicity and interim analysis results to various institutional review boards (IRBs), the UTMACC data monitoring committee, the DoD, and other regulatory agencies.
7. Generate statistical reports for all projects.
8. Collaborate with all project investigators and assist them in publishing scientific results.
9. Develop and adapt innovative statistical and genomic methods pertinent to biomarker-integrated translational lung cancer studies.

Summary of Research Findings

In the fifth and final funding year, the BDMC continued to work with all project investigators in providing biostatistics and data management support. The accomplishments are summarized below.

(A) Biostatistics and Bioinformatics

We have continued to work with clinical investigators in providing biostatistical support for the development and revision of PROSPECT protocols. We provide statistical report in our monthly project meetings to update the accrual, randomization, demographic data, etc.

We have performed (and continue to perform) analyses of PROSPECT data, including analyses of immunohistochemically stained tissue microarray data looking at markers of prognosis in lung cancer samples. Univariate analysis identified a number of markers that appear to be related either to important clinical covariates or and/to clinically relevant outcomes (overall survival, disease-free survival, or recurrence-free survival). We have also performed multivariate analyses to identify signatures of outcomes. Several abstracts were presented at the AACR and ASCO annual meetings as well as a number of manuscripts and papers written.

In the bioinformatics area, we have done number of analyses on the PROSPECT project:

- (1) miRNA data. We processed 96 mesothelioma miRNA arrays and performed the analyses on identifying differentially expressed miRNA between histology groups, between treatment groups; we also performed survival analysis. We have generated 21 reports on this part of analysis. Currently, we are preparing a publication.
- (2) RPPA data. We processed 215 samples with 197 protein measurements and performed a number of analyses including identifying differentially expressed proteins between *KRAS* mutation and wild-type as well as survival analyses. We produced 24 reports on this part of the analysis.

Initial analysis of copy number data, gene expression array data, and miRNA data on NSCLC samples from PROSPECT has been completed. The bioinformatics and biostatistics core personnel meet weekly with PROSPECT researchers to prioritize analyses.

(B) Data Management

PROSPECT Database Development

We have conducted elaborative database queries and management to define the DoD lung cancer data sets. The final results with data set (N) are: Vanguard (N=45), ReVitalization (N=370), PROSPECT_Retrospective (N=272), PROSPECT_Pro prospective (N=462). Among them, 87 were included in the TMA1 data set and 556 were in the TMA2 data set. These data were cleaned and were prepared for data analysis within the various projects.

In collaboration with the University of Texas Lung SPORE, we continue to work on developing semantic database models for the kinds of assay data being generated by both PROSPECT projects and the SPORE projects.

We have continued with the database maintenance, training and support as follows:

- Provided data integrity checking and data correction.
- Performed database server maintenance and data backup periodically.
- Created an audit table for the collaborative VITAL database.
- Cross-checked data with existing excel files from other sources and held discussion meetings on discrepancies, verified the new information, and merged the data from other sources to the database.
- Cleaned up and deleted duplicate accession numbers.

Key Research Accomplishments

We have supported the research team in the study design, data analysis and publications.

Conclusions

In collaboration with clinical investigators, research nurses, pathologists, and basic scientists, the Biostatistics and Data Management Core has continued to deliver the biostatistics, bioinformatics, and data management support as proposed.

KEY RESEARCH ACCOMPLISHMENTS

PROJECT 1

- Identified fundamental differences distinguishing SCLC and NSCLC by RPPA profiling, including the possible therapeutic target PARP1.
- Established a robust, cross-platform EMT signature capable of classifying NSCLC cell lines and patient tumors as epithelial-like or mesenchymal-like. The mesenchymal phenotype is a negative predictor of response to erlotinib and PI3/Akt pathway inhibitors. We also identified Axl as a novel marker of EMT and potential therapeutic target for NSCLC.
- Determined that LKB1 and KRAS mutations are associated with resistance to PI3K/Akt inhibitors. Combination of PI3K+MEK inhibitors largely overcomes resistance of mutated lines to single-agent PI3K inhibition. RPPA analysis revealed that IGF1R is upregulated in LKB1 mutated cell lines.
- In collaboration with Dr. Powis, demonstrated that not all KRAS mutants signal similarly. Patients whose tumors had KRASG12C and KRASG12V have worse progression-free survival compared with patients whose tumors had other KRAS mutations or the wild type KRAS protein.

PROJECT 2

- Obtained data on relapse patterns, overall survival and cause-specific survival in 985 patients with resected NSCLC.
- Derived detailed molecular profiles on tumors of 272 of these patients, and tissue microarray data on another 315 patients.
- Have banked high quality FFPE and fresh frozen tumor samples available for assessment from another 401 patients.
- Demonstrated that tumor shrinkage after platinum-based neoadjuvant chemotherapy is proportional to tumor platinum concentration and that uptake of platinum into tumor may be down-regulated after initial tumor exposure to drug.
- Demonstrated that overall survival and progression-free survival after neoadjuvant chemotherapy is inversely proportional to percentage of tumor cells that remain viable after neoadjuvant therapy.

PROJECT 3

- Published 3 papers and submitted 2 manuscripts describing novel clinical relevant molecular markers (mRNA signatures, FR α , KDR CNG, etc.) associated to prognosis in surgically resected NSCLCs and MPMs.
- Developed and tested a strategy for gene (mRNA) signature validation using high-throughput Quantitative Nuclease Protection Assay (qNPATM) and FluidigmTM microfluidic quantitative dynamic array.
- Identified a series of molecular pathways and markers, using gene profiling, as potential novel markers associated to development and chemotherapy in NSCLC (EZH2, miR-101 and ETS2) and MPM (GPRC5A).
- Developed a molecular understanding of NSCLC resistance to platin-taxane chemotherapy using tumor tissues and cell lines.

- Developed a novel ProteinChip array and mass spectrometry based high-through-put serum phosphor-peptide profiling and identification platform, and identified a novel serum phosphor-MOR-1 peptide marker that is significantly upregulated in lung cancer patients and in smokers. These data were published in 2 papers.

PROJECT 4

- We demonstrated that here is a subpopulation of MPM patients that may derive clinical benefit from oral dasatinib therapy.
- MPM is a very heterogeneous tumor. Molecular profiling will be necessary to ultimately optimize targeted therapy in this disease.
- There is preliminary evidence that higher baseline levels of p-Src Tyr⁴¹⁹ are predictive for improved PFS with dasatinib.
- Initial evidence suggests that modulation of p-SrcTyr⁴¹⁹ is also a reasonable pharmacodynamic marker for dasatinib treatment.
- The approach for this novel clinical trial was proven feasible and has the potential to advance the field of MPM in personalized medicine.

PROJECT 5

- Our proteomics study showed a different protein profile between the newly established metastatic cell line and its non-metastatic counterpart. Difference in the invasive capability and differential expression of several metastasis-related proteins in these two cell lines has been confirmed.
- The genetic origin of the highly metastatic and non-metastatic cell lines has been confirmed. Since the two cell lines have the same genetic background, they can provide a powerful tool in understanding the mechanism of lung metastasis and good model for development of new therapeutic agents for treatment of lung metastasis.
- Our study presents a positive correlation between RRM2 and Bcl-2 in tumor tissues from NSCLC patients. This novel finding adds to emerging knowledge of the regulatory effects of RRM2 on apoptosis induction by modulation of Bcl-2.

PATHOLOGY CORE

- Maintained the prospectively collected frozen tissue specimens from 565 NSCLC and 43 MPM cases, with annotated clinical and pathological data.
- Maintained a NSCLC and MPM cell line repository for distribution for molecular profiling in collaboration with PROSPECT Projects 1 and 4.
- Distributed nucleic acids (DNA and RNA) and tissue for protein analyses from large series of NSCLC and MPM tumor specimens with annotated clinico-pathological information for molecular profiling.
- Collected, processed, and analyzed nearly 400 MPM tumor tissue specimens from patients enrolled in the neo-adjuvant dasatinib clinical trial in collaboration with Project 4.
- Contributed to the publication of 6 papers and submission of 4 manuscripts in peer-reviewed journals, and 8 abstracts presentations in scientific meetings.

BIostatistics and Data Management Core

We have supported the research team in the study design, data analysis and publications

PERSONNEL

A list of all personnel that have received funding from this research grant is included in **Appendix A**.

REPORTABLE OUTCOMES

Publications (Attached in Appendix B)

1. He Y, Correa AM, Raso MG, Hofstetter WL, Fang B, Behrens C, Roth JA, Zhou Y, Yu L, Wistuba II, Swisher SG, Pataer A. The role of PKR/eIF2 α signaling pathway in prognosis of non-small cell lung cancer. PLoS One. 2011; 6(11):e24855. Epub 2011 Nov 10. PubMed PMID: 22102852; PubMed Central PMCID: PMC3213082.
2. Jayachandran G, Roth JA, Ji L. Analysis of protein-protein interaction using proteinchip array-based SELDI-TOF mass spectrometry. Methods Mol Biol. 2012; 818:217-26. PubMed PMID: 22083826; PubMed Central PMCID: PMC3369541.
3. Ji L, Jayachandran G, Roth JA. High throughput profiling of serum phosphoproteins/peptides using the SELDI-TOF-MS platform. Methods Mol Biol. 2012; 818:199-216. PubMed PMID: 22083825; PubMed Central PMCID: PMC3369544.
4. Li Y, Fan S, Koo J, Yue P, Chen ZG, Owonikoko TK, Ramalingam SS, Khuri FR, Sun SY. Elevated expression of eukaryotic translation initiation factor 4E is associated with proliferation, invasion and acquired resistance to erlotinib in lung cancer. Cancer Biol Ther. 2012 Mar; 13(5):272-80. Epub 2012 Mar 1. PubMed PMID: 22236867.
5. Lockwood WW, Wilson IM, Coe BP, Chari R, Pikor LA, Thu KL, Solis LM, Nunez MI, Behrens C, Yee J, English J, Murray N, Tsao MS, Minna JD, Gazdar AF, Wistuba II, MacAulay CE, Lam S, Lam WL. Divergent genomic and epigenomic landscapes of lung cancer subtypes underscore the selection of different oncogenic pathways during tumor development. PLoS One. 2012; 7(5):e37775. Epub 2012 May 21. PubMed PMID: 22629454; PubMed Central PMCID: PMC3357406.
6. Nunez MI, Behrens C, Woods DM, Lin H, Suraokar M, Kadara H, Hofstetter W, Kalhor N, Lee JJ, Franklin W, Stewart DJ, Wistuba II. High Expression of Folate Receptor Alpha in Lung Cancer Correlates with Adenocarcinoma Histology and Mutation. J Thorac Oncol. 2012 May; 7(5):833-840. PubMed PMID: 22729036; PubMed Central PMCID: PMC3383601.
7. Pataer A, Kalhor N, Correa AM, Raso MG, Erasmus JJ, Kim ES, Behrens C, Lee JJ, Roth JA, Stewart DJ, Vaporciyan AA, Wistuba II, Swisher SG; The University of Texas M. D. Anderson Lung Cancer Collaborative Research Group. Histopathologic Response Criteria Predict Survival of Patients with Resected Lung Cancer After Neoadjuvant Chemotherapy. J Thorac Oncol. 2012 Apr 4. [Epub ahead of print] PubMed PMID: 22481232
8. Solis LM, Behrens C, Raso MG, Lin HY, Kadara H, Yuan P, Galindo H, Tang X, Lee JJ, Kalhor N, Wistuba II, Moran CA. Histologic patterns and molecular characteristics of lung adenocarcinoma associated with clinical outcome. Cancer. 2012 Jun 1;118(11):2889-99. doi: 10.1002/cncr.26584. Epub 2011 Oct 21. PubMed PMID: 22020674; PubMed Central PMCID: PMC3369269.

9. Tsuta K, Raso MG, Kalhor N, Liu DD, Wistuba II, Moran CA. Histologic features of low- and intermediate-grade neuroendocrine carcinoma (typical and atypical carcinoid tumors) of the lung. *Lung Cancer*. 2011 Jan; 71(1):34-41. Epub 2010 May 11. PubMed PMID: 20462655.
10. Xie Y, Xiao G, Coombes KR, Behrens C, Solis LM, Raso G, Girard L, Erickson HS, Roth J, Heymach JV, Moran C, Danenberg K, Minna JD, Wistuba II. Robust gene expression signature from formalin-fixed paraffin-embedded samples predicts prognosis of non-small-cell lung cancer patients. *Clin Cancer Res*. 2011 Sep 1; 17(17):5705-14. Epub 2011 Jul 8. PubMed PMID: 21742808; PubMed Central PMCID: PMC3166982.
11. Yang F, Tang X, Riquelme E, Behrens C, Nilsson MB, Giri U, Varella-Garcia M, Byers LA, Lin HY, Wang J, Raso MG, Girard L, Coombes K, Lee JJ, Herbst RS, Minna JD, Heymach JV, Wistuba II. Increased VEGFR-2 gene copy is associated with chemoresistance and shorter survival in patients with non-small-cell lung carcinoma who receive adjuvant chemotherapy. *Cancer Res*. 2011 Aug 15; 71(16):5512-21. Epub 2011 Jul 1. PubMed PMID: 21724587; PubMed Central PMCID: PMC3159530.
12. Byers LA, Wang J, Nilsson M, Fujimoto J, Saintigny P, Yordy J, Giri U, Peyton M, Fan Y, Shen L, Liu W, Diao L, Duchemann B, Tumula P, Weber S, Glisson BS, Kalhor N, Wistuba I, Girard L, Hong WK, Mills GB, Coombes K, Weinstein J, Minna J, and Heymach JV. Proteomic Profiling Identifies Dysregulated Pathways in Small Cell Lung Cancer and PARP1 as a Novel Therapeutic Target. *Cancer Discovery*. *In Press*.
13. Byers LA, Diao L, Wang J, Saintigny P, Girard L, Peyton M, Shen L, Fan Y, Giri U, Tumula PK, Nilsson MN, Gudikote J, Tran H, Foulks JM, Kanner SB, Gandhi V, Krett N, Rosen ST, Kim ES, Herbst RS, Blumenschein GR, Lee JJ, Lippman SM, Ang K, Mills GB, Hong WK, Weinstein JN, Wistuba II, Coombes KR, Minna JD, Heymach JV. An epithelial-mesenchymal transition (EMT) gene signature predicts resistance to EGFR and PI3K pathway inhibitors and identifies Axl as a mesenchymal-associated target in non-small cell lung cancer. *Clin Cancer Research*, *Accepted pending revisions*

Abstracts (Attached in Appendix B)

1. Behrens C, Solis L, Lin H, Yuan P, Tang X, Kadara H, Riquelme E, Galindo H, Lee JJ, Wistuba II. Analysis of EZH2 and TTF-1 Protein expression identifies a subset of lung adenocarcinomas with better prognosis. AACR 2012 Annual Meeting, Chicago, March 31-April 4, 2012.
2. Bhardwaj V, Likhacheva A, Byers LA, Diao L, Allen PK, Minna JD, Ihle NT, Powis G, Das AK, Girard L, Peyton M, Yordy J, Liao Z, Ang KK, Story M, Kalhor N, Komaki R, Kim ES, Heymach JV, Welsh JW. Establishing role of KRAS mutation on NSCLC radio-sensitivity. AACR Annual Meeting, 4/2012.
3. Byers LA, Nilsson M, Fujimoto J, Saintigny P, Wang J, Diao L, Peyton M, Fan Y-H, Giri U, Weber S, Duchemann B, Girard L, Coombes K, Weinstein J, Minna JD, Wistuba I, Heymach JV. Investigation of poly (ADP-ribose) polymerase 1 (PARP1) as a novel therapeutic target in small cell lung cancer (SCLC). 14th World Conference on Lung Cancer (#2323), 7/2011.
4. Byers LA, Wang J, Diao L, Girard L, Peyton M, Coombes KR, Weinstein JN, Gandhi V, Krett N, Rosen ST, Minna JD, Heymach JV. An epithelial to mesenchymal transition (EMT) gene expression signature predicts resistance to PI3K/Akt pathway inhibitors in non-small cell lung cancer. AACR-NCI-EORTC International Conference on Molecular Targets and Cancer Therapeutics, 11/2011.

5. Byers LA, Diao L, Wang J, Girard L, Peyton M, Gazdar A, Groth P, Paul J, Liu N, Kim ES, Mauro D, Herbst RS, Papadimitrakopoulou V, Coombes KR, Weinstein JN, Minna JD, Heymach JV. LKB1 and KRAS mutations predict resistance to PI3K/Akt inhibitors in non-small cell lung cancer. AACR Annual Meeting, 4/2012.
6. Dai B, Liu W, Heymach JV, Byers LA, Wang J, Coombes KR, Fang B, Roth JA. Identify signaling responses to MEK inhibitor AZD6244 in lung cancer cells with proteomics reverse phase protein array. AACR Annual Meeting, 4/2012.
7. Dalvi MP, Behrens C, Suraokar M, Girard L, Xie Y, Wistuba II, Minna JD. Developing a molecular understanding of non-small cell lung cancer (NSCLC) resistance to platin-taxane chemotherapy. AACR 2012 Annual Meeting, Chicago, March 31-April 4, 2012.
8. Du L, DeSevo C, Borkowski R, Baker M, Wistuba II, Minna JD, Pertsemilidis A. MicroRNA regulation of cell viability and drug response in cancer. AACR 2012 Annual Meeting, Chicago, March 31-April 4, 2012.
9. Erickson HS, Hale KS, Diao L, Silvestro A, McDowel C, Raso MG, Behrens C, Ortenberg E, Roberts D, Heath JD, Hennessy BT, Mills GB, Wang J, Wistuba II. Nanoscale high-throughput quantitative RT-PCR for the characterization of targeted-therapy related molecular biomarkers from recurrent and non-recurrent NSCLC tissues. AACR 2012 Annual Meeting, Chicago, March 31-April 4, 2012.
10. Fujimoto J, Kadara H, Fukuoka J, Aoe K, Fujimoto N, Kishimoto T, Inai K, Hiroshima K, Suraokar M, Mehran R, Tsao A, Wistuba II. Expression patterns of the G protein-coupled receptor, GPRC5A, in human malignant pleural mesothelioma. AACR 2012 Annual Meeting, Chicago, March 31-April 4, 2012.
11. He Y, Zhou Z, Hofstetter VL, Zhou Y, Hu W, Pataer A, Correa AM, Lu Y, Wang J, Diao L, Byers LA, Wistuba I, Roth JA, Swisher SG, Heymach JV, Fang B. Aberrant signal transduction and DNA damage response pathways in primary lung cancer. 14th World Conference on Lung Cancer (#646), 7/2011.
12. Kabbout M, Garcia M, Fujimoto J, Woods D, Koch P, Solis LM, Behrens C, Wistuba II, Kadara H. Tumor suppressor effects of the ETS2 canonical transcriptional factor in human non-small cell lung cancer pathogenesis. AACR 2012 Annual Meeting, Chicago, March 31-April 4, 2012.
13. Kim ES, Chow C-W, Kalhor N, Fujimoto J, Swisher SG, Wistuba II, Stewart DJ, Siddik Z. Effects of tissue platinum concentration on tumor response in non-small cell lung cancer. Proc 14th World Conference on Lung Cancer, Amsterdam, July 3-7, 2011.
14. Riquelme E, Behrens C, Suraokar M, Chow C-W, Kadara H, Girard L, Minna JD, Wistuba II. EZH2High and miR-101Low expressions are associated with chemoresistance and shorter survival in patients with lung adenocarcinoma who received adjuvant chemotherapy. AACR 2012 Annual Meeting, Chicago, March 31-April 4, 2012.
15. Saintigny P, Blumenschein GR, Diao L, Wang J, Coombes K, Liu S, Kim E, Tsao A, Herbst R, Alden C, Lee JJ, Tang X, Stewart D, Kies M, Fossella F, Tran H, Mao L, Hicks M, Erasmus J, Gupta S, Girard L, Peyton M, Davis S, Lippman S, Hong WK, Minna J, Wistuba I, Heymach J. Gene-expression profiles predict sorafenib efficacy in wild-type EGFR non-small cell lung cancer (NSCLC). AACR Annual Meeting, 4/2012.
16. Stewart DJ, Nunez M, Behrens C, Swisher S, Roth JA, Heymach JV, Wistuba II. Factors associated with membrane carbonic anhydrase IX (mCAIX) immunohistochemistry (IHC) in non-small cell lung cancer (NSCLC). J Clin Oncol 29 (#abstr e21125), 6/2011.

17. Suraokar M, Kim D, Zhang Y, Diao L, Riquelme E, Behrens C, Mehran R, Wang J, Coombes K, Tsao A, Wistuba II. Exploring the role of Twist-1 in the pathogenesis of malignant pleural mesothelioma (MPM). AACR 2012 Annual Meeting, Chicago, March 31-April 4, 2012.
18. Yordy JS, Shen L, Diao L, Wang J, Coombes K, Giri U, Xie Y, Minna JD, Girard L, Weinstein J, Heymach JV, Ang K, Story MD, Meyn R. Use of a gene expression signature related to epithelial-to-mesenchymal transition (EMT) to predict for overall survival (OS) in cohorts of lung and head and neck cancer (HNSCC) patients. J Clin Oncol 29: 2011 (suppl; abstr 7010), 6/2011.
19. Zhang J, Giri U, Cantu K, Wang J, Beketaev I, Byers LA, Saintigny P, Heymach JV, Lin SH. Casitas B-lineage lymphoma-3 is an epigenetically regulated gene whose knockdown induces mesenchymal to epithelial transition and enhances erlotinib sensitivity in lung cancer cell lines. AACR Annual Meeting, 4/2012.

CONCLUSIONS

PROJECT 1: Using comprehensive gene expression and proteomic profiling, we have demonstrated that we can systematically profile lung cancer cell lines to identify molecular markers and signaling changes associated with mutation status and drug response. The resulting profiles can be correlated with patient tissue data for association with clinical outcome. These techniques have led to the development of novel therapeutic targets in SCLC (PARP1), mesenchymal NSCLC (Axl), and LKB1 mutated NSCLC (IGF1R). Clinical trials based on all three of these observations are currently being planned.

PROJECT 2: We have collected very detailed information on relapse patterns, overall survival and cause-specific survival in 985 patients with resected NSCLC, have detailed molecular profiles on tumors of 272 of these patients, have detailed tissue microarray data on another 315 patients, and have high quality FFPE and fresh frozen tumor samples available for assessment in a further 401 of these patients. We have demonstrated that tumor shrinkage after platinum-based neoadjuvant chemotherapy is proportional to tumor platinum concentration and that uptake of platinum into tumor may be down-regulated after initial tumor exposure to drug. Overall survival and progression-free survival after neoadjuvant chemotherapy is inversely proportional to percentage of tumor cells that remain viable after neoadjuvant therapy.

PROJECT 3: During the last year, the PROSPECT Project 3 investigators completed the goals established for all three Aims. We identified and characterized a number of novel clinical relevant molecular markers associated to the prognosis in surgically resected NSCLCs and MPMs. We developed and tested a strategy for gene (mRNA) signature validation using high-throughput Quantitative Nuclease Protection Assay (qNPA™) and Fluidigm™ microfluidic quantitative dynamic array. We developed a molecular understanding of NSCLC resistance to platin-taxane chemotherapy using neo-adjuvant-treated tumors tissues and cell lines. We identified the role of the Phospho-ORM-1 peptide as a novel nAChR-associated protein in lung cancer pathogenesis and smoking-associated carcinogenesis, and as a potential serum marker and target for lung cancer detection and treatment.

PROJECT 4: There is preliminary evidence that a subgroup of MPM patients gain clinical benefit from dasatinib therapy and that baseline p-Src Tyr⁴¹⁹ levels in MPM tumor tissue may be predictive of TTP. This is the first targeted therapy neoadjuvant trial to potentially identify a predictive biomarker in MPM. We have completed accrual to the trial and are awaiting the final

translational research studies. We will plan on completing these IHC and FISH studies by September of this year and having a draft manuscript by the end of this year. Future plans include correlating outcome and tumor p-Src Tyr⁴¹⁹ to peripheral surrogate markers in blood/serum/platelets and pleural effusion and to analyze pathways of resistance in MPM tumors.

PROJECT 5: In addition to the preparation of publications summarizing the studies on CXCR4/E-cadherin and EGFR/ β -catenin, we further characterized the new lung metastasis model. This model is currently being used by our group and our colleagues in a study of anti-lung-cancer agents and will provide a unique tool for further understanding lung metastasis and its microenvironment. In addition, QD-based technology developed through this grant support has been used in several collaborative projects. As one example, we identified a significantly positive correlation between RRM2 and Bcl-2 expression in tumor tissues from NSCLC patients. This imaging technique allows quantification of multiple biomarkers at the per-cell level, providing evidence to support the underlying biological significance of co-localized proteins.

PATHOLOGY CORE: During the last year, the PROSPECT Pathology Core finalized the completion of the goals established for all three Objectives. The Pathology Core has played an important role in the processing of NSCLC and MPM tissue and cell line specimens for comprehensive molecular profiling, and in the characterization of tissue specimens on the expression of protein expression by immunohistochemistry. The Pathology Core contributed to the publication of 6 papers and submission of 4 manuscripts in peer-reviewed journals, and 8 abstracts presentations in scientific meetings.

BIostatISTICS AND DATA MANAGEMENT CORE: In collaboration with clinical investigators, research nurses, pathologists, and basic scientists, the Biostatistics and Data Management Core has continued to deliver the biostatistics, bioinformatics, and data management support as proposed.

APPENDIX A

Personnel

DoD PROSPECT Funded Personnel 06/01/2007 to 06/30/12

EMPLOYEE NAME	JOB TITLE
Alden,Christine M	Supv, Research Nurse
An,Tong-tong	Research Intern
Basey,Annette L	Sr Research Histology Tech
Behrens,Maria del Carmen	Assistant Professor
Bhutani,Manisha	Postdoctoral Fellow
Brooks,Angela A	Grant Program Coordinator
Casey,Beverly D	Research Nurse
Chow,Chi-Wan B	Sr Research Asst
Chu,Zuo M	Tissue Procurement Specialist
Chung,Wen-Cheng	Postdoctoral Fellow
Coombes,Kevin R	Professor
Correa,Arlene M	Assistant Professor
Corvalan,Alejandro	Assistant Professor
Davis,Suzanne E	Dir, Res Planning & Dev
Fan,You-Hong	Coord, Research Laboratory
Feng,Lei	Sr Statistical Analyst
Fiorentino,Stefania	Sr Research Asst
Francisco,Ma Rhodora D	Sr Research Nurse
George,John T	Financial Analyst
Gil,James M	Sr Research Nurse
Gudikote,Jayanthi	Research Scientist
Heymach,John Victor	Associate Professor
Hong,Waun K	Division Head
Iwamaru,Arifumi	Postdoctoral Fellow
Jayachandran,Gitanjali	Research Scientist
Jenkins,Deborah J	Vocational Nurse
Ji,Lin	Associate Professor
Jones Jr,Paul J	Sr Research Histology Tech
Kim,Yoon Sung	Research Asst I
Lee,Jangsoon	Postdoctoral Fellow
Lee, Jiun-Kae Jack	Professor
Lin,Yan	Sr Statistical Analyst
Mao,Li	Professor
Martinez,Carmen R	Grant Program Manager
Morris,Damien K	Financial Analyst
Nunez,Maria I	Research Investigator
Nweke,Gift K	Research Asst II
Price,Mellanie J	Mgr, Clinical Protocol Admin
Riquelme Sanchez,Erick Marcelo	Postdoctoral Fellow
Saigal,Babita	Research Investigator
Saintigny,Pierre	Postdoctoral Fellow
Sakai,Ryo	Postdoctoral Fellow
Schaerer,Rainell G	Sr Research Nurse
Smith,Beverly J	Grant Program Coordinator
Solis Soto,Luisa Maren	Postdoctoral Fellow
Song,Wei Sonya	Project Director
Suraokar,Milind B	Instructor

Tsao,Anne	Associate Professor
Tse,Warner H	Sr Research Nurse
Tumula,Praveen K.	Research Intern
Wang,Jing	Assistant Professor
Watanabe,Yuichi	Postdoctoral Fellow
Weissferdt,Annikka	Fellow
Willis,Veshae P	Clinical Invest Technician
Wismach,Marnie	Postdoctoral Fellow
Wistuba,Ignacio Ivan	Professor
Yang,Bijun	Dir, Prod Research and Develop
Yang,Fei	Postdoctoral Fellow
Yuan,Ping	Research Investigator

APPENDIX B

Abstracts and Publications

The Role of PKR/eIF2 α Signaling Pathway in Prognosis of Non-Small Cell Lung Cancer

Yong He^{1,2}, Arlene M. Correa², Maria Gabriela Raso³, Wayne L. Hofstetter², Bingliang Fang², Carmen Behrens⁴, Jack A. Roth², Yihong Zhou⁵, Liping Yu⁶, Ignacio I. Wistuba^{3,4}, Stephen G. Swisher², Apar Pataer^{2*}

1 Department of Thoracic Surgery, Daping Hospital, Third Military Medical University, Chongqing, China, **2** Department of Thoracic and Cardiovascular Surgery, The University of Texas M.D. Anderson Cancer Center, Houston, Texas, United States of America, **3** Department of Pathology, The University of Texas M.D. Anderson Cancer Center, Houston, Texas, United States of America, **4** Department of Thoracic Head and Neck Medical Oncology, The University of Texas M.D. Anderson Cancer Center, Houston, Texas, United States of America, **5** Department of Neurological Surgery and Biological Chemistry, University of California Irvine, Irvine, California, United States of America, **6** Ziren Research LLC, Irvine, California, United States of America

Abstract

Background: In this study, we investigated whether PKR protein expression is correlated with mRNA levels and also evaluated molecular biomarkers that are associated with PKR, such as phosphorylated PKR (p-PKR) and phosphorylated eIF2 α (p-eIF2 α).

Methodology and Findings: We determined the levels of PKR protein expression and mRNA in 36 fresh primary lung tumor tissues by using Western blot analysis and real-time reverse-transcriptase PCR (RT-PCR), respectively. We used tissue microarrays for immunohistochemical evaluation of the expression of p-PKR and p-eIF2 α proteins. We demonstrated that PKR mRNA levels are significantly correlated with PKR protein levels (Spearman's $\rho = 0.55$, $p < 0.001$), suggesting that PKR protein levels in tumor samples are regulated by PKR mRNA. We also observed that the patients with high p-PKR or p-eIF2 α expression had a significantly longer median survival than those with little or no p-PKR or p-eIF2 α expression ($p = 0.03$ and $p = 0.032$, respectively). We further evaluated the prognostic effect of combined expression of p-PKR plus PKR and p-eIF2 α plus PKR and found that both combinations were strong independent prognostic markers for overall patient survival on stage I and all stage patients.

Conclusions: Our findings suggest that PKR protein expression may be controlled by transcription level. Combined expression levels of PKR and p-PKR or p-eIF2 α can be new markers for predicting the prognosis of patients with NSCLC.

Citation: He Y, Correa AM, Raso MG, Hofstetter WL, Fang B, et al. (2011) The Role of PKR/eIF2 α Signaling Pathway in Prognosis of Non-Small Cell Lung Cancer. PLoS ONE 6(11): e24855. doi:10.1371/journal.pone.0024855

Editor: John D. Minna, University of Texas Southwestern Medical Center at Dallas, United States of America

Received: March 25, 2011; **Accepted:** August 22, 2011; **Published:** November 10, 2011

This is an open-access article, free of all copyright, and may be freely reproduced, distributed, transmitted, modified, built upon, or otherwise used by anyone for any lawful purpose. The work is made available under the Creative Commons CC0 public domain dedication.

Funding: This work is supported in part by the National Institutes of Health through M.D. Anderson's Cancer Center Support Grant CA-016672 - Lung Program, a Specialized Program of Research Excellence (SPORE) Grant CA-070907 (to IW), and an R01 Grant CA-124591 (to BF). Further support came from Department of Defense grant W81XWH-07-1-0306 (to IW), the National Natural Science Foundation of China (30600611, 81071912) (to YH) and "1510 project" of Third Military Medical University of China (to YH), and from the Homer Flower Gene Therapy Fund, the Charles Rogers Gene Therapy Fund, the Margaret Wiess Elkins Endowed Research Fund, the Flora and Stuart Mason Lung Cancer Research Fund, the Phalanx Thoracic Gene Therapy Fund, and the George P. Sweeney Esophageal Research Fund (to SS). The funders had no role in study design, data collection and analysis, decision to publish, or preparation of the manuscript.

Competing Interests: The authors have read the journal's policy and have the following conflicts. LY is an employee of Ziren Research LLC. This does not alter the authors' adherence to all the PLoS ONE policies on sharing data and materials.

* E-mail: apataer@mdanderson.org

Introduction

The protein kinase (PKR) is an interferon-inducible serine/threonine kinase that mediates protein synthesis, a tightly regulated process that is critical in cellular proliferation and differentiation [1–3]. Increased PKR expression has been shown to correlate with better prognoses in head and neck cancer and colon cancer [2,3], and accumulating evidence demonstrates that PKR may act as a tumor suppressor in leukemia and other hematopoietic malignancies [4,5]. Binding of either double-stranded RNA (dsRNA) or structured single-stranded RNAs can mediate PKR phosphorylation [6,7]. Activated PKR phosphorylates its well-documented downstream target, the α subunit of protein synthesis initiation factor eIF2 (eIF2 α), leading to

inhibition of protein synthesis and eliciting antiviral and antitumor activities [8,9]. In addition to its role in translational control, PKR has been implicated in antiviral innate immunity, apoptosis, cell proliferation, and stress signaling [10]. Moreover, PKR expression and autophosphorylation are increased in several types of cancer, including melanoma, colon cancer, and breast cancer [11,12]. The results of several studies have demonstrated the importance of phosphorylated eIF2 α (p-eIF2 α) in cancer therapy [10,13,14]: activation of the PKR-eIF2 α phosphorylation pathway is essential for the antiproliferative and proapoptotic functions of the tumor suppressor gene [15].

Recently, we found that low expression of dsRNA-dependent PKR was significantly associated with shorter survival in NSCLC patients, suggesting that biologic functions of PKR or its

downstream molecules could be valuable prognostic factors in NSCLC [1]. In this new study, our goal was to determine whether PKR protein expression is associated with its mRNA levels and whether its downstream targets, such as phosphorylated PKR (p-PKR) and p-eIF2a, are also prognostic factors in NSCLC. We first determined the PKR mRNA levels and protein expression in fresh-frozen NSCLC tissue and found a positive correlation between PKR protein expression and mRNA levels. Next, using immunohistochemical staining, we investigated the expression of p-PKR and its well-characterized downstream molecule p-eIF2a in archived tissue microarray specimens. Our results show that p-PKR and p-eIF2a are predictive biomarkers of NSCLC outcomes and that when expression of PKR was combined with expression of p-PKR or p-eIF2a, the effect on predicting patient survival was enhanced.

Results

PKR protein expression correlates with mRNA levels

To investigate whether PKR protein expression is associated with mRNA levels, we determined the PKR and p-PKR protein expression and PKR mRNA levels in 36 fresh primary lung tumor

tissues using Western blot analysis and real time RT-PCR, respectively. Protein expression of β -actin and its mRNA levels were also determined and used as controls. The results of the Western blotting analyses showed that tumor samples expressed different levels of PKR at both protein and mRNA levels (Figure 1A and 1B). Statistical analysis revealed a significant correlation between PKR protein expression and its mRNA levels. (Spearman's $\rho = 0.55$, $p < 0.001$; Figure 1C). These results suggest that PKR gene expression may cause of the differing levels of PKR protein expression in tumors.

Correlation between p-PKR and p-eIF2a protein expression in NSCLC tumors with clinicopathologic features

Because the biological function of PKR is closely associated with its phosphorylation, and eIF2a phosphorylation is a hallmark of PKR activation, we next evaluated the expression of p-PKR and p-eIF2a proteins in TMA specimens using immunohistochemical staining. Table 1 summarizes the relationships between p-PKR or p-eIF2a expression and other clinicopathologic features. High p-PKR expression was associated with the adenocarcinomas subtype

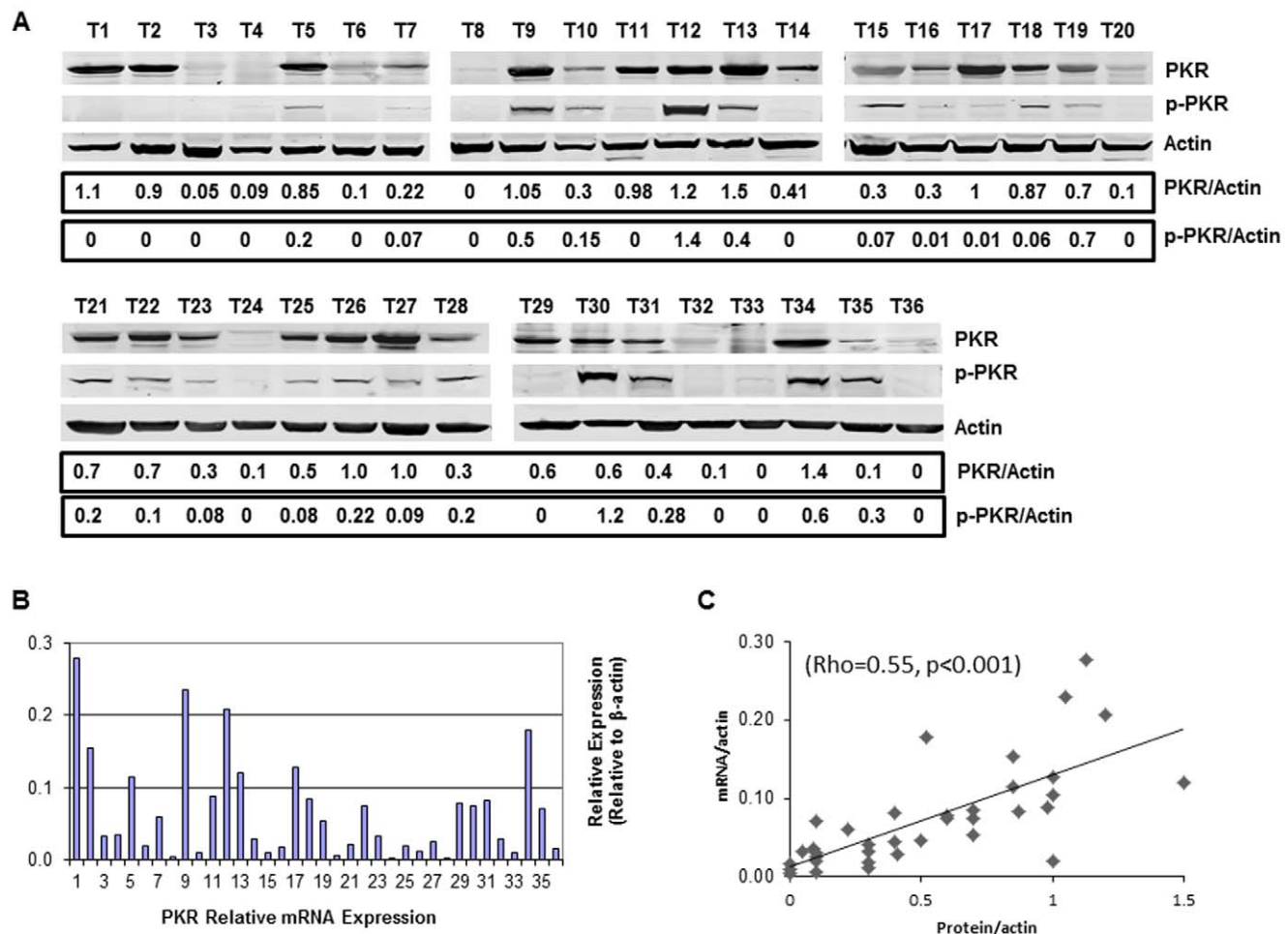


Figure 1. PKR mRNA levels are correlated with PKR protein levels in primary NSCLC tissues. **A.** Western blot analysis of PKR and p-PKR protein in tumor samples. A densitometric analysis of the ratio of PKR or PKR to β -actin is represents normalized protein levels. Each lane represents a tumor sample from an individual patient. **B.** mRNA levels of corresponding samples were determined using quantitative real-time PCR. Levels of β -actin protein and its mRNA of the same sample were used as controls. **C.** Scatter plot of PKR protein expression correlated with mRNA expression (Spearman's $\rho = 0.55$, $p < 0.001$).

doi:10.1371/journal.pone.0024855.g001

Table 1. Relationships between the level of p-PKR and p-eIF2 α expression and clinicopathologic characteristics in TMA of NSCLC patients.

Characteristics	p-PKR Score		p-Value	p-eIF2 α Score		p-Value
	Low (≤ 70)	High (>70)		Low (≤ 150)	High (>150)	
Gender			0.11			0.45
Male	49 (50.0)	34 (37.6)		39 (43.3)	44 (49.4)	
Female	49 (50.0)	56 (62.4)		51 (56.7)	45 (50.6)	
Pathological TNM			0.33 ^a			0.25 ^a
Stage I	62 (62.9)	58 (64.4)		55 (60.0)	57 (64.8)	
Stage II	19 (19.6)	13 (14.4)		17 (18.9)	16 (18.2)	
Stage III–IV	17 (17.5)	19 (21.2)		19 (21.1)	15 (17.0)	
pT			0.11 ^b			0.46 ^b
T1	26 (26.5)	35 (38.9)		27 (30.1)	30 (33.7)	
T2	64 (65.3)	47 (52.2)		56 (62.2)	48 (53.9)	
T3	3 (3.1)	5 (5.6)		3 (3.3)	6 (6.8)	
T4	5 (5.1)	3 (3.3)		4 (4.4)	5 (5.6)	
pN			0.48 ^c			0.06 ^c
N0	67 (68.4)	62 (68.9)		57 (63.3)	67 (75.3)	
N1	20 (20.4)	13 (15.4)		19 (21.1)	14 (15.7)	
N2	11 (11.2)	14 (15.7)		14 (15.6)	8 (9.0)	
pM			0.07			0.36
M0	96 (97.9)	84 (93.3)		86 (95.5)	86 (96.6)	
M1	2 (2.1)	6 (6.7)		4 (4.4)	3 (3.4)	
Histologic type			<0.01			0.19
ACC	41 (41.4)	73 (82.0)		51 (56.7)	56 (62.5)	
SCC	58 (58.6)	16 (18.0)		39 (43.3)	33 (37.5)	
Tobacco history			0.11			0.13
No	25 (25.5)	33 (36.3)		29 (32.2)	19 (21.8)	
Yes	72 (74.5)	58 (63.7)		61 (67.8)	68 (78.2)	

^aThe *p*-value was calculated between pathologic stage I and II–IV.^bBetween T1 and T2–T4.^cBetween N0 and N1–N2.

SCC, squamous cell carcinoma. ACC, Adenocarcinoma.

doi:10.1371/journal.pone.0024855.t001

($p < 0.001$). No correlation was observed between p-PKR expression and gender sex, TNM stage, or smoking status. We also found no correlation between p-eIF2 α expression and clinicopathologic features. Representative images of immunohistochemical staining results for p-PKR and p-eIF2 α are shown in Figure 2. The p-PKR and p-eIF2 α proteins were expressed in the cytoplasm of tumor cells.

Correlation between p-PKR and p-eIF2 α protein expression in NSCLC tumors with disease outcomes

To further evaluate whether p-PKR or p-eIF2 α protein expression correlates with clinical outcomes of patients with NSCLC, Kaplan–Meier analysis revealed that for stage I and all stages, patients with relatively elevated p-PKR had significantly longer survival than those with little or no p-PKR expression (Figure 3A and 3C). For all stage patients, the median survival time was 105 months for patients with high p-PKR expression and 51 months for those with little or no p-PKR expression. A significant association was also observed between high p-eIF2 α protein expression and longer survival on stage I and all stages (Figure 3D and 3F). There is no significant association was

observed between high p-PKR or high p-eIF2 α protein expression and longer survival on stages II–IV (Figure 3B and 3E).

In a univariate analysis, a Cox proportional hazards model indicated that p-PKR and p-eIF2 α had prognostic significance (Table 2). In a multivariate analysis, we found that p-PKR and p-eIF2 α expression were statistically significant associated with survival (Table 2). These results indicate that p-PKR and p-eIF2 α expression are independent biomarkers of patients' survival.

We also examined the associations between the expression levels of PKR, p-PKR, and p-eIF2 α . Our results indicated that p-PKR expression significantly correlated with p-eIF2 α expression (Spearman's $\rho = 0.48$, $p < 0.001$). PKR expression also significantly correlated with expression of p-PKR (Spearman's $\rho = 0.31$, $p = 0.004$) and p-eIF2 α (Spearman's $\rho = 0.45$, $p < 0.001$). We further evaluated the prognostic effect of combined expression of p-PKR plus PKR and p-eIF2 α plus PKR and found that both combinations were strong independent prognostic markers for overall patient survival on stage I (Figure 4A and 4B) and all stage patients (Figure 4C and 4D). For all stage patients, patients with high PKR and high p-PKR expression had a median survival time of 132 months, which was significantly longer than that of patients

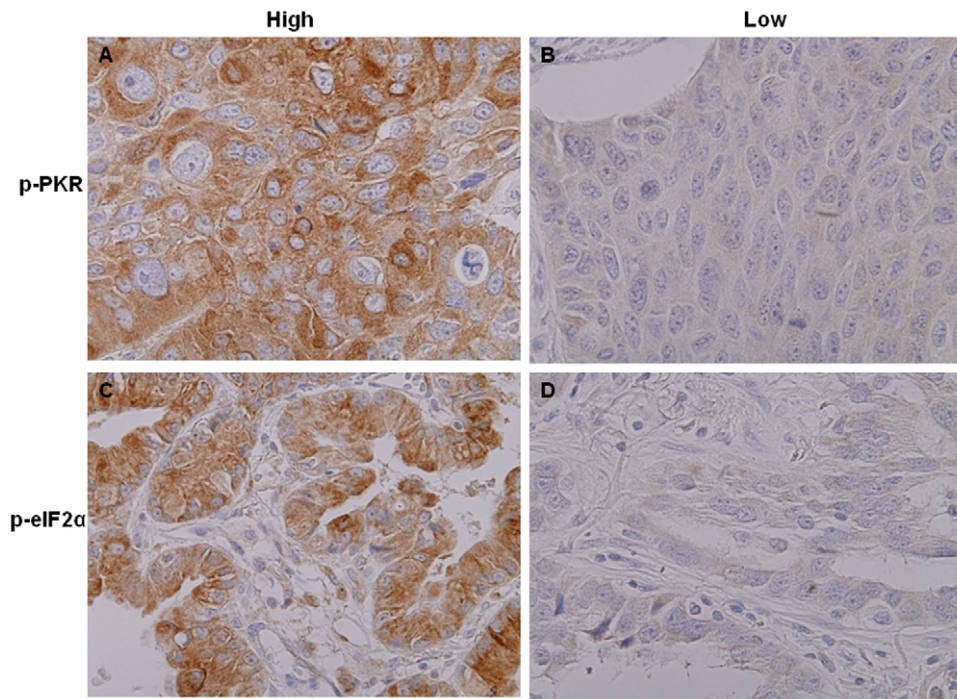


Figure 2. Representative results of immunohistochemical staining of NSCLC tumor specimens for p-PKR and p-eIF2 α . High-expressing cases (A and C). Low-expressing cases (B and D). Expression of p-PKR and p-eIF2 α was detected in the cytoplasm.
doi:10.1371/journal.pone.0024855.g002

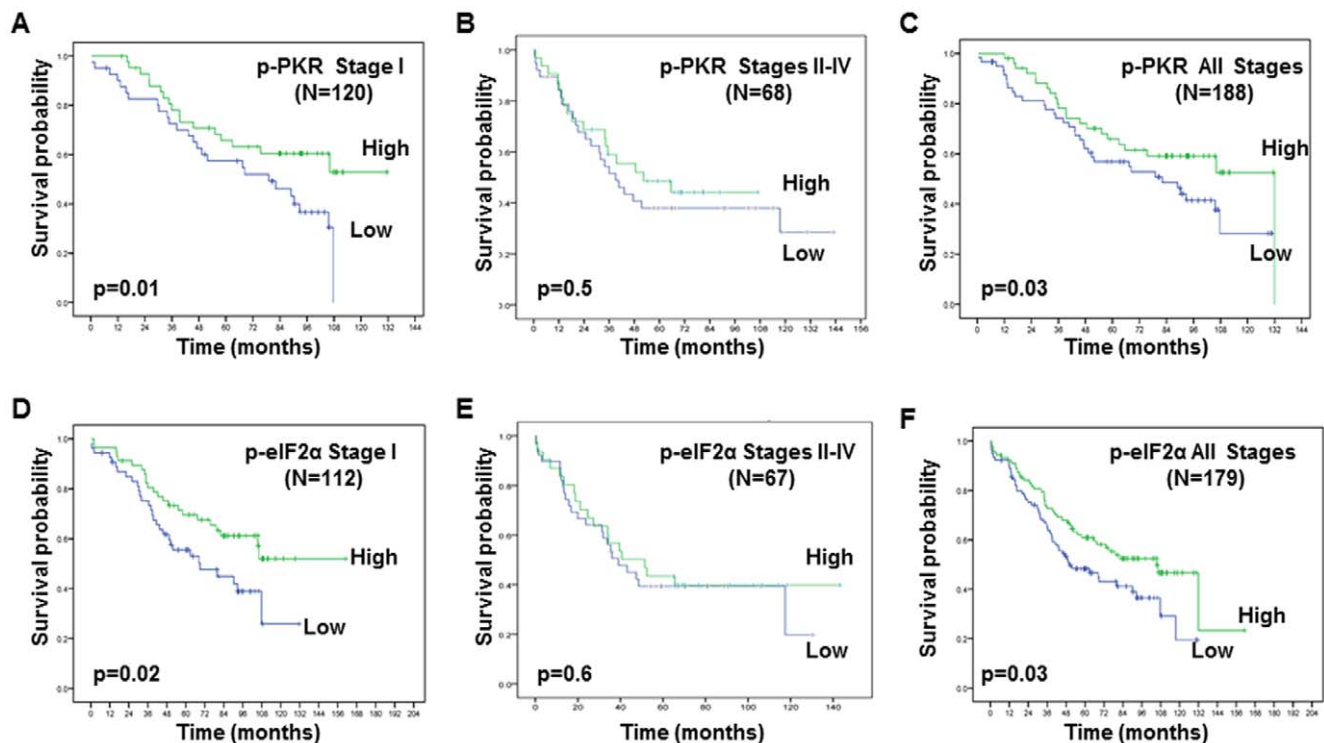


Figure 3. The prognostic significance assessed by using Kaplan-Meier survival estimates and long-rank test. A–F. Kaplan-Meier survival curves according to the differences in (A, B, C) p-PKR and (D, E, F) p-eIF2 α expression in patients with stage I (A, D), stages II–IV (B, E) and all stage (C, F) NSCLC. The survival rates were significantly worse in the patients with low p-PKR or p-eIF2 α expression than in those with high p-PKR or p-eIF2 α expression (Stage I: $p=0.01$ and $p=0.02$; All stages: $p=0.03$ and $p=0.03$, respectively).
doi:10.1371/journal.pone.0024855.g003

Table 2. Univariate and multivariate Cox model assessing effects of covariates on overall survival.

Characteristics	Stage I		All Stages	
	Hazard ratio (95% CI)	p-Value	Hazard ratio (95% CI)	p-Value
A. Univariate Cox regression model				
Age	0.99 (0.99–1.00)	0.21	0.99 (0.96–1.02)	0.48
Gender (male vs female)	1.49 (0.88–2.51)	0.14	1.31 (0.87–1.96)	0.19
Tobacco history (yes vs no)	1.50 (0.78–2.89)	0.22	0.85 (0.54–1.33)	0.48
Pathological TNM stage				
Stage II+III+IV vs I	-	-	2.79 (1.65–4.71)	0.001
Histologic type (ACC vs SCC)	1.36 (0.67–2.78)	0.39	2.00 (0.58–6.85)	0.27
p-PKR (High vs Low)	0.45 (0.24–0.84)	0.01	0.51 (0.28–0.96)	0.02
p-eIF2a (High vs Low)	0.53 (0.31–0.92)	0.03	0.54 (0.32–0.96)	0.03
B. Multivariate Cox regression model				
Pathological TNM stage				
Stage II+III+IV vs I	-	-	2.71 (1.53–4.82)	0.001
p-PKR (High vs Low)	-	-	0.56 (0.34–0.95)	0.03
p-eIF2a (High vs Low)	-	-	0.61 (0.42–0.97)	0.04

doi:10.1371/journal.pone.0024855.t002

with high PKR and low p-PKR expression (median survival, 80 months; Figure 4C). Patients with little or no PKR and p-PKR expression had a significantly shorter median survival (43 months; Figure 4C). There is a difference in outcome for PKR(H)/p-PKR(H) vs PKR(L)/p-PKR(H) patients on Figure 4A. Our IHC score range is 0–300 for PKR and p-PKR. In current study, we are using median cut-off (150 for PKR and 70 for p-PKR). On Figure 4A, 106 stage I patients divided into four groups, 43 patients with high PKR and high p-PKR, 21 patients with high PKR and low p-PKR expression, 32 Patients with low PKR and p-PKR expression and 10 patients with low PKR and high p-PKR expression. These 10 patients have p-PKR score range 80–120, are very close to median cut-off score (70), and may also belong to low PKR low p-PKR group. For all stage patients, patients with high PKR and high p-eIF2 α expression had a median survival time of 132 months, which was significantly longer than that of patients with high PKR plus low p-eIF2 α expression (median survival, 80 months) and those with low PKR plus high p-eIF2 α expression (median survival, 47 months; Figure 4D). Finally, patients with little or no expression of both PKR and p-eIF2 α had a significantly short median survival (median survival, 35 months; Figure 4D).

Discussion

The results of this study show that PKR mRNA levels are associated with PKR protein expression in primary NSCLC tumors. Our findings suggest that PKR protein expression may control transcription levels. Further, our data suggest that real time RT-PCR, a sensitive method for quantitatively analyzing mRNA levels, can be used to determine mRNA levels in biopsy samples and might therefore be useful for predicting patient survival. We also found that patients with high p-PKR expression had significantly longer median survival than those with little or no p-PKR protein expression. Results of various studies of human malignancies have suggested that high PKR expression indicates favorable prognosis for patients with squamous cell carcinoma of the head or liver [2,16], thus suggesting that PKR may play an important role in suppressing tumor progression and affecting

apoptosis [17]. We have also studied PKR pathways and have found them to be clearly necessary for inducing apoptosis in some cancer cells, including lung cancer, after certain treatments such as melanoma differentiation-associated gene 7 (*MDA7*), E2F-1, and TNF α [18,19]. More recently, we and others demonstrated that some small compounds can induce PKR-dependent apoptosis in both cancer cells and murine embryonic fibroblasts [20,21], indicating that modulating PKR activity could be an interesting approach to cancer therapy. Our finding that NSCLC tumor cells that express a high level of p-PKR correlate with a favorable prognosis is consistent with previous observations that PKR activation is associated with apoptosis induction.

Our findings also demonstrated that patients with high expression of both PKR and p-PKR had significantly longer survival than did those with other combinations of expression levels, including those positive for PKR and negative for p-PKR and those negative for both PKR and p-PKR. Our observation that 53% of the NSCLC tumor samples highly expressed PKR and that 61% of them highly expressed p-PKR [data not shown] These results led us to speculate that PKR expression (i.e., PKR) and PKR activation (i.e., p-PKR) are affected by differing expression of the PKR activator or PKR inhibitor. Other investigators have reported that the function of PKR can be regulated by cellular proteins either positively (e.g., MDA-7/interleukin-24 and PKR-activating protein [PACT]) or negatively (e.g., p58IPK, nucleophosmin and heat shock proteins 90 and 70) [18,19]. In future studies, we will seek to determine which PKR activators and inhibitors affect the PKR signaling pathway in NSCLC tumor samples.

We observed that tumors with high p-eIF2 α expression had a significantly longer median survival. In additional, we demonstrated that patients with high expressions of both PKR and p-eIF2 α also had significantly longer survival than did those with other combinations of expression levels. Our finding that 47% of the tumor samples had low PKR expression and 27% had high p-eIF2 α expression [data not shown]. These results suggest that eIF2 α phosphorylation in some NSCLC tumors occurs independent of the PKR pathway. Besides PKR, three different eIF2 α kinases that can phosphorylate eIF2 α in response to various stress

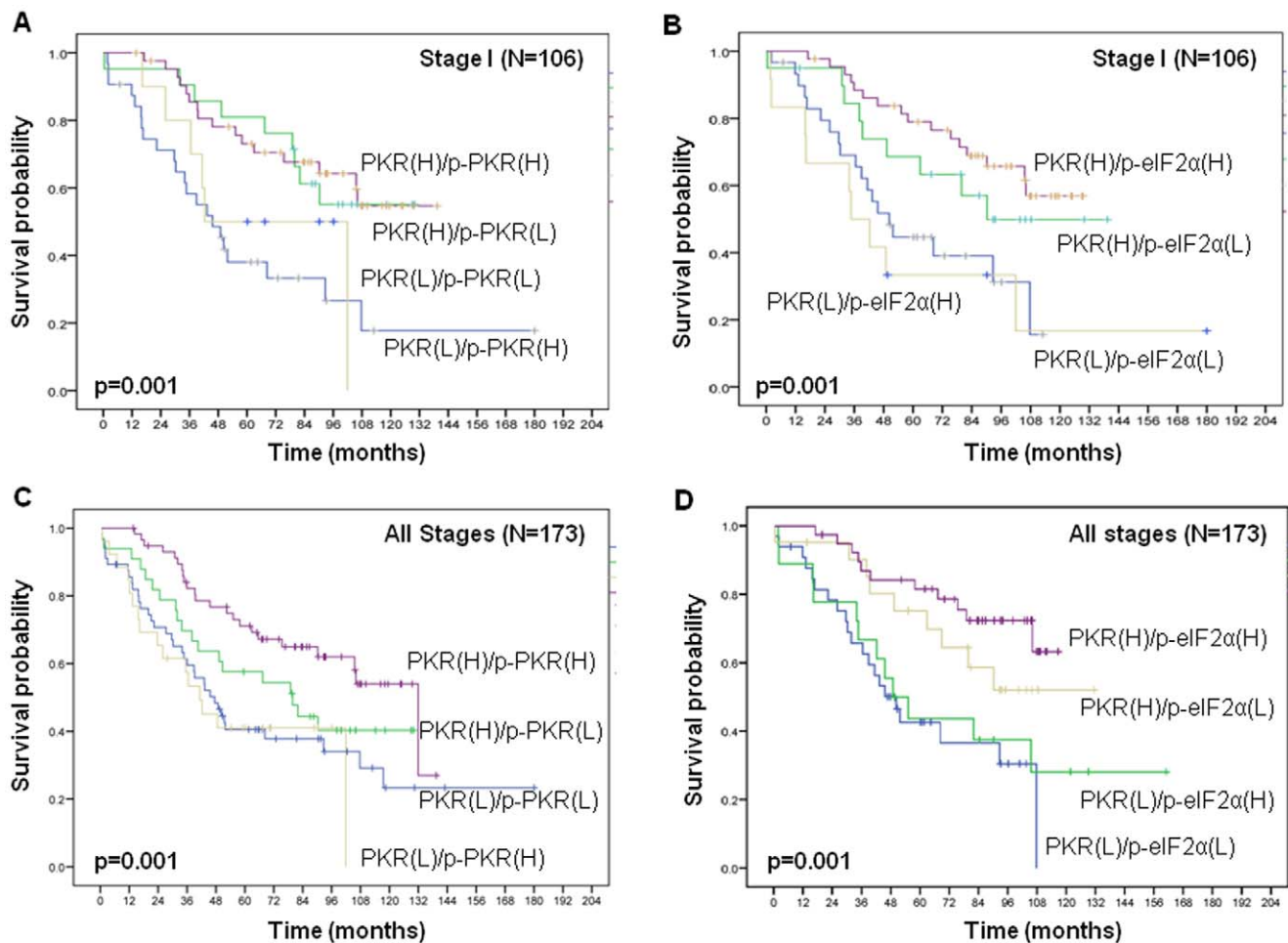


Figure 4. The prognostic significance assessed by using Kaplan-Meier survival estimates and long-rank test. A and C. Survival rate was significantly lower patients with low PKR or low p-PKR expression than in those with high PKR or high p-PKR expression on stage I (A) and all stages (C) ($p=0.001$ and $p=0.001$, respectively). B and D. Survival rate was also significantly lower in patients with low PKR or low p-eIF2 α expression than in those with high PKR or high p-eIF2 α expression on stage I (B) and all stages (D) ($p=0.001$ and $p=0.001$, respectively). doi:10.1371/journal.pone.0024855.g004

conditions have been identified: heme-regulated inhibitor, the homologue of *Saccharomyces cerevisiae* protein kinase general control non-derepressible-2, and RNA-dependent-protein-kinase-like endoplasmic reticulum (ER) kinase (PERK; also known as pancreatic eIF2 α kinase) [13].

In conclusion, our data suggest that the PKR/phosphorylated PKR/phosphorylated eIF2 α signaling pathway plays an important role in the prognosis for non-small cell lung cancer (NSCLC). PKR pathway activities may be useful for predicting NSCLC outcomes, and modulating PKR pathway activities might be a potential NSCLC treatment option.

Methods

Patients and Tissues

NSCLC patients who were undergoing radical resection of their primary cancer at The University of Texas M. D. Anderson Cancer Center between 2007 and 2008 were used for this study based on availability. Patients were excluded from the study if they had previously undergone radiotherapy or chemotherapy for cancer. Patients all provided written informed consent for the use of their tissues, and the study was approved by our Institutional Review Board (University of Texas, MD Anderson Cancer

Center). After being surgically resected, each fresh tumor was immediately divided into two portions; one was instantly frozen and stored in liquid nitrogen for protein and RNA extraction, and the other was fixed with formalin and embedded in paraffin for routine histopathologic evaluation and diagnosis. Tissues with an estimated tumor cell content of 70% or more were used for molecular analyses. In addition to our patients' tissues, we obtained 193 NSCLC Tissue microarray (TMA) specimens (114 adenocarcinomas, and 74 squamous cell carcinomas) between 1997 and 2001 from the Lung Cancer Specialized Program of Research Excellence Tissue Bank at M. D. Anderson Cancer Center (Houston, TX). All specimens were histologically examined and classified using the 2004 World Health Organization classification system [22]. In most cases, detailed clinical and pathologic information, including the patients' demographic data, smoking history, and overall survival plus the disease TNM staging and time to recurrence, was available (Table 1).

Western Blot Analysis

Frozen tumor tissues were initially prepared by being washed twice in cold PBS. Approximately 20 mg of tissue from each fresh sample was homogenized in 0.5 ml ice-cold lysis buffer (1% NP40, 50 mM HEPES [pH 7.4], 150 mM NaCl, 1.5 mM MgCl₂,

100 mM NaF, 1 mM EGTA, 1 mM Na₃VO₄, 10% glycerol, and 10 mM Na pyrophosphate [Roche Applied Science]), containing freshly added protease and phosphate inhibitor. The lysates were spun at 14,000 g in a microcentrifuge at 4°C for 10 min, and the resulting supernatants were used as tissue extracts. The extracts, equivalent to 60 µg of the total protein, were separated by using a 10% SDS-polyacrylamide gel and then transferred to nitrocellulose membranes. The membranes were blocked with TBS containing 5% nonfat dried milk and then probed in PBS containing 5% bovine serum. The following antibodies were used: rabbit anti-PKR (K-17; Santa Cruz Biotechnology), rabbit anti-p-PKR (pT446) (Epitomics), rabbit anti-p-eIF2a (Epitomics), and mouse anti-β-actin (Sigma). Immunoreactive bands were detected and quantified using a Li-Cor Odyssey infrared imaging system.

Reverse Transcription and Real-time Absolute Quantitative Reverse-Transcription-Polymerase Chain Reaction (Real-Time AqRT-PCR)

The total RNA (1 µg) from each frozen clinical sample was extracted using a Trizol extraction kit (Invitrogen) and reverse transcribed in a 20 µL reaction volume by using Taqman reverse-transcription reagents (Applied Biosystems) according to the manufacturer's instructions. The cDNAs were diluted and quantified for expression PKR using real-time RT-PCR (SYBR Green I) (performed by Ziren Research LLC, Irvine, CA). A single standard was incorporated to determine the absolute ratio of expression of each target and reference gene, as previously described [23]. The primer sequences for PKR were as follows: forward, 5'-TCTTCATGTATGTGACACTGC-3', and reverse, 5'-CACACAGTCAAGGTCCTT AG-3'.

Immunohistochemical Staining and Evaluation

The antibodies used for Western blot analysis were also used for immunohistochemical staining. Formalin-fixed and paraffin-embedded tissue histology sections (5-µm thick) were deparaffinized, hydrated and heated in a steamer for 10 min with 10 mmol/L of sodium citrate (pH 6.0) for antigen retrieval. Peroxidase was blocked with 3% H₂O₂ in methanol at room temperature for 15 min, followed by incubation in 10% bovine serum albumin in TBS-t for 30 min. The slides were next incubated with primary antibody at 1:100 dilutions for 65 min at room temperature. After being washed with PBS, the slides were incubated with biotin-

labeled secondary antibody for 30 min. Finally, the samples were incubated with streptavidin-peroxidase at a 1:40 dilution for 30 min. The samples were then stained with 0.05% 3', 3'-diaminobenzidine tetrahydrochloride prepared in 0.05 mol/L of Tris buffer (pH 7.6) containing 0.02% H₂O₂ and subsequently counterstained with hematoxylin. As a positive control, formalin-fixed and paraffin-embedded lung tissues with normal bronchial epithelia were used. As a negative control, tissue samples not incubated with the primary antibody were used. Immunohistochemical staining was quantified by two independent pathologists (Drs. Raso and Pataer) with a four-value intensity score described previously [1].

Statistical Analysis

The median was used as the cutoff point for p-PKR and p-eIF2a. The biomarkers were dichotomized into low- and high-level groups as follows: p-PKR: low (score ≤ 70), high (score > 70); and p-eIF2a: low (score ≤ 150), high (score > 150). In univariate analysis, independent sample *t* and χ^2 tests were used to analyze continuous and categorical variables, respectively. Survival probability as a function of time was computed by using the Kaplan-Meier estimator. The log-rank test was used for between-group comparisons of patient survival time. The Cox proportional hazards model was used to calculate the influence of p-PKR and p-eIF2a expression on survival time, with adjustments made for clinical and histopathologic parameters (age, sex, smoking status and tumor histologic subgroup). The two-sided test was used to test equal proportion between groups in two-way contingency tables. The generalized estimating equation approach was used to estimate differences in the means for the data. Statistical significance was set at $P < 0.05$.

Acknowledgments

We thank Markeda Wade for editorial review. We thank Denise M. Woods and Lakshimi Kakarala for their technical assistance.

Author Contributions

Conceived and designed the experiments: YH AP SS. Performed the experiments: YH AP MR YZ LY. Analyzed the data: AP AC. Contributed reagents/materials/analysis tools: IW CB JR BF WH. Wrote the paper: YH AP.

References

1. Pataer A, Raso MG, Correa AM, Behrens C, Tsuta K, et al. (2010) RNA-dependent protein kinase is an independent prognostic variable for non-small cell lung cancer patients. *Clin Cancer Res* 16: 5522–5528.
2. Haines GK, 3rd, Becker S, Ghadge G, Kies M, Pelzer H, et al. (1993) Expression of the double-stranded RNA-dependent protein kinase (p68) in squamous cell carcinoma of the head and neck region. *Arch Otolaryngol Head Neck Surg* 119: 1142–1147.
3. Singh C, Haines GK, Talamonti MS, Radosevich JA (1995) Expression of p68 in human colon cancer. *Tumour Biol* 16: 281–289.
4. Li S, Koromilas AE (2001) Dominant negative function by an alternatively spliced form of the interferon-inducible protein kinase PKR. *J Biol Chem* 276: 13881–13890.
5. Hii SI, Hardy L, Crough T, Payne EJ, Grimmett K, et al. (2004) Loss of PKR activity in chronic lymphocytic leukemia. *Int J Cancer* 109: 329–335.
6. Bilanges B, Stokoe D (2007) Mechanisms of translational deregulation in human tumors and therapeutic intervention strategies. *Oncogene* 26: 5973–5990.
7. Holland EC, Sonenberg N, Pandolfi PP, Thomas G (2004) Signaling control of mRNA translation in cancer pathogenesis. *Oncogene* 23: 3138–3144.
8. Hovanessian AG (1989) The double stranded RNA-activated protein kinase induced by interferon: dsRNA-PK. *J Interferon Res* 9: 641–647.
9. Williams BR (2001) Signal integration via PKR. *Sci STKE* 2001: re2.
10. Toth AM, Zhang P, Das S, George CX, Samuel CE (2006) Interferon action and the double-stranded RNA-dependent enzymes ADAR1 adenosine deaminase and PKR protein kinase. *Prog Nucleic Acid Res Mol Biol* 81: 369–434.
11. Kim SH, Forman AP, Mathews MB, Gunnery S (2000) Human breast cancer cells contain elevated levels and activity of the protein kinase, PKR. *Oncogene* 19: 3086–3094.
12. Kim SH, Gunnery S, Choe JK, Mathews MB (2002) Neoplastic progression in melanoma and colon cancer is associated with increased expression and activity of the interferon-inducible protein kinase, PKR. *Oncogene* 21: 8741–8748.
13. Schewe DM, Aguirre-Ghisso JA (2009) Inhibition of eIF2alpha dephosphorylation maximizes bortezomib efficiency and eliminates quiescent multiple myeloma cells surviving proteasome inhibitor therapy. *Cancer Res* 69: 1545–1552.
14. Zhu K, Chan W, Heymach J, Wilkinson M, McConkey DJ (2009) Control of HIF-1alpha expression by eIF2 alpha phosphorylation-mediated translational repression. *Cancer Res* 69: 1836–1843.
15. Mounir Z, Krishnamoorthy JL, Robertson GP, Scheuner D, Kaufman RJ, et al. (2009) Tumor suppression by PTEN requires the activation of the PKR-eIF2alpha phosphorylation pathway. *Sci Signal* 2: ra85.
16. Shimada A, Shiota G, Miyata H, Kamahara T, Kawasaki H, et al. (1998) Aberrant expression of double-stranded RNA-dependent protein kinase in hepatocytes of chronic hepatitis and differentiated hepatocellular carcinoma. *Cancer Res* 58: 4434–4438.
17. Vorburger SA, Pataer A, Swisher SG, Hunt KK (2004) Genetically targeted cancer therapy: tumor destruction by PKR activation. *Am J Pharmacogenomics* 4: 189–198.
18. Pataer A, Vorburger SA, Barber GN, Chada S, Mhashilkar AM, et al. (2002) Adenoviral transfer of the melanoma differentiation-associated gene 7 (mda7)

- induces apoptosis of lung cancer cells via up-regulation of the double-stranded RNA-dependent protein kinase (PKR). *Cancer Res* 62: 2239–2243.
19. D'Acquisto F, Ghosh S (2001) PACT and PKR: turning on NF-kappa B in the absence of virus. *Sci STKE* 2001: re1.
 20. Hu W, Hofstetter W, Wei X, Guo W, Zhou Y, et al. (2009) Double-stranded RNA-dependent protein kinase-dependent apoptosis induction by a novel small compound. *J Pharmacol Exp Ther* 328: 866–872.
 21. Trisciuglio D, Uranchimeg B, Cardellina JH, Meragelman TL, Matsunaga S, et al. (2008) Induction of apoptosis in human cancer cells by candidaspongolide, a novel sponge polyketide. *J Natl Cancer Inst* 100: 1233–1246.
 22. Travis WD, Garg K, Franklin WA, Wistuba II, Sabloff B, et al. (2006) Bronchioloalveolar carcinoma and lung adenocarcinoma: the clinical importance and research relevance of the 2004 World Health Organization pathologic criteria. *J Thorac Oncol* 1: S13–19.
 23. Zhou YH, Hess KR, Liu L, Linskey ME, Yung WK (2005) Modeling prognosis for patients with malignant astrocytic gliomas: quantifying the expression of multiple genetic markers and clinical variables. *Neuro Oncol* 7: 485–494.

Published in final edited form as:

Methods Mol Biol. 2012 ; 818: 217–226. doi:10.1007/978-1-61779-418-6_15.

Analysis of Protein–Protein Interaction Using ProteinChip Array-Based SELDI-TOF Mass Spectrometry

Gitanjali Jayachandran, Jack A. Roth, and Lin Ji

Abstract

Protein–protein interactions are key elements in the assembly of cellular regulatory and signaling protein complexes that integrate and transmit signals and information in controlling and regulating various cellular processes and functions. Many conventional methods of studying protein–protein interaction, such as the immuno-precipitation and immuno-blotting assay and the affinity-column pull-down and chromatographic analysis, are very time-consuming and labor intensive and lack accuracy and sensitivity. We have developed a simple, rapid, and sensitive assay using a ProteinChip array and SELDI-TOF mass spectrometry to analyze protein–protein interactions and map the crucial elements that are directly involved in these interactions. First, a purified “bait” protein or a synthetic peptide of interest is immobilized onto the pre-activated surface of a PS10 or PS20 ProteinChip and the unoccupied surfaces on the chip are protected by application of a layer ethanolamine to prevent them from binding to other non-interactive proteins. Then, the target-containing cellular protein lysate or synthetic peptide containing the predicted amino acid sequence of protein–interaction motif is applied to the protected array with immobilized bait protein/ peptide. The nonspecific proteins/peptides are washed off under various stringent conditions and only the proteins specifically interacting with the bait protein/peptide remain on the chip. Last, the captured interacting protein/peptide complexes are then analyzed by SELDI-TOF mass spectrometry and their identities are confirmed by their predicted distinctive masses. This method can be used to unambiguously detect the specific protein–protein interaction of known proteins/peptides, to easily identify potential cellular targets of proteins of interest, and to accurately analyze and map the structural elements of a given protein and its target proteins using synthetic peptides with the predicted potential protein interaction motifs.

Keywords

SELDI-TOF-MS; ProteinChip; Peptide interactions; SEND-ID; Fus1; Apaf1

1. Introduction

Signal transduction events in eukaryotic cells involve the reversible assembly of large multi-protein complexes which integrate and transmit the information that controls various cellular processes such as ion fluxes, cytoskeletal rearrangements, gene expression, cell cycle progression, and apoptosis (1, 2). Protein–protein interactions are key elements in the assembly of functional cellular regulatory and signaling protein complexes. Many proteins involved in intracellular signaling contain multiple distinct sequence modules that direct their constitutive and signal-regulated interaction with other proteins in a signaling network (3, 4). These interaction domains can target proteins to a specific subcellular location, provide a means for recognition of protein post-translational modifications such phosphorylation, mediate the formation of multi-protein signaling complexes, maintain

functional conformations, and control substrate specificity of enzymes (5, 6). Some of these interactions are mediated by structurally conserved protein domains which recognize specific short peptide motifs such as the well characterized Src-homology SH2 and SH3 domains and the phospho-tyrosine-binding PTB domains (7) in protein tyrosine kinases (PTKs). The most recently identified PDZ domains are modular protein-binding domains that can bind to specific recognition sequences at the C-termini of unrelated proteins or dimerize with other PDZ domains or bind to internal peptide motifs to create networks associated with the plasma membrane (8, 9). Hence, deciphering protein–protein interaction cascades is essential for understanding cellular functions of proteins.

Analysis of protein–protein interaction and determination of the precise mechanism and communication among key components in an interactive protein complex such as apoptosome is a very complicated and time-consuming process. The conventional methods currently used to screen potential interacting protein partners, such as the yeast two hybrid assay or phage display systems, are notorious in generating excessive false positives. The Tandem Affinity Purification (TAP) method developed at EMBL (Heidelberg, Germany) has been shown to be a powerful tool for capturing and analyzing cellular proteins potentially interacting with each other under physiological conditions without prior knowledge of the protein composition, activity, or function (10). The TAP assay when combined with mass spectrometry analysis allows the identification of cellular protein targets interacting with a given protein. However, this process is very complex, needs to clone the gene of interest in the TAP-tagged vectors, and requires stringent and lengthy purification efforts (10). Moreover, the TAP system requires validation of targets by means of classical co-immunoprecipitation/immunoblotting experiments and/or gel filtration chromatography. The biochemical approach with FPLC or HPLC for studying protein–protein interaction requires not only expensive equipment, but also highly purified proteins and substantial expertise of the user. To circumvent these operational difficulties, a rapid and sensitive approach is needed for accurately and effectively analyzing protein–protein interaction. Mass spectrometry can serve as a powerful and sensitive tool to attain that goal (11).

We have developed a simple, rapid, and sensitive assay using a ProteinChip array and SELDI-TOF mass spectrometry to analyze protein–protein interactions and map the crucial elements that are directly involved in these interactions. First, a purified “bait” protein or a synthetic peptide of interest is immobilized onto the pre-activated surface of a ProteinChip array and the unoccupied surfaces on the array are protected by application of ethanolamine to prevent them from binding to other non-interactive proteins. Then, the target-containing cellular protein lysate or synthetic peptide containing the predicted amino acid sequence of protein-interaction motif is applied to the protected array with immobilized bait protein/peptide. The nonspecific proteins/peptides are washed off under various stringent conditions and only the proteins specifically interacting with the bait protein/peptide remain on the chip. Last, the captured interacting protein/peptide complexes are then analyzed by SELDI-TOF mass spectrometry and their identities are confirmed by their predicted distinctive masses. This method can be used to unambiguously detect the specific protein–protein interaction of known proteins/peptides, to easily identify potential cellular targets of proteins of interest, and to accurately analyze and map the structural elements of a given protein and its target proteins using synthetic peptides with the predicted potential protein interaction motifs. This simplified assay system with ProteinChip array-based SELDI-TOF-MS platform can also ideally be used in the confirmatory studies following exploratory studies with the yeast two-hybrid system, the TAP-tag assay, and the computer-aided protein interaction modeling (see Note 1). Several databases and bioinformatics tools with a multitude of algorithms, such as BOND (Biomolecular Object Network Databank), PIP (Potential Interactions of Proteins) (12), and PDB (Protein Data Bank), are currently

available for the prediction and visualization of interacting protein partners. “Interweaver” is one other versatile program developed by the Institute for InfoComm Research in Singapore that uses BIND, DIP (Database of Interacting proteins) and PDB collectively for generating experimental data. The hit candidates obtained from these databases can be applied in this SELDI-TOF-based protocol to confirm not just direct protein interactions but also the exact interacting motifs of the individual protein partners.

2. Materials

2.1. Protein Chips

Several ProteinChip arrays with chemically modified surfaces (pre-activated) that form covalent bonds with free amine groups are available from Bio-Rad Laboratories (Hercules, CA) (see Note 2). They are developed for diverse biological applications including biomarker discovery, protein profiling, protein–protein interaction studies, peptide mapping for protein ID, immunoassays, and receptor–ligand binding studies. These arrays have eight 2-mm diameter spots (A–H format) that correlate with the spacing of wells in a single column of a standard 96-well microplate and are therefore amenable for high-throughput applications in varied robotics. Here, we describe two types of arrays that are particularly amenable to covalently immobilize biomolecules for subsequent capture of targeted proteins from complex biological samples. The arrays differ in their surface chemistry and hence both should be tested to determine the most suitable array for the application envisioned. Other considerations include lower non-specific binding and higher sensitivity.

1. PS10: The pre-activated surface is composed of carbonyl diim-idazole moities to capture amine groups on the protein.
2. PS20: The pre-activated surface is composed of epoxy moities to capture amine groups on the protein.

2.2. Reagents

1. EAM (energy absorbing molecule): CHCA (α -Cyano-4-hydroxycinnamic acid) was purchased from Ciphergen Biosystems (Freemont, CA). These molecules can now be procured from Bio-Rad Laboratories (Hercules, CA).
2. Molecular weight standards (All-in-One Peptide) were purchased from Ciphergen Biosystems (Freemont, CA). They can now be procured from BioRad Laboratories (Hercules, CA).
3. Ethanolamine was purchased from Sigma (St. Louis, MO). Ethanolamine (ETA), also called 2-aminoethanol or mono-ethanolamine (MEA), is an organic chemical compound that is both a primary amine (due to an amino group in its molecule) and a primary alcohol (due to a hydroxyl group).

2.3. Peptide Synthesis

The peptides used in this study were formulated in the Peptide Synthesis Facility at The University of Texas M. D. Anderson Cancer Center.

¹For the characterization of protein-interacting motifs, this technique requires prior knowledge of candidate molecules to be tested and hence cannot function as a screening strategy. It can be useful for validating and confirming the observation and knowledge obtained from screening procedures or database searches.

²This study describes the use of SELDI-TOF based proteinchip arrays to capture interacting partners after covalent immobilization of bait protein/peptide molecules onto pre-activated surfaces. According to the manufacturer, these arrays are pre-activated with carbonyldiimidazole that have a high affinity toward amino groups. Hence, the amino groups in the peptides applied onto the spots form durable covalent bonds with carbonyldiimidazole already present on the arrays.

1. FUS1: KLRRVHKNLIPQGIVKLDHER (2,418 Da).
2. Stearated FUS1: Stearate-KLRRVHKNLIPQGIVKLDHER (2,767 Da).
3. Mutant FUS1: KREHLRKNRPQPGPKPREDHR (2,386 Da).
4. Apaf1: LGILYILQTLE (1,272 Da).

3. Methods

A schematic representation of the overall methodology is depicted in Fig. 1. PS10 arrays are processed as described by Liu and coworkers (13) (see Note 3).

1. Apply 10 μ l (1 ng/ μ l) of bait protein or peptide to individual spots on PS10 chips as bait molecules. The arrays are incubated at room temperature in a humidified chamber for 1 h.
2. Add 10 μ l of 1 M ethanolamine onto each spot of the array to block the unoccupied functional surface and incubate at room temperature for 30 min.
3. Wash individual spots three times with (10 μ l) of 1 \times PBS, pH 7.5, containing 0.25% Triton X100 (see Note 4).
4. Apply the second target protein or peptide (10 μ l: concentration to be determined empirically) onto the spots containing the immobilized bait protein/peptide and incubated in a humidity chamber for 5–8 h at room temperature or overnight at 4°C.
5. Wash the captured targets on each spot three times in (10 μ l) of PBS, pH 7.5, containing 0.25% Triton X100 (see Note 4).
6. Quickly wash each spot two times in distilled water without detergent and air-dry the surface.
7. Add 1 μ l of 25 \times diluted EAM solution (CHCA) onto each spot and air-dry.
8. Acquire mass spectrum using the ProteinChip reader.
9. The molecular mass of the resultant peptide peaks are analyzed and confirmed by externally calibrating the spectra with All-in-One peptide standards with pre-determined molecular weights (Bio-Rad Laboratories, Hercules, CA).

We used this method to study the molecular events in the mitochondria-dependent intrinsic apoptosis pathway mediated by the tumor suppressor FUS1-Apaf-1 protein–protein interaction in lung cancer cells. One of the FUS1-mediated tumor suppressing activities is its ability to induce apoptosis when ectopically expressed by wt-FUS1 gene transfer in FUS1-deficient tumor cells in vitro and in vivo (14, 15). However, the exact molecular mechanism in FUS1-induced apoptosis is unknown. To determine the mechanism of the FUS1-mediated tumor suppression and apoptosis induction, we carried out immuno-precipitations using rabbit anti-FUS1 polyclonal antibodies to pull down FUS1 and its interacting cellular

³Akin to other mass spectrometry-based proteomic techniques, crude samples are not amenable to this procedure. Quality of the input protein sample determines the quality of the data generated with it. A high degree of purity in the protein/peptide samples loaded onto arrays is desirable to generate best results and avoid ambiguous and erroneous data. The best results are obtained with pure synthetic peptides. In our hands, partially purified protein samples did work to a considerable extent, although they did not generate spectacular data. However, it can be used for partially purified over-expressed protein candidates. Liu and coworkers (16) used this elegant technique to determine the interaction between calbindin-D_{28k} and caspase 3 in their study of glucocorticoid-induced apoptosis in osteocytes and osteoblasts. Their study provides a real-world example of application of this technique to decipher meaningful molecular interactions.

⁴Stringency of the washes (amount of detergent used in the wash buffer) should be experimentally determined for each project based on the sensitivity the assay and specificity of the binding involved.

protein partners in crude protein lysates prepared from FUS1-transfected lung cancer cells. We identified one of the potential cellular targets of FUS1 to be the Apaf-1 protein, which has been extensively studied and implicated to be a major component in the apoptosome found in the intrinsic apoptosis pathway (16). We applied this technique to confirm the FUS1-Apaf-1 protein interaction and identify the interacting motifs between two proteins. A computer-aided prediction of the functional motifs in FUS1 and Apaf1 protein sequence revealed a Class I and Class II PDZ protein binding motif in FUS1 and Apaf-1 proteins, respectively. We synthesized peptides containing wild-type or mutated amino acid sequences of the predicted PDZ motifs in both proteins. As demonstrated in Fig. 2, we alternatively used the peptide derived from the PDZ domain of Apaf1 protein or from the PDZ or other functional motifs of FUS1 protein as a bait to test against different peptides derived from both proteins with a wild-type or a mutated amino acid sequence within their PDZ motifs, using PS10 array (see Note 5) by SELDI-TOF-MS analysis. The specific interaction between the FUS1 and Apaf-1 proteins is clearly demonstrated by the interaction between the peptides derived from wild type amino acid sequences containing the PDZ protein-binding motifs from both proteins. However, no interaction in the non-PDZ sequence containing peptide and the mutated peptides can be detected (Fig. 2). The other attractive feature of this technique is the sensitivity of detection. As demonstrated in Fig. 3, even a very low concentration of peptides and their interactions can be detected. Protein/peptide quantity as low as 10 ng can easily be detected using this method with several modifications and different arrays.

Acknowledgments

This work was partially supported by grants from NIH/NCI SPORE P50CA070907, RO1CA116322, DOD PROSPECT W81XWH-0710306; and the M. D. Anderson Cancer Center Support Core Grant (CA16672) for using the Peptide Synthesis Facility to synthesize all the peptides used in this study.

References

1. Yaffe MB, Cantley LC. Signal transduction. Grabbing phosphoproteins. *Nature*. 1999; 402:30–31. [PubMed: 10573413]
2. Yaffe MB, Smerdon SJ. PhosphoSerine/threonine binding domains: you can't pSERious? *Structure*. 2001; 9:R33–R38. [PubMed: 11286893]
3. Schlessinger J. A solid base for assaying protein kinase activity. *Nat Biotechnol*. 2002; 20:232–233. [PubMed: 11875418]
4. Schlessinger J, Lemmon MA. SH2 and PTB domains in tyrosine kinase signaling. *Sci STKE*. 2003; 2003:RE12. [PubMed: 12865499]
5. Pawson T, Nash P. Protein-protein interactions define specificity in signal transduction. *Genes Develop*. 2000; 14:1027–1047. [PubMed: 10809663]
6. Pawson T, Nash P. Assembly of cell regulatory systems through protein interaction domains. *Science*. 2003; 300:445–452. [PubMed: 12702867]
7. Fanning AS, Anderson JM. Protein modules as organizers of membrane structure. *Curr Opin Cell Biol*. 1999; 11:432–439. [PubMed: 10449334]
8. Fanning AS, Anderson JM. PDZ domains and the formation of protein networks at the plasma membrane. *Curr Topics Microbiol Immunol*. 1998; 228:209–233.
9. Fanning AS, Anderson JM. Protein modules as organizers of membrane structure. *Curr Opin Cell Biol*. 1999; 11:432–439. [PubMed: 10449334]

⁵This procedure can also be accomplished using another proteinchip array with a slightly different chemistry, PS20. It can also be performed using other compatible blocking agents between the two protein-binding steps. As suggested by the manufacturer, Tris-HCl or Glycine (0.1–0.5 M), pH 8.0 can also function as a blocking vehicle.

10. Rigaut G, Shevchenko A, Rutz B, Wilm M, Mann M, Séraphin B. A generic protein purification method for protein complex characterization and proteome exploration. *Nat Biotechnol.* 1999; 17:1030–1032. [PubMed: 10504710]
11. Wilkins MR, Gasteiger E, Gooley AA, Herbert BR, Molloy MP, Binz PA, Ou K, Sanchez JC, Bairoch A, Williams KL, Hochstrasser DF. High-throughput mass spectrometric discovery of protein post-translational modifications. *J Mol Biol.* 1999; 289:645–657. [PubMed: 10356335]
12. Jonsson PF, Cavanna T, Zicha D, Bates PA. Cluster analysis of networks generated through homology: automatic identification of important protein communities involved in cancer metastasis. *BMC Bioinformatics.* 2006; 7:2–14. [PubMed: 16398927]
13. Liu Y, Porta A, Peng X, Gengaro K, Cunningham EB, Li H, Dominguez LA, Bellido T, Christakos S. Prevention of glucocorticoid-induced apoptosis in osteocytes and osteoblasts by calbindin-D-28k. *J Bone Miner Res.* 2004; 19:479–490. [PubMed: 15040837]
14. Ito I, Ji L, Tanaka F, Saito Y, Gopalan B, Branch CD, Xu K, Atkinson EN, Bekele BN, Stephens LC, Minna JD, Roth JA, Ramesh R. Liposomal vector mediated delivery of the 3p *FUS1* gene demonstrates potent antitumor activity against human lung cancer in vivo. *Cancer Gene Ther.* 2004; 11:733–739. [PubMed: 15486560]
15. Kondo M, Ji L, Kamibayashi C, Tomizawa Y, Randle D, Sekido Y, Yokota J, Kashuba V, Zabarovsky E, Kuzmin I, Lerman M, Roth J, Minna JD. Overexpression of candidate tumor suppressor gene *FUS1* isolated from the 3p21.3 homozygous deletion region leads to G1 arrest and growth inhibition of lung cancer cells. *Oncogene.* 2001; 20:6258–6262. [PubMed: 11593436]
16. Liu X, Miller CW, Koeffler PH, Berk AJ. The p53 activation domain binds the TATA box-binding polypeptide in Holo-TFII-D, and a neighboring p53 domain inhibits transcription. *Cell.* 1992; 13:3291–3300.

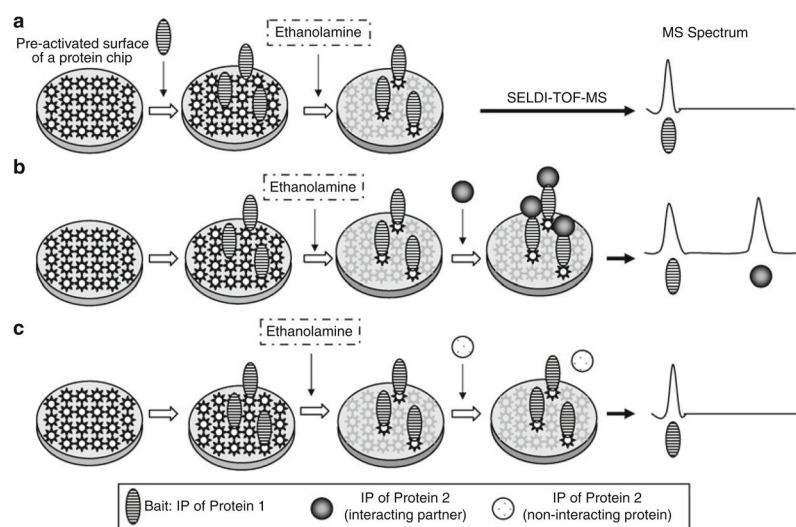
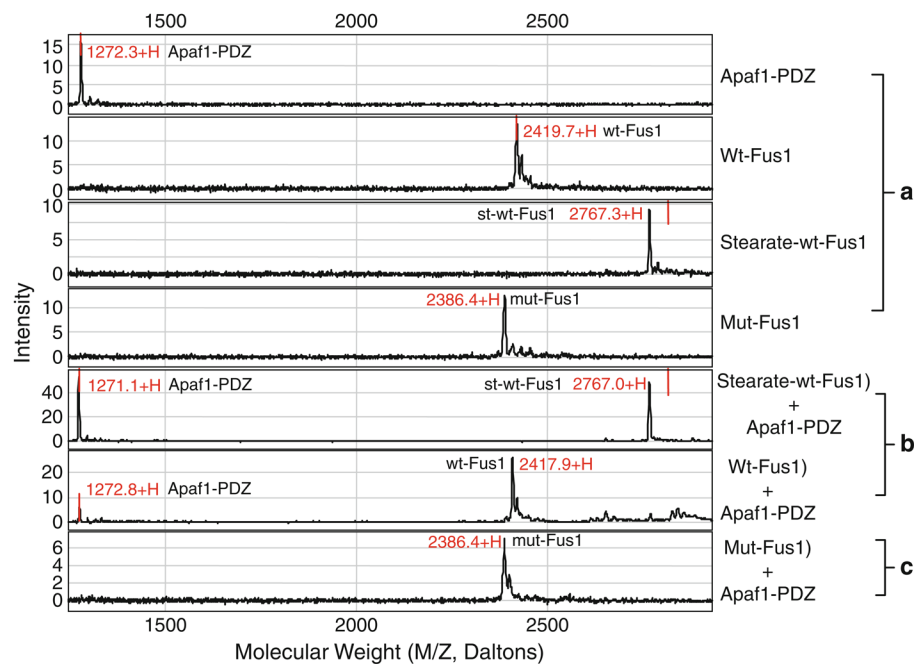


Fig. 1. Schematic presentation of analysis of the protein–protein interaction by an ethanolamine protection on a ProteinChip array with SELDI-TOF-MS. **(a)** a single peak will be detected in the mass spectrum when a single protein/peptide is immobilized onto the array surface; **(b)** two peaks will be detected when the target protein/peptide specifically interacts with the bait; and **(c)** failure of the second peak to show up in the mass spectrum data when the protein/peptide applied subsequently does not interact with the bait protein/peptide.

**Fig. 2.**

Analysis of Fus1-Apaf-1 interaction using synthetic peptides designed from predicted protein interaction motifs by an ethanolamine protection assay on a ProteinChip array with SELDI-MS. The specific interaction of the Fus1 PDZ domain with Apaf-1 c-terminal peptide was detected as indicated by accurate mass of each peptide and by comparison with negative mutant and nonspecific control peptides. **(a)** Panels show individual peaks of various Fus1 or Apaf1 peptides when single peptides were loaded onto proteinchip arrays; **(b)** two distinctive peaks are detected only when the peptides specifically interact with each other; and **(c)** when a mutation is introduced in the PDZ binding motif of Fus1, no Apaf1 peptide peak appears in the spectrum.

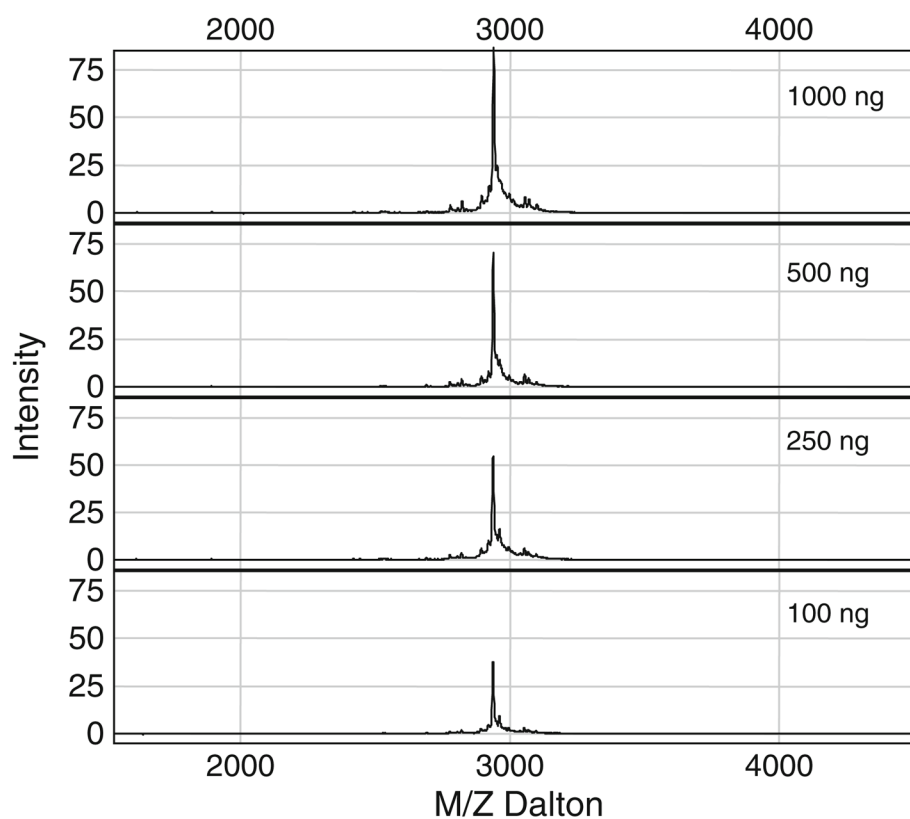


Fig. 3. Quantification of peptide bound to the surface and determination of detection sensitivity on PS10 ProteinChip array by SELDI-TOF-MS. A serial dilution of known concentrations of purified synthetic peptides is loaded onto PS10 chip individually and the amount of peptide is quantified based on the peak intensity.

Published in final edited form as:

Methods Mol Biol. 2012 ; 818: 199–216. doi:10.1007/978-1-61779-418-6_14.

High Throughput Profiling of Serum Phosphoproteins/Peptides Using the SELDI-TOF-MS Platform

Lin Ji, Gitanjali Jayachandran, and Jack A. Roth

Abstract

Protein phosphorylation is a dynamic post-translational modification that plays a critical role in the regulation of a wide spectrum of biological events and cellular functions including signal transduction, gene expression, cell proliferation, and apoptosis. Determination of the sites and magnitudes of protein phosphorylation has been an essential step in the analysis of the control of many biological systems. A high throughput analysis of phosphorylation of proteins would provide a simple, logical, and useful tool for a functional dissection and prediction of biological functions and signaling pathways in association with these important molecular events. We have developed a functional proteomics technique using the ProteinChip array-based SELDI-TOF-MS analysis for high throughput profiling of phosphoproteins/phosphopeptides in human serum for the early detection and diagnosis as well as for the molecular staging of human cancer. The methodology and experimental approach consists of five steps: (1) generation of a total peptide pool of serum proteins by a global trypsin digestion; (2) rapid isolation of phosphopeptides from the total serum peptide pool by an affinity selection, purification, and enrichment using a novel automated micro-bioprocessing system with phospho-antibody-conjugated paramagnetic beads and a hybrid magnet plate; (3) high throughput phosphopeptide analysis on ProteinChip arrays by automated SELDI-TOF-MS; and (4) bioinformatics and statistical methods for data analysis. This method with appropriate modifications may be equally applicable to serine-, threonine- and tyrosine-phosphorylated proteins and for selectively isolating, profiling, and identifying phosphopeptides present in a highly complex phosphor-peptide mixture prepared from various human specimens such as cells, tissue samples, and serum and other body fluids.

Keywords

Phosphoprotein; Phosphopeptide; Phosphoproteome; High throughput Phosphoprotein/Peptide Profiling; ProteinChip Arrays; SELDI-TOF-MS

1. Introduction

The reversible protein phosphorylation is a key regulating switch that controls a wide range of biological functions and activities (1–8). Particularly, phosphorylation of protein kinases plays a critical role in signaling pathways involved in oncogenesis and pathogenesis of various human cancers (6, 8–10). It is clear that the abnormal protein phosphorylation is associated with many major diseases, such as diabetes, rheumatoid arthritis, cardiovascular disease, and cancers (1, 10, 11). Therefore it is vitally important to understand the intracellular signaling events that control protein phosphorylation. Many toxins that are known to cause cancers act by affecting the functions of kinases or phosphatases (5, 9–12). Although protein kinases are now one of the major groups of proteins being targeted by drug discovery and therapeutics programs, the substrates, or proteins that these kinases and

phosphatases affect, are largely unknown. Thus, determination of the sites and magnitudes of protein phosphorylation has been an essential step in the analysis of the control of many biological systems. A high throughput analysis of phosphorylation of serum proteins would provide a simple, logical, and useful tool for a functional diagnosis and prediction of human cancers in association with these important molecular events (5, 8, 9, 13–16). Moreover, the current advanced cancer treatment with anti-angiogenesis agents and protein kinase inhibitors showed profound impact on phosphorylation/dephosphorylation of proteins involved in cell proliferation, apoptosis, angiogenesis, tumor progression, and metastasis in laboratory and in preclinical and clinical settings (10, 11, 17). These phospho-modified proteins are secreted from cells and into the circulation system and are easily available in the serum. Thus, a high-throughput proteomic profiling of phosphopeptides in serum samples exposed to these agents will allow the identification of specific serological biomarkers associated with their biological action (3, 8, 14, 17–20). However, direct determination of phosphorylation of individual proteins in a biological system has been difficult to date (5, 9, 14, 15, 21). It typically requires the purification to homogeneity of the phosphoprotein of interest before analysis and there is currently no method available to study this aspect in detail and consistently. Thus, there has been a substantial need for a more rapid, global, and general method for the analysis of protein phosphorylation in complex protein mixtures (3, 14, 17–20, 22). In addition, a large-scale global phosphoproteome analysis poses challenges in several fronts including to simultaneously isolate and enrich phosphopeptides in several hundred parallel samples without introduction of significant experimental errors and to maintain consistent integrity of proteome among all the samples (2, 3, 14, 15, 18, 19, 21, 23). To address these challenges, we developed an innovative, rapid, and simplified method for serum phosphopeptide separation and enrichment using a one-step affinity capture of phosphopeptides on phospho-antibody-conjugated paramagnetic beads or nanoparticles and separation by a hybrid magnet. This method offers the advantage of automation to avoid human errors and enable a high throughput serum phosphopeptide preparation, which is readily coupled with an automated peptide profiling and analysis on ProteinChip arrays by SELDI-TOF-MS.

2. Materials

2.1. Reagents

1. Phospho-tyrosine antibody: the phospho-tyrosine mouse mAbs (P-Tyr-100) developed by Cell Signaling Technology (Danvers, MA) is a high affinity mouse monoclonal antibody and provides an exceptionally sensitive new tool with increased utility for studying tyrosine phosphorylation and monitoring tyrosine kinase activity in high throughput tyrosine phosphor-protein/peptide analysis. The antibody is supplied in 10 mM sodium HEPES (pH 7.5), 150 mM NaCl, 100 μ BSA and 50% glycerol. Store at -20°C .
2. Surface Activated Dynabeads: the Dynabeads[®] MyOne[™] Tosylactivated (Invitrogen, Carlsbad, CA) are superparamagnetic and uniform polystyrene beads (1.0 μ in diameter) coated with a polyurethane layer. The dynabeads are used for conjugation with phosphor-antibodies and for biomagnetic separation and enrichment of phosphor-antibodycaptured phosphor-peptides.
3. Sequencing Grade Modified Trypsin: Sequencing Grade Modified Trypsin (Promega, Madison, WI) is a porcine trypsin modified by reductive methylation, rendering it resistant to proteolytic digestion (24). Sequencing Grade Modified Trypsin is supplied as lyophilized powder and can be reconstituted in 50 mM acetic acid. The substrate is dissolved in 50 mM Tris-HCl (pH 7.6), 1 mM CaCl_2 , and the enzyme is diluted in 50 mM acetic acid.

4. Human Serum: human clinical serum samples are collected and prepared using approved clinical protocols and standard methods. Serum samples are stored at -80°C .

2.2. Magnetic Plate

A new class of hybrid magnet plates has recently been developed at the Joint Genome Institute and Lawrence Berkeley National Laboratory (JGI/LBNL, Berkeley, CA) for high throughput purification of biological samples for functional genomics and proteomics and for affinity drug screening due to its superior capability of selectively separating proteins and DNA from complex biological mixtures based on a magnetic field (25, 26). These magnet plates are ideal for any process that requires automated bead manipulation in high-density microtiter plates containing sample volumes in a range of 3–300 μl . The novel hybrid magnetic structure combines a permanent magnet with ferromagnetic materials that produces magnetic fields significantly higher than those of any commercially available magnetic plate. More importantly, the fields at a distance of 1 cm above the magnet are more than 1,000-fold stronger than those of the commercial 96-well magnet. This feature allows for more vigorous washing and sample recovering. The second generation 96-well hybrid magnet plate has been designed and constructed for our proteomics platform by physicists and engineers at JGI/LBNL, producing fields well above 10,000.0 G, which allows a more efficient separation of affinity-captured phosphopeptides from crude serum peptide mixtures and thus improves reproducibility and sensitivity of proteomic analysis by reducing processing loss and increasing peptide recovery while retaining a high peptide-proteome integrity. Alternatively, the commercially available 96-well magnetic plates can also be used.

2.3. ProteinChip Arrays and Peptide Standards

1. SEND-ID ProteinChip arrays (Bio-Rad, Hercules, CA) have C18 as a functional group and are used for phosphopeptide profiling and fingerprinting on SELDI-TOF-MS. IMAC30 ProteinChip arrays (Bio-Rad) can also be used for phosphopeptide analysis.
2. All-in-1 Peptide standards (Bio-Rad) for SELDI-TOF-MS is supplied as a dry powder in a glass vial with rubber stopper and is freshly reconstituted in Reconstitution Solution.

2.4. Buffers and Solutions

1. Trypsin Resuspension Buffer: 50 mM acetic acid.
2. Protein Denaturation Solution: 6 M guanidine HCl (or 6–8 M urea), 50 mM Tris-HCl (pH 8), 2–4 mM DTT (or β -mercaptoethanol).
3. 1 \times PBS (phosphate buffered saline) (pH 7.4): 0.26 g $\text{NaH}_2\text{PO}_4 \times \text{H}_2\text{O}$ (MW 137.99), 1.44 g $\text{Na}_2\text{HPO}_4 \times 2\text{H}_2\text{O}$ (MW 177.99), 8.78 g NaCl (MW 58.5). Dissolve in 900 ml dH_2O . Adjust pH to 7.4 and the volume to 1,000 ml.
4. 10 \times Phosphate Buffered Saline (PBS): To prepare 1 L add 80 g sodium chloride (NaCl), 2 g potassium chloride (KCl), 14.4 g sodium phosphate, dibasic (Na_2HPO_4), and 2.4 g potassium phosphate, monobasic (KH_2PO_4) to 1 L dH_2O . Adjust pH to 7.4.
5. Coating buffer: 0.1 M sodium borate buffer (pH 9.5): 6.183 g H_3BO_3 (MW 61.83). Dissolve in 800 ml distilled water. Adjust pH to 9.5 using 5 M NaOH and adjust volume to 1,000 ml with distilled water. The coating buffer is used for pre-washing and coating of Dynabeads.

6. 3 M ammonium sulphate stock solution: 39.6 g (NH₄)₂SO₄ (MW 132.1). Dissolve in 0.1 M sodium borate buffer (pH 9.5), adjust pH to 9.5 and adjust volume to 100 ml.
7. Blocking buffer: PBS pH 7.4 with 0.5% (w/v) BSA and 0.05% Tween 20 in 100 ml PBS. Blocking buffer is used for blocking of all precoated Dynabeads. Do not use this buffer or any buffer containing protein or amino-groups (glycine, Tris etc.) for pre-washing or coating of Dynabeads.
8. Washing buffer: PBS pH 7.4 with 0.1% (w/v) BSA and 0.05% Tween-20 in 100 ml PBS. If a preservative is needed in the coated product, a final concentration of 0.02% (w/v) sodium azide (NaN₃) may be added to washing buffer. This preservative is cytotoxic and must be carefully removed before use by washing.
9. Elution buffers: Any conventional method for protein elution can be used, e.g., 0.1 M citrate pH 3, 0.1 M glycine-HCl pH 2.5, or 0.1 M glycine-NaOH pH 10. All reagents used should be analytical grade. Organic solvent containing 50% acetonitrile (CAN) and 0.1% Trifluoroacetic acid (TFA) (Sigma, St. Louis, MO) is best for the SEND-ID chip.
10. Peptide Standards Reconstitution Solution: 10 mM ammonium acetate, 25% acetonitrile, and 1.25% trifluoroacetic acid.

3. Methods

An important goal of clinical proteomics is to develop sensitive, specific, and robust proteomic platforms to simultaneously measure the human proteome in clinically relevant specimens and to establish protein signature profiles for discriminating between the normal and disease states (27–35). Serum potentially carries a rich archive of histological and biological information and is attracting increasing interest in clinical proteomics. A throughput profiling and an accurate measurement of these serum proteome would serve to improve early detection, diagnosis, and prognosis of cancers and identify new therapeutic targets (27–35). While the importance of studying the serum proteome is obvious, the characterization and analysis of serum proteins, however, are analytically challenging due to their extremely high dynamic range of concentration that spans more than 9–10 orders of magnitude and to the complexity that is composed of biomolecules ranging from large proteins and lipids to small metabolite hormones, peptides, amino acids, and electrolytes. Particularly, the serum protein contents are dominated by a handful of abundant proteins such as albumin, immunoglobulins, haptoglobin, transferrin, and lipoproteins that account for more than 99% of serum protein masses and overwhelmingly shadow the detection of those low abundant but biologically important molecules (30). The reduction of sample complexity and depletion of the level of these abundant proteins are essential first steps for a successful and efficient analysis of the serum proteome. Affinity depletion methods have therefore been developed to remove abundant serum proteins such as albumin and immunoglobulin from serum prior to mass spectrometric analysis (36–38). One of the major pitfalls of these protein depletion methods, however, is that many important low molecular weight proteins or peptides can be concomitantly removed during the sample processing as well (27, 28, 30). Classical methods such as sample fractionation and purification by liquid chromatography with various media, separation by gel electrophoresis, sample desalting and concentration by dialysis, centrifugation, and immuno-precipitation, are often labor-intensive and demand large quantities of sample, suffer from attendant analyte loss due to non-specific binding and dilution effects, and easily introduce experimental errors during multi-task and multi-step sample preparation thus hampering sample quantification and parallel comparison (30, 38, 39). A simple, direct, and efficient mass spectrometric sample preparation and protein/peptide detection in heterogeneous samples is much needed.

In this method, we use innovative antibody-conjugated magnetic beads to specifically capture a subset of biologically important phosphopeptides from the trypsin-digested serum peptide mixtures. The captured peptides are rapidly and efficiently separated and purified by a novel hybrid magnet specifically developed for our proteomic analysis. This method will significantly reduce the complexity of serum proteins, completely eliminate the interference of abundant serum proteins but not affect the integrity of serum proteome, and avoid multi-steps of serum sample fractionation and purification, thus, allowing a high throughput sample preparation, quantification, and parallel comparison. A comparison of technologies and applications between the existing proteomic approaches (Method 1) and our new serum phosphopeptide proteomic platform (Method 2) is shown in Fig. 1.

The ProteinChip-based SELDI technology is currently being used to successfully detect disease-associated proteins in complex biological specimens and has primarily been applied to search for the cancer-relevant biomarkers in clinical serum samples (33, 34, 40–45). These studies emphasize the capability and potential of SELDI for the detection and characterization of differentially expressed proteins or proteomic patterns for detection and prediction of diseases. For serum proteomics to realize its full potential, however, several potential problems and controversy in sensitivity and reproducibility concerning the SELDI profiling approach needs to be addressed (32, 34, 46, 47). Semmes et al. (48) has recently assessed the platform reproducibility using SELDI-mediated serum protein profiling for the detection of prostate cancer and demonstrated the reproducibility of SELDI serum profiling between laboratories and suggested that this approach could provide a reproducible diagnostic assay platform. The most severe limitation for the reproducibility may be a result of loss of the majority of proteins and peptides present in the sample while using SELDI for the protein profiling (27, 28, 43, 48). This in turns leads to the rather low-resolution pattern that represents only a minority of proteins and peptides in the serum. Other limitations for SELDI protein profiling are due to variability such as in instrumental laser desorption energy level and ProteinChip array quality and in sample collection, processing, and storage (32, 49–53). These changes resulted in reproducible changes in serum proteome, and can sometimes overshadow the biological changes in the serum samples (32). In this study, we use SELDI-TOF-MS to profile serum phosphopeptide sub-proteome instead of total proteins and, thus, will partially circumvent these problems and enhance reproducibility because it concentrates all measurements in a small region of low mass peptides within 200–5,000 Da with an extremely high mass resolution by SELDI-TOF-MS spectrometry. Furthermore, because the affinity capture is performed after a complete global proteolytic digestion of serum proteins, phosphopeptides cleaved from larger proteins are equally captured together with other phosphopeptides in the pool and can be easily and precisely detected on MS spectroscopy, therefore circumventing the difficulty and inefficiency of using mass spectrometry such as SELDI or MALDI in detection of large protein species (>30–50 kDa), improve the measurement sensitivity, and gain a higher coverage of serum proteome.

3.1. Preparation of Phospho-Antibody-Conjugated Magnetic Beads

The Tosylactivated Dynabeads® (1–2 µm in diameter) (Invitrogen, Carlsbad, CA) is used as a solid phase to conjugate phosphor-antibodies for a biomagnetic separation of phosphopeptides from the trypsin-digested serum peptide mixtures. The general protocols given below are based on experience with either phosphotyrosine (pY)-specific antibodies (Cell Signaling Technology) or phospho-Serine/Threonine (pS/pT)-specific antibodies (BD Biosciences). When incubating the beads with the ligand of choice, it will be physically adsorbed onto the surface of Dynabeads MyOne™ Tosylactivated first and followed by the formation of covalent bonds over time (see Note 1).

1. The volume of beads used is based on the number of serum samples to be analyzed (1 mg beads per 200 µl serum sample). The conjugation is at a ratio of 40 µg

antibodies to 1 mg beads (w/w). These conditions are for the coating of 1.0 mg phosphor-antibody to 25 mg Dynabeads MyOne™ Tosylactivated (250 µl at 100 mg beads/ml).

2. Resuspend Dynabeads thoroughly by vortexing for 30 min. Transfer 250 µl of beads into a test tube. Place the tube on a magnet (DynaL MPC, Invitrogen) for 2 min or until the beads have migrated to the side of the tube and the liquid is clear.
3. Pipette the supernatant off carefully, leaving beads undisturbed.
4. Remove the test tube from the magnet and resuspend the beads thoroughly in 1 ml of Coating buffer (Solution 5) by vortexing.
5. Repeat steps 3–4.
6. Resuspend the washed beads in 100 µl volume coating buffer and the beads are ready for conjugation with antibodies.
7. Dilute 1.0 mg of antibodies in coating buffer to a total of 600 µl. For optimized coating, the antibodies may be pre-treated and acidified (see Note 2)
8. Add 970 µl of coating buffer to the above washed beads (100) and mix properly.
9. Add the diluted antibodies (1.0 mg/600 µl) to the suspended beads and mix properly.
10. Add 830 µl of 3 M ammonium sulphate stock solution to the antibody/beads mixture to a total of 2,500 µl of conjugation reaction.
11. Incubate the conjugation reaction for 16–24 h at 37°C with slow tilt rotation. Do not let the beads settle during the incubation period (see Note 3 for optimized coating time, temperature, and pH).
12. After incubation, place the tube on the magnet for 2 min, or until the beads have migrated to the side of the tube, and remove the supernatant.
13. Add the same total volume (2,500 µl) of PBS with 0.5% BSA and 0.05% Tween-20 and incubate at 37°C over night.
14. Wash three times with PBS with 0.1% BSA and 0.05% Tween-20, and resuspend the washed conjugates to the desired volume or concentration. The Dynabeads are now coated and ready for use (see Note 4).
15. For storage, the desired preservative, e.g., 0.02% sodium azide may be added and store at 2–8°C. The coated beads can usually be stored for several months at 2–8°C, depending on the stability of your immobilized antibodies.

¹The efficacy of immunomagnetic separation is critically dependant on the specificity and avidity of the antibody or other ligand applied. A concentration of 40 µg antibody/mg Dynabeads is generally optimal for coating. Antibody/protein to be coated directly onto the surface of Dynabeads must be purified, since all proteins will bind to the bead surface. Sugars or stabilizers may disturb the binding and should be removed from the antibody preparation.

²For antibody pre-treatment and acidification, in general, lowering pH to 2.5 for 15 min at room temperature or 1 h at 1–4°C, and then raising the pH to approximately neutral prior to addition of the beads, will increase binding and function of antibodies, but this must be optimized for your specific antibodies.

³The physical adsorption to the bead surface is rapid, while the formation of covalent bonds will need more time. After the recommended 16–24 h at 37°C, a maximal chemical binding is achieved. Coating at 20°C will require an extended incubation time to 48 h and longer to obtain the same degree of chemical binding. At 4°C the chemical binding is very slow (>48 h). Both higher temperatures and a higher pH will speed up the formation of covalent bonds, provided that the antibodies in question are stable and functional under these conditions. Sodium borate buffer pH 9.5 is recommended. Molarities between 0.1 and 0.5 are optimal.

⁴If the presence of BSA will interfere with your downstream application, this protein can be omitted from the buffer. Detergent may similarly be omitted.

3.2. Protease Digestion of Serum Proteins

1. Serum Protein Denaturation: Serum proteins require denaturation and disulfide bond cleavage before enzymatic digestion can go to completion. 200 μ l (10–15 mg of total proteins) of serum is used for each individual assay. Dilute serum sample 1:1 (v/v) in 100 mM NH_4HCO_3 , pH 8.2, in each well of a 96-well plate.
2. Boil for 5 min in a heating-block that fits a 96-well plate. If smaller amounts of protein are to be digested, the recommended conditions given can be scaled down proportionally. However, under no conditions should less than 25 μ l of dissolving agent be used.
3. After denaturation, allow the reaction to cool to room temperature.
4. Protease Digestion: add sequencing grade modified trypsin (Promega) to a final protease:serum proteins ratio of 1:50 (w/w). Incubate at 37°C overnight.
5. Remove a small aliquot and chill the reaction on ice or freeze. Add an inhibitor to the aliquot to terminate the protease activity or precipitate the sample by the addition of TCA to a 10% final concentration.
6. Determine the extent of digestion by subjecting a portion of the digestion products to reverse phase HPLC or SDS-PAGE. If further proteolysis is required, return the reaction tube to 37°C and continue incubating until the desired digestion is obtained.
7. The reaction can be terminated by freezing or by the addition of specific inhibitors (see Note 5).

3.3. Capture, Separation, and Enrichment of Serum Phosphopeptides

1. For affinity capture and enrichment of serum phosphopeptides, wash the phosphor-antibody-conjugated magnetic beads with two volumes of 1 \times PBS three times to remove any unbound antibodies.
2. Resuspend the phosphor-antibody (p-Ab)-beads conjugates in PBS at a desired concentration (1 mg per 200 μ l of serum sample).
3. Transfer the p-Ab/beads conjugates at a ratio of 200 μ l trypsin-digested serum proteins to 1 mg p-Ab/beads into each well of the 96-well plates containing digested serum proteins.
4. Incubate the plate for 1 h at room temperature with gentle shaking.
5. Place the plate on a 96-well magnet plate and allow phosphopeptide-captured beads to settle down.
6. Gently remove the supernatant and the unbound peptides by washing three times with 400 μ l of PBS.
7. The captured phosphor-peptides are then eluted in 15 μ l of elution buffer comprising 50% acetonitrile (CAN) and 0.1% Trifluoroacetic acid (TFA).
8. Place the plate on a 96-well hybrid magnet plate. After the beads settle down, carefully collect the eluted phosphopeptides into a fresh 96-well plate.

⁵Trypsin can also be inactivated by lowering the pH of the reaction to below 4. Trypsin will regain activity as the pH is raised above 4. Reducing the temperature will decrease the digestion rate. Longer incubation periods, up to 24 h, may be required depending on the nature of the protein.

9. All these steps of process are performed automatically using a Biomek-2000 Laboratory Automation Workstation (Beckman, Fullerton, CA).

3.4. Phosphopeptide Profiling on ProteinChip Arrays by SELDI-TOF-MS

The enriched phosphopeptides are further processed automatically using a micro bio-processor (Bio-Rad) and a Biomek-2000 Laboratory Automation Workstation (Beckman, Fullerton, CA) and loaded onto a SEND (Surface Enhanced Neat Desorption) or IMAC proteinchip array purchased from (Bio-Rad). SEND arrays are unique compared to other arrays by having the energy-absorbing molecule (EAM) incorporated into the array chemistry and is added after sample addition. They are best suited for small molecule analysis, which in our case are phosphopeptides. Pooled serum samples are used as quality assurance (QA) controls and samples are randomly loaded onto each ProteinChip array with duplicates. One spot is loaded on each array with peptide standards for peptide mass calibration. The chips are automatically loaded and analyzed by SELDI-TOF-MS spectrometer (Model PSII or new model PCS 4000, Bio-Rad).

1. Add 5 μ l of 0.1% TFA to each spot of a SEND-ID array and then quickly remove.
2. Add 10 μ l of the eluted phosphopeptides onto each spot of the SEND-ID array that is placed in a humidity chamber and incubate for 30 min.
3. Remove samples from the array surface and wash bound phospho-peptides quickly once with 5 μ l of 0.1% TFA.
4. Then add 2 μ l of 25% ACN and 0.1% TFA to each spot. Air-dry.
5. Read arrays with desired and optimized instrumental parameters and settings in a ProteinChip reader, according to manufacturer's instruction.

3.5. Data Processing and Analysis

The SELDI-MS spectral data collected from the mass spectrometer are calibrated and subjected to further analysis using bioinformatics tools and statistical methods developed by Dr. Coombes (52, 54). Advanced proteomic data processing and analysis methodologies and bioinformatics algorithms are needed to address concerns regarding reliability, sensitivity, and reproducibility of peak detection, quantification, and identification in clinical serum proteomics (32). Some advanced methodologies and algorithms for spectral alignment, baseline correction and normalization, peak detection and quantification, and statistical analysis of peaks are also needed for evaluating clinical significance of cancer diagnostic peptides (32, 49–55). These methods will improve the reproducibility of peak quantifications and provide tools for evaluating the variations in this phosphor-peptide proteomics platform and more accurately interpret serum phosphor-peptide profiling results.

To overcome the technology barriers and circumvent the potential problems and limitations facing MS spectrometry-based serum proteomics and as demonstrated in the above serum protein-profiling experiments, we have developed an innovative and integrated functional proteomics technique using the ProteinChip array-based SELDI-MS analysis for a high throughput profiling of phospho-peptides in human serum. To demonstrate the feasibility of this proteomic platform for clinical serum sample processing and analysis, we performed phosphopeptide (phosphor-Tyrosine) proteomic profiling on serum samples from human normal and lung cancer patients in different stages and with different smoking histories. We analyzed three groups of samples: (1) 20 serum samples from lung cancer patients collected by Dr. Roth in the Department of Thoracic & Cardiovascular Surgery (Cancer Group 1, C-G1), (2) 20 lung cancer serum samples collected by Dr. Spitz in the Department of Epidemiology (Cancer Group 2, C-G2), and (3) 20 serum samples from normal controls. Tyrosin-phosphopeptides (pYs) were prepared and selectively isolated from these serum

samples as described in the Subheading 3. The purified pYPs were randomly loaded onto SEND ProteinChip arrays in duplicate. Phosphopeptide MS-spectra and data were analyzed using bioinformatics tools and statistical methods developed by Dr. Coombes (52, 54).

We used wavelets and the mean spectrum for peak detection. Briefly, we first computed the mean of the aligned, baseline-corrected, normalized spectra. We used an undecimated discrete wavelet transform (UDWT) to denoise the mean spectrum by hard thresholding the wavelet coefficients that were less than ten times the standard deviation. Peaks were defined as local maxima in the denoised mean spectrum. Along with the location of each peak, we also recorded an interval that contained the peak by finding the nearest local minimum on either side of the peak. Using this procedure, we detected 622 distinct peaks spanning a m/z range from 50 to 5,500 Da (Fig. 2a). The smallest signal-to-noise ratio (S/N) of any of these peaks was 4.92; the median S/N was 416. In order to quantify the peaks in the individual spectra, we began by locating the time interval containing the peak. We then took the maximum value of the spectrum in that interval and subtracted the three minimum values in the interval to define the peak height. Peak quantification was performed on the aligned, baseline-corrected, normalized spectra. Implicitly, the minimum value was used as a local estimate of the baseline in the interval. Because no smoothing was performed, the peak heights might be slightly biased on the high side. However, this is a reasonable trade-off because it decreases the variance.

Information on the peak locations and heights was further exported from MATLAB and imported to the software program R for statistical analysis. To answer the primary question whether there are any peaks that are different between cancer samples and normal samples, we performed a one-way analysis of variance (ANOVA) using a single factor that takes on three levels (Cancer-G1 Cancer-G2, versus Normal). We performed a separate ANOVA for each of the 622 peaks, using the base-two logarithm of the peak height to try to separate the three sample groups. For each peak, we recorded the p -value from an F -test of the model; small p -values suggest that the peak height is different between at least two of the three groups in the study. In order to account for multiple testing, we modeled the set of p -values using a beta-uniform mixture (BUM) model to estimate the false discovery rate (FDR) (56–59). Setting FDR at 1, 5, and 10%, we found 0, 1, and 2 significant peaks, respectively (Fig. 2b). However, using a BUM analysis after accounting with other technological factors including laser intensity, vacuum chamber pressure, and spot positions on the ProteinChip arrays, we found 1, 15, and 39 significant peaks with FDR = 1, 5, and 10%, respectively (Fig. 2c). The fold changes in intensity detected on MS profiles between the normal and cancer serum samples are plotted in Fig. 2d. Using this phosphopeptide proteomic profiling technology and data analysis we are able to find peaks that significantly differ between the three groups. The data generated from these phosphopeptide profiles are also highly reproducible, as shown by the consistent mass spectra among each sample group (Fig. 3). Differences in sample handling explain some of the peaks that are found to be differentially expressed. Nevertheless, many of the changes can clearly be attributed to differences between normal samples and cancer samples, regardless of who collected them. These pilot experiments clearly demonstrate the feasibility of our serum phosphopeptide proteomic platform in detecting temporal changes of phosphopeptide proteome in clinically relevant serum samples. Our proteomics platform also demonstrated the capability of overcoming and circumventing a number of technological problems and barriers facing the current MS spectrometry-based proteomics technologies, including reduction of proteome complexity, enhancement of specificity and sensitivity of detection of low abundance proteins and peptides, increase of throughput rate of sample process and analysis, and improvement of identification and quantification of specific peptides and proteins on MS profiles and proteomic data processing and analysis.

Acknowledgments

The authors would like to thank Drs. Xifeng Wu and Margaret Spitz for providing lung cancer serum samples for serum phosphopeptide profiling and analysis and Dr. Kevin Coombes for bioinformatics and statistical analysis, at The University of Texas M. D. Anderson Cancer Center, Houston, TX, and David Humphries at Lawrence Berkeley National Laboratory, Oak Land, CA for developing hybrid magnetic plates for serum phosphopeptide enrichment. This work was partially supported by grants from NIH/NCI SPORE P50CA070907, RO1CA116322, and MMHCC U01CA105352; DOD PROSPECT W81XWH-0710306; The University of Texas M. D. Anderson Cancer Center Support Core Grant (CA16672).

References

1. Hunter T. Signaling—2000 and beyond. *Cell*. 2000; 100:113–127. [PubMed: 10647936]
2. Oda Y, Huang K, Cross FR, Cowburn D, Chait BT. Accurate quantitation of protein expression and site-specific phosphorylation. *Proc Natl Acad Sci USA*. 1999; 96:6591–6596. [PubMed: 10359756]
3. Oda Y, Nagasu T, Chait BT. Enrichment analysis of phosphorylated proteins as a tool for probing the phosphoproteome. *Nat Biotechnol*. 2001; 19:379–382. [PubMed: 11283599]
4. Peters EC, Brock A, Ficarro SB. Exploring the phosphoproteome with mass spectrometry. *Mini-Rev Med Chem*. 2004; 4:313–324. [PubMed: 15032677]
5. Johnson SA, Hunter T. Kinomics: methods for deciphering the kinome. *Nat Methods*. 2005; 2:17–25. [PubMed: 15789031]
6. York JD, Hunter T. Signal transduction. Unexpected mediators of protein phosphorylation. *Science*. 2004; 306:2053–2055. [PubMed: 15604398]
7. Johnson SA, Hunter T. Phosphoproteomics finds its timing. *Nat Biotechnol*. 2004; 22:1093–1094. [PubMed: 15340474]
8. Manning G, Whyte DB, Martinez R, Hunter T, Sudarsanam S. The protein kinase complement of the human genome. *Science*. 2002; 298:1912–1934. [PubMed: 12471243]
9. Rush J, Moritz A, Lee KA, Guo A, Goss VL, Speck EJ, et al. Immunoaffinity profiling of tyrosine phosphorylation in cancer cells. *Nat Biotechnol*. 2005; 23:94–101. [PubMed: 15592455]
10. Hunter T. Tyrosine phosphorylation in cell signaling and disease. *Keio J Med*. 2002; 51:61–71. [PubMed: 12125907]
11. Hunter T. The role of tyrosine phosphorylation in cell growth and disease. *Harvey Lectures*. 1998; 94:81–119. [PubMed: 11070953]
12. Alonso A, Sasini J, Bottini N, Friedberg I, Osterman A, et al. Protein tyrosine phosphatases in the human genome. *Cell*. 2004; 117:699–711. [PubMed: 15186772]
13. Hornbeck PV, Chabra I, Kornhauser JM, Skrzypek E, Zhang B. PhosphoSite: A bioinformatics resource dedicated to physiological protein phosphorylation. *Proteomics*. 2004; 4:1551–1561. [PubMed: 15174125]
14. Gerber SA, Rush J, Stemman O, Kirschner MW, Gygi SP. Absolute quantification of proteins and phosphoproteins from cell lysates by tandem MS. *Proc Natl Acad Sci USA*. 2003; 100:6940–6945. [PubMed: 12771378]
15. Steen H, Jeblanathirajah JA, Rush J, Morrice N, Kirschner MW. Phosphorylation analysis by mass spectrometry: myths, facts, and the consequences for qualitative and quantitative measurements. *Mol Cell Proteomics*. 2006; 5:172–181. [PubMed: 16204703]
16. Pan S, Zhang H, Rush J, Eng J, Zhang N, Patterson D, et al. High throughput proteome screening for biomarker detection. *Mol Cell Proteomics*. 2005; 4:182–190. [PubMed: 15637048]
17. Brill LM, Salomon AR, Ficarro SB, Mukherji M, Stettler-Gill M, Peters EC. Robust phosphoproteomic profiling of tyrosine phosphorylation sites from human T cells using immobilized metal affinity chromatography and tandem mass spectrometry. *Anal Chem*. 2004; 76:2763–2772. [PubMed: 15144186]
18. Mann M, Ong SE, Gronborg M, Steen H, Jensen ON, Pandey A. Analysis of protein phosphorylation using mass spectrometry: deciphering the phosphoproteome. *Trends Biotechnol*. 2002; 20:261–268. [PubMed: 12007495]

19. Salomon AR, Ficarro SB, Brill LM, Brinker A, Phung QT, Ericson C, et al. Profiling of tyrosine phosphorylation pathways in human cells using mass spectrometry. *Proc Natl Acad Sci USA*. 2003; 100:443–448. [PubMed: 12522270]
20. Zhou H, Watts JD, Aebersold R. A systematic approach to the analysis of protein phosphorylation. *Nat Biotechnol*. 2001; 19:375–378. [PubMed: 11283598]
21. Zhang H, Zha X, Tan Y, Hornbeck PV, Mastrangelo AJ, Alessi DR, et al. Phosphoprotein analysis using antibodies broadly reactive against phosphorylated motifs. *J Biol Chem*. 2002; 277:39379–39387. [PubMed: 12151408]
22. Rush J, Moritz A, Lee KA, Guo A, Goss VL, Spek EJ, et al. Immunoaffinity profiling of tyrosine phosphorylation in cancer cells. *Nat Biotechnol*. 2005; 23:94–101. [PubMed: 15592455]
23. Mann M. Quantitative proteomics? *Nat Biotechnol*. 1999; 17:954–955. [PubMed: 10504691]
24. Rice RH, Means GE, Brown WD. Stabilization of Bovine Trypsin by Reductive Methylation. *Biochim Biophys Acta*. 1977; 492:316–321. [PubMed: 560214]
25. Elkin H, Kapur T, Humphries D, Pollard M, Nammon N, Hawkins T. Magnetic bead purification of labeled DNA fragments for high throughput capillary electrophoresis sequencing. *Biotechniques*. 2002; 32:1296–1307. [PubMed: 12074160]
26. Humphries, DE.; Pollard, MJ.; Elkin, CJ. High Performance Hybrid Magnetic Structure for Biotechnology Applications. 10/305658 (6954128B2)2002. (Patent)
27. Aebersold R, Rist B, Gygi SP. Quantitative proteome analysis: methods and applications. *Annal New York Acad Sci*. 2000; 919:33–47.
28. Aebersold R, Mann M. Mass spectrometry-based proteomics. *Nature*. 2003; 422:198–207. [PubMed: 12634793]
29. Anderson NL, Matheson AD, Steiner S. Proteomics: applications in basic and applied biology. *Curr Opin Biotechnol*. 2000; 11:408–412. [PubMed: 10975462]
30. Anderson NL, Anderson NG. The human plasma proteome: history, character, and diagnostic prospects. *Mol Cell Proteomics*. 2002; 1:845–867. [PubMed: 12488461]
31. Celis JEG. Proteomics in translational cancer research: Toward an integrated approach. *Cancer Cell*. 2003; 3:9–15. [PubMed: 12559171]
32. Coombes KR, Morris JS, Hu J, Edmonson SR, Baggerly KA. Serum proteomics profiling—a young technology begins to mature. *Nat Biotechnol*. 2005; 23:291–292. [PubMed: 15765078]
33. Petricoin EF, Zoon KC, Kohn EC, Barrett JC, Liotta LA. Clinical proteomics: translating benchside promise into bedside reality. *Nat Rev Drug Discov*. 2002; 1:683–695. [PubMed: 12209149]
34. Petricoin EF, Liotta LA. SELDI-TOF-based serum proteomic pattern diagnostics for early detection of cancer. *Curr Opin Biotechnol*. 2004; 15:24–30. [PubMed: 15102462]
35. Sauer S, Lange BM, Gobom J, Nyarsik L, Seitz H, Lehrach H. Miniaturization in functional genomics and proteomics. *Nat Rev Genet*. 2005; 6:465–476. [PubMed: 15931170]
36. Shrivastava A, von Wronski MA, Sato AK, et al. A distinct strategy to generate high-affinity peptide binders to receptor tyrosine kinases. *Prot Engin, Design Select*. 2005; 18:417–424.
37. Sato AK, Sexton DJ, Morganelli LA, et al. Development of mammalian serum albumin affinity purification media by peptide phage display. *Biotechnol Prog*. 2002; 18:182–192. [PubMed: 11934284]
38. Adkins JN, Varnum SM, Auberry KJ, et al. Toward a human blood serum proteome: analysis by multidimensional separation coupled with mass spectrometry. *Mol Cell Proteomics*. 2002; 1:947–955. [PubMed: 12543931]
39. Chan KC, Lucas DA, Hise DGM, et al. Analysis of the human serum proteome. *Clin Proteomics J*. 2004; 1:101–225.
40. Ransom HW, Varghese RS, Abdel-Hamid M, et al. Analysis of mass spectral serum profiles for biomarker selection. *Bioinformatics*. 2005; 21:4039–4045. [PubMed: 16159919]
41. Veenstra TD, Prieto DA, Conrads TP. Proteomic patterns for early cancer detection. *Drug Discov Today*. 2004; 9:889–897. [PubMed: 15475322]
42. Yu LR, Zhou M, Conrads TP, Veenstra TD. Diagnostic proteomics: serum proteomic patterns for the detection of early stage cancers. *Dis Markers*. 2003; 19:209–218. [PubMed: 15258335]

43. Issaq HJ, Conrads TP, Prieto DA, Tirumalai R, Veenstra TD. SELDI-TOF MS for diagnostic proteomics. *Anal Chem.* 2003; 75:148A–155A.
44. Issaq HJ, Veenstra TD, Conrads TP, Felschow D. The SELDI-TOF MS approach to proteomics: protein profiling and biomarker identification. *Biochem Biophys Res Commun.* 2002; 292:587–592. [PubMed: 11922607]
45. Rosenblatt KP, Bryant-Greenwood P, Killian JK, et al. Serum proteomics in cancer diagnosis and management. *Ann Rev Med.* 2004; 55:97–112. [PubMed: 14746511]
46. Diamandis EP. Analysis of serum proteomic patterns for early cancer diagnosis: drawing attention to potential problems. *J Natl Cancer Inst.* 2004; 96:353–356. [PubMed: 14996856]
47. Koomen JM, Li D, Xiao LC, et al. Direct tandem mass spectrometry reveals limitations in protein profiling experiments for plasma biomarker discovery. *J Prot Res.* 2005; 4:972–981.
48. Semmes OJ, Feng Z, Adam BL, et al. Evaluation of serum protein profiling by surface-enhanced laser desorption/ionization time-of-flight mass spectrometry for the detection of prostate cancer: I. Assessment of platform reproducibility. *Clin Chem.* 2005; 51:102–112. [PubMed: 15613711]
49. Baggerly KA, Morris JS, Wang J, Gold D, Xiao LC, Coombes KR. A comprehensive approach to the analysis of matrix-assisted laser desorption/ionization-time of flight proteomics spectra from serum samples. *Proteomics.* 2003; 3:1667–1672. [PubMed: 12973722]
50. Baggerly KA, Morris JS, Coombes KR. Reproducibility of SELDI-TOF protein patterns in serum: comparing datasets from different experiments. *Bioinformatics.* 2004; 20:777–785. [PubMed: 14751995]
51. Baggerly KA, Morris JS, Edmonson SR, Coombes KR. Signal in noise: evaluating reported reproducibility of serum proteomic tests for ovarian cancer. *J Natl Cancer Inst.* 2005; 97:307–309. [PubMed: 15713966]
52. Coombes KR, Tsavachidis S, Morris JS, Baggerly KA, Hung MC, Kuerer HM. Improved peak detection and quantification of mass spectrometry data acquired from surface-enhanced laser desorption and ionization by denoising spectra with the undecimated discrete wavelet transform. *Proteomics.* 2005; 5:4107–4117. [PubMed: 16254928]
53. Coombes KR. Analysis of mass spectrometry profiles of the serum proteome. *Clin Chem.* 2005; 51:1–2. [PubMed: 15613701]
54. Coombes KR, Fritsche HA Jr, Clarke C, et al. Quality control and peak finding for proteomics data collected from nipple aspirate fluid by surface-enhanced laser desorption and ionization. *Clin Chem.* 2003; 49:1615–1623. [PubMed: 14500586]
55. Baggerly KA, Edmonson SR, Morris JS, Coombes KR. High-resolution serum proteomic patterns for ovarian cancer detection. *Endocr Relat Cancer.* 2004; 11:583–584. [PubMed: 15613439]
56. Benjamini Y, Drai D, Elmer G, Kafkafi N, Golani I. Controlling the false discovery rate in behavior genetics research. *Behav Brain Res.* 2001; 125:279–284. [PubMed: 11682119]
57. Morris JS, Coombes KR, Koomen J, Baggerly KA, Kobayashi R. Feature extraction and quantification for mass spectrometry in biomedical applications using the mean spectrum. *Bioinformatics.* 2005; 21:1764–1775. [PubMed: 15673564]
58. Pounds S, Cheng C. Improving false discovery rate estimation. *Bioinformatics.* 2004; 20:1737–1745. [PubMed: 14988112]
59. Pounds S, Cheng C. Sample size determination for the false discovery rate. *Bioinformatics.* 2005; 21:4263–4271. [PubMed: 16204346]

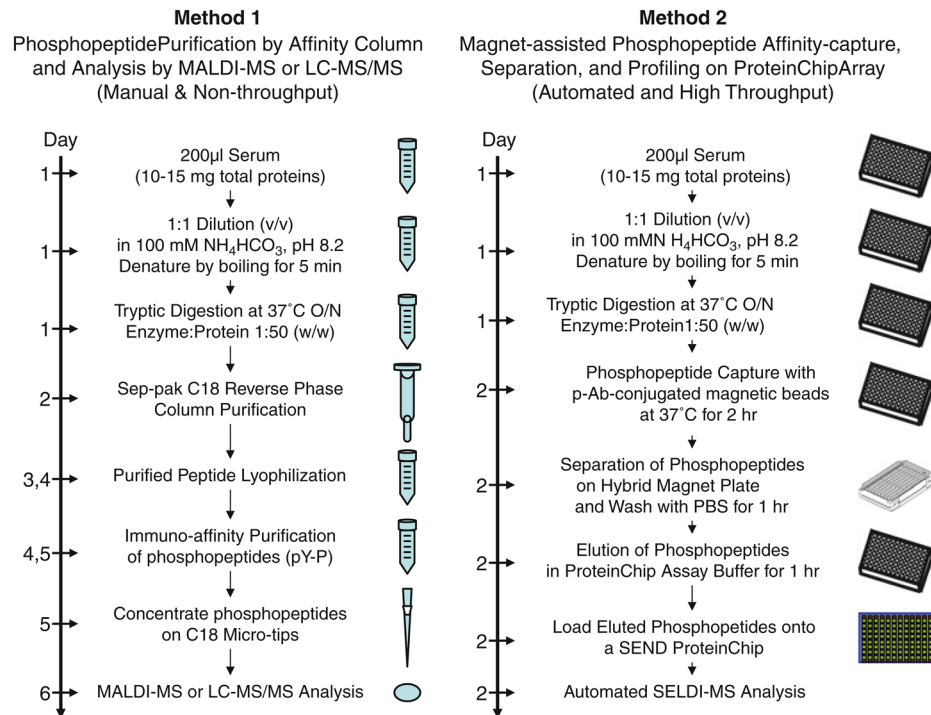
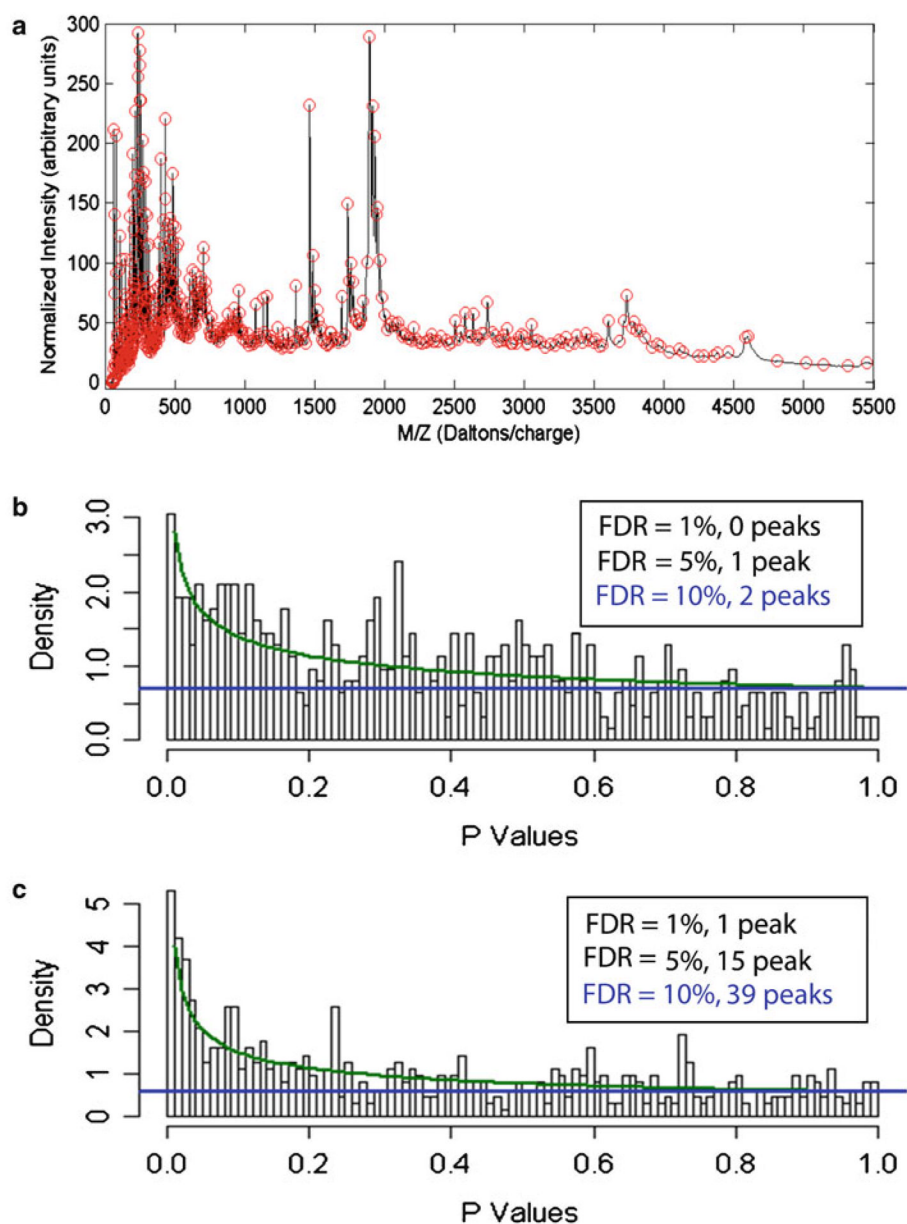


Fig. 1. Comparison of methods and platforms for phosphoprotein/phosphopeptide proteomics analysis by mass spectrometry. Method 1, the conventional phosphopeptide purification by affinity column and analysis by MALDI-MS or LC-MS/MS. Method 2, the magnet-assisted phosphopeptide affinity-capture, separation, enrichment, and profiling on ProteinChip arrays by SELDI-TOF-MS.



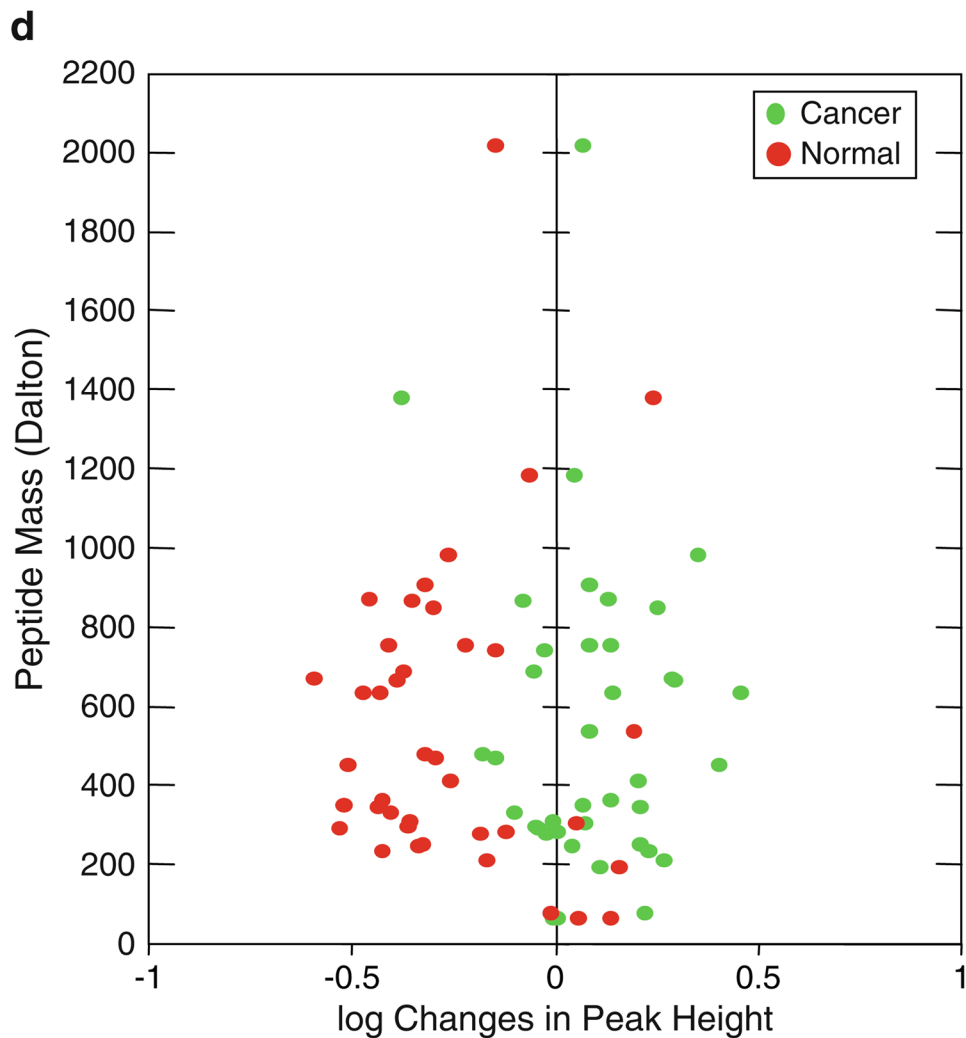


Fig. 2. Detection, quantification, and statistical analysis of specific human serum phosphopeptide peaks determined by ProteinChip array-based SELDI-TOF-MS. **(a)** Phosphopeptide peaks are detected using wavelets and determined by the mean spectrum of the aligned, base-line-corrected, and normalized spectra. More than 600 phospho-tyrosine peptide peaks are detected from the magnet-assisted and affinity-enriched human serum phosphopeptide pools. Statistical analysis of phosphor-peptide modulations between the normal and lung cancer serum samples using a beta-uniform mixture (BUM) Fig. 2. (continued) model to estimate the false discovery rate (FDR). **(b)** BUM analysis of peaks that are different between the three groups of samples using one-way NOVA, and **(c)** BUM analysis of p -values from an F -test of the significance of group effects after accounting for other technological factors, including laser intensity, pressure, and spot position. Peaks with significant changes ($p < 0.05$) between the normal and the cancer groups are determined at FDR = 1, 5, and 10%, respectively. **(d)** Scattered plot of 39 pairs of phosphor-tyrosine peptides with significant changes between the normal and lung cancer serum samples, as determined by BUM in **c**.

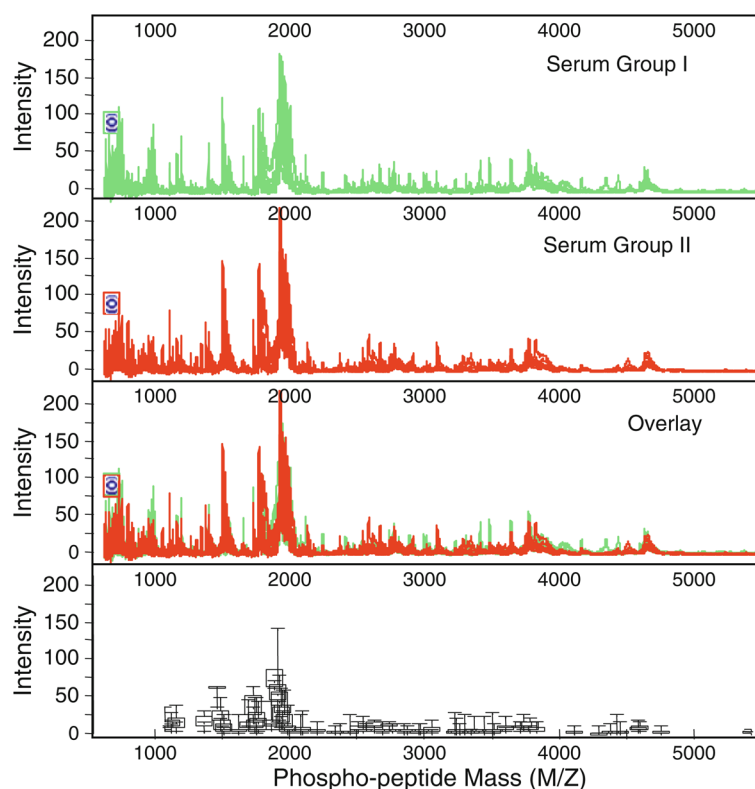


Fig. 3. Profiles and analysis of tyrosine-specific phosphopeptides in normal and lung cancer serum samples on SEND ProteinChip arrays by SELDI-TOF-MS. The variations of phosphopeptide levels as defined by peak intensity on the mass spectra among serum samples are shown by the overlapping spectra (*top three panels*) and by the *box plots* (*bottom panel*) with *error bars* indicating the ranges of each paired peptide peak among three serum sample groups.

Elevated expression of eukaryotic translation initiation factor 4E is associated with proliferation, invasion and acquired resistance to erlotinib in lung cancer

Yikun Li,¹ Songqing Fan,^{1,2} Junghui Koo,¹ Ping Yue,¹ Zhuo (Georgia) Chen,¹ Taofeek K. Owonikoko,¹ Suresh S. Ramalingam,¹ Fadlo R. Khuri¹ and Shi-Yong Sun^{1,*}

¹Department of Hematology and Medical Oncology; Emory University School of Medicine and Winship Cancer Institute; Atlanta, GA USA; ²Department of Pathology; The Second Xiang-Ya Hospital; Central South University; Changsha; Hunan, China

Keywords: eIF4E, proliferation, invasion, erlotinib, resistance, lung cancer

Eukaryotic translation initiation factor 4E (eIF4E) is the rate-limiting factor for cap-dependent translation initiation, which is known to regulate oncogenesis. Elevated eIF4E and its negative impact on prognosis in human non-small cell lung cancer (NSCLC) have been reported previously. However, its potential as a therapeutic target and role in regulation of sensitivity to EGFR inhibitors is an area of ongoing investigations. In this study, we detected increased levels of eIF4E in 16 human NSCLC cell lines compared with their normal bronchial epithelial cells. Consistently, human tissue array analysis showed that eIF4E expression was significantly higher in human NSCLC tissues than normal tissues. Inhibition of eIF4E using eIF4E siRNA inhibited the growth and invasion of NSCLC cells. These data suggest that eIF4E overexpression plays a crucial role in positive regulation of the growth and invasion of NSCLC cells. By proteomics, we found that eIF4E levels were elevated in erlotinib-resistant cell lines compared with the sensitive parental cell line. In agreement, assembly of the eIF4F cap complex and several oncogenic proteins regulated by the cap-dependent translation mechanism, were also increased in erlotinib-resistant cells. Thus, erlotinib-resistant cells exhibit elevated eIF4E expression and cap-dependent translation. Inhibition of eIF4F with different means (e.g., gene knockdown) downregulated c-Met expression and partially restored cell sensitivity to erlotinib, suggesting that elevated eIF4E contributes to development of erlotinib resistance, likely through positive regulation of c-Met expression. Taken together, we suggest that elevated eIF4E in NSCLC cells is associated with proliferation, invasion and acquired erlotinib resistance.

Introduction

The long-established role of eukaryotic translation initiation factor 4E (eIF4E) in the cytoplasm is in the initiation of cap-dependent translation of cellular mRNAs. eIF4E is a cap-binding protein component of the eIF4F complex, which includes the RNA helicase eIF4A and the scaffolding protein eIF4G. Binding of eIF4E to the cap structure on the 5' end of cellular mRNAs recruits the eIF4F complex to the mRNA. As a result, the eIF4F complex can scan from the 5' cap through the untranslated region (5'-UTR), unwinding secondary structure to reveal the translation initiation codon, enable ribosome loading and facilitate final protein translation.^{1,2} Thus, recruitment of mRNA to the ribosomal apparatus constitutes a key event in the initiation of translation of mRNAs that are otherwise translationally repressed due to their long 5'-UTRs.

Because eIF4E is the least abundant among these initiation factors and is considered to be the rate-limiting factor for

cap-dependent translation initiation, changes in the levels of eIF4E profoundly affect translation rates. While increasing global protein synthesis rates, higher levels of eIF4E preferentially enhance the synthesis of potent growth promoting proteins and oncogenic proteins (e.g., c-Myc, cyclin D1, HIF-1 and Mcl-1), which usually have lengthy, G/C-rich and highly structured 5'-UTRs in the mRNAs and, under normal cellular conditions, are translationally repressed. By this mechanism, cancer-related events such as transformation, tumorigenesis, angiogenesis, invasion and metastasis could be facilitated.^{1,3,4} It has been well documented that eIF4E expression is frequently elevated in many types of cancers and is associated with malignant progression. Inhibition of eIF4E effectively suppresses cellular transformation and tumor growth, invasiveness and metastasis.^{3,5,6}

In human non-small cell lung cancer (NSCLC), elevated eIF4E expression has been documented in several previous studies in reference 7–10. Moreover, elevated eIF4E expression is associated with short survival of patients with NSCLC.¹⁰⁻¹² These

*Correspondence to: Shi-Yong Sun; Email: ssun@emory.edu
Submitted: 10/10/11; Revised: 12/01/11; Accepted: 12/02/11
<http://dx.doi.org/10.4161/cbt.13.5.18923>

results suggest that eIF4E may play an important role in positive regulation of the growth and other oncogenic phenotypes of NSCLC cells. However, whether eIF4E can serve as a good therapeutic target in NSCLC has not been demonstrated.

The epidermal growth factor receptor (EGFR) tyrosine kinase inhibitors (TKIs), erlotinib and gefitinib, are effective therapies for NSCLC patients with somatic mutations in EGFR. However, all patients eventually develop resistance (i.e., acquired resistance) to these agents.¹³ Thus, there is an urgent need to understand the mechanism(s) of acquired resistance to develop effective strategies to overcome the resistance. Until now, two different EGFR-TKI resistance mechanisms have been described: i.e., a secondary EGFR mutation-790M and amplification of the c-Met oncogene.¹³

eIF4E has been suggested to be involved in resistance to chemotherapy and androgen ablation (in prostate cancer cells).^{14,15} However, no study has linked eIF4E to EGFR-TKI resistance. Proteomics studies in comparing erlotinib-sensitive and resistant NSCLC cell lines uncovered an increase of eIF4E in erlotinib-resistant cells. Therefore, our present study analyzed eIF4E expression in human NSCLC cells and tissues, demonstrated its potential as a therapeutic target against NSCLC and elucidated its involvement in acquired EGFR-TKI resistance.

Results

Human NSCLC cells and tissues exhibit elevated eIF4E expression. We first examined eIF4E expression with western blotting in a panel of 16 NSCLC cell lines in comparison with two immortalized normal human bronchial epithelial (NHBE) cell lines (i.e., BEAS-2B and HBEC3KT). As presented in **Figure 1A**, all 16 NSCLC cell lines possessed much higher levels of eIF4E than both BEAS-2B and HBEC3KT cells, indicating that NSCLC cells exhibit elevated eIF4E expression. Moreover, we detected eIF4E expression with immunohistochemistry (IHC) in a tissue microarray (TMA) consisting of 40 cases of stage I–III lung cancer tissues (two cases of small cell lung cancer), 10 cases of metastatic cancer tissues from the primary lung cancer, and 9 cases of adjacent normal human lung tissues. In agreement with cell line data, we detected positive eIF4E staining in 71.1% (27/38) of NSCLC tissues, but only in 11.1% (1/9) of adjacent normal tissues (**Fig. 1B and C**). The eIF4E expression was significantly higher in NSCLC tissues than in adjacent normal tissues ($p = 0.0016$). Among these NSCLC tissues, we detected eIF4E expression in 92.3% (12/13) of squamous cell carcinoma, in 55.6% (10/18) of adenocarcinoma, and in 71.4% (5/7) of other NSCLC sub-types. Collectively, it is clear that eIF4E expression is elevated in human NSCLCs.

siRNA-mediated knockdown of eIF4E inhibits the growth of NSCLC cells. If elevated eIF4E is critical for the growth of NSCLC, we hypothesized that downregulation of eIF4E would result in inhibition of the growth of NSCLC cells. To verify this, we used eIF4E siRNA to downregulate eIF4E expression and then determined its impact on the growth of NSCLC cells. As shown in **Figures 2A, D and E**, transfection of eIF4E siRNA into four NSCLC cell lines (i.e., H157, A549, 801C and 801D)

substantially reduced the levels of eIF4E in comparison with control siRNA, indicating successful knockdown of eIF4E. Consequently, we found that all eIF4E siRNA-transfected cell lines grew much slower than cell lines transfected with the control siRNA (**Fig. 2B**), indicating that silencing of eIF4E inhibits the growth of NSCLC cells. Moreover, we tested the effects of eIF4E siRNA transfection on the growth of NSCLC colonies on soft agar. Again, we detected much less colonies in cells transfected with eIF4E siRNA than in control siRNA-transfected cells (**Fig. 2C**), further indicating that inhibition of eIF4E expression suppresses the growth of NSCLC cells. Using cleaved PARP as a readout of apoptosis, we further determined whether knockdown of eIF4E induces apoptosis in the tested cell lines. As presented in **Figure 2D**, we detected cleaved form of PARP in eIF4E siRNA-transfected 801D cells, but not in eIF4E siRNA-transfected H157 cells. As a positive control, tumor necrosis factor-related apoptosis-inducing ligand induced strong cleavage of PARP in the both cell lines. Thus, knockdown of eIF4E induces a cell line-dependent apoptosis.

We also determined whether knockdown of eIF4E expression affected cap-dependent protein translation by detecting several proteins regulated by cap-dependent translation in eIF4E siRNA-transfected cells. As presented in **Figure 2E**, we detected reduced levels of c-Myc, cyclin D1, survivin and Mcl-1 in eIF4E siRNA-transfected H157 and 801D cells in comparison with control siRNA-transfected cells, suggesting that silencing of eIF4E expression in the tested cell systems inhibits cap-dependent translation.

Elevated eIF4E expression is associated with cell invasion. We detected that eIF4E levels were higher in 801D cells (a highly metastatic cell line) than in 801C cells (a low metastatic cell line) (**Fig. 3A**). Moreover, we noted that metastatic NSCLC tissues tended to have increased eIF4E staining rate than their matched primary tumor tissues (100 vs. 60%) (**Fig. 3B**). These data suggest that eIF4E may be involved in regulation of cancer metastasis. Therefore, we next determined whether inhibition of eIF4E expression impacted invasion of NSCLC cells. The matrigel chamber invasion assay showed that 801D cells had higher invasive capacity than 801C cells. Regardless, knockdown of eIF4E expression significantly reduced the number of invasive cells in both cell lines compared with control siRNA-transfected cells (**Fig. 3C and D**). Thus, inhibition of eIF4E expression suppresses the invasion of NSCLC cells, suggesting that elevated eIF4E expression is associated with positive regulation of cell invasion.

EGFR-TKI-resistant NSCLC cells possess elevated eIF4E expression and cap-dependent translation. In an effort to understand the biology of acquired EGFR-TKI resistance, we conducted proteomics by comparing HCC827/ER (derived from HCC827 with acquired resistance to erlotinib) with HCC827 cells using SILAC (stable isotope labeling with amino acids in cell culture) technique. Interestingly, eIF4E was among the proteins that were increased in HCC827/ER cells. By western blot analysis, we further confirmed increased eIF4E expression in HCC827/ER cells. In agreement, PC-9/GR cell also showed increased levels of eIF4E compared with PC-9 cells (**Fig. 4A**). Erlotinib treatment did not alter the expression of eIF4E both

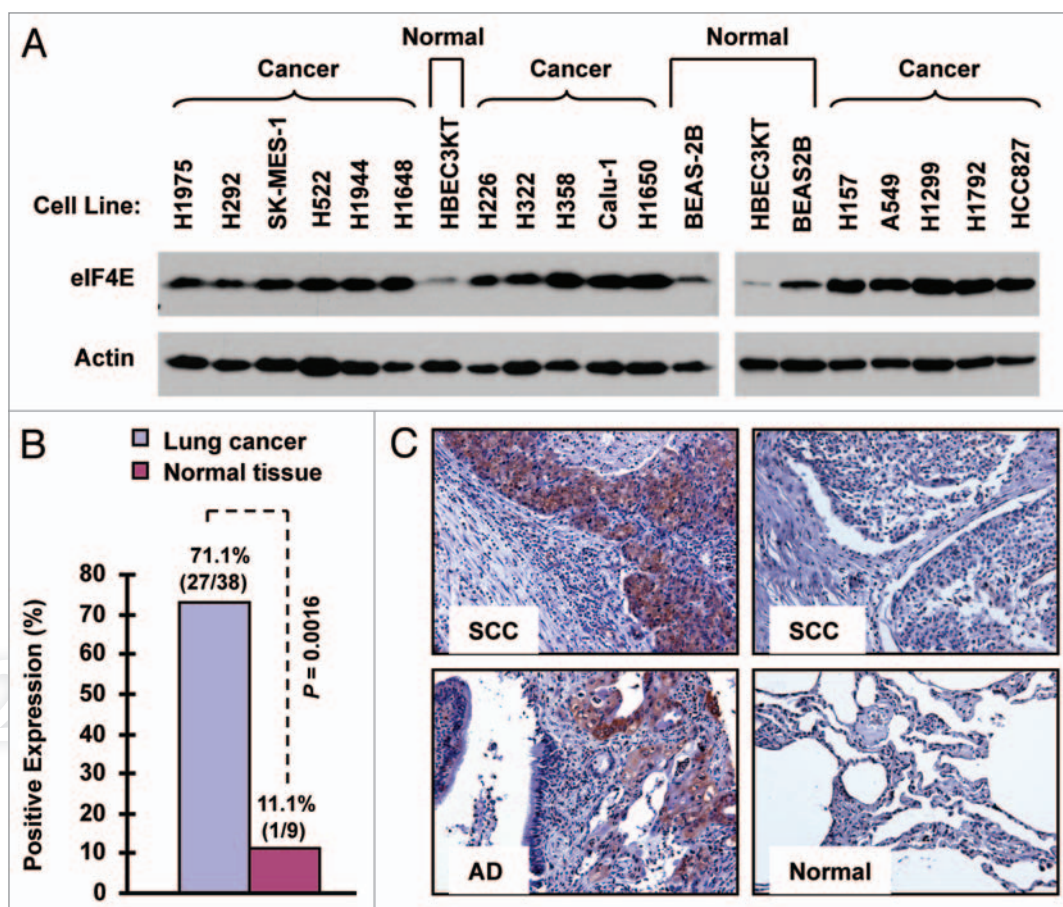


Figure 1. eIF4E expression is elevated in human NSCLC cell lines (A) and tissues (B and C). (A) Whole-cell protein lysates were extracted from the indicated normal and NSCLC cell lines and used for detection of eIF4E expression with western blotting. (B and C) eIF4E expression in human NSCLC tissues was detected with IHC and scored as positive or negative expression (B). The representative images were also presented (C). SCC, squamous cell carcinoma; AD, adenocarcinoma; Normal, adjacent normal lung tissue.

in HCC827 and HCC827/ER cells (Fig. 4B). By RT-PCR, we detected increased levels of eIF4E mRNA in HCC827/ER cells (Fig. 4C). Transfection of eIF4E promoter reporter plasmid (i.e., pGL3-eIF4E-luc) resulted in much higher luciferase activity in HCC827/ER cell than in HCC827 cells (Fig. 4D), indicating that HCC827/ER cells possess increased transcriptional activity of eIF4E. Thus, it appears that increased eIF4E in HCC827/ER cells occurs at the transcriptional level. Collectively, these data clearly demonstrate that eIF4E expression is upregulated in EGFR-TKI-resistant NSCLC cells.

Moreover, we analyzed whether EGFR-TKI resistant cells exhibit elevated cap-dependent translation by examining the formation of eIF4F complex and expression of proteins regulated by cap-dependent translation. Interestingly we found that both PC-9/GR and HCC827/ER cells expressed higher levels of eIF4G in addition to eIF4E than their corresponding counterparts. Accordingly, we detected more eIF4G bound to m⁷GTP in both PC-9/GR and particularly HCC827/ER cells than their respective parent cells in our m⁷GTP-pull down assay (Fig. 5A). This result indicates that EGFR-TKI-resistant NSCLC cells possess elevated eIF4F assembly. Furthermore, we detected higher levels of HIF1 α , c-Myc and Mcl-1, which are typical proteins subject

to regulation by the cap-dependent translation, in HCC827/ER cells than in HCC827 cells (Fig. 5B). Taken together we suggest that EGFR-TKI-resistant cells possess elevated cap-dependent translation.

Inhibition of eIF4E partially restores sensitivity of EGFR-TKI-resistant cells to erlotinib. If elevated eIF4E is involved in development of acquired resistance to EGFR-TKIs, we speculated that inhibition of eIF4E would overcome EGFR-TKI-resistance and restore the sensitivity of to EGFR-TKIs. To test this hypothesis, we used eIF4E siRNA to knock down eIF4E expression in HCC827/ER cells and then examined its impact on cell response to erlotinib. As presented in Figure 6A, erlotinib at 2 μ M inhibited the growth of control siRNA-transfected HCC827/ER cells only by < 15%; however, it suppressed the growth of eIF4E siRNA-transfected HCC827/ER cells by > 55%, which was also greater than that cause by knockdown of eIF4E alone (< 35% growth inhibition). Thus, it is clear that silencing of eIF4E enhances the growth-inhibitory effect of erlotinib in HCC827/ER cells.

4EGI-1 is a small molecule that inhibits eIF4E and eIF4G interaction and cap-dependent translation.¹⁶ Thus, we further determined whether addition of 4EGI-1 would enhance the

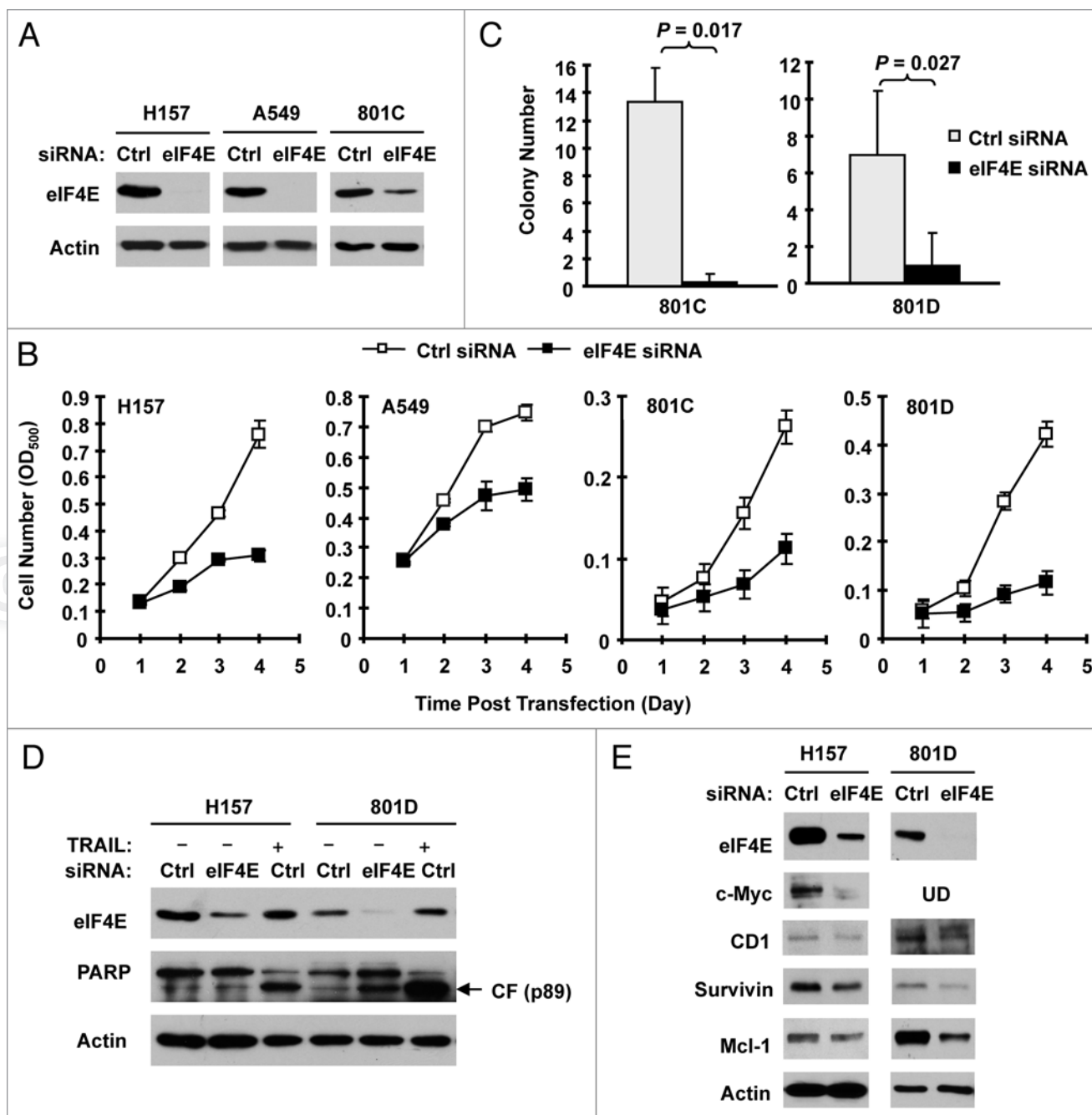


Figure 2. Knockdown of eIF4E (A, D and E) inhibits the growth of NSCLC cells (B and C) and induces apoptosis (D) with suppression of cap-dependent translation (E). (A and B) The indicated NSCLC cell lines were transfected with control (Ctrl) or eIF4E siRNA (20 nM) for 48 h and then subjected to western blot analysis for detection of eIF4E (A). The cells were also re-plated in 96-well plates. Cell numbers were estimated every 24 h with the SRB assay (B). The data are means \pm SDs of four replicates. (C) 801-C and 801-D cells were transfected with control or eIF4E siRNA for overnight and equal numbers of cells were then used for soft agar in 35 mm diameter Petri dishes. After 14 d, colony numbers were counted and averaged from five random microscopic field or view. The final data are means \pm SDs of triplicate independent determinations. The Student t-test was used to compare growth-inhibitory effects between two groups. (D and E) The indicated cell lines were transfected with control or eIF4E siRNA for 72 h (D) or 48 h (E). The cells were then harvested for preparation of whole-cell protein lysates and subsequent western blotting for detection of the given proteins. In (D) the control siRNA-transfected cells were exposed to 50 ng/ml tumor necrosis factor-related apoptosis-inducing ligand (TRAIL) for 20 h before harvesting the cells. UD, undetected.

growth inhibitory effects of erlotinib on HCC827/ER cells. In a 3 d assay, the combination of erlotinib and 4EGI-1 was more potent than either agent alone in inhibiting the growth of HCC827/ER cells. The combination indexes were < 1 for all

combination treatments (Fig. 6B), indicating synergy between erlotinib and 4EGI-1 in inhibiting the growth of HCC827/ER cells. In agreement, the long-term colony formation assay generated similar results as presented in Figure S1. The presence of

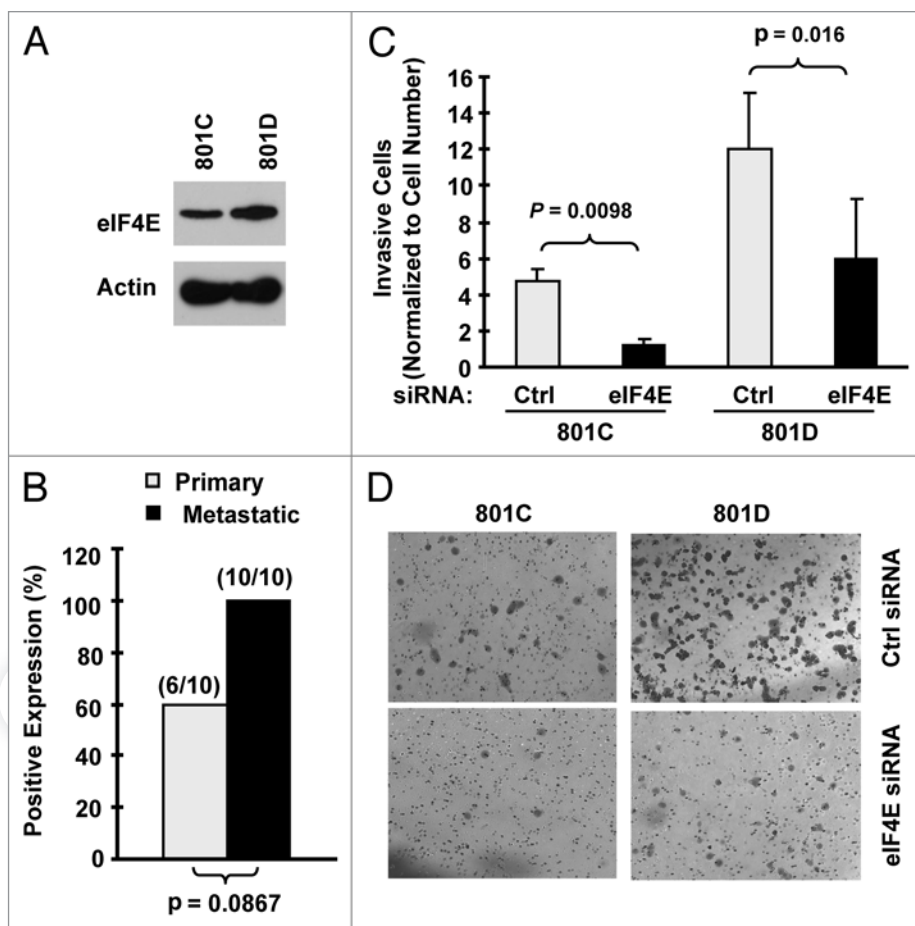


Figure 3. eIF4E expression is increased in metastatic NSCLC cells (A) and tissues (B) and is associated with cell invasion (C and D). (A) eIF4E expression in 801C and 801D cells was detected with western blot analysis. (B) eIF4E expression in primary and matched metastatic NSCLC tissues was detected with IHC. (C and D) Both 801C and 801D cells were transfected with control (Ctrl) or eIF4E siRNA for 48 h and then subjected to matrigel chamber invasion assay. After 36 h, the non-invaded cells and collagen matrix on top of the membranes were removed. Invasive cells on the bottoms of the membranes were counted and normalized by the live cells cultured under the same conditions (C). Representative images of invasive cells on the membranes were also shown (D). The data are means \pm SDs of triplicate determinations. The Student t-test was used to compare inhibitory effects on invasion between two groups.

4EGI-1 enhanced the ability of erlotinib to inhibit the formation and growth of the colonies of HCC827/ER cells. Taken together, these results indicate that the combination of erlotinib and 4EGI-1 synergistically inhibits the growth of HCC827/ER cells.

eIF4G is also the major component in the eIF4F complex. Thus, we further knocked down eIF4G in HCC827/ER cells and analyzed its impact on cell sensitivity to erlotinib. As presented in Figure 6C, erlotinib at up 2 μ M inhibited the growth of control siRNA-transfected HCC827/ER cells by approximately 25%, but the growth of eIF4G-transfected HCC827/ER cells by about 70%. Thus, the knockdown of eIF4G greatly sensitizes HCC827/ER cells to erlotinib, furthering the notion that inhibition of eIF4F cap complex restores TKI-resistant cells to TKIs.

Elevated eIF4E is associated with increased Met expression in TKI-resistant cells. c-Met amplification represents one of the major mechanisms accounting for EGFR TKI-resistance.¹³

In HCC827/ER cells, c-Met expression is elevated compared with their parent HCC827 cells (Fig. S2). Since eIF4E is primarily involved in regulation of cap-dependent protein translation, we then asked whether elevated eIF4E enhances c-Met translation. To this end, we knocked down eIF4E and eIF4G, respectively, and then examined their impact on c-Met expression. Indeed, knockdown of either eIF4E or eIF4G reduced the levels of c-Met protein (Fig. 7A and B). Similarly, treatment of HCC827/ER cells with 4EGI-1 also reduced c-Met levels (Fig. 7C). These data collectively indicate that inhibition of eIF4F cap complex inhibits c-Met expression.

Discussion

In this study, we have shown that human NSCLC cell lines and tissues possess significantly elevated expression of eIF4E in comparison with their normal counterparts (Fig. 1). These findings are in agreement with previous observations.⁷⁻¹⁰ In variance with a report that eIF4E is rarely increased in squamous cell carcinoma of lung,⁷ we detected eIF4E expression in 92% (12/13) of squamous cell carcinoma.

Given that elevated eIF4E expression is significantly associated with short survival of NSCLC patients,¹⁰⁻¹² it is plausible to speculate a role of eIF4E in positive regulation of the growth of NSCLC cells.

Indeed, knockdown of eIF4E expression by siRNA in our study substantially inhibited the growth of NSCLC cells (Fig. 2), suggesting that eIF4E plays a critical role in mediating the growth of NSCLC cells. In this study, we found that knockdown of eIF4E induced apoptosis in 801D cells, but not in H157 cells although it effectively inhibited the growth of both cell lines, suggesting that inhibition of eIF4E inhibit the growth of cancer cells through growth arrest or both growth arrest and apoptosis. It has been recently shown that eIF4E-specific antisense oligonucleotides effectively inhibit the growth of cancer xenografts in mice with minimal toxicity,¹⁷ hence providing robust validation for eIF4E-targeted cancer therapy. Our results also support eIF4E as a promising target for therapy of NSCLCs.

We noted that eIF4E knockdown potently reduced the levels of Mcl-1 in 801D cells, but only minimally in H157 cells even though it effectively decreased survivin levels in the both cell

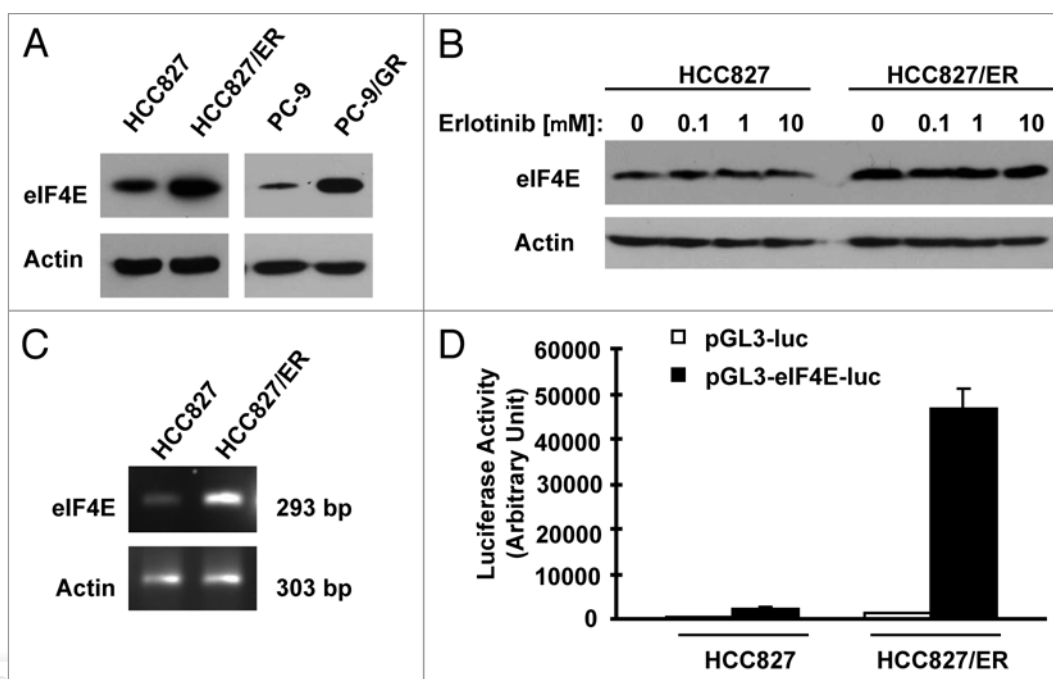


Figure 4. Erlotinib-resistant NSCLC cells possess elevated levels of eIF4E protein (A and B) and mRNA (C and D). (A and B) Whole-cell protein lysates were prepared from the indicated cell lines (A) or cell lines exposed to different concentrations of erlotinib for 6 h (B) and then used for western blot analysis to detect the given proteins as indicated. (C) Total cellular RNA was isolated from both parental and HCC827/ER cells for detection of eIF4E mRNA by RT-PCR. (D) eIF4E promoter activities in the given cell lines were performed with transfection of the given reporter constructs into HCC827 or HCC827/ER cells followed with a luciferase activity assay after 48 h. Each column represents the mean \pm SD of triplicate determinations.

lines (Fig. 2E). Coincidentally, knockdown of eIF4E induced apoptosis in 801D cells, but not in H157 cells (Fig. 2D). Whether this suggests that Mcl-1 downregulation plays a critical role in mediating eIF4E inhibition-induced apoptosis needs further investigation.

The early work with antisense of eIF4E in Ras-transformed rat embryo fibroblasts showed that cells with reduced levels of eIF4E had delayed and reduced invasiveness and decreased experimental metastasis,¹⁸ suggesting that eIF4E plays a role in regulation of invasion and metastasis.¹ In our study, we detected elevated eIF4E expression in metastatic NSCLC cells and tissues. Moreover, knockdown of eIF4E significantly inhibited invasion of NSCLC cells (Fig. 3), suggesting that elevated eIF4E expression is associated with positive regulation of invasion of NSCLC cells. Thus, our findings support the notion that eIF4E is involved in regulation of cancer invasion and metastasis.

Acquired resistance to EGFR-TKIs is a major obstacle and challenge in the treatment of NSCLCs with EGFR-TKIs.¹³ Our exciting finding in this study that eIF4E expression is elevated

in NSCLC cells with acquired resistance to EGFR-TKIs (e.g., HCC827/ER and PC-9/GR) is significant for future efforts to overcome EGFR-TKI resistance. Moreover we have shown that these EGFR-TKI-resistant NSCLC cells possess increased capacity of eIF4F assembly and elevated expression of oncogenic proteins known to be regulated by the cap-dependent translation mechanism (e.g., HIF1 α , c-Myc and Mcl-1) (Figs. 4 and

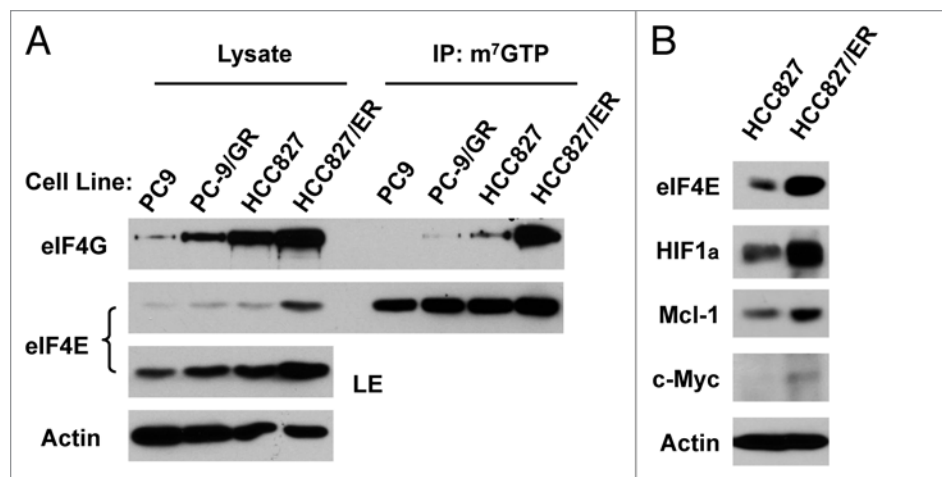


Figure 5. Erlotinib-resistance cells exhibit elevated eIF4F assembly (A) and expression of oncogenic proteins regulated by the cap-dependent translation (B). (A) Whole-cell protein lysates prepared from the given cell lines were used for m⁷GTP pull-down assay followed with western blot analysis to detect the indicated proteins. LE, long exposure. (B) Whole-cell protein lysates were prepared from the indicated cell lines and then used for western blot analysis to detect the given proteins as indicated.

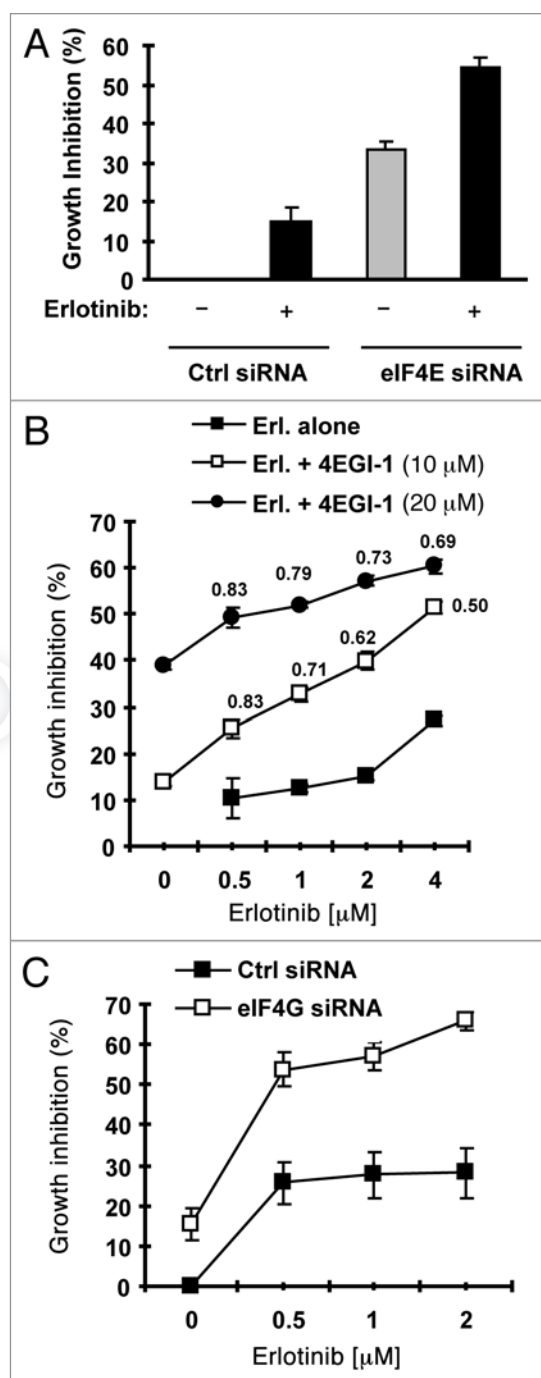


Figure 6. Inhibition of eIF4F formation by knocking down eIF4E (A) or eIF4G (C) or by inhibiting eIF4E and eIF4G interaction with 4EGI-1 (B) sensitizes erlotinib-resistant cells to erlotinib. (A) HCC828/ER cells were transfected with control (Ctrl) or eIF4E siRNA for overnight and then exposed to 2 μ M erlotinib for 3 d. (B) HCC828/ER cells were treated with indicated concentrations of erlotinib in the absence and presence of 4EGI-1 for 3 d. (C) HCC828/ER cells were transfected with control (Ctrl) or eIF4G siRNA for overnight and then exposed to the indicated concentrations of erlotinib for 3 d. After the aforementioned treatments, the cell numbers were estimated by the SRB assay. The data are means \pm SDs of four replicate determinations. The numbers by the lines in (B) are combination indexes for the combinations of erlotinib and 4EGI-1.

5). These results together indicate that eIF4E expression and cap-dependent translation are elevated in EGFR-TKI-resistant NSCLC cells. To the best of our knowledge, this is the first study that links eIF4E and cap-dependent translation to the acquired EGFR-TKI resistance of NSCLCs.

In our study, inhibition of eIF4F assembly by knocking down of eIF4E or eIF4G with eIF4E or eIF4G siRNA enhanced the effect of erlotinib against the growth of HCC827/ER cells. Moreover, the combination of erlotinib and 4EGI-1, an inhibitor of eIF4E and eIF4G interaction, synergistically inhibited the growth of HCC827/ER cells (Figs. 6 and S2). These data collectively suggest that elevated eIF4E expression is involved in development of acquired EGFR-TKI resistance. However, we noted that inhibition of eIF4F with the aforementioned approaches did not fully restore the sensitivity of HCC827/ER cell to erlotinib. Thus, we suggest that elevated eIF4E alone may not be sufficient to confer cell full resistance to EGFR-TKIs although it does contribute to development of acquired EGFR-TKI resistance.

One of the known mechanisms underlying acquired EGFR-TKI resistance is c-Met amplification.¹³ Here, we showed that HCC827/ER cells possessed elevated expression of c-Met (Fig. S2). Importantly, we found that inhibition of eIF4F cap complex with either eIF4E or eIF4G siRNA or the small molecule 4EGI-1 reduced c-Met protein levels (Fig. 7), indicating that elevated eIF4E and cap-dependent cap initiation regulates c-Met expression. Thus, it is likely that elevated eIF4E contributes to development of acquired EGFR-TKI resistance through facilitating c-Met expression in addition to gene amplification. Our findings warrant further investigation in this direction.

Since we detected increased levels of eIF4E mRNA and transcriptional activity in HCC827/ER cells (Fig. 4), it appears that elevated eIF4E expression in EGFR-TKI-resistant cells occurs at the transcriptional level. Thus, our current findings warrant further study to fully elucidate the mechanisms by which eIF4E expression is upregulated in EGFR-TKI-resistant cells.

In summary, the current study has demonstrated that eIF4E expression is elevated in human NSCLCs. The elevated eIF4E expression is associated with positive regulation of cell proliferation and invasion of NSCLC cells and contributes to development of acquired resistance to EGFR-TKIs.

Materials and Methods

Reagents. Erlotinib and gefitinib were purchased from LC Laboratories. 4EGI-1 was purchased from EMD Chemicals, Inc. or Calbiochem. They were dissolved in DMSO at the concentration of 20 or 100 mM, and aliquots were stored at -80°C . Stock solutions were diluted to the appropriate concentrations with growth medium immediately before use. eIF4E, eIF4G, Mcl-1, survivin, PARP, p-EGFR (Tyr1068), EGFR, p-Erb3 (Tyr1289), p-Met (Tyr1234/1235), Met and Akt antibodies were purchased from Cell Signaling Technology, Inc. Rabbit anti-HIF-1 α and p-Akt (S473) were purchased from Epitomics. Mouse monoclonal anti-c-Myc and rabbit anti-Erb3 antibodies were purchased from Santa Cruz Biotechnology, Inc. Mouse monoclonal cyclin D1 antibody (clone DCS-6) was purchased from Dako. Mouse

monoclonal anti-actin and anti-tubulin antibodies were purchased from Sigma Chemical Co., 7-methyl GTP (m⁷GTP)-sepharose 4B was purchased from GE Healthcare Biosciences.

Cell lines and cell culture. H1975, HCC827 and H1650 were purchased from the American Type Culture Collection. The SV40-immortalized normal human bronchial epithelial (NHBE) cell line, BEAS-2B,¹⁹ and other NSCLC cell lines were generously provided by Dr. R. Lotan (MD Anderson Cancer Center). The Cdk4/hTERT-immortalized NHBE cell line, HBEC3KT,²⁰ was obtained from Dr. J. Minna (University of Texas Southwestern Medical Center). PLA-801C and PLA-801D cell lines²¹ were obtained from Dr. Y.L. Lu (Institute of Basic Medical Science, Academy of Military Medical Sciences). PC-9 and gefitinib-resistant PC-9 (PC-9/GR) cell lines were provided by Dr. P.A. Jänne (Dana Farber Cancer Institute). All NSCLC cell lines were cultured with RPMI 1640 containing 5% fetal bovine serum and HBEC3KT and BEAS-2B cells were cultured with K-SFM medium containing 50 µg/mL bovine pituitary extract and 5 ng/mL EGF (Life Technologies) at 37°C in a humidified atmosphere of 5% CO₂ and 95% air.

Establishment of an erlotinib-resistant NSCLC cell line. The erlotinib-resistant HCC827 cell line (HCC827/ER) was established by exposing HCC827 cells to 3.5 µM erlotinib for 2 mo followed with one more month of exposure to 7.5 µM with 5 d drug on and 5 d drug off cycle. The resistant cell population was then routinely cultured with medium containing 1 µM erlotinib. HCC827/ER cell is also cross-resistant to gefitinib (Fig. S2A). Compared with HCC827 cells, HCC827/ER cells have down-regulated EGFR/p-EGFR and elevated levels of Met/p-Met, Akt/p-Akt and ERKs/p-ERKs, which are resistant to modulation by erlotinib (Fig. S2B). The resistance remains unchanged after withdrawal of erlotinib from culture medium for 6 mo, suggesting an irreversible phenotype (Fig. S2C).

Growth inhibition assay. Cell number in monolayer culture in 96-well plates was estimated by the sulforhodamine B (SRB) assay and the growth inhibition was calculated as previously described in reference 22. Combination index (CI) for drug interaction (e.g., synergy) was calculated using the CompuSyn software (ComboSyn, Inc.).

Colony formation assays. Colony formation assay on plastic surface was conducted in 6-well plate (approximately 600/well) as described previously in reference 23. To perform colony formation assay on soft agar, 0.5% bottom agar and 0.35% top agar were prepared and used for each 35 mm Petri dish. The top agar contained 5,000 cells. The dishes were cultured for 14 d and then stained with 0.005% crystal violet for 30 min. The colonies were then counted under a microscope.

Cell invasion assay. Cell invasion assay were performed using BD BioCoat™ Matrigel™ Invasion (BD Biosciences) coated with BD Matrigel Basement Membrane Matrix in a working concentration of 350 µg/ml. For each coated chamber, 25,000 cells in 500 µl of serum-free medium were seeded in the cell insert and pre-cultured for 8 h. After that, 750 µl complete

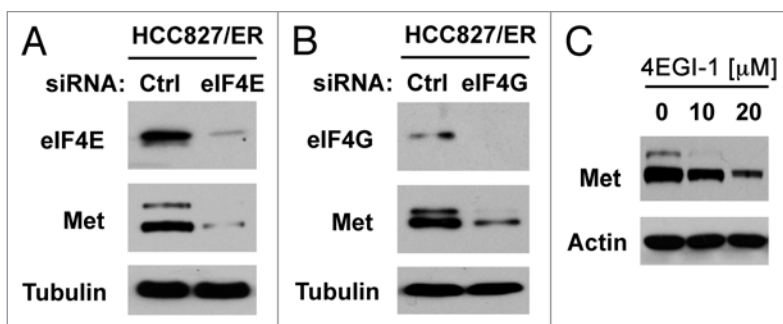


Figure 7. Inhibition of eIF4F formation by knocking down eIF4E (A) or eIF4G (B) or by inhibiting eIF4E and eIF4G interaction with 4EGI-1 (C) reduces c-Met protein levels. (A and B) HCC827/ER cells were transfected with control (Ctrl), eIF4E or eIF4G siRNA for 48 h. (C) HCC827/ER cells were treated with the indicated concentrations of 4EGI-1 for 24 h. After the aforementioned treatments, the cells were harvested for preparation of whole-cell protein lysates and subsequent western blotting.

medium supplemented with 10% fetal bovine serum was added to each lower chamber and culture for another 36 h. The invasive cells on the bottoms of the membranes were then counted after staining with Fisher Hema 3 Manual Staining System (Fisher Scientific) and normalized by live cells (determined by trypan blue) cultured at the same condition.

Western blot analysis. The procedures for preparation of whole-cell protein lysates and for western blotting were the same as described previously in reference 24.

IHC. Human lung cancer TMA was purchased from Imgenex (IMH-358). The TMA was stained with IHC using the EnVision + Dual Link System-HRP Kit (Dako) following the protocol. The rabbit polyclonal antibody against eIF4E (9742) was purchased from Cell signaling and used at 1:100 dilutions. eIF4E staining was scored as negative (<10% staining) and positive staining (≥ 10% staining), respectively.

m⁷GTP pull-down for analysis of eIF4F complex. eIF4F complex in cell extracts was detected using affinity chromatography m⁷GTP-sepharose as described previously in reference 25.

Small interfering RNA (siRNA)-mediated eIF4E and eIF4G knockdown. The siRNA duplexes for non-silencing control and eIF4E and their transfections were described previously in reference 25. eIF4G siRNA (sc-35286) was purchased from Santa Cruz Biotechnology.

Detection of eIF4E mRNA. The forward primer 5'-GGT TGC TAA CCC AGA ACA C-3' and reverse primer 5'-CAC TTC GTC TCT GCT GTT TG-3' were used for the RT-PCR to detect the eIF4E mRNA level. Forward primer 5'-GAA ACT ACC TTC AAC TCC ATC-3' and reverse primer 5'-CTA GAA GCA TTT GCG GTG GAC GAT GGA GGG GCC-5' were used to detect actin mRNA level as an internal control.

Construction of eIF4E reporter plasmid and luciferase activity assay. To make an eIF4E reporter construct, RT-PCR was used to amplify eIF4E promoter region (-1,507 to +72) from genomic DNA extracted from H157 cells using the following primers: forward 5'-GCG GGT ACC GCA CAG GCA GCC TGC ATA CA-3' and reverse 5'-CCC AAG CTT TCT CCT CTT CTG TAG TCG GGG G-3'. The final PCR product was

then cloned into pGL3-basic luciferase reporter vector (Promega Inc.) through KpnI and Hind III cloning sites to generate pGL3-eIF4E-luc construct. The transient transfection and subsequent luciferase assay have been described previously in reference 26.

Statistical analyses. The statistical significance between two groups was analyzed with two-sided unpaired Students t-tests or with Fishers exact test. All of these analyses were done by use of Graphpad InStat 3 software (GraphPad Software). Results were considered to be statistically significant at $p < 0.05$.

Disclosure of Potential Conflicts of Interest

No potential conflicts of interest were disclosed.

Acknowledgments

This study was supported by the Georgia Cancer Coalition Distinguished Cancer Scholar award (to S.Y.S.), NIH R01 CA118450 (S.Y.S.) and P01 CA116676 (Project 1 to F.R.K. and S.Y.S.), DOD BATTLE award W81XWH-06-1-0303 (Project 4 to F.R.K. and S.Y.S.) and Emory Winship Cancer Institute Cancer Cell Biology seed grant. S.S.R., T.K.O., F.R.K. and S.Y.S. are Georgia Cancer Coalition Distinguished Cancer Scholars.

Supplementary Material

Supplemental material can be found at:

www.landesbioscience.com/journals/cbt/article/18923/

References

- De Benedetti A, Graff JR. eIF-4E expression and its role in malignancies and metastases. *Oncogene* 2004; 23:3189-99; PMID:15094768; <http://dx.doi.org/10.1038/sj.onc.1207545>.
- Goodfellow IG, Roberts LO. Eukaryotic initiation factor 4E. *Int J Biochem Cell Biol* 2008; 40:2675-80; PMID:18069043; <http://dx.doi.org/10.1016/j.biocel.2007.10.023>.
- Thumma SC, Kratzke RA. Translational control: a target for cancer therapy. *Cancer Lett* 2007; 258:1-8; PMID:17923280; <http://dx.doi.org/10.1016/j.canlet.2007.08.022>.
- Graff JR, Zimmer SG. Translational control and metastatic progression: enhanced activity of the mRNA cap-binding protein eIF-4E selectively enhances translation of metastasis-related mRNAs. *Clin Exp Metastasis* 2003; 20:265-73; PMID:12741684; <http://dx.doi.org/10.1023/A:1022943419011>.
- Graff JR, Konicek BW, Carter JH, Marcusson EG. Targeting the eukaryotic translation initiation factor 4E for cancer therapy. *Cancer Res* 2008; 68:631-4; PMID:18245460; <http://dx.doi.org/10.1158/0008-5472.CAN-07-5635>.
- Clemens MJ. Targets and mechanisms for the regulation of translation in malignant transformation. *Oncogene* 2004; 23:3180-8; PMID:15094767; <http://dx.doi.org/10.1038/sj.onc.1207544>.
- Rosenwald IB, Hutzler MJ, Wang S, Savas L, Fraire AE. Expression of eukaryotic translation initiation factors 4E and 2alpha is increased frequently in bronchioloalveolar but not in squamous cell carcinomas of the lung. *Cancer* 2001; 92:2164-71; PMID:11596034; [http://dx.doi.org/10.1002/1097-0142\(20011015\)92:8<2164::AID-CNCR1559>3.0.CO;2-A](http://dx.doi.org/10.1002/1097-0142(20011015)92:8<2164::AID-CNCR1559>3.0.CO;2-A).
- Seki N, Takasu T, Mandai K, Nakata M, Saeki H, Heike Y, et al. Expression of eukaryotic initiation factor 4E in atypical adenomatous hyperplasia and adenocarcinoma of the human peripheral lung. *Clin Cancer Res* 2002; 8:3046-53; PMID:12374671.
- Yang SX, Hewitt SM, Steinberg SM, Liewehr DJ, Swain SM. Expression levels of eIF4E, VEGF and cyclin D1, and correlation of eIF4E with VEGF and cyclin D1 in multi-tumor tissue microarray. *Oncol Rep* 2007; 17:281-7; PMID:17203162.
- Wang R, Geng J, Wang JH, Chu XY, Geng HC, Chen LB. Overexpression of eukaryotic initiation factor 4E (eIF4E) and its clinical significance in lung adenocarcinoma. *Lung Cancer* 2009; 66:237-44; PMID:19261348; <http://dx.doi.org/10.1016/j.lungcan.2009.02.001>.
- Seki N, Takasu T, Sawada S, Nakata M, Nishimura R, Segawa Y, et al. Prognostic significance of expression of eukaryotic initiation factor 4E and 4E binding protein 1 in patients with pathological stage I invasive lung adenocarcinoma. *Lung Cancer* 2010; 70:329-34; PMID:20621385; <http://dx.doi.org/10.1016/j.lungcan.2010.03.006>.
- Khoury T, Alrawi S, Ramnath N, Li Q, Grimm M, Black J, et al. Eukaryotic initiation factor-4E and cyclin D1 expression associated with patient survival in lung cancer. *Clin Lung Cancer* 2009; 10:58-66; PMID:19289374; <http://dx.doi.org/10.3816/CLC.2009.n.009>.
- Engelman JA, Janne PA. Mechanisms of acquired resistance to epidermal growth factor receptor tyrosine kinase inhibitors in non-small cell lung cancer. *Clin Cancer Res* 2008; 14:2895-9; PMID:18483355; <http://dx.doi.org/10.1158/1078-0432.CCR-07-2248>.
- Wendel HG, De Stanchina E, Fridman JS, Malina A, Ray S, Kogan S, et al. Survival signalling by Akt and eIF4E in oncogenesis and cancer therapy. *Nature* 2004; 428:332-7; PMID:15029198; <http://dx.doi.org/10.1038/nature02369>.
- Andrieu C, Taieb D, Baylot V, Ettinger S, Soubeyran P, De-Thonel A, et al. Heat shock protein 27 confers resistance to androgen ablation and chemotherapy in prostate cancer cells through eIF4E. *Oncogene* 2010; 29:1883-96; PMID:20101233; <http://dx.doi.org/10.1038/onc.2009.479>.
- Moerke NJ, Aktas H, Chen H, Cantel S, Reibarkh MY, Fahmy A, et al. Small-molecule inhibition of the interaction between the translation initiation factors eIF4E and eIF4G. *Cell* 2007; 128:257-67; PMID:17254965; <http://dx.doi.org/10.1016/j.cell.2006.11.046>.
- Graff JR, Konicek BW, Vincent TM, Lynch RL, Monteith D, Weir SN, et al. Therapeutic suppression of translation initiation factor eIF4E expression reduces tumor growth without toxicity. *J Clin Invest* 2007; 117:2638-48; PMID:17786246; <http://dx.doi.org/10.1172/JCI32044>.
- Graff JR, Boghaert ER, De Benedetti A, Tudor DL, Zimmer CC, Chan SK, et al. Reduction of translation initiation factor 4E decreases the malignancy of ras-transformed cloned rat embryo fibroblasts. *Int J Cancer* 1995; 60:255-63; PMID:7829225; <http://dx.doi.org/10.1002/ijc.2910600221>.
- Sun SY, Kurie JM, Yue P, Dawson MI, Shroot B, Chandraratna RA, et al. Differential responses of normal, premalignant and malignant human bronchial epithelial cells to receptor-selective retinoids. *Clin Cancer Res* 1999; 5:431-7; PMID:10037194.
- Ramirez RD, Sheridan S, Girard L, Sato M, Kim Y, Pollack J, et al. Immortalization of human bronchial epithelial cells in the absence of viral oncoproteins. *Cancer Res* 2004; 64:9027-34; PMID:15604268; <http://dx.doi.org/10.1158/0008-5472.CAN-04-3703>.
- Zhang JQ, Wang Y, Wang T, Du ZY, Xu YJ, Lu YL. Differentially expressed genes in human giant-cell lung cancer lines with different metastatic potentials. *Zhonghua Zhong Liu Za Zhi* 2004; 26:590-3; PMID:15634517.
- Sun SY, Yue P, Dawson MI, Shroot B, Michel S, Lamph WW, et al. Differential effects of synthetic nuclear retinoid receptor-selective retinoids on the growth of human non-small cell lung carcinoma cells. *Cancer Res* 1997; 57:4931-9; PMID:9354460.
- Wang X, Hawk N, Yue P, Kauh J, Ramalingam SS, Fu H, et al. Overcoming mTOR inhibition-induced paradoxical activation of survival signaling pathways enhances mTOR inhibitors' anticancer efficacy. *Cancer Biol Ther* 2008; 7:1952-8; PMID:18981735; <http://dx.doi.org/10.4161/cbt.7.12.6944>.
- Sun SY, Rosenberg LM, Wang X, Zhou Z, Yue P, Fu H, et al. Activation of Akt and eIF4E Survival Pathways by Rapamycin-Mediated Mammalian Target of Rapamycin Inhibition. *Cancer Res* 2005; 65:7052-8; PMID:16103051; <http://dx.doi.org/10.1158/0008-5472.CAN-05-0917>.
- Fan S, Li Y, Yue P, Khuri FR, Sun SY. The eIF4E/eIF4G interaction inhibitor 4EGI-1 augments TRAIL-mediated apoptosis through c-FLIP Downregulation and DR5 induction independent of inhibition of cap-dependent protein translation. *Neoplasia* 2010; 12:346-56; PMID:20360945.
- Sun SY, Liu X, Zou W, Yue P, Marcus AI, Khuri FR. The Farnesyltransferase Inhibitor Lonafarnib Induces CCAAT/Enhancer-binding Protein Homologous Protein-dependent Expression of Death Receptor 5, Leading to Induction of Apoptosis in Human Cancer Cells. *J Biol Chem* 2007; 282:18800-9; PMID:17493934; <http://dx.doi.org/10.1074/jbc.M611438200>.

Divergent Genomic and Epigenomic Landscapes of Lung Cancer Subtypes Underscore the Selection of Different Oncogenic Pathways during Tumor Development

William W. Lockwood^{1*¤}, Ian M. Wilson¹, Bradley P. Coe¹, Raj Chari¹, Larissa A. Pikor¹, Kelsie L. Thu¹, Luisa M. Solis², Maria I. Nunez³, Carmen Behrens², John Yee⁴, John English⁵, Nevin Murray⁶, Ming-Sound Tsao⁷, John D. Minna⁸, Adi F. Gazdar⁸, Ignacio I. Wistuba^{2,3}, Calum E. MacAulay¹, Stephen Lam¹, Wan L. Lam¹

1 Department of Integrative Oncology, British Columbia Cancer Research Centre, Vancouver, British Columbia, Canada, **2** Department of Pathology, The University of Texas MD Anderson Cancer Center, Houston, Texas, United States of America, **3** Departments of Thoracic/Head and Neck Medical Oncology, The University of Texas MD Anderson Cancer Center, Houston, Texas, United States of America, **4** Department of Surgery, Vancouver General Hospital, Vancouver, British Columbia, Canada, **5** Department of Pathology, Vancouver General Hospital, Vancouver, British Columbia, Canada, **6** Department of Medical Oncology, British Columbia Cancer Agency, Vancouver, British Columbia, Canada, **7** Department of Pathology, University Health Network – Princess Margaret Hospital and Ontario Cancer Institute, University of Toronto, Toronto, Ontario, Canada, **8** Hamon Center for Therapeutic Oncology Research, University of Texas Southwestern Medical Center, Dallas, Texas, United States of America

Abstract

For therapeutic purposes, non-small cell lung cancer (NSCLC) has traditionally been regarded as a single disease. However, recent evidence suggest that the two major subtypes of NSCLC, adenocarcinoma (AC) and squamous cell carcinoma (SqCC) respond differently to both molecular targeted and new generation chemotherapies. Therefore, identifying the molecular differences between these tumor types may impact novel treatment strategy. We performed the first large-scale analysis of 261 primary NSCLC tumors (169 AC and 92 SqCC), integrating genome-wide DNA copy number, methylation and gene expression profiles to identify subtype-specific molecular alterations relevant to new agent design and choice of therapy. Comparison of AC and SqCC genomic and epigenomic landscapes revealed 778 altered genes with corresponding expression changes that are selected during tumor development in a subtype-specific manner. Analysis of >200 additional NSCLCs confirmed that these genes are responsible for driving the differential development and resulting phenotypes of AC and SqCC. Importantly, we identified key oncogenic pathways disrupted in each subtype that likely serve as the basis for their differential tumor biology and clinical outcomes. Downregulation of *HNF4α* target genes was the most common pathway specific to AC, while SqCC demonstrated disruption of numerous histone modifying enzymes as well as the transcription factor *E2F1*. *In silico* screening of candidate therapeutic compounds using subtype-specific pathway components identified HDAC and PI3K inhibitors as potential treatments tailored to lung SqCC. Together, our findings suggest that AC and SqCC develop through distinct pathogenetic pathways that have significant implication in our approach to the clinical management of NSCLC.

Citation: Lockwood WW, Wilson IM, Coe BP, Chari R, Pikor LA, et al. (2012) Divergent Genomic and Epigenomic Landscapes of Lung Cancer Subtypes Underscore the Selection of Different Oncogenic Pathways during Tumor Development. PLoS ONE 7(5): e37775. doi:10.1371/journal.pone.0037775

Editor: Alfons Navarro, University of Barcelona, Spain

Received: November 8, 2011; **Accepted:** April 27, 2012; **Published:** May 21, 2012

This is an open-access article, free of all copyright, and may be freely reproduced, distributed, transmitted, modified, built upon, or otherwise used by anyone for any lawful purpose. The work is made available under the Creative Commons CC0 public domain dedication.

Funding: This work was supported by grants from the Canadian Institutes for Health Research (CIHR) (MOP-86731, MOP-77903, MOP-110949), Canadian Cancer Society (CCS20485), NCI Early Detection Research Network, and Department of Defence (CDMRP W81XWH-10-1-0634). W.W.L., I.M.W., B.P.C., R.C., K.L.T. and L.A.P. were supported by scholarships from CIHR and NSERC (Natural Sciences and Engineering Research Council), and W.W.L. by a CIHR Jean-Francois Saint Denis Fellowship in Cancer Research, R.C. by a Banting Postdoctoral Fellowship, K.L.T. and L.A.P. by Vanier Canada Graduate Scholarships. The funders had no role in study design, data collection and analysis, decision to publish, or preparation of the manuscript.

Competing Interests: The authors have declared that no competing interests exist.

* E-mail: william.lockwood@nih.gov

¤ Current address: Cancer Biology and Genetics Section, Cancer Genetics Branch, National Human Genome Research Institute, National Institutes of Health, Bethesda, Maryland, United States of America

Introduction

Lung cancer is the leading cause of cancer-related deaths worldwide and despite current treatments, prognosis remains poor, with a five year survival of <18% [1,2,3]. Non-small cell lung cancer (NSCLC) and small cell lung cancer (SCLC) are the two main histologic groups. SCLC arises mainly in the central airways while NSCLC may occur centrally or peripherally. The

differing pathology of the two types is reflected in their clinical management.

NSCLC is a heterogeneous disease with squamous cell carcinoma (SqCC) and adenocarcinoma (AC) being the predominant histological subtypes. Traditionally, these subtypes have been treated as a single disease entity with treatment strategies determined solely by disease stage. However, recent evidence from clinical trials has demonstrated that histological subtypes of

NSCLC respond differently to both targeted drugs and newly developed chemotherapies, possibly related to differences in cell derivation and pathogenetic origins [3,4,5,6,7,8,9]. One of the most striking examples is the folate antimetabolite Pemetrexed, which exhibits superior efficacy and is restricted for use in patients with non-SqCC, presumably due to the higher expression of thymidylate synthase in SqCC tumors [9]. Likewise, numerous studies have associated a higher response rate upon treatment of AC with the EGFR tyrosine kinase inhibitors Gefitinib and Erlotinib, reflecting the higher prevalence of *EGFR* mutations in this subtype [6,10]. These discrepancies in tumor biology and clinical response highlight the need to determine the underlying genetic, epigenetic and metabolic similarities as well as differences between the NSCLC subtypes in order to define more appropriate avenues for therapeutic intervention.

Initial gene expression profiling studies were able to segregate AC and SqCC tumors into their respective histologic groupings based on multi-gene models; however, critical events in tumorigenesis may be masked by reactive changes when examining expression profiles alone [11,12,13]. Conversely, DNA copy number or DNA methylation changes corresponding with gene expression changes are often regarded as evidence of causality. Such DNA level changes are critical deregulation events driving progression and other cancer phenotypes [14,15,16]. Since SqCC and AC are thought to develop from distinct cell lineages in different regions of the lung, the range of genetic alterations required for tumor initiation may occur in a lineage-restricted manner. For example, the amplification of the lineage survival oncogenes *SOX2* and *TTF1/NKX2-1* have recently been identified as key events specific to the development of lung SqCC and AC, respectively [17,18]. However, these genes alone are insufficient to explain the phenotypic diversity of the subtypes, suggesting that the vast majority of genes responsible for their differential development remain unknown. Although genetic and epigenetic differences between SqCC and AC have been described, low genome coverage and/or small sample sizes have been limiting [19,20,21,22,23,24].

In this study, we performed the first large-scale analysis of primary NSCLC tumors (261 total – 169 AC and 92 SqCC), integrating high resolution DNA copy number, methylation and gene expression profiles to identify critical subtype-specific molecular features. The characterization of the genomic and epigenomic landscapes of AC and SqCC revealed an astounding number of differences at the DNA level with subsequent gene expression changes that are selected for during subtype-specific lung tumor development. Importantly, we identified key oncogenic pathways disrupted by these alterations that likely serve as the basis for differential behaviors in tumor biology and clinical outcomes. Lastly, through prognostic analysis and *in silico* screening of candidate therapeutic compounds using subtype-specific pathway components, we show how these new findings may influence our approach to the clinical management of NSCLC.

Results

Assessment of global genomic instability in AC and SqCC

Carcinomas of all types are known to harbor many DNA-level alterations linked, in part, to carcinogen exposure [25]. Indeed, tobacco smoke has been linked to the induction of not only DNA mutations, but also broad chromosomal instability [26]. Based on the differing exposure to tobacco carcinogens of cells in the central (SqCC) and peripheral (AC) airways, we sought first to determine whether global genomic instability was more prevalent in either of the two subtypes. We generated and compared whole genome

copy number profiles for 261 NSCLC tumors 169 AC and 92 SqCC – by tiling-resolution array comparative genomic hybridization (CGH) (Sample Set #1, Table S1) [27,28,29,30]. After hybridization, standard removal of systematic biases, and computational segmentation to identify regions of gain and loss, the number of gained, lost, and neutral probes was assessed for each tumor. The relative genomic instability observed in AC and SqCC groups was then compared (Figure 1a). The average number of altered probes (per sample) was compared between groups using the Mann-Whitney U-test. No significant differences between the two subtypes were found, consistent with previous work that showed similar DNA content across subtypes [31]. This analysis demonstrates that neither subtype has a proclivity for gain or loss of DNA. Therefore, observed differences in alteration frequency at a given locus can be attributed to sub-type specific selection of genes included within altered regions and not to different degrees of random genomic instability associated with tumor development.

Disparate genomic landscapes characterize lung SqCC and AC

Although the NSCLC subtypes exhibit similar levels of genomic instability, if specific genetic pathways are involved in their differential development, differences in the genomic alterations selected during tumorigenesis should be present. To determine if genetic alterations unique to each NSCLC subtype exist, we looked for recurrent non-random regions of aberration in each group. Samples were grouped by subtype and probes were aggregated into regions based on similar copy number status. The frequency of alteration across autosomes was determined and compared between subtypes using the Fisher's exact test and the resulting *p*-values were corrected for multiple comparisons with a cut-off of ≤ 0.01 considered significant. In addition, we required regions to be altered in $>20\%$ of samples from a subtype group and a difference between groups of $>10\%$ to be considered "of interest". Figure 1b displays the resulting genomic landscapes of AC and SqCC based on the frequency of gain and loss across the genome, and highlights the corresponding regions of difference between the subtypes that were identified.

This analysis revealed 294 regions of copy number disparity between SqCC and AC, 205 of which were SqCC-specific, whereas 89 were AC specific (Table S2). Although some regions overlapped, the character of the alteration (i.e. gain versus loss) was specific to an individual group. Since the alteration status between the subtypes differed strongly, we classed these as subtype-specific copy number alterations. In total, these alterations covered approximately 550 Mbp of the genome, ranging in size from large segments on chromosome arms (64.8 Mbp on 4q) to discrete peaks only kilobases in size (0.05 Mbp in multiple places).

Interestingly, copy number profiling of 20 preinvasive lung carcinoma *in situ* lesions, the assumed precursors to lung SqCC tumors, revealed that the vast majority (186/204, $\sim 92\%$) of SqCC-specific alterations are present at this stage of tumor development, suggesting that these events may commence early in SqCC tumorigenesis (Table S3). The remaining alterations that are present in the SqCC tumors and not found in the carcinoma *in situ* lesions may represent potential drivers of SqCC progression (Table S3, with potential target genes of these regions identified in Table S4, discussed below). Together, these findings support our hypothesis that the subtypes develop through different genetic pathways.

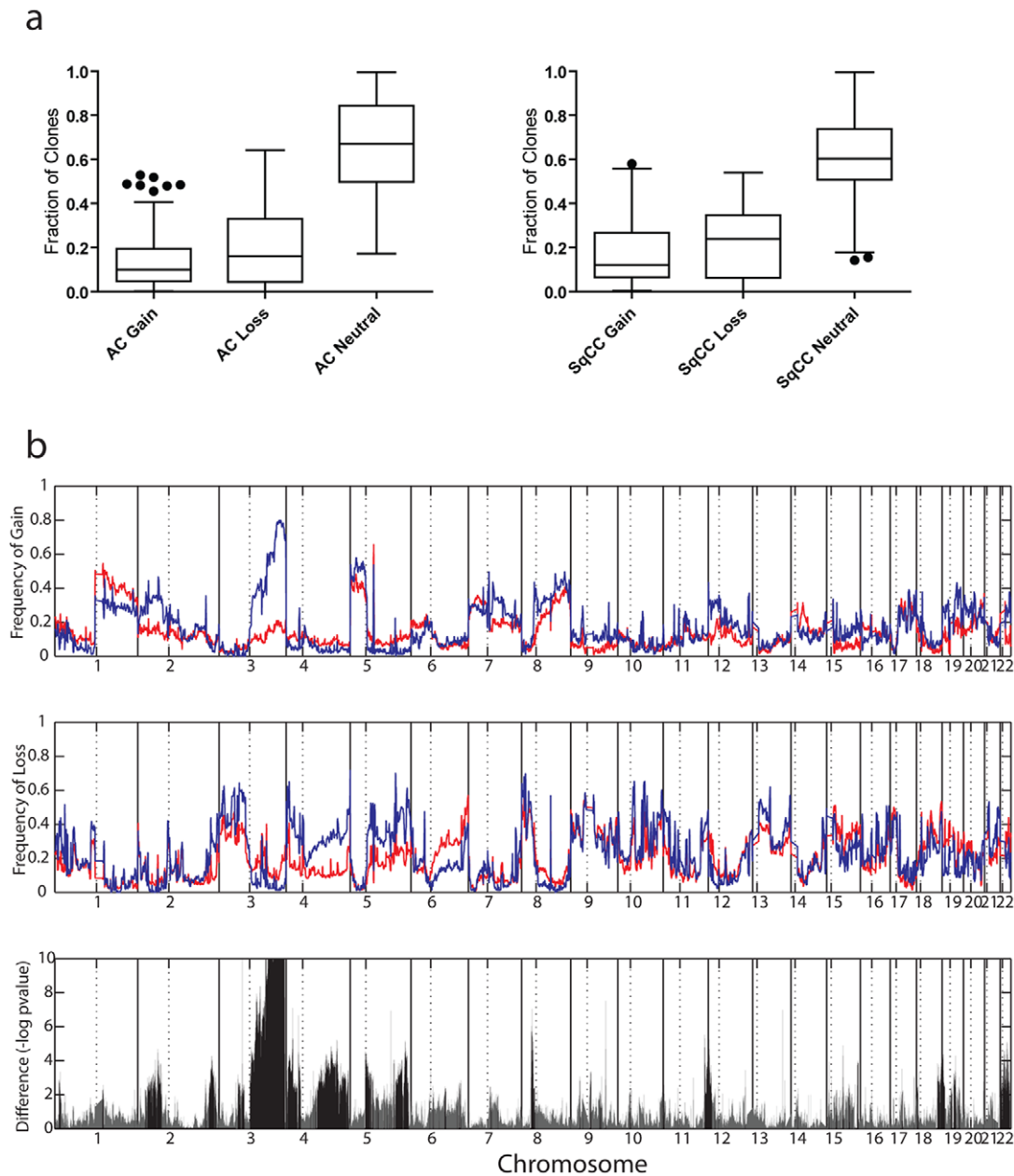


Figure 1. Genomic landscapes of lung AC and SqCC. (a) Percentage of clones of each state in both subtypes. Box plots illustrate the percentage of clones with status -1 (loss/deletion), 0 (neutral), and $+1$ (gain/amplification) in each of the subtypes. Percentages were calculated for each sample and for each status. These plots demonstrate the similarity in total genome alteration percentages between AC and SqCC tumors and suggest that recurrently altered regions of genome are the result of selection rather than a higher frequency of gain or loss of DNA in either subtype. (b) Alteration frequencies for 169 AC (red) and 92 SqCC (blue) tumors are displayed across the entire human genome. Solid vertical black lines represent chromosome boundaries whereas the dotted black lines represent chromosome arm boundaries. The frequency of copy number gain is denoted in the top panel. Note the high frequency of 3q gain in the SqCC subtype, consistent with previous reports. Additional regions of copy-number difference are also clear, such as the more common gain of chromosome 2p in AC. The second panel (middle) shows the frequency of copy number loss. Common tumor suppressor gene loci such as chromosome 3p are common between AC and SqCC, but large differences exist in regions such as chromosome 4q. The significance of copy number disparity (inverse p-value corrected for multiple comparisons) between AC and SqCC subtypes is depicted in the third (bottom) panel. Solid black lines represent regions considered statistically different ($p \leq 0.01$) whereas grey lines are not.

doi:10.1371/journal.pone.0037775.g001

Gene disruptions are selected in a subtype specific manner during NSCLC development

The discovery of DNA copy number disparities between NSCLC subtypes suggests that genes within these areas might be preferentially selected during tumorigenesis and thus, responsible

for the differential development and pathological characteristics of the subtypes. To identify the potential target genes of these alterations, we integrated DNA copy number and gene expression levels [32]. Gene expression profiles were generated for a subset of tumors that were analyzed by array CGH (20 SqCC and 29 AC

tumors, Sample Set #2, Table S1). We hypothesized that genes targeted by subtype-specific alterations would be different at the DNA level with matching differences at the gene expression level. Further, we also analyzed normal lung tissue to ensure that only genes differentially expressed in tumor tissues (relative to normal) remained as candidates, a characteristic consistent with a role in tumor development.

Genes located within each subtype-specific copy number alteration were identified and the expression levels compared between the SqCC and AC samples to determine those that were differentially expressed ($p < 0.001$, after multiple testing correction). For SqCC, 4669 unique genes mapped to the subtype-specific copy number alterations (~23 genes per region), and 797 (17%) of these were differentially expressed between subtypes in the anticipated direction. In AC, 2050 unique genes were located in subtype-specific copy number alterations (~23 per region) and 171 (8%) were differentially expressed between subtypes in the anticipated direction.

Although some genes overlapped, their disruption patterns were specific to the individual cancer type, suggestive of opposing roles (oncogenic vs tumor suppressive) depending on cellular context. Thus, these genes were also considered to be subtype-specific targets. When combined, the SqCC and AC subtype-specific copy number regulated candidates represented 968 unique genes and showed a clear distinction in expression levels between the two subtypes.

In addition to demonstrating a relationship between expression and copy number alteration, a candidate subtype-specific gene was also required to be deregulated in cancer tissues relative to normal tissue [33]. We analyzed the expression levels of candidates in an independent panel of 53 SqCC and 58 AC lung tumors and 67 samples of exfoliated bronchial cells from cancer-free individuals (Sample Sets #3 and #4, Table S1). In total, 655 of the 797 SqCC-specific and 143 of the 171 AC-specific genes had corresponding probes on this array platform. These genes were compared between the respective cancer subtype and the normal bronchial cells in order to determine those that were significantly differentially expressed ($p < 0.001$) in the direction predicted by the corresponding copy number alteration in which they were located. This analysis revealed that 447 (68%) of the SqCC-specific and 71 (49%) of the AC-specific genes were deregulated in cancerous tissues (492 unique gene alterations, Table S4). Since these genes met all three criteria for defining candidate subtype-specific, copy number alteration regulated targets as described above, we concluded they might represent the critical gene alterations driving the development of each subtype (Figure 2).

Different oncogenic pathways are associated with the development of AC and SqCC

Cellular pathways and processes specifically disrupted in individual subtypes may reveal key oncogenic mechanisms driving the differential development of AC and SqCC. Thus, after identifying the genes responsible for the differences between the subtypes, we next wanted to investigate their biological functions. To discover subtype-related networks of biologically related genes we performed Ingenuity Pathway Analysis (IPA) of the 71 AC and 447 SqCC specific target genes (Figure 3, Table S5). SqCCs exhibited disruptions in gene networks that function in regulating DNA replication, recombination and repair, with additional roles in lymphoid tissue structure and development (Table S4). Genes involved in the top SqCC network were associated with the binding and modification of histone protein H4, as well as the regulation of the NFkB complex (Figure 3b). In contrast, the primary networks in AC displayed functions associated with cell-to-cell signaling, development, and drug metabolism (Table S5).

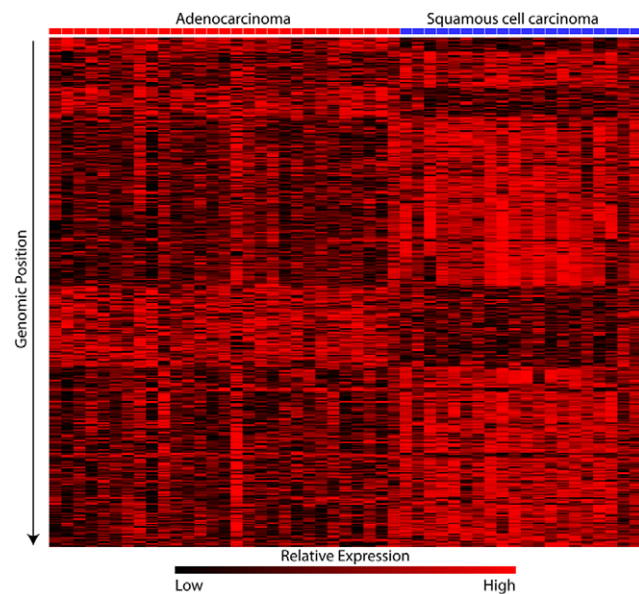


Figure 2. Differential expression as a result of subtype specific copy number alterations. Transformed absolute expression data for the 492 unique genes exhibiting disruption in expression levels as a result of copy number differences are displayed. In addition, these genes are up or down-regulated in the subtype which they are disrupted compared to normal lung tissue (see results). High-level expression is indicated by red while black indicates progressively lower levels of expression. The AC samples are indicated by red highlighting on the top of each column, while SqCC samples are indicated by blue highlighting. Each gene is sorted according to its chromosomal position. There is a clear distinction in the expression of these genes indicating their specific involvement in the subtypes. doi:10.1371/journal.pone.0037775.g002

The main AC-specific gene network was composed primarily of genes regulated by the transcription factor HNF4 α (Figure 3a), whereas AC network 2 contained numerous genes controlled by TGF β and TP53. The differential disruption of gene networks in AC and SqCC was further suggestive of distinct mechanisms of tumorigenesis for the subtypes.

Global subtype variations in DNA methylation levels reflect differences in cells of origin

Unlike the genome, which is identical for most normal cells in the body, the epigenome differs between tissue types [34,35]. Similarly, cancer genomes exhibit global hypomethylation to varying degrees depending on the tissue of origin [36]. DNA methylation profiles are also influenced by mutational profiles within different cancer types, as DNA hyper- and hypomethylation alterations are also known to be related to tissue and genetic background [37] as well as smoking behavior [38]. Given the differing mutational spectra of the two NSCLC subtypes and their likely differing cells of origin, we investigated the overall DNA methylation level of 30 AC and 13 SqCC samples (Sample Set #4, Table S1). To enable comparisons of SqCC and AC tumors to appropriate matched normal cells, DNA methylation profiles were also generated for 30 non-malignant lung parenchyma samples (AC reference) and 18 histologically normal exfoliated bronchial epithelial cell samples (SqCC reference) from patients with NSCLC (Sample Set #1, Table S1). Analysis of 27,578 CpG dinucleotides probes within >13000 CpG islands shows that DNA methylation in the bronchial epithelia and the SqCC tumors was slightly lower than in the normal lung or AC tumors (Figure 4a).

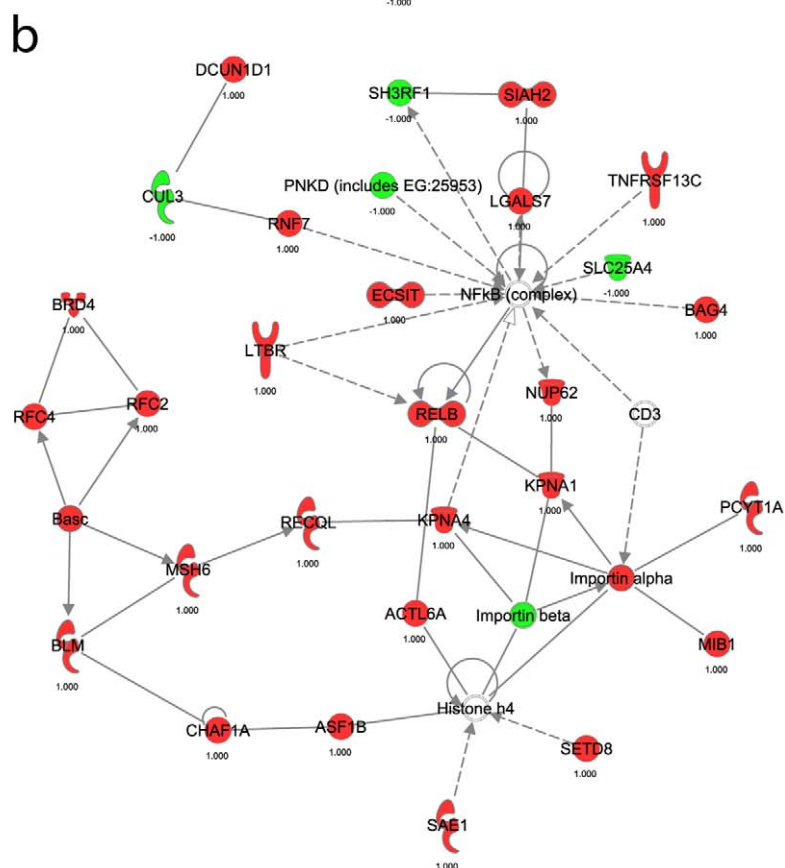
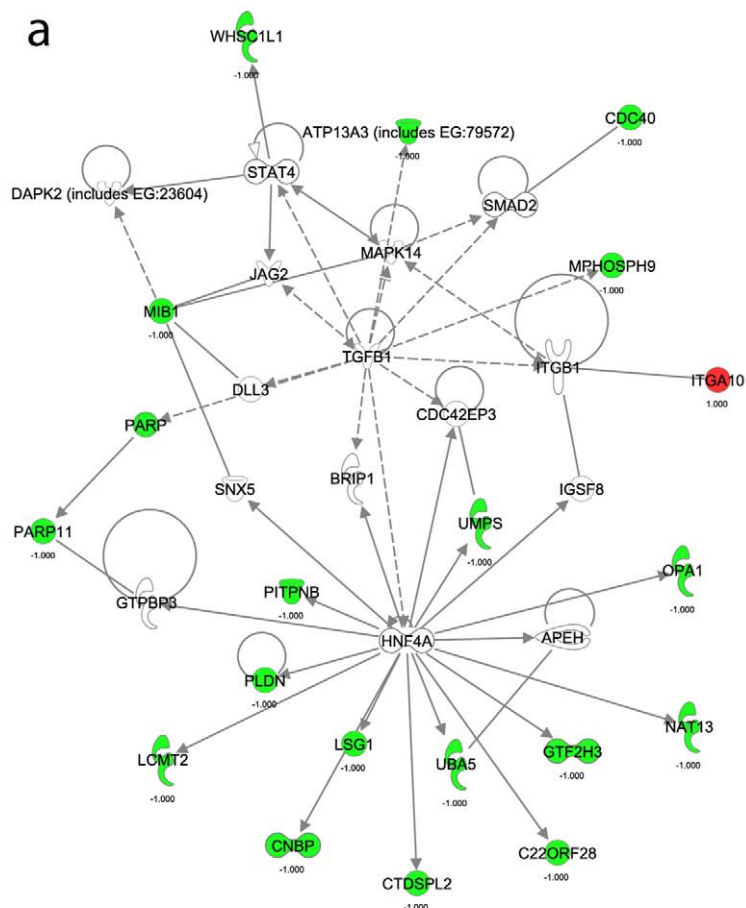


Figure 3. Gene networks involved in the development of SqCC and AC. Ingenuity Pathway Analysis was used to identify biologically related networks from the subtype specific genes deregulated by subtype-specific copy number alterations (see Methods). The top resultant gene networks for each subtype are displayed. a) AC network #1 of genes related to HNF4 signaling. b) SqCC network #1 displaying potential interactions between multiple histone regulating genes for both a) and b), solid lines denote direct interactions while dotted lines represent indirect interactions between the genes. Network components highlighted in red are upregulated in the corresponding subtype whereas those highlighted green are downregulated. Those not highlighted are used by the software to display relationships. Additional information about the genes and their interactions can be found at www.ingenuity.com. or within the discussion. In this diagram molecules are represented as such; corkscrews represent enzymes, y-shaped molecules are transmembrane receptors, thimble-shaped molecules are transporters, kinases are triangular, and circular molecules encompass all other gene products.
doi:10.1371/journal.pone.0037775.g003

This is mirrored and exaggerated in the CpG dinucleotides outside of CpG islands, suggesting that the cells of the central airway are globally hypomethylated relative to the cells of the peripheral airways, whether cancerous or not (Figure 4b). In this case the two groups are significantly different when compared using a Mann-Whitney U test ($p < 0.0001$).

To determine whether these trends were evident in tumor-specific epigenetic alterations, (i.e. those that exist within the tumor subtype when compared to an appropriate normal cell), we compared the differential methylation profiles of AC and SqCC tumors. These profiles were generated by subtracting the average normal DNA methylation profile for the references from each of

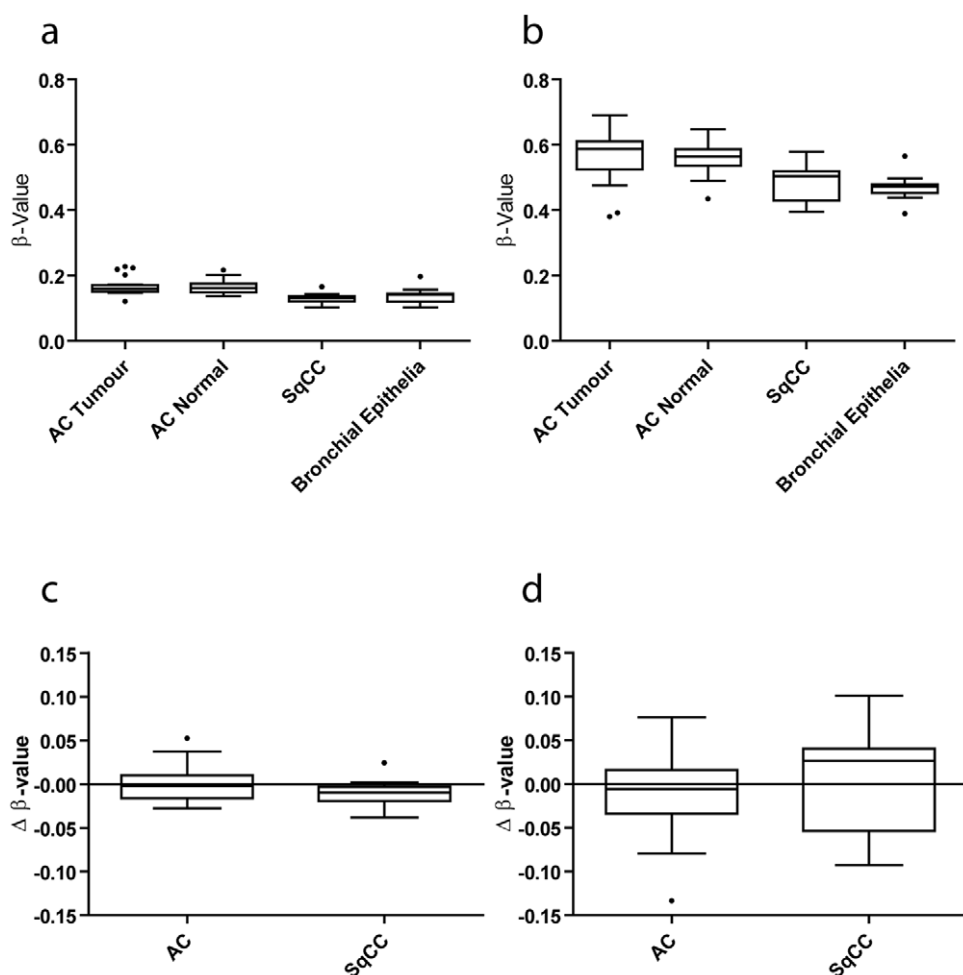


Figure 4. Global DNA methylation patterns of NSCLC tumors and associated normal tissues. Comparison of average DNA methylation levels between AC tumor, AC normal (histologically normal lung parenchyma), SqCC tumor, and bronchial epithelia. a) CpG island probe averages. The average of each of the profiles at probes located within CpG islands is plotted as a component within the box plot. In this panel, SqCC and bronchial epithelia samples appear to have slightly lower DNA methylation levels than the AC tumor and AC normal groups, indicating that outside of CpG islands, where the bulk of genomic methylation occurs, the central airway samples are more hypomethylated. b) Non-CpG island probe averages. The average of each of the profiles at probes not located within CpG islands is plotted as a component within the box plot. In this figure β -value is the level of methylation as defined by the methylated signal/total signal for each probe. In this panel, SqCC and bronchial epithelia are significantly lower in methylation level compared to the AC tumor or AC normal groups, indicating that outside of CpG islands, where the bulk of genomic methylation occurs, the central airway samples are more hypomethylated. c) Average differential methylation levels at CpG islands. The average differential is plotted for the 30 AC samples and the 13 SqCC samples. The two groups are very similar in their differential profile within CpG island probes. d) Average differential methylation levels at CpG sites not located within CpG islands. In this plot the average differential methylation level is plotted for probes that are not located within CpG islands. Again, the two groups are not significantly different by a Mann-Whitney U test.
doi:10.1371/journal.pone.0037775.g004

the 30 AC and 13 SqCC tumors, respectively. Similar to the global assessment of copy number alterations (gain and loss), there were no significant differences between the AC differential profiles and the SqCC differential profiles (Figure 4c) in CpG island probes or non-CpG island probes (Figure 4d). Based on this, we again reasoned that any observed differences in hypermethylation or hypomethylation frequencies between the subtypes are likely to be due to subtype-specific selection of these alterations.

Different epigenetic alterations are involved in the development of AC and SqCC subtypes

Although no differences in global methylation changes were observed between subtypes, the two subtypes may possess differential alteration frequencies at individual loci. To determine whether AC and SqCC tumors possess locus-specific differences in DNA methylation, we examined the frequencies of methylation alteration at gene-associated loci in both subtypes. Tumor DNA methylation levels were compared to the average of available normal reference tissue profiles. The frequency of probe hypermethylation and hypomethylation (tumor-normal $|\geq 0.15$) in AC and SqCC samples was compared using the Fisher's exact test. Following correction for multiple comparisons, 2708 probes corresponding to 2384 genes were found to be differentially methylated ($p \leq 0.05$). The SqCC group contained markedly more recurrently hyper- and hypomethylated loci than the AC group, similar to the disparity in the numbers of subtype-specific copy number-regulated genes observed in the analysis of genomic alterations. In fact, only 8% of the 2708 significant probes were more frequently altered in AC, the rest being more commonly hyper- or hypomethylated in SqCC.

To further refine the list of differentially methylated genes to those whose gene expression reflects levels expected based on their epigenetic alteration, we assessed the 2384 genes with differential methylation for differential expression between the subtypes, as well as differential expression from normal tissues, using a corrected p -value threshold of $p < 0.05$. 32 AC candidate genes and 297 SqCC genes met these stringent criteria and were further analyzed as subtype-specific epigenetically regulated genes (Table S6).

Epigenetically regulated genes complement genetically regulated genes

To determine whether the 32 AC-specific and 297 SqCC-specific epigenetically-regulated genes carried out functions similar to those subtype-specific genes discovered by the DNA copy number analysis described above, pathway disruption analysis was performed. This revealed that the most significant epigenetically-regulated gene network in AC is involved in cell cycle, cell death, and cellular development (Table S7). This is partly in contrast to the top AC network of copy number regulated genes, which similarly have functions associated with tissue development, but also possess cell signaling and hematological system function in common (Table S4). The overall degree of similarity between AC-specific genes that are genetically or epigenetically regulated is quite small, likely due to the low number of AC-specific genes identified (potential reasons for this are discussed below). In contrast, the SqCC gene networks in both analyses are very similar. For example, DNA replication, recombination and repair are highly featured functions of genes identified by both DNA copy number and DNA methylation analyses of SqCC (Tables S5 and S7, respectively). Additionally, genes involved in immunological disease and lymphoid tissue structure and development were prominent. Of particular interest was the enrichment of aberrantly methylated genes in the small cell lung cancer signaling pathway

(comprised of genes known to deregulated in small cell lung cancer as annotated by Ingenuity) (Figure 5a). This was the most significantly enriched canonical pathway in either subtype that was affected by DNA methylation alterations and it is of interest because both of these lung cancers (SCLC and SqCC) arise in the central airways with similar exposure to cigarette smoke carcinogens. *E2F1* is among the hypomethylated and overexpressed genes represented in this pathway, and is known to be overexpressed in SCLC and to drive expression of *EZH2*, which is also overexpressed in SCLC [39,40]. To explore this pathway further, we investigated whether *EZH2* was more highly expressed in SqCC than AC tumors (as a consequence of differential *E2F1* expression). As expected, we found that *EZH2* was expressed at a significantly higher level in SqCC tumors than AC tumors, demonstrating the biological consequence of *E2F1* disruption (Figure 5b). The differential expression of *EZH2* in the two subtypes is significant, given the numerous differences in aberrant DNA methylation observed between subtypes; this could reflect the key role of EZH2 in the polycomb group, a protein complex involved in DNA methylation [41].

DNA copy number and DNA methylation data are complementary from a gene-specific perspective as well. This is highlighted by seven genes (*ATP2C1*, *PCYT1A*, *ZWILCH*, *CENTB2*, *BAG4*, *PARP11* and *CSDA*, Table S8) that are disrupted by gene-dosage in one subtype and DNA methylation in the other. *PARP11* is one such example of differential activation/inactivation by DNA copy number and DNA methylation, which is discussed further below.

Concerted genetic and epigenetic disruption of subtype-specific genes

In order to determine if both DNA copy number and DNA methylation aberrations simultaneously disrupted any genes, we combined the subtype-specific gene lists derived using the two analytical approaches described above (Table S9). Combining the 71 AC genes identified through their association with DNA copy number alteration and the 32 genes associated with DNA methylation aberrations did not yield any overlapping genes. This result was not surprising given the observed lack of similarity at the level of function/network analysis. In SqCC however, combining the 447 copy-number associated genes with the 297 DNA methylation genes yielded overlap of 38 genes (Table S9). These genes exhibit frequent concurrent genetic, epigenetic, and subsequent gene-expression alterations that discriminate them from AC tumors. Notably, the well-known 3p tumor suppressor gene (TSG) *FHIT* was among these genes. The differential methylation levels of *FHIT* are shown in Figure 5c. Loss of *FHIT* expression is associated with smoking and is more frequent in SqCC tumors than AC tumors, consistent with our data [42,43,44]. Hypermethylation of this gene has also been investigated as a potential biomarker for centrally-occurring lung cancers [45,46]. Concerted genetic and epigenetic disruption was not limited to hypermethylation/loss however, as numerous genes displayed hypomethylation coupled with increased copy number and gene expression in SqCC. For example, *BRF2*, which we recently identified as a lineage specific oncogene in lung SqCC, was deregulated in this manner, highlighting its importance to the development of this lung cancer subtype [47]. Furthermore, in addition to those genes previously associated with lung cancer, TSGs and oncogenes known to be deregulated in other cancer types—such as *PRDM2* and *SLAH2*, respectively—were also altered at the genetic, epigenetic and gene expression levels. Such multidimensional disruption is indicative of strong selective

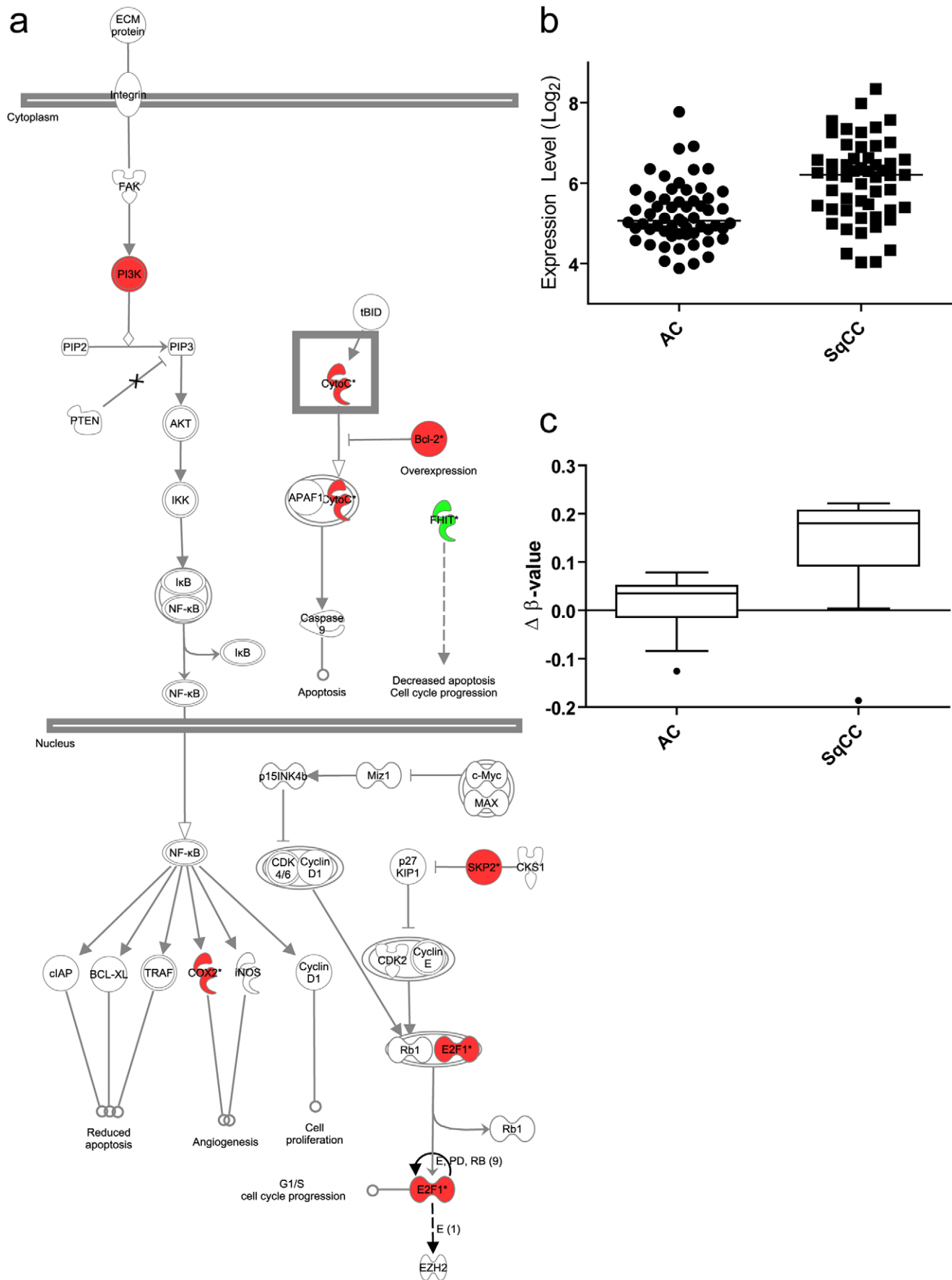


Figure 5. Epigenetically altered SqCC genes are significantly enriched for SCLC signaling. a) SCLC signaling components altered by DNA methylation in SqCC. In this schematic of the SCLC signaling pathway, genes that are hypomethylated and overexpressed are shown in red, and those that are hypermethylated and underexpressed are shown in green. Components at all levels of the pathway are affected, including the transcription factor *E2F1*, which drives the expression of the oncogenic polycomb group member *EZH2*. b) *EZH2* expression in 58 AC tumors and 53 SqCC tumors. *EZH2* expression was assessed in an external dataset, and it was found to be higher, as predicted, in SqCC tumors compared to AC tumors using a Mann-Whitney U test ($p < 0.0001$). c) *FHIT* differential methylation levels in SqCC and AC tumors. *FHIT* was shown to be deregulated by both deletion and hypermethylation in a manner that was specific to SqCC tumors. Show here are the differential DNA methylation levels for 30 AC tumors and 13 SqCC tumors. The SqCC tumors are hypermethylated to a much higher degree than the AC tumors, consistent with previous published findings. doi:10.1371/journal.pone.0037775.g005

pressures for gene silencing/activation during tumorigenesis, suggesting that these genes may play a pivotal role in SqCC.

Subtype specific genes are responsible for AC and SqCC phenotypes

Next, we aimed to confirm that the genes differentially disrupted at the genomic and epigenomic level are responsible for the different biological characteristics of AC and SqCC. Since they are regulated by subtype specific alterations, we hypothesized that the expression levels of these genes should be able to accurately segregate NSCLC tumors into distinct AC and SqCC groups. As predicted, when using the expression values for the 49 NSCLC tumors from our data set, principle component analysis with the 778 unique genetically and/or epigenetically deregulated genes clearly delineated distinct subtype specific clusters (Figure 6a). A receiver operating characteristic (ROC) area under the curve (AUC) value of 0.9690 ($P < 0.0001$) confirmed that principle component 1 was a strong discriminator of the subtypes (Figure 6a). This was not surprising as the genes were uncovered based on differences between the subtypes using this same set of samples. Therefore, to further confirm the role of the genes in subtype development, we applied the same analysis to two independent sample sets generated by different institutions. The first consisted of 111 (58 AC and 53 SqCC, Sample Set #3, Table S1) and the second of 138 (62 AC and 76 SqCC, Sample Set #6, Table S1) clinical lung tumors [48]. Strikingly, this analysis was also able to separate the AC and SqCC samples with a great deal of accuracy (ROC AUC values of 0.9076 and 0.9442, $P < 0.0001$, respectively) (Figure 6b and c). Validation in these large, independent panels of NSCLC tumors from separate institutions provides further evidence that the genes regulated by subtype specific genomic and epigenomic disruptions are responsible for driving the differential development of AC and SqCC. Furthermore, our results highlight the impact of this novel integrative genome, epigenome and transcriptome analysis in identifying robust target genes that can be used as biomarkers of disease.

Subtype-specific genetic differences are translated to the protein level

In order to confirm that the genome and transcriptome differences between the subtypes affect the relative protein levels of the identified genes, we performed immunohistochemical (IHC) analysis on a large, independent panel of >200 lung tumors. Protein levels for three subtype specific genes with available antibodies validated for IHC were analyzed: ERCC1 (inactivated in AC), KEAP1 (inactivated in AC) and SOX2 (activated in SqCC) (Figure 7). Average protein levels for all three genes were significantly different between the subtypes in the direction predicted by the integrative genetic and epigenetic analysis (Figure 7a, d, and g). The average immunohistochemical nuclear ERCC1 expression was much lower in AC tumors (43.45 ± 5.389 , $N = 175$) compared to SqCC tumors (79.99 ± 9.095 , $N = 106$, two-tailed $p < 0.001$, unpaired t test with Welch's correction) consistent with this gene being inactivated specifically in AC. Similar results were seen for cytoplasmic levels of KEAP1, which is also

inactivated specifically in AC (AC: 126.5 ± 4.179 , $N = 184$; SqCC: 160.9 ± 5.401 , $N = 110$, two-tailed $p < 0.0001$, unpaired t test with Welch's correction). Conversely, nuclear levels of SOX2, which is activated specifically in SqCC, were significantly higher in this subtype (206.5 ± 8.839 , $N = 106$) than in AC (70.39 ± 6.342 , $N = 170$, two-tailed $p < 0.0001$, unpaired t test with Welch's correction). Together, these data demonstrate that the genomic, epigenomic and gene transcription differences between the subtypes are translated to the protein level, providing more credence to the hypothesis that these changes have a functional consequence on the phenotypes of AC and SqCC.

Subtype-specific genes are associated with distinct clinical characteristics in AC and SqCC

We next aimed to determine the influence of the subtype specific genes on the clinical characteristics of AC and SqCC. Since these genes are responsible for defining the distinct biology of these diseases, we reasoned that their expression should only correlate with specific clinical features in one subtype and not the other subtype or NSCLC (AC + SqCC) in general. To test this, we determined the survival associations using a Mantel-Cox log rank test for each of the 778 subtype specific genes in AC, SqCC and NSCLC in the dataset with overall survival information available (Sample Set #3, Table S1). Collectively, this analysis revealed 131 AC and 46 SqCC specific genes that had significant ($P < 0.05$) associations with overall survival (Table S10). Remarkably, the associations were completely specific to an individual subtype as no genes were correlated with survival in the same manner across both subtypes. Six genes (*DSG2*, *PLAC2*, *ATP9A*, *TPM4*, *CD9* and *PSMD11*) were significantly associated with survival in both subtypes; however, they displayed a completely opposite pattern in terms of survival with low expression associated with poor survival in one subtype and high expression with poor survival in the other (Figure 8). Thus, although associated with survival in both subtypes, the genes exhibit distinct subtype-specific associations. Interestingly, low levels of *CD9* expression have been previously implicated in the poor prognosis of lung cancer patients [49]. However, we now show that this association is subtype specific with low levels of *CD9* correlated with poor prognosis in SqCC and high levels with poor prognosis in AC (Figure 8). Importantly, only eight genes that were associated with survival in one of the subtypes were also significant when analyzing NSCLC as a whole, providing further evidence to the importance of treating the subtypes as separate disease entities. Together, these findings underscore the potential clinical relevance of subtype specific alterations.

Defining putative treatment strategies tailored to lung cancer subtypes using *in silico* screening of candidate therapeutic compounds

Lastly, after defining and validating our AC and SqCC specific cancer genes, we applied these findings to define potential treatment strategies tailored to each lung cancer subtype. To do this, we queried the Connectivity Map (CMAP) database using our subtype

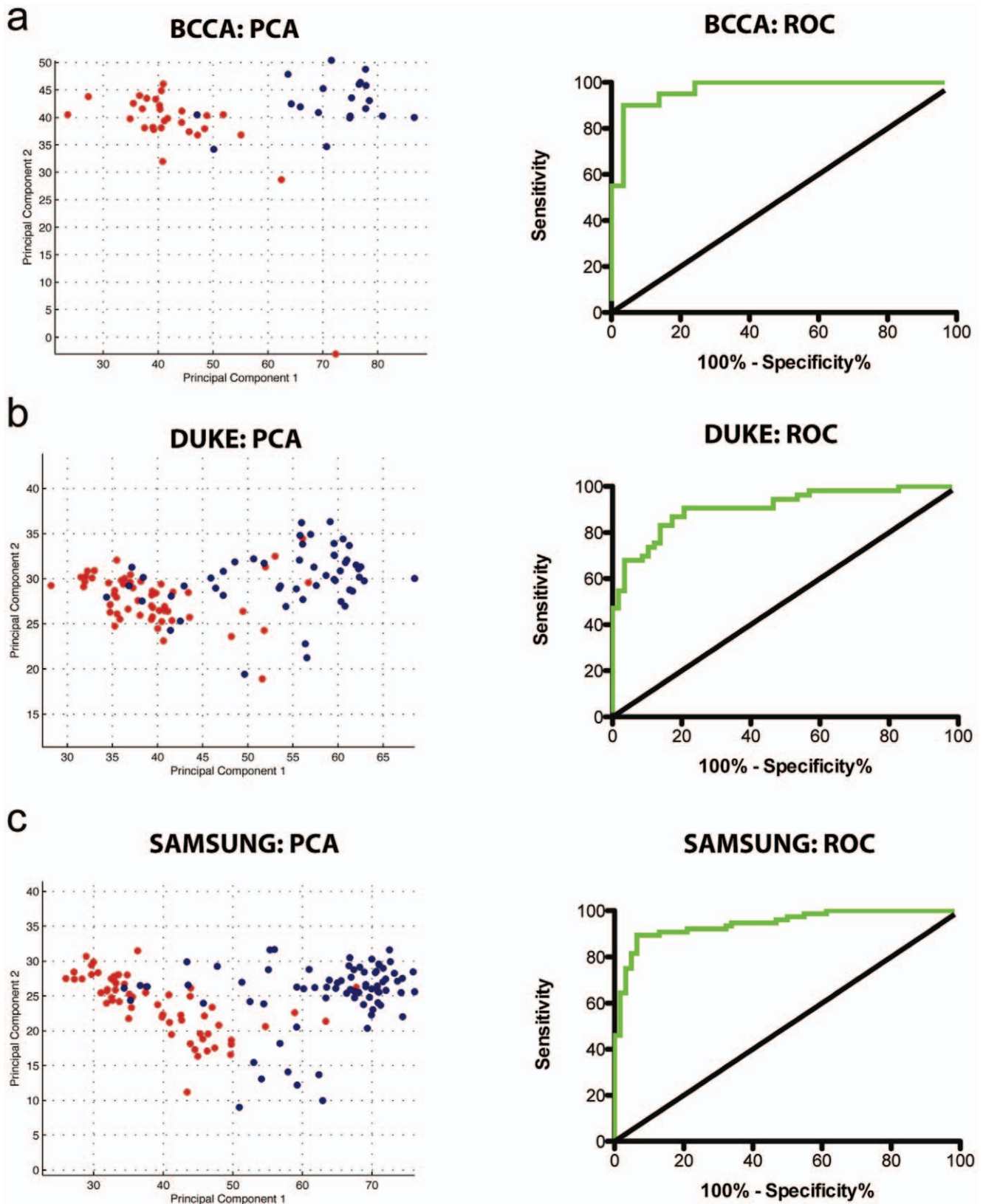


Figure 6. Subtype specific genes explain AC and SqCC phenotypes. Principal components analysis was performed utilizing all genes demonstrating expression differences between the subtypes as a result of genetic and/or epigenetic alterations using: A) Data generated for 49 NSCLC tumors (29 AC, 20 SqCC) as part of this study which was used in gene discovery; B) Publically available data from 111 NSCLC tumors (58 AC and 53 SqCC, Dataset #3-Duke, Table S1) used as test set #1; C) Publically available data from 138 NSCLC tumors (62 AC and 76 SqCC, Dataset #6-Samsung, Table S1) used as test set #2. Red circles indicate AC samples, while the blue circles indicate SqCC samples. Strong separation of the AC

and SqCC tumors along principal component 1 in all sets demonstrates the contribution of these genes to the differential phenotypes. On the right are the respective ROC curves for each dataset using the respective principle component 1 values for each sample. AUC values of 0.9690, 0.9076 and 0.9442 for A), B) and C), respectively, suggest that the gene expression signature is an extremely good discriminator of the subtypes. doi:10.1371/journal.pone.0037775.g006

specific genes to identify compounds that could “reverse” the expression direction of each signature. The CMAP consists of thousands of gene expression profiles from different cancer cell lines treated with a vast collection of small molecules [50]. By comparing the subtype specific signatures of up and down regulated genes with preexisting small molecule response signatures in the database, the program can identify small molecules whose effects on gene expression changes are positively or negatively correlated. Negative correlation scores imply that the matched molecules have a mode of action that can reverse the expression direction of query genes, and therefore serve as potential therapeutic compounds. Using this *in silico* screening approach, we identified numerous instances (cell line/treatment combination) that were significantly correlated with both the AC and SqCC specific gene signatures identified in our study (Table S11). Remarkably, SqCC had an expression signature that was negatively correlated with multiple HDAC and PI3K/mTOR instances including trichostatin A, vorinostat (also known as SAHA) and MS-275 (all HDAC inhibitors) and LY-294002,

quinostatin, sirolimus (also known as Rapamycin) and wortmannin (all PI3K/mTOR inhibitors). These findings were interesting for two reasons, firstly as the alteration of histone modifying enzymes was the major network disrupted in SqCC (see above). Secondly, the relevance of these epigenetically-targeted drugs is pertinent as we identified concerted disruption of PRC2 components responsible for *de novo* methylation as well. In addition, *PIK3CA* activation (mutation and/or amplification) is known to occur more frequently in SqCC than AC [51] and many downstream components of this pathway were also altered specifically in SqCC (Table S4). The CMAP analysis for AC, on the other hand, was not very informative, as none of the negatively correlated molecules shared the same functions (Table S10). This may be a byproduct of the heterogeneity between AC tumors (discussed below).

To confirm the results from the CMAP analysis, we treated a panel of six NSCLC cell lines (three AC and three SqCC) with the HDAC inhibitor Trichostatin A, which was the most significantly negative correlated HDAC inhibitor from the SqCC analysis.

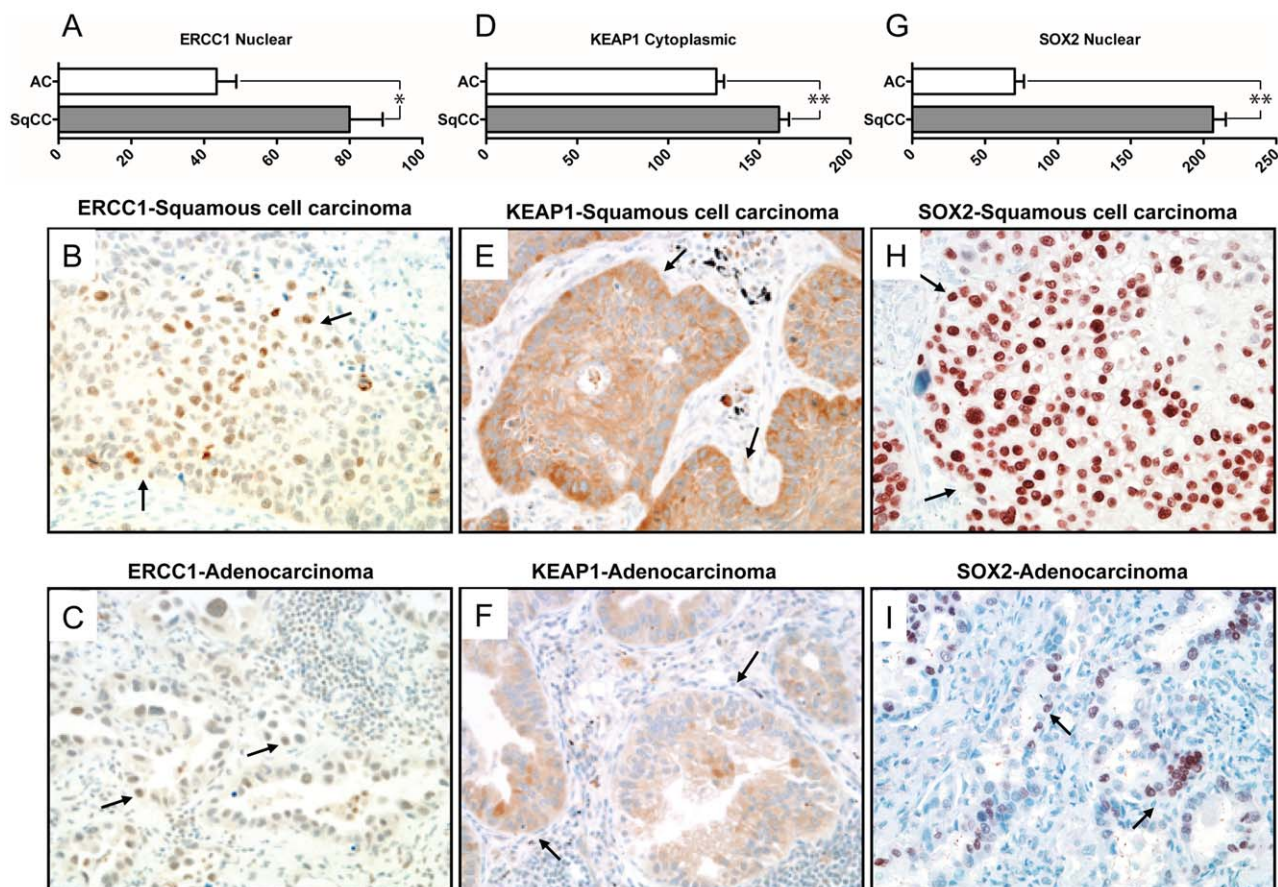


Figure 7. Subtype-specific genomic differences are reflected at the protein level. Immunohistochemical analysis of protein levels for ERCC1 (A–C), KEAP1 (D–F) and SOX2 (G–I) in squamous and adenocarcinoma lung tumors. Average immunohistochemical protein expression levels for each subtype are plotted \pm SEM of each group. Representative microphotographs showing tumoral cells (arrows) with higher levels of immunohistochemistry expression of nuclear ERCC1 (B and C), cytoplasmic KEAP1 (E and F) and nuclear SOX2 (H and I) in squamous cell carcinomas (B, E and H) compared to lung adenocarcinomas (C, F, and I). Images are of samples reflecting the average protein expression for each group (ERCC1: SqCC = \sim 80, AC = \sim 43; KEAP1: SqCC = \sim 161, AC = \sim 126; SOX2: SqCC = \sim 207, AC = \sim 70). Magnification 200x. * and ** = $p < 0.001$ and $p < 0.0001$, two-tailed unpaired t test with Welch’s correction, respectively. doi:10.1371/journal.pone.0037775.g007

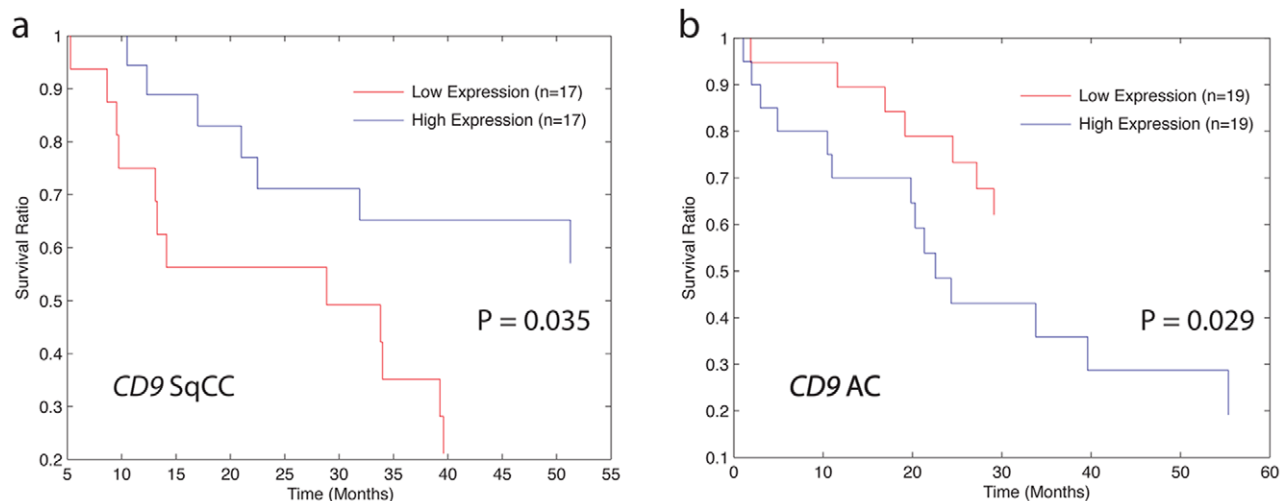


Figure 8. CD9 alteration and survival is different in AC and SqCC tumors. a) Low *CD9* levels are associated with poor prognosis in SqCC. The prognostic value of *CD9* expression levels was evaluated in 53 SqCC tumors. Survival of the 1/3 lowest *CD9* expressers is shown in red, and the top 1/3 is shown in blue. In this case, low expression of *CD9* is significantly associated with poor prognosis when using a Mantel-Cox log test ($p=0.035$). b) High *CD9* levels are associated with poor prognosis in AC. The prognostic value of *CD9* expression levels was evaluated in 58 AC tumors. Survival of the 1/3 lowest *CD9* expressers is shown in red, and the top 1/3 is shown in blue. In this case, low expression of *CD9* is significantly associated with poor prognosis when using a Mantel-Cox log test ($p=0.029$).
doi:10.1371/journal.pone.0037775.g008

Importantly, we selected the available cell lines that best represented their respective clinical tumor subtypes by performing principle component analysis with the subtype-specific genes using publically available gene expression profiles for a large panel of

NSCLC cell lines (Figure S1). As predicted by the *in silico* analysis, SqCC cell lines (average $IC_{50} = 69$ nM) were, on average, five times more sensitive to Trichostatin A than AC cell lines (average $IC_{50} = 346$ nM), a statistically significant difference ($P=0.05$, Mann-Whitney U Test) (Figure 9).

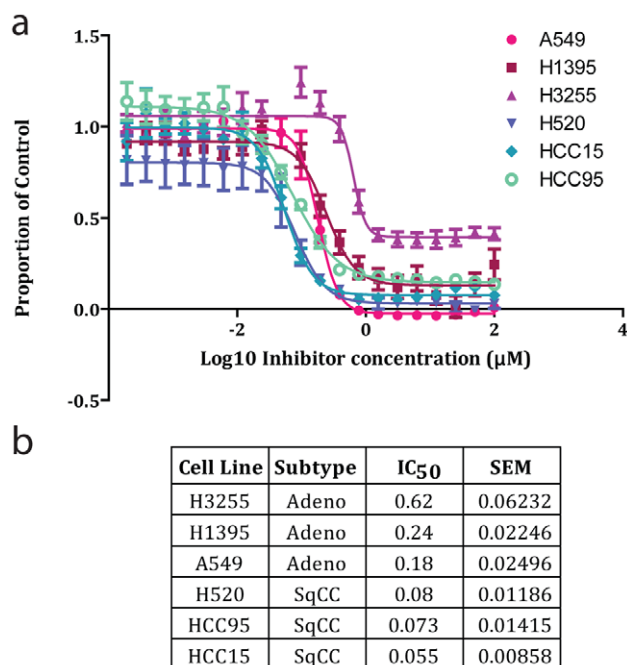


Figure 9. SqCC cell lines are more sensitive to the HDAC inhibitor Trichostatin A than AC cell lines. a) Dose-response analysis of Trichostatin A on the relative viability of three AC (A549, H3255 and H1395) and three SqCC (H520, HCC15 and HCC15) cell lines. Each curve was generated from the average data points from four separate experiments. b) Table with the average IC_{50} and SEM for each cell line tested derived from four separate experiments.
doi:10.1371/journal.pone.0037775.g009

Discussion

The emergence of tumor cells from normal precursors is thought to involve a complex interplay between genetics and cell lineage [8]. Due to the different cell types involved as well as the attributes of an individual cell's local environment or niche, it is logical to assume different mechanisms are required in tumorigenesis for each lung cancer subtype. Cell lineage may also have a dramatic effect on the manifestation of genetic/epigenetic alterations during the development of each lung cancer subtype as only those promoting a malignant phenotype in the specific cellular context will be selected and maintained [8]. Previous studies suggest that distinct patterns of DNA alteration exist for AC and SqCC; however, the specific genes responsible for the different tumor phenotypes are largely unknown [20,21,22,52].

In this study, we provide the first comprehensive investigation of the key genetic and epigenetic alterations distinguishing AC and SqCC lung tumors. We achieved this by integrating whole-genome DNA copy number, DNA methylation, and gene expression data to identify genes altered in a subtype-specific manner. These genes are associated with distinct gene networks in each lung cancer subtype, flagging distinct signaling pathways as contributing to tumorigenesis. We also found subtype-type specific changes to be correlated with clinical outcomes and highlight putative treatment strategies based on the subtype specific molecular signatures.

The 294 subtype-specific copy number alterations detected in this study demonstrate that different genetic pathways are involved in the pathogenesis of AC and SqCC. Importantly, previously identified lineage specific oncogenes including *SOX2* and *BRF2* were identified, validating our approach [17,47]. Although some of the regions and genes have previously been shown to be

important in NSCLC development, our findings suggest their newfound importance to a specific lung cancer subtype. For example, previously identified oncogenes such as *NOTCH3* and *FOXM1* were overexpressed through increased gene dosage specifically in SqCC while the tumor suppressor *KEAP1* was deleted and underexpressed specifically in AC [53,54,55]. This is the first report suggesting that these previously established lung cancer-associated genes are actually involved in subtype-specific tumorigenesis.

A broader gene network-based analysis of the copy number-regulated genes revealed additional insights into the differential oncogenic mechanisms driving the pathogenesis of AC and SqCC. The top SqCC gene network was mainly associated with DNA replication, recombination and repair. In addition to these functions, histone modification genes were represented as well. Histones are fundamental building blocks of eukaryotic chromatin and are involved in myriad cellular processes, including replication, repair, recombination and chromosome segregation [56,57,58]. Recently, global alterations of histone modification patterns have been reported in human cancers [59]. Our data suggest that direct deregulation of histone modification enzymes including *ASF1B*, *PRMT1*, *SAE1*, *SET8*, *CHAF1A* and *UHRF1* may drive this phenomenon and play a key role during the development of lung SqCC. As histone modifications also play an essential role in DNA replication, there may be a synergistic effect between the histone modifying genes and replication/recombination associated genes that contribute to tumor development. Interestingly, histone modification alterations occur more frequently in lung SqCC than AC, consistent with our findings [60].

The gene network detected as perturbed in AC subtype tumors contained genes mainly involved in regulating tissue development and cell-to-cell signaling and known to be targeted by the transcription factor *HNF4 α* . *HNF4 α* regulates a large set of genes in a cell-specific manner and is necessary for cell differentiation and maintenance of a differentiated epithelial phenotype [61]. In other carcinomas, deregulation of *HNF4 α* leads to increased cellular proliferation, progression and dedifferentiation [62,63,64,65,66]. This suggests that *HNF4 α* may act as a tumor suppressor in epithelial carcinogenesis [61]. Interestingly, although *HNF4 α* was not affected, we found that numerous downstream targets of this gene are downregulated specifically in AC. Thus, this may have the same net affect as inactivation of *HNF4 α* itself and lead to increased cellular proliferation during AC tumorigenesis.

Concerted alterations to gene networks and pathways are not a feature that is limited to copy-number regulated genes. Indeed, we found that coupling subtype-specific DNA methylation profiles with matched gene expression alterations implicated numerous canonical signaling pathways in the differential development of SqCC and AC tumors. The enrichment of small-cell lung cancer signaling pathway members within the epigenetically altered SqCC genes was of particular interest. For example, one of the deregulated components of this pathway, the transcription factor *E2F1*, was found to exhibit SqCC-specific hypomethylation and overexpression. *E2F1* is upregulated in SCLC tumors [40], which suppresses apoptosis and induces expression of *EZH2*, an oncogenic polycomb histone-methyltransferase [39]. The relevance of this pathway in SqCC tumors is strengthened by our observation that *EZH2* expression is significantly higher in SqCC than AC (Figure 5). This is particularly interesting given the potential dual role of *EZH2* in different cancer types [67]. The disruption of the polycomb group (preferentially in SqCC) is relevant because we have also identified SqCC-specific deregulation

of numerous histone-modifying enzymes by DNA copy number alterations.

In addition to the deregulation of histone modifying genes by DNA copy number and DNA methylation alterations, we have uncovered evidence of global SqCC-specific epigenetic disruption. Our analysis of global DNA methylation levels in AC and SqCC tumors showed that SqCC tumors were more hypomethylated overall, suggesting that the epigenetic machinery is highly deregulated in SqCC (Figure 4). There is precedent for this finding, as altered global methylation is thought to be a consequence of exposure to the carcinogens found in tobacco smoke [37,38,68]. Global hypomethylation, such as that caused by cigarette smoke, is also known to be associated with chromosomal instability. Although we did not observe any difference in the percentage of AC or SqCC genomes that were altered by copy number, we did identify a greater number of recurrent copy number alterations in the SqCC subtype. This may be indicative of similar selective pressures in the SqCC tumors that facilitate the development of recurrent alterations, whereas those in AC may be more diverse, leading to greater heterogeneity.

Concerted DNA copy number and DNA methylation alterations yield insight into tumor biology as well. We show hypermethylation and deletion of *FHIT* to be a SqCC-specific event, confirming earlier studies describing inactivation of the gene at a higher frequency in SqCC than AC tumors [42,46,69,70]. While there were relatively few genes that were simultaneously activated/inactivated in SqCC by DNA copy number and methylation alterations (32), there was no overlap seen in AC. In fact, compared to SqCC tumors, AC tumors possessed fewer subtype-specific alterations linked to both DNA copy number and DNA methylation. The reason for this is not clear, but it is possible that AC tumors have higher levels of cellular and/or genetic heterogeneity than SqCC tumors. Heterogeneity of patient clinical-characteristics may also contribute to this, as lung cancer in non-smokers are more likely to appear as AC tumors, and cigarette smoke may play a role in contributing to specific genetic or epigenetic alterations [71,72]. Nevertheless, although a high proportion of our AC tumors were from never smokers (22.5%), no significant differences in copy number were identified between AC tumors from ever and never smokers (data not shown), suggesting that this is not a confounding factor in our analysis.

The specific alterations selected during the development of each subtype may also play a role in the clinical management of disease, such as influencing treatment outcomes. Indeed, genes already known to influence NSCLC response to conventional chemotherapy were deregulated in a subtype-specific manner. For example, the finding that *ERCC1* disruption was subtype-specific is significant. *ERCC1* is a nucleotide excision repair gene which repairs DNA adducts and lesions induced by smoking-related carcinogens [73]. As such, low expression levels of *ERCC1* have been implicated in lung cancer susceptibility [74] and tumorigenesis, whereas high expression levels are associated with favorable overall prognosis [73]. However, since *ERCC1* is also involved in the repair of cisplatin-induced DNA adducts in cancer cells, high expression levels increase resistance to platinum-based chemotherapies [75,76], while low expression leads to drug sensitivity [77]. Underscoring the relevance of this finding are the results of recent clinical trials that have described a significantly better outcome for patients who received adjuvant cisplatin-based combination chemotherapy if their resected tumors expressed low levels of *ERCC1* [73,75]. Our finding that this gene is inactivated specifically in AC tumors has major clinical consequences in terms of guiding disease management and treatment strategies in order to define appropriate treatment regimens for

patients. This is consistent with a previous report demonstrating the subtype specificity of *ERCC1* expression levels in NSCLC, and further highlights how biological differences between AC and SqCC may influence patient response to therapy [78].

Importantly, numerous genomic regions showed opposite patterns of alteration in each lung cancer subtype. For example, a discrete alteration spanning 2.4 Mbp on chromosome bands 8p12-p11.23 was commonly gained in SqCC and lost in AC, implying that genes in these regions may play opposite roles during the development of the individual NSCLC subtypes, acting as TSGs in AC and as oncogenes in SqCC. Such diametric alteration is seen when including epigenomic alterations as well. This is the case for *PARP11*, which is upregulated in SqCC by DNA hypomethylation and downregulated in AC by copy number loss (Table S8). This information will become particularly important as targeted therapeutic strategies based around these genes develop. The development of MEK inhibitors highlights this point [72]: since activated MEK1 and MEK2 phosphorylate and activate ERK (MAPK1), the differential deregulation of *MAPK1* in AC (inactivated) and SqCC (activated) tumors may be an important consideration in determining the efficacy of this treatment against lung cancer subtypes [79].

Similarly, numerous studies have aimed to identify genes associated with prognosis in NSCLC in order to better determine patient outcome [80]. Our data suggest that these relationships may be subtype-specific as well (Table S10). Importantly, we discovered that specific genes may be indicative of totally different clinical outcomes depending on which subtype they are disrupted in. For example, *CD9* was gain/overexpressed in SqCC and high expression of this gene correlated with favorable survival in this subtype as well (Figure 7). However, the opposite was true in AC, which displayed copy number loss and underexpression; low expression was associated with good survival and high expression with poor survival. Together, these results indicate that the genes involved in defining clinical characteristics are largely exclusive to individual NSCLC subtypes and influenced by the acquisition of distinct genetic alterations during tumor development. In addition, this underlines the importance of separating AC and SqCC when assessing genes involved in predicting patient prognosis and other clinical outcomes.

Furthermore, in order to demonstrate how these findings can be used to define treatment strategies tailored to the individual lung cancer subtypes, we performed CMAP analysis using our AC and SqCC specific gene signatures to identify compounds that can potentially reverse the expression of these genes. Although the results for AC were uninformative, the SqCC CMAP analysis identified numerous HDAC and PI3K/mTOR inhibitors as compounds that could potentially induce a gene expression signature negatively correlated with that associated with SqCC (Table S11). The HDAC inhibitor result was remarkable as the alteration of histone modifying enzymes was the most prominent network disrupted in this subtype, providing a biological basis for this finding. Furthermore, cancer cells with elevated activity of E2F1 have been shown to be highly susceptible to HDAC inhibitor induced cell death and more recently HDAC inhibitors such as SAHA have been shown to suppress the activity of EZH2 [81,82]. As E2F1 and EZH2 are both upregulated in SqCC (Figure 5), this data suggests that treatment with HDAC inhibitors, in conjunction with standard chemotherapy, could be a promising avenue for disease treatment. In addition, since *PIK3CA* activation (mutation and/or amplification) is known to occur more frequently in SqCC than AC the finding of multiple PI3K/mTOR inhibitors as potential therapeutics for SqCC is also logical [51,75]. Together, this data demonstrates the potential to use information

about the underlying molecular biology of the cancer subtypes to make informed decisions about clinical management strategies and suggests that HDAC and PI3K/mTOR inhibitors, in combination with current treatment regimes, may provide a novel treatment tailored to lung SqCC.

Lastly, it is important to note that although they display broadly unifying characteristics, AC and SqCC themselves are very heterogeneous tumor types, with many molecular, pathologic and clinical subtypes [83,84]. We suggest that our analysis has revealed the common initiating molecular changes for AC and SqCC, which may be followed by secondary driver mutations that cause the subsequent heterogeneity seen in advanced tumors. This is supported by the fact that we identified SqCC specific alterations in preinvasive CIS lesions, suggesting that these alterations commence early in tumor development (Table S3). By identifying these “root” changes, one may be able to utilize type specific therapies either in combination with, or followed by, individualized therapies that target the secondary alterations to achieve a more complete antitumor response.

Conclusions

Fundamental discrepancies in tumor biology may be a primary factor determining the differential outcomes of lung cancer patients. Biological differences that segregate with cell lineages may also lead to differences in response to therapies [85]. Therefore, tumor cell lineage may be an important consideration when selecting and developing therapeutic approaches for lung cancer. An example of this is already in common practice as SCLC and NSCLC are treated separately due to the observation that cancers of the former lineage tend to be much more responsive to initial treatment with conventional cytotoxic agents. In contrast, no clinical distinction is made between the different subtypes of NSCLC and stage is the primary factor that determine treatment options. Our high-resolution integrative analysis of NSCLC genomes and epigenomes delineated novel tumor subtype-specific genetic and epigenetic alterations responsible for driving the differential pathogenesis and phenotypes of AC and SqCC. The specific genes and networks identified in this study provide essential starting insights for elucidating mechanisms of tumor differentiation and developing tailored therapeutics for lung cancer treatment. More generally, our results confirm at the molecular level that these lung cancer subtypes are distinct disease entities. When designing new treatment strategies and testing new drugs in clinical trials, these subtype differences as well as the biological pathways should be taken into account.

Materials and Methods

Ethics Statement

All patient samples were collected under informed, written patient consent and anonymized as approved by the University of British Columbia–British Columbia Cancer Agency Research Ethics Board (REB number H04-60060).

DNA samples

Formalin-fixed, paraffin embedded (FFPE) and fresh-frozen tissues were collected from St. Paul's Hospital, Vancouver General Hospital and Princess Margaret Hospital following approval by the Research Ethics Boards. Hematoxylin and eosin stained sections for each sample were graded by a lung pathologist for use in selecting regions for microdissection. DNA was isolated using standard procedure with proteinase K digestion followed by phenol-chloroform extraction as previously described [86]. Patient information is located in Table 1.

Table 1. Sample set clinical characteristics.

		AC (n = 169)	SqCC (n = 92)
Stage*	I	76 (44.9%)	32 (34.7%)
	II	40 (23.6%)	32 (34.7%)
	III	22 (13%)	14 (15.2%)
	IV	27 (16.0%)	10 (10.9%)
	n/a	4 (2.4%)	4 (4.4%)
Sex	Female	106 (62.7%)	26 (28.3%)
	Male	63 (37.3%)	66 (71.7%)
Smoking Status	Current smoker	48 (28.4%)	30 (32.6%)
	Ex-smoker	80 (47.3%)	61 (66.3%)
	n/a	3 (1.8%)	
	Non-smoker	38 (22.5%)	1 (1.1%)

*6th Edition UICC/AJCC classification criteria.

doi:10.1371/journal.pone.0037775.t001

Tiling path array comparative genomic hybridization

Array hybridization was performed as previously described [30,87,88]. Briefly, equal amounts (200–400 ng) of sample (extracted from either fresh-frozen or FFPE tissues) and single male reference genomic DNA were differentially labelled and hybridized to SMRT array v.2 (BCCRC Array Laboratory, Vancouver, BC), which is previously described to give optimal genome coverage [27,89].

Hybridized arrays were imaged using a charge-coupled device (CCD) camera system and analyzed using *SoftWoRx Tracker Spot Analysis* software (Applied Precision, Issaquah, WA). Systematic biases were removed from all array data files using a stepwise normalization procedure as previously described [29,32]. *SeeGH* software was used to combine replicates and visualize all data as log₂ ratio plots [90,91]. Stringently, all replicate spots with a standard deviation above 0.075 or signal to noise ratios below three were removed from further analysis. The probes were then positioned based on the human March 2006 (hg 18) genome assembly. Genomic imbalances (gains and losses) within each sample were identified using *aCGH-Smooth* [28] with lambda and breakpoint per chromosome settings at 6.75 and 100, respectively (as previously described) [30]. The resulting frequency of alteration was then determined for each lung cancer cell type as described previously [30].

DNA Methylation Analysis

For 30 AC samples, 30 patient-matched non-malignant lung samples, 13 SqCC samples and 18 non-patient matched bronchial epithelia samples (all fresh-frozen samples), DNA methylation profiling was performed using the Illumina HumanMethylation27 chip. Five hundred nanograms of DNA from each sample were analyzed by this technology. Normalized β -values were obtained and only those with a detection p -value of ≤ 0.05 were used. When comparing tumor samples (AC/SqCC) and normal non-malignant samples (AC non-malignant parenchyma and bronchial epithelia), probes were deemed aberrantly methylated if the absolute difference between tumor and the average of the appropriate normal samples was ≥ 0.15 .

Comparison of subtype alteration frequencies

Regions of differential copy number alteration between AC and SqCC genomes were identified as follows. Each array element was

scored as 1 (gain/amplification), 0 (neutral/retention), or -1 (loss/deleted) for each individual sample. Values for elements filtered based on quality control criteria were inferred by using neighbouring probes within 10 Mb. Probes were then aggregated into genomic regions if the similarity in copy number status between adjacent probes was at least 90% across all samples from the same subtype. The occurrence of copy number gain/amplification, loss/deletion, and retention at each locus was then compared between AC and SqCC data sets using the Fisher's exact test. Testing was performed using the *R* statistical computing environment on a 3×2 contingency table as previously described, generating a p -value for each probe [30]. A Benjamini-Hochberg multiple hypothesis testing correction based on the number of distinct regions was applied and resulting p -values ≤ 0.01 were considered significant. Adjacent regions within 1 Mb which matched both the direction of copy number difference and statistical significance were then merged. Finally, regions had to be altered in $>20\%$ of samples in a group and the difference between groups $>10\%$ to be considered.

A similar approach was used for determining subtype-specific DNA methylation alterations. Frequencies of hypermethylation and hypomethylation for each probe were compared using a Fisher's exact test, followed by a Benjamini-Hochberg multiple testing correction. A corrected p -value cut-off of $p < 0.05$ was used to deem a probe differentially methylated between the two groups.

Gene expression microarray analysis

Fresh-frozen lung tumors were obtained from Vancouver General Hospital as described above. Microdissection of tumor cells was performed and total RNA was isolated using RNeasy Mini Kits (Qiagen Inc., Mississauga, ON). Samples were labeled and hybridized to a custom Affymetrix microarray according to the manufacturer's protocols (Affymetrix Inc., Santa Clara, CA). In addition, RNA was obtained from exfoliated bronchial cells of lung cancer free individuals obtained during fluorescence bronchoscopy [71]. All individuals were either current or former smokers. Expression profiles were generated for all cases using the Affymetrix U133 Plus 2 platform (Affymetrix Inc., Santa Clara, CA). All data was normalized using the Robust Multichip Average (RMA) algorithm in [92]. In addition, publically available datasets downloaded from the *Gene Expression Omnibus* were used: Affymetrix U133 Plus 2 expression data was downloaded for accession numbers GSE3141 [93] and GSE8894 [48].

Statistical analysis of gene expression data

Gene expression probes were mapped to March 2006 (hg 18) genomic coordinates and those within the regions of copy number difference between the subtypes were determined. Comparisons between expression levels for AC and SqCC tumors were performed using the Mann-Whitney U test and computed with the *ranksum* function in *Matlab*. As the direction of gene expression difference was predicted to match the direction of copy number difference, one tailed p -values were calculated. A Benjamini-Hochberg multiple hypothesis testing correction was applied based on the total number of gene expression probes analyzed for each region. Probes with a corrected p -value ≤ 0.001 were considered significant. If multiple probes mapped to the same gene, the one with the lowest p -value was used. Resulting genes were then mapped to the corresponding probes on the Affymetrix U133 Plus 2 array in order to compare their expression in a second set of NSCLC tumors (GSE3141 above) against normal bronchial epithelial cells. If multiple probes were present for a gene, the one with the strongest p -value was used. All comparisons were performed using a one-tailed t-test with unequal variances in *Excel* and genes with a $p < 0.001$ were considered significant. The fold-change for tumors versus normal tissues was

then determined in order to determine genes expressed in the direction predicted by copy number.

Principle component analysis was performed using expression data for the three independent tumor data sets (described above) in MATLAB. All genes of interest with probes on the corresponding arrays were used. Briefly, the first and second principal components were generated from the original dataset. In the subsequent validation in secondary datasets, these principal components are then used to weight the expression data for a gene based on the original distribution. The Receiver Operating Characteristic (ROC) area under the curve (AUC) analysis was performed to determine the ability of principle component 1 to separate the AC and SqCC samples into their appropriate histological groups. Calculations were performed using the *GraphPad Prism* software.

Connectivity Map (<http://www.broad.mit.edu/cmap/>) analysis was performed using the up and downregulated genes specific to each subtype as previously described [50].

Survival analysis

Survival analysis was performed using the statistical toolbox in *Matlab*. Expression data for each gene were sorted and survival times were compared between the top 1/3 and bottom 1/3 in expression using a publicly available gene expression microarray dataset with survival data (Table S1). Two tailed *p*-values were generated using a Mantel-Cox log test and those <0.05 were considered significant. Kaplan-Meier plots were then generated for each gene of interest.

Network identification

Functional identification of gene networks and canonical signalling pathways was performed using Ingenuity Pathway Analysis program (Ingenuity® Systems, www.ingenuity.com). AC and SqCC specific gene lists were imported as individual experiments using the Core Analysis tool. The analysis was performed using Ingenuity Knowledge Database with the Affymetrix U133 Plus 2 platform as the reference set and was limited to direct and indirect relationships.

Human lung tissue tissue microarray case selection

To determine the expression of ERCC1, KEAP1 and SOX2 in primary NSCLC, we selected 330 NSCLCs (AC, *n* = 220; SqCC, *n* = 110) from surgically resected lung cancer specimens from the Lung Cancer Specialized Program of Research Excellence Tissue-Bank at The University of Texas M.D. Anderson Cancer Center. We used archived, formalin-fixed, paraffin-embedded (FFPE) tumor tissue samples placed in tissue micro-array (TMA). The tumor tissue samples were collected between 1997 and 2003, and were histologically analyzed and classified using the 2004 WHO classification system [94]. The characteristics of these TMAs have been previously described in detail [95,96].

Immunohistochemical analysis

The immunohistochemical analysis was done using commercially available antibodies against KEAP1 (dilution 1:25; Proteintech, Chicago, IL), ERCC1 (dilution 1:25; Labvision, Fremont, CA) and SOX2 (dilution 1:50; R&D system, Minneapolis, MN). Immunohistochemical staining was done using an automated stainer (Dako, Inc.) with 5-μm-thick TMA sections from FFPE tissues. Tissue sections were deparaffinized and hydrated. Antigen retrieval was done in pH 6.0 citrate buffer in a decloaking chamber (121°C×30 - seconds, 90°C×10 seconds) and washed on Tris buffer. Peroxide blocking was done at ambient temperature with 3% H₂O₂ in methanol. The slides were incubated with primary antibody

(KEAP1 and ERCC1 for 60 minutes; SOX2 for 90 minutes) at ambient temperature and washed with Tris buffer, followed by incubation with biotin-labeled secondary antibody for 30 minutes (EnVision Dual Link System-HRP-Dako for KEAP1 and ERCC1; LSAB system-Dako for SOX2). The immunostaining was developed with 0.5% 3,3'-diaminobenzidine, freshly prepared with imidazole-HCl buffer (pH 7.5) containing hydrogen peroxide and an antimicrobial agent (Dako) for 5 minutes, and then the slides were counterstained with hematoxylin, dehydrated, and mounted.

Nuclear ERCC1, cytoplasmic KEAP1, and nuclear SOX2 expressions were quantified using a four-value intensity score (0, 1+, 2+, or 3+) and the percentage (0–100%) of the extent of reactivity. An immunohistochemical expression score was obtained by multiplying the intensity and reactivity extension values (range, 0–300), and these expression scores were used to determine expression levels.

Trichostatin A dose-response analysis

The effect of HDAC inhibitor Trichostatin A, (Cayman Chemicals, Denver, CO, USA) on six NSCLC cell lines; three adenocarcinoma (H3255, H1395 and A549) and three SqCC lines (HCC95, HCC15 and H520) was assessed by cell viability assays. Cells were plated in triplicate in 96 well plates at optimal densities for growth (A549 at 2000 cells/well, HCC95, HCC15 and H520 at 3000 cells/well, and H3255 and H1395 at 6000 cells/well). Cells were subjected to a series of 2-fold dilutions of Trichostatin A prepared in cell growth media and DMSO. The experimental inhibitor concentrations ranged from 100 μM to 109 pM and the final DMSO concentration for treated and untreated (control) cells was 1%. Blank wells contained equal volumes of growth media with 1% DMSO. Cells were incubated for 72 hours at 37°C and then treated with 10 μl of Alamar Blue cell viability reagent (Invitrogen, Carlsbad, CA, USA) according to manufacturer's instructions. The reaction product was quantified by measuring absorbance at 570 nm with reference to 600 nm using an EMax plate reader (Molecular Devices, Sunnyvale, CA, USA). The response of treated cells was measured as a proportion of the viability of untreated cells, with the mean background subtracted treatment absorbance divided by the mean background subtracted untreated absorbance for each inhibitor concentration. Dose response curves and IC₅₀ values were generated in Graph Pad v5 using the proportionate response of all 20 drug concentrations. Experiments were repeated in quadruplicate and differences in IC₅₀ values were determined using a student's t-test with a *p*-value <0.05 considered significant.

Supporting Information

Figure S1 Principle component analysis of NSCLC cell lines using subtype-specific genes. (TIF)

Table S1 Clinical Samples used in Analyses. (DOCX)

Table S2 List of copy number alterations specific to each subtype. (XLSX)

Table S3 SqCC-Specific Copy Number Alteration Present in CIS Cases. (XLSX)

Table S4 Genes deregulated by copy number specifically in each subtype. (XLSX)

Table S5 IPA network analysis of subtype specific copy number alteration target genes.
(XLSX)

Table S6 Genes deregulated by DNA methylation in each subtype.
(XLSX)

Table S7 IPA network analysis of subtype specific methylation target genes.
(XLSX)

Table S8 Genes disrupted by gene-dosage in one subtype and DNA methylation in the other.
(XLSX)

Table S9 Genes demonstrating concerted genetic, epigenetic and transcriptional disruption in SqCC.
(XLSX)

References

- Coleman MP, Forman D, Bryant H, Butler J, Rachet B, et al. (2011) Cancer survival in Australia, Canada, Denmark, Norway, Sweden, and the UK, 1995–2007 (the International Cancer Benchmarking Partnership): an analysis of population-based cancer registry data. *Lancet* 377: 127–138.
- Jemal A, Bray F, Center MM, Ferlay J, Ward E, et al. (2011) Global cancer statistics. *CA Cancer J Clin* 61: 69–90.
- Sato M, Shames DS, Gazdar AF, Minna JD (2007) A translational view of the molecular pathogenesis of lung cancer. *J Thorac Oncol* 2: 327–343.
- Giangreco A, Groot KR, James SM (2007) Lung cancer and lung stem cells: strange bedfellows? *Am J Respir Crit Care Med* 175: 547–553.
- Travis WD (2002) Pathology of lung cancer. *Clin Chest Med* 23: 65–81, viii.
- Mok TS, Wu YL, Thongprasert S, Yang CH, Chu DT, et al. (2009) Gefitinib or carboplatin-paclitaxel in pulmonary adenocarcinoma. *N Engl J Med* 361: 947–957.
- Broet P, Camilleri-Broet S, Zhang S, Alifano M, Bangarusamy D, et al. (2009) Prediction of clinical outcome in multiple lung cancer cohorts by integrative genomics: implications for chemotherapy selection. *Cancer Res* 69: 1055–1062.
- Garraway LA, Sellers WR (2006) Lineage dependency and lineage-survival oncogenes in human cancer. *Nat Rev Cancer* 6: 593–602.
- Scagliotti G, Hanna N, Fossella F, Sugarman K, Blatter J, et al. (2009) The differential efficacy of pemetrexed according to NSCLC histology: a review of two Phase III studies. *Oncologist* 14: 253–263.
- Langer CJ, Besse B, Gualberto A, Brambilla E, Soria JC (2010) The evolving role of histology in the management of advanced non-small-cell lung cancer. *J Clin Oncol* 28: 5311–5320.
- Bhattacharjee A, Richards WG, Staunton J, Li C, Monti S, et al. (2001) Classification of human lung carcinomas by mRNA expression profiling reveals distinct adenocarcinoma subclasses. *Proc Natl Acad Sci USA* 98: 13790–13795.
- Thomas RK, Weir B, Meyerson M (2006) Genomic approaches to lung cancer. *Clin Cancer Res* 12: 4384s–4391s.
- Coe BP, Chari R, Lockwood WW, Lam WL (2008) Evolving strategies for global gene expression analysis of cancer. *J Cell Physiol* 217: 590–597.
- Feinberg AP, Tycko B (2004) The history of cancer epigenetics. *Nat Rev Cancer* 4: 143–153.
- Hyman E, Kauraniemi P, Hautaniemi S, Wolf M, Mousses S, et al. (2002) Impact of DNA amplification on gene expression patterns in breast cancer. *Cancer Res* 62: 6240–6245.
- Pollack JR, Sorlie T, Perou CM, Rees CA, Jeffrey SS, et al. (2002) Microarray analysis reveals a major direct role of DNA copy number alteration in the transcriptional program of human breast tumors. *Proc Natl Acad Sci USA* 99: 12963–12968.
- Bass AJ, Watanabe H, Mermel CH, Yu S, Perner S, et al. (2009) SOX2 is an amplified lineage-survival oncogene in lung and esophageal squamous cell carcinomas. *Nat Genet* 41: 1238–1242.
- Weir BA, Woo MS, Getz G, Perner S, Ding L, et al. (2007) Characterizing the cancer genome in lung adenocarcinoma. *Nature* 450: 893–898.
- Luk C, Tsao MS, Bayani J, Shepherd F, Squire JA (2001) Molecular cytogenetic analysis of non-small cell lung carcinoma by spectral karyotyping and comparative genomic hybridization. *Cancer Genet Cytogenet* 125: 87–99.
- Pei J, Balsara BR, Li W, Litwin S, Gabrielson E, et al. (2001) Genomic imbalances in human lung adenocarcinomas and squamous cell carcinomas. *Genes Chromosomes Cancer* 31: 282–287.
- Sy SM, Wong N, Lee TW, Tse G, Mok TS, et al. (2004) Distinct patterns of genetic alterations in adenocarcinoma and squamous cell carcinoma of the lung. *Eur J Cancer* 40: 1082–1094.
- Tonon G, Wong KK, Maulik G, Brennan C, Feng B, et al. (2005) High-resolution genomic profiles of human lung cancer. *Proc Natl Acad Sci U S A* 102: 9625–9630.
- Toyooka S, Maruyama R, Toyooka KO, McLerran D, Feng Z, et al. (2003) Smoke exposure, histologic type and geography-related differences in the methylation profiles of non-small cell lung cancer. *Int J Cancer* 103: 153–160.
- Toyooka S, Toyooka KO, Maruyama R, Virmani AK, Girard L, et al. (2001) DNA methylation profiles of lung tumors. *Mol Cancer Ther* 1: 61–67.
- Sozzi G, Sard L, De Gregorio L, Marchetti A, Musso K, et al. (1997) Association between cigarette smoking and FHIT gene alterations in lung cancer. *Cancer Res* 57: 2121–2123.
- Bardelli A, Cahill DP, Lederer G, Speicher MR, Kinzler KW, et al. (2001) Carcinogen-specific induction of genetic instability. *Proc Natl Acad Sci U S A* 98: 5770–5775.
- Ishkanian AS, Malloff CA, Watson SK, DeLeeuw RJ, Chi B, et al. (2004) A tiling resolution DNA microarray with complete coverage of the human genome. *Nat Genet* 36: 299–303.
- Jong K, Marchiori E, Meijer G, Vaart AV, Ylstra B (2004) Breakpoint identification and smoothing of array comparative genomic hybridization data. *Bioinformatics* 20: 3636–3637.
- Khojasteh M, Lam WL, Ward RK, MacAulay C (2005) A stepwise framework for the normalization of array CGH data. *BMC Bioinformatics* 6: 274.
- Coe BP, Lockwood WW, Girard L, Chari R, Macaulay C, et al. (2006) Differential disruption of cell cycle pathways in small cell and non-small cell lung cancer. *Br J Cancer* 94: 1927–1935.
- Petersen I, Kotb WF, Friedrich KH, Schluns K, Bocking A, et al. (2009) Core classification of lung cancer: correlating nuclear size and mitoses with ploidy and clinicopathological parameters. *Lung Cancer* 65: 312–318.
- Lockwood WW, Chari R, Coe BP, Girard L, Macaulay C, et al. (2008) DNA amplification is a ubiquitous mechanism of oncogene activation in lung and other cancers. *Oncogene* 27: 4615–4624.
- Croce CM (2008) Oncogenes and cancer. *N Engl J Med* 358: 502–511.
- Doi A, Park IH, Wen B, Murakami P, Aryee MJ, et al. (2009) Differential methylation of tissue- and cancer-specific CpG island shores distinguishes human induced pluripotent stem cells, embryonic stem cells and fibroblasts. *Nat Genet* 41: 1350–1353.
- Choi SH, Worswick S, Byun HM, Shear T, Soussa JC, et al. (2009) Changes in DNA methylation of tandem DNA repeats are different from interspersed repeats in cancer. *Int J Cancer* 125: 723–729.
- Hoffmann MJ, Schulz WA (2005) Causes and consequences of DNA hypomethylation in human cancer. *Biochem Cell Biol* 83: 296–321.
- Yang HH, Hu N, Wang C, Ding T, Dunn BK, et al. Influence of genetic background and tissue types on global DNA methylation patterns. *Plos One* 5: e9355.
- Vaissiere T, Hung RJ, Zaridze D, Moukeria A, Cuenin C, et al. (2009) Quantitative analysis of DNA methylation profiles in lung cancer identifies aberrant DNA methylation of specific genes and its association with gender and cancer risk factors. *Cancer Res* 69: 243–252.
- Wu ZL, Zheng SS, Li ZM, Qiao YY, Aau MY, et al. (2009) Polycomb protein EZH2 regulates E2F1-dependent apoptosis through epigenetically modulating Bim expression. *Cell Death Differ*.
- Eymin B, Gazzeri S, Brambilla C, Brambilla E (2001) Distinct pattern of E2F1 expression in human lung tumours: E2F1 is upregulated in small cell lung carcinoma. *Oncogene* 20: 1678–1687.
- Hussain M, Rao M, Humphries AE, Hong JA, Liu F, et al. (2009) Tobacco smoke induces polycomb-mediated repression of Dickkopf-1 in lung cancer cells. *Cancer Res* 69: 3570–3578.
- Gerads J, Fong KM, Zimmerman PV, Minna JD (2000) Loss of Fhit expression in non-small-cell lung cancer: correlation with molecular genetic abnormalities and clinicopathological features. *Br J Cancer* 82: 1191–1197.

Table S10 Survival analysis of subtype-specific genes.
(XLSX)

Table S11 CMAP analysis of subtype-specific genes.
(XLS)

Acknowledgments

We would like to thank Emily Vucic and Timon Buys for their insightful comments.

Author Contributions

Conceived and designed the experiments: WWL IMW BPC RC IIW JDM AFG CEM SL WLL. Performed the experiments: WWL IMW BPC RC LMS MIN CB IIW. Analyzed the data: WWL IMW BPC RC LAP KLT LMS MIN CB IIW SL WLL. Contributed reagents/materials/analysis tools: BPC RC LMS MIN CB IIW JY JE NM MST JDM AFG CEM SL. Wrote the paper: WWL IMW JDM AFG CEM SL WLL.

43. Tomizawa Y, Nakajima T, Kohno T, Saito R, Yamaguchi N, et al. (1998) Clinicopathological significance of Fhit protein expression in stage I non-small cell lung carcinoma. *Cancer Res* 58: 5478–5483.
44. Sozzi G, Pastorino U, Moiraghi L, Tagliabue E, Pezzella F, et al. (1998) Loss of Fhit function in lung cancer and preinvasive bronchial lesions. *Cancer Res* 58: 5032–5037.
45. de Fraipont F, Moro-Sibilot D, Michelland S, Brambilla E, Brambilla C, et al. (2005) Promoter methylation of genes in bronchial lavages: a marker for early diagnosis of primary and relapsing non-small cell lung cancer? *Lung Cancer* 50: 199–209.
46. Maruyama R, Sugio K, Yoshino I, Maehara Y, Gazdar AF (2004) Hypermethylation of Fhit as a prognostic marker in nonsmall cell lung carcinoma. *Cancer* 100: 1472–1477.
47. Lockwood WW, Chari R, Coe BP, Thu KL, Garnis C, et al. (2010) Integrative genomic analyses identify BRF2 as a novel lineage-specific oncogene in lung squamous cell carcinoma. *PLoS Med* 7: e1000315.
48. Lee ES, Son DS, Kim SH, Lee J, Jo J, et al. (2008) Prediction of recurrence-free survival in postoperative non-small cell lung cancer patients by using an integrated model of clinical information and gene expression. *Clin Cancer Res* 14: 7397–7404.
49. Higashiyama M, Taki T, Ieki Y, Adachi M, Huang CL, et al. (1995) Reduced motility related protein-1 (MRP-1/CD9) gene expression as a factor of poor prognosis in non-small cell lung cancer. *Cancer Res* 55: 6040–6044.
50. Lamb J, Crawford ED, Peck D, Modell JW, Blat IC, et al. (2006) The Connectivity Map: using gene-expression signatures to connect small molecules, genes, and disease. *Science* 313: 1929–1935.
51. Yamamoto H, Shigematsu H, Nomura M, Lockwood WW, Sato M, et al. (2008) PIK3CA mutations and copy number gains in human lung cancers. *Cancer Res* 68: 6913–6921.
52. Petersen I, Bujard M, Petersen S, Wolf G, Goeze A, et al. (1997) Patterns of chromosomal imbalances in adenocarcinoma and squamous cell carcinoma of the lung. *Cancer Res* 57: 2331–2335.
53. Dang TP, Eichenberger S, Gonzalez A, Olson S, Carbone DP (2003) Constitutive activation of Notch3 inhibits terminal epithelial differentiation in lungs of transgenic mice. *Oncogene* 22: 1988–1997.
54. Wang IC, Meliton L, Tretiakova M, Costa RH, Kalinichenko VV, et al. (2008) Transgenic expression of the forkhead box M1 transcription factor induces formation of lung tumors. *Oncogene* 27: 4137–4149.
55. Lee DF, Kuo HP, Liu M, Chou CK, Xia W, et al. (2009) KEAP1 E3 ligase-mediated downregulation of NF-kappaB signaling by targeting IKKbeta. *Mol Cell* 36: 131–140.
56. Strahl BD, Allis CD (2000) The language of covalent histone modifications. *Nature* 403: 41–45.
57. Esteller M (2008) Epigenetics in cancer. *N Engl J Med* 358: 1148–1159.
58. Esteller M (2007) Cancer epigenomics: DNA methylomes and histone-modification maps. *Nat Rev Genet* 8: 286–298.
59. Barlesi F, Giaccone G, Gallegos-Ruiz MI, Loundou A, Span SW, et al. (2007) Global histone modifications predict prognosis of resected non small-cell lung cancer. *J Clin Oncol* 25: 4358–4364.
60. Van Den Broeck A, Brambilla E, Moro-Sibilot D, Lantuejoul S, Brambilla C, et al. (2008) Loss of histone H4K20 trimethylation occurs in preneoplasia and influences prognosis of non-small cell lung cancer. *Clin Cancer Res* 14: 7237–7245.
61. Lazarevich NL, Fleishman DI (2008) Tissue-specific transcription factors in progression of epithelial tumors. *Biochemistry (Mosc)* 73: 573–591.
62. Grigo K, Wirsing A, Lucas B, Klein-Hitpass L, Ryffel GU (2008) HNF4 alpha orchestrates a set of 14 genes to down-regulate cell proliferation in kidney cells. *Biol Chem* 389: 179–187.
63. Lazarevich NL, Cheremnova OA, Varga EV, Ovchinnikov DA, Kudrjavtseva EI, et al. (2004) Progression of HCC in mice is associated with a downregulation in the expression of hepatocyte nuclear factors. *Hepatology* 39: 1038–1047.
64. Lucas B, Grigo K, Erdmann S, Lausen J, Klein-Hitpass L, et al. (2005) HNF4alpha reduces proliferation of kidney cells and affects genes deregulated in renal cell carcinoma. *Oncogene* 24: 6418–6431.
65. Sel S, Ebert T, Ryffel GU, Drewes T (1996) Human renal cell carcinogenesis is accompanied by a coordinate loss of the tissue specific transcription factors HNF4 alpha and HNF1 alpha. *Cancer Lett* 101: 205–210.
66. Watt AJ, Garrison WD, Duncan SA (2003) HNF4: a central regulator of hepatocyte differentiation and function. *Hepatology* 37: 1249–1253.
67. Morin RD, Johnson NA, Severson TM, Mungall AJ, An J, et al. (2010) Somatic mutations altering EZH2 (Tyr641) in follicular and diffuse large B-cell lymphomas of germinal-center origin. *Nat Genet* 42: 181–185.
68. Hillemecher T, Frieling H, Moskau S, Muschler MA, Semmler A, et al. (2008) Global DNA methylation is influenced by smoking behaviour. *Eur Neuropsychopharmacol* 18: 295–298.
69. Kim H, Kwon YM, Kim JS, Lee H, Park JH, et al. (2004) Tumor-specific methylation in bronchial lavage for the early detection of non-small-cell lung cancer. *J Clin Oncol* 22: 2363–2370.
70. Kim JS, Kim H, Shim YM, Han J, Park J, et al. (2004) Aberrant methylation of the Fhit gene in chronic smokers with early stage squamous cell carcinoma of the lung. *Carcinogenesis* 25: 2165–2171.
71. Chari R, Lonergan KM, Ng RT, MacAulay C, Lam WL, et al. (2007) Effect of active smoking on the human bronchial epithelium transcriptome. *BMC Genomics* 8: 297.
72. Sun S, Schiller JH, Gazdar AF (2007) Lung cancer in never smokers – a different disease. *Nat Rev Cancer* 7: 778–790.
73. Olausson KA, Mountzios G, Soria JC (2007) ERCC1 as a risk stratifier in platinum-based chemotherapy for nonsmall-cell lung cancer. *Curr Opin Pulm Med* 13: 284–289.
74. Cheng L, Spitz MR, Hong WK, Wei Q (2000) Reduced expression levels of nucleotide excision repair genes in lung cancer: a case-control analysis. *Carcinogenesis* 21: 1527–1530.
75. Herbst RS, Heymach JV, Lippman SM (2008) Lung cancer. *N Engl J Med* 359: 1367–1380.
76. Vilmar A, Sorensen JB (2009) Excision repair cross-complementation group 1 (ERCC1) in platinum-based treatment of non-small cell lung cancer with special emphasis on carboplatin: a review of current literature. *Lung Cancer* 64: 131–139.
77. Felip E, Rosell R (2007) Testing for excision repair cross-complementing 1 in patients with non-small-cell lung cancer for chemotherapy response. *Expert Rev Mol Diagn* 7: 261–268.
78. Olausson KA, Dunant A, Fouret P, Brambilla E, Andre F, et al. (2006) DNA repair by ERCC1 in non-small-cell lung cancer and cisplatin-based adjuvant chemotherapy. *N Engl J Med* 355: 983–991.
79. Gollob JA, Wilhelm S, Carter C, Kelley SL (2006) Role of Raf kinase in cancer: therapeutic potential of targeting the Raf/MEK/ERK signal transduction pathway. *Semin Oncol* 33: 392–406.
80. Guo NL, Wan YW, Tosun K, Lin H, Msiska Z, et al. (2008) Confirmation of gene expression-based prediction of survival in non-small cell lung cancer. *Clin Cancer Res* 14: 8213–8220.
81. Zhao Y, Tan J, Zhuang L, Jiang X, Liu ET, et al. (2005) Inhibitors of histone deacetylases target the Rb-E2F1 pathway for apoptosis induction through activation of proapoptotic protein Bim. *Proc Natl Acad Sci U S A* 102: 16090–16095.
82. Orzan F, Pellegatta S, Poliani L, Pisati F, Caldera V, et al. (2010) Enhancer of Zeste 2 (Ezh2) is up-regulated in Malignant Gliomas and in Glioma Stem-Like Cells. *Neuropathol Appl Neurobiol*.
83. Travis WD, Brambilla E, Noguchi M, Nicholson AG, Geisinger KR, et al. (2011) International association for the study of lung cancer/american thoracic society/european respiratory society international multidisciplinary classification of lung adenocarcinoma. *J Thorac Oncol* 6: 244–285.
84. Wilkerson MD, Yin X, Hoadley KA, Liu Y, Hayward MC, et al. (2010) Lung squamous cell carcinoma mRNA expression subtypes are reproducible, clinically important, and correspond to normal cell types. *Clin Cancer Res* 16: 4864–4875.
85. Garraway LA, Sellers WR (2006) From integrated genomics to tumor lineage dependency. *Cancer Res* 66: 2506–2508.
86. Garnis C, Davies JJ, Buys TP, Tsao MS, MacAulay C, et al. (2005) Chromosome 5p aberrations are early events in lung cancer: implication of glial cell line-derived neurotrophic factor in disease progression. *Oncogene* 24: 4806–4812.
87. Baldwin C, Garnis C, Zhang L, Rosin MP, Lam WL (2005) Multiple microalterations detected at high frequency in oral cancer. *Cancer Res* 65: 7561–7567.
88. Lockwood WW, Coe BP, Williams AC, MacAulay C, Lam WL (2007) Whole genome tiling path array CGH analysis of segmental copy number alterations in cervical cancer cell lines. *Int J Cancer* 120: 436–443.
89. Watson SK, DeLeeuw RJ, Ishkanian AS, Malloff CA, Lam WL (2004) Methods for high throughput validation of amplified fragment pools of BAC DNA for constructing high resolution CGH arrays. *BMC Genomics* 5: 6.
90. Chi B, DeLeeuw RJ, Coe BP, MacAulay C, Lam WL (2004) SeeGH – A software tool for visualization of whole genome array comparative genomic hybridization data. *BMC Bioinformatics* 5: 13.
91. Chi B, deLeeuw RJ, Coe BP, Ng RT, MacAulay C, et al. (2008) MD-SeeGH: a platform for integrative analysis of multi-dimensional genomic data. *BMC Bioinformatics* 9: 243.
92. Irizarry RA, Hobbs B, Collin F, Beazer-Barclay YD, Antonellis KJ, et al. (2003) Exploration, normalization, and summaries of high density oligonucleotide array probe level data. *Biostatistics* 4: 249–264.
93. Bild AH, Yao G, Chang JT, Wang Q, Potti A, et al. (2006) Oncogenic pathway signatures in human cancers as a guide to targeted therapies. *Nature* 439: 353–357.
94. Travis WD, Brambilla E, Muller-Hemelinck HK, Harris CC (2004) World Health Organization Classification of tumours. Pathology and Genetics of Tumours of the Lung, Pleura, Thymus, WD Heart; Travis, eds. editor. Lyon: IARC Press.
95. Solis LM, Behrens C, Dong W, Suraokar M, Ozburn NC, et al. (2010) Nrf2 and Keap1 abnormalities in non-small cell lung carcinoma and association with clinicopathologic features. *Clin Cancer Res* 16: 3743–3753.
96. Yuan P, Kadara H, Behrens C, Tang X, Woods D, et al. (2010) Sex determining region Y-Box 2 (SOX2) is a potential cell-lineage gene highly expressed in the pathogenesis of squamous cell carcinomas of the lung. *PLoS One* 5: e9112.

High Expression of Folate Receptor Alpha in Lung Cancer Correlates with Adenocarcinoma Histology and Mutation

Maria Ines Nunez, MD,* Carmen Behrens, MD,† Denise M. Woods, BS,* Heather Lin, MD,‡ Milind Suraokar, PhD,† Humam Kadara, PhD,† Wayne Hofstetter, MD,§ Neda Kalhor, MD,* J. Jack Lee, PhD,‡ Wilbur Franklin, MD,|| David J. Stewart, MD,† and Ignacio I. Wistuba, MD*†

Introduction: Folate receptor alpha (FR α) and reduced folate carrier-1 (RFC1) regulate uptake of folate molecules inside the cell. FR α is a potential biomarker of tumors response to antifolate chemotherapy, and a target for therapies using humanized monoclonal antibody. Information on the protein expression of these receptors in non-small-cell lung carcinoma (NSCLC) is limited.

Material and Methods: Expressions of FR α and RFC1 were examined by immunohistochemistry (IHC) in 320 surgically resected NSCLC (202 adenocarcinomas and 118 squamous cell carcinomas) tissue specimens and correlated with patients' clinico-pathologic characteristics. Folate receptor α gene (*FOLR1*) mRNA expression was examined using publicly available microarray datasets. FR α expression was correlated with thymidylate synthase and p53 expression in NSCLCs, and with epidermal growth factor receptor (*EGFR*) and V-Ki-ras2 Kirsten rat sarcoma viral (*KRAS*) gene mutations in adenocarcinomas.

Results: NSCLC overexpressed FR α and RFC1. In a multivariate analysis, lung adenocarcinomas were more likely to express FR α in the cytoplasm (OR = 4.39; $p < 0.0001$) and membrane (OR = 5.34; $p < 0.0001$) of malignant cells than squamous cell carcinomas. Tumors from never-smokers were more likely to express cytoplasmic (OR = 3.35; $p < 0.03$) and membrane (OR = 3.60; $p = 0.0005$) FR α than those from smokers. In adenocarcinoma, *EGFR* mutations correlated with higher expression of membrane FR α and *FOLR1* gene expressions. High levels of FR α expression was detected in 42 NSCLC advanced metastatic tumor tissues.

Conclusions: FR α and RFC1 proteins are overexpressed in NSCLC tumor tissues. The high levels of FR α in lung adenocarcinomas may

be associated to these tumors' better responses to antifolate chemotherapy and represents a potential novel target for this tumor type.

Key Words: Non-small-cell lung carcinoma, Epidermal growth factor receptor, membrane transporter, Folate receptor alpha, Reduced folate carrier-1.

(*J Thorac Oncol*. 2012;7: 833–840)

Lung cancer represents the first cause of death for cancer worldwide.¹ Most patients with lung cancer are diagnosed at advanced metastatic stage (IV), requiring systemic treatment.¹ Two types of non-small-cell carcinoma (NSCLC), adenocarcinoma and squamous cell carcinoma (SCC), are the most frequent (~80%) histological types of lung cancer.² Despite intensive research on molecular targeted therapy, chemotherapy still represents the main treatment option for patients with advanced NSCLC.³ In addition, over recent years chemotherapy after surgical resection has become the standard of care for treatment of selected patients with early-stage (i.e., stage IB, II, or IIIA) NSCLC.⁴ However, a subset of tumors does not respond to chemotherapy, and most tumors develop drug resistance, leading to chemotherapy failure.² The factors associated with chemotherapy resistance are not well understood, but some phenomena have been associated with this resistance, including, among others, decreases or alterations in the membrane transporters involved in drug-uptake systems or increase in drug-efflux pumps.⁵

Folate receptor alpha (FR α) and reduced folate carrier-1 (RFC1) regulate cellular uptake of folate molecules inside the cell.^{5–7} Folates are required in the synthesis of nucleotide bases, amino acids, and other methylated compounds, and consequently, they are required in larger quantities by proliferating cells.⁵ FR α is a glycoprotein that is anchored to the apical cell membrane of normal epithelial cells,⁸ and binds folate at a high affinity to mediate transport into the cytoplasm of cells.⁵ RFC1 is more ubiquitously expressed in normal cells, binds folate at low affinity, and represents the sole folate-uptake pathway for most normal cells.⁷

FR α expression is upregulated in a range of human tumors, including ovarian, mesothelioma, lung, and colorectal cancer.^{9–13} However, the level of expression of RFC1 in

Departments of *Pathology, †Thoracic/Head and Neck Medical Oncology, ‡Biostatistics, and §Thoracic and Cardiovascular Surgery, The University of Texas M. D. Anderson Cancer Center, Houston, TX; and ||Department of Pathology, University of Colorado at Denver and Health Sciences Center, Aurora, CO.

Disclosure: The authors declare no conflict of interest.

Address for correspondence: Ignacio I. Wistuba, MD, Department of Pathology, The University of Texas M. D. Anderson Cancer Center, 1515 Holcombe Blvd., Box 085, Unit 54, Houston, TX 77030. E-mail: iiwistuba@mdanderson.org

Copyright © 2012 by the International Association for the Study of Lung Cancer

ISSN: 1556-0864/12/833-840

tumors is less known. FR α has emerged as a potential marker for response to treatment of human carcinomas with the drug pemetrexed,¹⁴ a potent inhibitor of thymidylate synthase (TS) and other folate-dependent enzymes.^{15–17} Interestingly, FR α has been also investigated as a potential novel molecular target for human tumors.^{18–20} Recently, a humanized monoclonal antibody against FR α has been tested in a phase I clinical trial in patients with advanced chemorefractory ovarian carcinomas.¹⁹

In this study, we aimed to characterize the expression of FR α and RFC1 proteins in a large series ($n = 320$) of surgically resected NSCLC tissue specimens with annotated clinico-pathologic features. In addition, we investigated the expression of FR α in a small series ($n = 42$) of advanced metastatic NSCLC tumor tissues. In surgically resected tumors we correlated the expression of FR α with the expression of TS. Our findings of higher expression of FR α expression in lung tumors with adenocarcinoma histology and tumors obtained from never-smokers prompted us to correlate the expression of FR α with tumors' *epidermal growth factor receptor (EGFR)* and *KRAS* mutation status in adenocarcinomas, and with tumors' p53 protein expression in all NSCLCs.

METHODS

Case Selection and Tissue Microarray Construction

We obtained archived formalin-fixed and paraffin-embedded (FFPE) NSCLC tissues from the Lung Cancer Tissue Bank at The University of Texas M. D. Anderson Cancer Center (Houston, TX). We selected lung cancer tissue specimens from surgically resected NSCLCs with curative intent between 1997 and 2001, and constructed TMAs using three 1-mm diameter cores. Detailed clinico-pathologic information

was available for most cases (Table 1). In addition, we selected FFPE NSCLC tumor tissues from diagnostic tissue specimens from 42 advanced metastatic NSCLCs. The tissue specimens were histologically classified according to the 2004 World Health Organization classification.² The institutional review board at M. D. Anderson Cancer Center approved our study.

Immunohistochemical Staining and Evaluation

To test the expression of the membrane transporters, we used a monoclonal homemade antibody against FR α (clone Mb343, immunoglobulin G), dilution 1:500,¹³ and a polyclonal antibody against RFC1 (Abcam, Cambridge, MA), dilution 1:100. To assess the expression of TS, we used a monoclonal antibody (Zymed Carlsbad, CA), dilution 1:100. For p53 analysis, we used mouse monoclonal antihuman p53, clone DO7 (Dako, Carpinteria, CA), dilution 1:400.

For FR α we used a previously published IHC protocol.¹³ For RFC1 and TS, immunohistochemical staining was performed as follows: 5- μ M FFPE tissue sections were deparaffinized and hydrated, and underwent heat-induced epitope retrieval in a DAKO antigen retrieval bath (Dako) at 121°C for 30 seconds and 90°C for 10 seconds in a decloaking chamber (Biocare, Concord, CA), followed by a 30-minute cool down. Before antibody immunostaining, endogenous peroxidase activity was blocked with 3% H₂O₂ in methanol for 30 minutes. To block nonspecific antibody binding, tissue sections were incubated with 10% fetal bovine serum in Tris-buffered saline solution with Tween 20 for 30 minutes. The slides were incubated with primary antibody at ambient temperature for 60 minutes for all antibodies. This was followed by incubation with biotin-labeled secondary antibody (Envision Dual Link +, DAKO) for 30 minutes.

TABLE 1. Summary of Clinico-Pathologic Features of Patients with NSCLC Examined for Membrane Transporter and Thymidylate Synthase Expression

Feature	NSCLC Histologic Type		
	Squamous Cell Carcinoma ($n = 118$)	Adenocarcinoma ($n = 202$)	Total ($n = 320$)
Mean age, years (SD), (range)	68.4 (9.20), (43–90)	64.9 (11.5), (33–88)	66.2 (10.85), (33–90)
Sex			
Male	73	77	150
Female	45	125	170
Smoking status ^a			
Never	4	52	56
Ever	113	150	263
TNM stage			
I	62	134	196
II	36	25	61
III	18	36	54
IV	2	7	9

^aSmoking status and history were not available for one patient with squamous cell carcinoma.
NSCLC, non-small-cell lung carcinoma; TNM, Tumor, Node, Metastasis.

Staining was developed with 0.05% 3',3'-diaminobenzidine tetrahydrochloride, which had been freshly prepared in 0.05 mol/L Tris buffer at pH 7.6 containing 0.024% H₂O₂, and then the slides were counterstained with hematoxylin, dehydrated, and mounted.

Two observers (M.N. and I.W.) jointly quantified the immunohistochemical expression of the membrane transporters (magnification $\times 20$) in normal bronchial epithelium and lung tumor malignant epithelial cells. For each membrane transporter and TS, we defined three categories of intensity of immunostaining (0–3+). Next, an expression score (range, 0–300) was obtained by multiplying the intensity of staining by the percent of cells (0%–100%) staining. p53 expression was categorized by percentage of tumor cells expressing nuclear p53 as positive (greater than or equal to 5%) or negative (0%–5%).

EGFR and KRAS Mutation Analysis

Exons 18 through 21 of *EGFR* and exon 1 of *KRAS* were amplified by polymerase chain reaction (PCR) using intron-based primers as previously described.^{21,22}

Assessment of Membrane Transporter Expression in Microarray Data Sets

The cancer microarray database and integrated data-mining platform Oncomine²³ was utilized to analyze the expression of *FOLR1* (FR α) and *SLC19A1* (RFC1), and in microarray databases of NSCLC available online.^{24–27} The statistical significances of differences in expression of the genes were provided by Oncomine and confirmed by a two-tailed *t* test with random variance. Gene expression data of lung adenocarcinomas with annotated mutation data of *EGFR* and *KRAS* were obtained from the Ladanyi and Gerald laboratories at the Memorial Sloan-Kettering Cancer Center (http://cbio.mskcc.org/Public/lung_array_data/).²⁸ Available Affymetrix raw data files of the transcriptomes of 190 adenocarcinomas

(set I, *n* = 88; set II, *n* = 102) were analyzed using the BRB-ArrayTools version 3.7.0 software developed by using the BRB-ArrayTools v.3.7.0 developed by Dr. Richard Simon and BRB-ArrayTools Development Team.²⁹ Robust multiarray analysis was used for normalization of gene expression data using the R language environment.³⁰ *FOLR1* mRNA expression levels in both Memorial Sloan-Kettering Cancer Center data sets were median-centered by the Cluster v.2.11 software. Differences in normalized median-centered *FOLR1* expression levels were assessed for statistical significance by the two-tailed *t* test and *p* < 0.05 was considered statistically significant.

Statistical Methods

Associations between biomarker expression scores and patient clinico-pathologic data were assessed using the Wilcoxon ranked sum test or Kruskal-Wallis test, as appropriate, for continuous variables and the Chi-square test for categorical variables. The immunohistochemical expression of the markers was dichotomized in negative (score = 0) and positive (score > 0) expressions based on the graphical distribution of the scores. For recurrence free survival (RFS) and overall survival (OS) analyses, we tested binary cutoff points of biomarkers using the median expression score for each marker. Univariate and multivariate Cox proportional hazards regression models were used to assess the effects of covariates on survival. All statistical tests were two-sided, and *p* values < 0.05 were considered statistically significant.

RESULTS

Expression of FR α and RFC1 in Surgically Resected Tumors

Both adenocarcinoma and SCC expressed relatively high levels of FR α and RFC1 in the malignant cells (Fig. 1

TABLE 2. Frequency of Membrane Transporters and Thymidylate Synthase Immunohistochemical Expression in NSCLC by Tumor Histology

Marker	Any Expression (Score > 0)			Average Score		
	Adenocarcinoma Positive/Total (%)	SCC Positive/Total (%)	<i>p</i> Value ^a	Adenocarcinoma Score (SD)	SCC Score (SD)	<i>p</i> Value ^b
FR α						
Cytoplasm	152/174 (87)	63/110 (57)	<0.001	91.6 (66.4)	35.9 (40.3)	<0.001
Membrane	107/174 (61)	29/110 (26)	<0.001	72.2 (89.0)	11.29 (28.8)	<0.001
RFC1						
Cytoplasm	181/182 (99)	110/112 (98)	0.56	162.7 (83.2)	153.2 (72.0)	0.34
Membrane	164/182 (90)	103/112 (92)	0.68	128.1 (95.9)	119.2 (86.1)	0.59
TS						
Cytoplasm	130/165 (79)	82/102 (80)	0.75	52.2 (40.1)	55.6 (42.0)	0.565
Nuclear	58/165 (35)	59/102 (58)	0.0003	9.3 (21.1)	13.8 (27.7)	0.0043

^aFisher's exact test.

^bWilcoxon ranked sum test.

SCC, squamous cell carcinoma; FR α , folate receptor alpha; RFC1, reduced folate carrier-1; TS, thymidylate synthase.

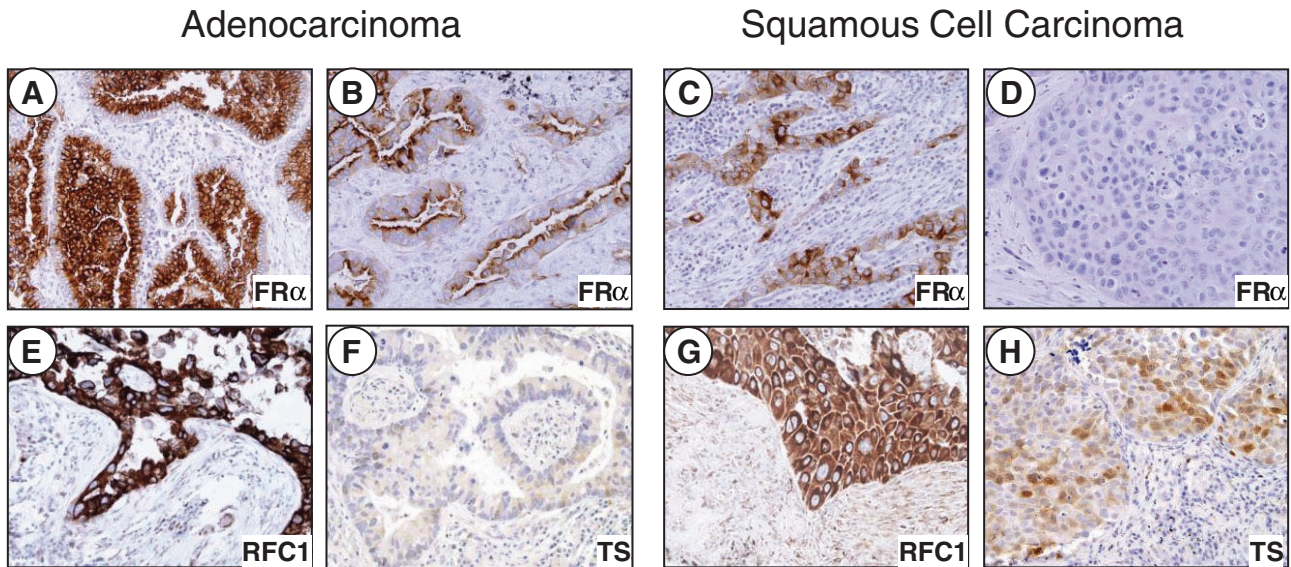


FIGURE 1. Photomicrographs showing immunohistochemical expression of folate receptor alpha (FR α), reduced folate carrier-1 (RFC1) and thymidylate synthase (TS) in non-small-cell lung carcinoma tissue specimens by histologic type. FR α : (A), strong cytoplasmic and membrane expression in tumor cells; (B and C), moderate expression in tumor cells; (D), lack of expression in malignant cells. RFC1: (E and G), strong cytoplasmic expression in malignant cells. TS: (F and H), negative and moderate cytoplasmic and nuclear expression in tumor cells, respectively. Original magnification, $\times 200$. FR α , folate receptor alpha; TS, thymidylate synthase; RFC1, reduced folate carrier-1.

and Table 2). For FR α , the average expression scores and frequency of any expression (score > 0) were significantly higher in adenocarcinomas than in SCCs at membrane ($p < 0.001$) and cytoplasmic ($p < 0.001$) localizations (Fig. 2). Both NSCLC histologies demonstrated similar levels of cytoplasmic and membrane RFC1 expression. For both markers the tumor cells exhibited stronger immunohistochemical expression than the 11 samples of normal bronchial epithelia adjacent to tumors (data not shown).

Correlation of FR α and RFC1 Expression with Clinico-Pathologic Features in Surgically Resected Tumors

The multivariate analysis of the immunohistochemical expression of the two membrane transporters as a dichotomized variable (positive, score > 0 , vs. negative, score $= 0$), after adjustment for patient's tumor histology, smoking history, sex, and disease stage, revealed that adenocarcinomas were more likely

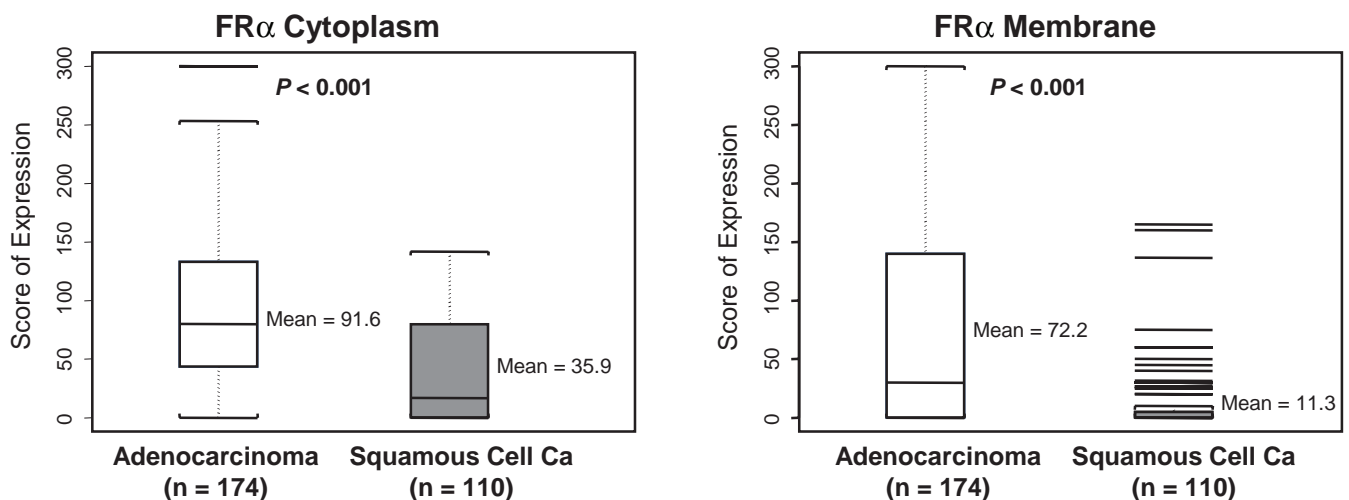


FIGURE 2. FR α expression scores by tumor histology. In the box-plots, indicates median scores. FR α , folate receptor alpha.

than SCCs to express cytoplasmic (odds ratio [OR] = 4.39; $p < 0.0001$) and membrane (OR = 5.34; $p < 0.0001$) FR α . In addition, tumors from never-smokers were significantly more likely to express cytoplasmic (OR = 3.35; $p < 0.03$) and membrane (OR = 3.60; $p = 0.0005$) FR α than those of smokers. In the multivariate analysis, the patient's sex was not an independent significant factor influencing tumor expression of FR α . No correlation was found between expression of both membrane transporters and RFS or OS in 230 patients with stage I or II NSCLCs (median follow-up, 7.2 years).

Correlation between FR α Expression and Tumors' p53 Expression and EGFR and KRAS Mutation Status

Our findings of higher expression of FR α expression in lung tumors with adenocarcinoma histology and tumors

obtained from never-smokers prompted us to correlate the expression of FR α with tumors' EGFR and KRAS mutation status in adenocarcinomas, and with tumors' p53 protein expression in all NSCLCs.

In lung adenocarcinomas, EGFR mutant tumors demonstrated significantly higher expression scores for membrane FR α (mean scores: mutant 134.8 versus wild-type 67.1; $p = 0.002$) than wild-type tumors (Fig. 3A). No correlation between FR α expression and adenocarcinoma tumors' KRAS mutation status was detected.

Of all NSCLCs tested, 38% (75 of 195) of adenocarcinomas and 69% (80 of 116) of SCCs had a positive p53 level (5% or more). Interestingly, we found that the scores for FR α expression in both membrane ($p = 0.001$) and cytoplasm ($p < 0.001$) were significantly lower in malignant cells from NSCLC tumors with positive p53 expression (mean score: membrane 33.4, SD 59.9, and cytoplasm 58.3, SD 60.0) than

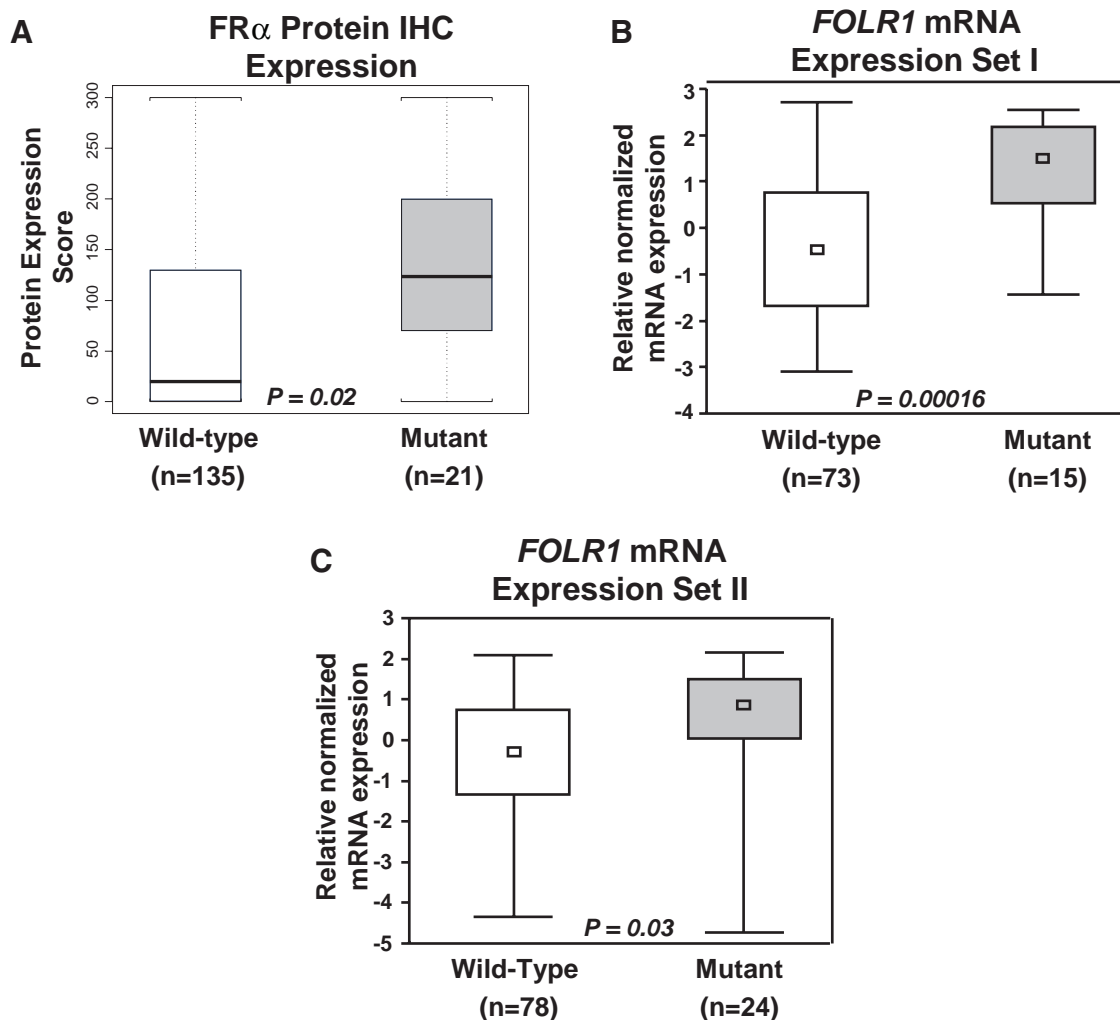


FIGURE 3. Folate Receptor alpha (FR α) protein and mRNA expression scores in lung adenocarcinoma by mutation status. FR α protein expression was determined by immunohistochemistry (IHC), and mRNA expression is based in 2 publicly microarray data sets available.²⁸ In the box-plots, indicates median mRNA expression scores.

in tumors with negative p53 expression (mean score: membrane 65.3, SD 90.6, and cytoplasm 83.55.3, SD 65.3).

Expression of FR α in Advanced Metastatic Tumors

To determine the levels of FR α expression in the entire spectrum of NSCLC, we examined FR α expression in 42 tumor tissues obtained from advanced NSCLCs (27 from lung/pleural tumors and 15 from metastatic sites). The tumor histologies corresponded to 23 adenocarcinomas, 5 SCCs, and 14 tumors classified as NSCLCs without features of specific histology (NSCLC—not otherwise specified). We found that advanced tumors demonstrated similar levels of FR α expression than surgically resected tumors by examining the average expression scores and frequency of any expression (score >0). Although small numbers, in the advanced tumors the FR α average expression scores were higher in adenocarcinomas than SCCs at membrane (mean score: adenocarcinoma 62.2, SD 81.2; SCC 20.0, SD 44.7; $p = 0.042$) and cytoplasmic (mean score: adenocarcinoma 104.1, SD 88.5; SCC 22.0, SD 39.0; $p = 0.319$) locations. NSCLC—not otherwise specified showed intermediate levels of FR α expression (mean score: membrane 20.7, SD 56.9, and cytoplasm 64.6, SD 96.5). In advanced tumors, any membrane expression (score > 0) of FR α was detected in 48% (11 of 23) of adenocarcinomas and 20% (1 of 5) of SCCs, whereas cytoplasmic expression was observed in 78% (18 of 23) and 40% (2 of 5) SCCs. No significant difference in the expression of FR α was detected when comparing lung/pleural tumors with metastatic sites (data not shown).

FOLR1 mRNA Expression in Tumor Tissues

Our findings that protein levels of FR α was greater in adenocarcinomas than in SCCs incited us to analyze expression levels of the mRNA of the *FOLR1* in published microarray data sets of surgically resected (satges I–III) NSCLC tumor specimens and compare them by histologic type.^{24–27} In accordance with our IHC data, *FOLR1* mRNA expression levels were significantly higher in adenocarcinomas ($n = 197$) than in SCCs ($n = 210$) in all four data sets available: 1.8 versus 1.0 ($p < 0.0001$),²⁵ 0.81 versus 0.73 ($p = 0.03$),²⁷ 2.61 versus 0.98 ($p < 0.0001$),²⁶ and 0.93 versus 0.31 ($p < 0.0001$).²⁴

To confirm our findings on the increased FR α immunoreactivity in tumors obtained from *EGFR* mutant lung adenocarcinomas compared with wild type tumors, we probed this association using the mRNA expression levels of *FOLR1* in publicly available microarray data sets with information on *EGFR* and *KRAS* mutation status.²⁸ Notably, the analysis of the microarray data further revealed the statistically significant upregulation of *FOLR1* mRNA levels in *EGFR* mutant lung adenocarcinomas compared with wild-type tumors in both available data sets ($p = 0.00016$ and $p = 0.003$) (Fig. 3B and C). In addition, no statistically significant differences were found in *FOLR1* expression levels between *KRAS* mutant lung adenocarcinomas and wild-type tumors (data not shown). These findings confirm the close positive association between *FOLR1* expression and *EGFR* mutation status, which we had found at the protein level by assessment of FR α immunoreactivity.

Correlation of Immunohistochemical Expression of TS and FR α

TS was expressed frequently in the nucleus and cytoplasm of malignant NSCLC cells. However, the frequency of any TS expression (score > 0) was higher in the cytoplasm (212 of 267, 79%) than in the nucleus (117 of 267, 44%). Although cytoplasmic expression of TS was similar in both NSCLC histologic types (Table 2), nuclear expression was significantly higher ($p = 0.003$) in SCCs (mean score: 13.8, SD 27.7) than in adenocarcinomas (mean score: 9.3, SD 27.1). The level of TS expression did not correlate with clinico-pathologic characteristics, including RFS and OS. In all NSCLC, significantly ($p = 0.02$) higher expression of nuclear TS immunostaining was detected in tumors with positive p53 expression (67 of 114, 58%) than in those with negative p53 staining (65 of 147, 44%). In adenocarcinomas, there was no correlation between TS expression and *EGFR* or *KRAS* mutation status.

We correlated the expression of TS and FR α in NSCLC tissue specimens. The score for nuclear TS expression correlated negatively with the score for cytoplasmic FR α expression in SCCs ($r = -0.20$; $p = 0.04$), and showed marginally significant negative correlation with membrane FR α expression in adenocarcinomas ($r = -0.16$; $p = 0.05$). When we examined the correlation of any expression (score > 0) of both markers in tumors, we found that in SCCs expression of nuclear TS was significantly inversely correlated ($p = 0.03$) with membrane expression of FR α , and that most tumors positive for TS (62 of 79, 79%) lacked membrane FR α . This correlation was not detected in adenocarcinomas.

DISCUSSION

Membrane transporters FR α and RFC1 are considered potential biomarkers of tumor response to antifolate chemotherapy.¹⁴ In addition, FR α represents a novel target for therapy in human carcinomas utilizing monoclonal antibodies.^{19,20} Information on the protein expression of these receptors in NSCLC is limited. Here, we report for the first time that NSCLC frequently overexpresses both FR α and RFC1 proteins by studying a large series of cases with annotated clinico-pathologic information. Importantly, we report that tumor cells from lung adenocarcinoma histology expressed significantly higher levels of cytoplasmic and membrane FR α than SCC, and tumors from never-smokers were significantly more likely to express cytoplasmic FR α than those from smokers. In lung adenocarcinomas, the presence of *EGFR* mutations correlated with higher expression of membrane FR α and *FOLR1* gene expression. NSCLC tissue specimens from advanced metastatic tumors showed similar levels of FR α expression than surgically resected tumors. We postulate that this information may be useful in selecting which patients with NSCLC may benefit from receiving treatment with antifolate inhibiting agents and monoclonal antibodies against FR α .

Our study showed that RFC1 is expressed frequently in the membrane and cytoplasm of malignant cells of NSCLC tumor tissues. Although RFC1 performs its important biological functions at the cell membrane, the cytoplasmic expression can be explained as part of synthesis of the protein.³¹ The only report available on the expression of RFC1 in human tumors showed relatively high

levels of mRNA gene expression in NSCLC, with similar expression in adenocarcinomas and SCCs.¹¹ These data are consistent with our protein expression data showing that levels of expression of RFC1 were similar in the two histologic types.

Interestingly, in our study the expression of membrane and cytoplasmic FR α was significantly higher in surgically resected lung adenocarcinomas compared with SCCs. FR α is bound to the cell membrane which binds to folate and internalizes it in the cytoplasm through endocytosis.⁶ Similar trend was detected in a small set of advanced metastatic NSCLC tumor tissues. FR α has been shown by immunohistochemical studies to be overexpressed previously in small sets of NSCLC tissue specimens.^{11,12} However, to the best of our knowledge, there is no published report of FR α protein expression in NSCLC tumors and correlation with clinical and pathological features. Our protein expression findings agree with the significantly higher levels of expression of *FOLR1* (FR α gene) mRNA in adenocarcinomas than in SCCs in all four public microarray data sets available.^{24–27} Similar findings have been reported in a quantitative PCR study of mRNA expression of 119 NSCLC tissue specimens.¹¹

The findings of higher levels of FR α protein and *FOLR1* mRNA expression in adenocarcinomas than in SCCs of the lung may have important clinical implications. The higher level of FR α protein expression in adenocarcinoma cells may explain the better response of advanced NSCLC of nonsquamous histology when treated with the combination of cisplatin and the multitargeted antifolate agent pemetrexed.³² However, this needs to be further tested in NSCLC tumor tissue specimens obtained from patients treated with pemetrexed. In addition, FR α is currently considered an attractive target for biologic therapy in tumors in which it is overexpressed compared with corresponding normal epithelium such as ovarian cancer by using the humanized monoclonal antibody against FR α Farletuzumab.^{19,20} Our findings of high expression of FR α in NSCLC compared with normal bronchial epithelium suggest that this protein could be considered a novel potential target for NSCLC, particularly in lung adenocarcinomas.

Our finding that NSCLCs of never-smokers have a higher expression of FR α than those of smokers is of interest. Our data showing significantly higher cytoplasmic and membrane FR α expression in NSCLCs obtained from never-smokers are in agreement with the previous report of higher levels of mRNA *FOLR1* by quantitative PCR in adenocarcinomas from nonsmokers and light smokers than in those from heavy smokers.¹¹ These differences in the expression of FR α by smoking status are consistent with our findings of higher FR α expression in NSCLCs lacking p53 expression and in adenocarcinomas harboring *EGFR* mutation, two features associated with the pathogenesis of non-smoking-related lung cancer.³³ Of interest, the analysis of the publicly available microarray data confirmed at mRNA gene expression level our observation that *EGFR* mutant adenocarcinoma tumors expressed higher levels of FR α protein. There are not data available on the response to antifolate chemotherapy agents in lung adenocarcinomas based on *EGFR* mutation status. However, it has been shown that advanced stage adenocarcinoma harbouring this mutation showed improved response to other type of (carboplatin and paclitaxel) chemotherapy.³⁴

Because of their roles in metabolism of the chemotherapy agent pemetrexed,^{14,35} we correlated the expressions of TS and FR α in NSCLC tissue specimens by histologic type. As previously reported,^{36,37} TS protein was expressed frequently in the nucleus (44%) and cytoplasm (79%) of malignant NSCLC cells. In our analysis, we determined that nuclear expression was significantly higher in SCCs than in adenocarcinomas. Ceppi et al.³⁶ previously reported that immunohistochemical expression of TS mRNA and protein was significantly higher in SCCs of the lung than in adenocarcinomas. In this previously reported immunohistochemical analysis, however, expression of TS in the malignant cells was not distinguished as nuclear or cytoplasmic. It has been shown that low levels of TS mRNA expression significantly correlated with in vitro chemosensitivity of freshly explanted human tumor specimens to pemetrexed.³⁸ It has been hypothesized that the higher mRNA and protein expressions of TS observed in SCCs explains the lower rate of response to pemetrexed in this NSCLC type.³² Recently, Sun et al.³⁹ reported that low immunohistochemical TS protein expression in tumors correlated with worse progression-free survival in stage IIIB and IV patients with nonsquamous cell lung carcinomas treated with pemetrexed.

When we correlated FR α and TS protein expression in NSCLC tumors, we found that in SCCs the expression of nuclear TS had a significant inverse correlation with expression of membrane FR α , and most TS-positive SCCs (79%) lacked membrane FR α immunostaining. Furthermore, we speculate that the more frequent occurrence of the FR α -membrane-negative/TS-nuclear-positive expression pattern in lung SCCs than in adenocarcinomas could be associated with the lower response rate to pemetrexed in this tumor type. Although FR α is most biologically active at the cell membrane,⁶ there is strong evidence of the important role of TS as translational regulation in the nucleus of cells.⁴⁰

In summary, our findings indicate that membrane transporter FR α and RFC1 proteins are frequently overexpressed in NSCLC tissues. The higher level of FR α in adenocarcinomas than in SCCs may help explain differences in efficacy of antifolate chemotherapy between these tumor types. We postulate that this information may be useful in selecting which patients with NSCLC may benefit from and should receive treatment with antifolate inhibiting agents and with monoclonal antibodies against FR α .

ACKNOWLEDGMENTS

This study was supported in part by grants from the Department of Defense (W81XWH-07-1-0306 to David J. Stewart, MD and Ignacio I. Wistuba, MD), the Specialized Program of Research Excellence in Lung Cancer (P50CA70907 to Ignacio I. Wistuba), and the National Cancer Institute (Cancer Center Support Grant CA-16672).

REFERENCES

- Herbst RS, Heymach JV, Lippman SM. Lung cancer. *N Engl J Med* 2008;359:1367–1380.
- Travis WD, Brambilla E, Muller-Hermelink HK, et al. Tumours of the lung. In Travis WD, Brambilla E, Muller-Hermelink HK, et al., (Eds), *Pathology and Genetics: Tumours of the Lung, Pleura, Thymus and Heart*. Lyon: International Agency for Research on Cancer (IARC), 2004. Pp. 9–124.

3. Pfister DG, Johnson DH, Azzoli CG, et al.; American Society of Clinical Oncology. American Society of Clinical Oncology treatment of unresectable non-small-cell lung cancer guideline: update 2003. *J Clin Oncol* 2004;22:330–353.
4. Arriagada R, Bergman B, Dunant A, Le Chevalier T, Pignon JP, Vansteenkiste J; International Adjuvant Lung Cancer Trial Collaborative Group. Cisplatin-based adjuvant chemotherapy in patients with completely resected non-small-cell lung cancer. *N Engl J Med* 2004;350:351–360.
5. Huang Y. Pharmacogenetics/genomics of membrane transporters in cancer chemotherapy. *Cancer Metastasis Rev* 2007;26:183–201.
6. Kelemen LE. The role of folate receptor alpha in cancer development, progression and treatment: cause, consequence or innocent bystander? *Int J Cancer* 2006;119:243–250.
7. Matherly LH, Hou Z, Deng Y. Human reduced folate carrier: translation of basic biology to cancer etiology and therapy. *Cancer Metastasis Rev* 2007;26:111–128.
8. Weitman SD, Weinberg AG, Coney LR, Zurawski VR, Jennings DS, Kamen BA. Cellular localization of the folate receptor: potential role in drug toxicity and folate homeostasis. *Cancer Res* 1992;52:6708–6711.
9. Hartmann LC, Keeney GL, Lingle WL, et al. Folate receptor overexpression is associated with poor outcome in breast cancer. *Int J Cancer* 2007;121:938–942.
10. Bueno R, Appasani K, Mercer H, Lester S, Sugarbaker D. The alpha folate receptor is highly activated in malignant pleural mesothelioma. *J Thorac Cardiovasc Surg* 2001;121:225–233.
11. Iwakiri S, Sonobe M, Nagai S, Hirata T, Wada H, Miyahara R. Expression status of folate receptor alpha is significantly correlated with prognosis in non-small-cell lung cancers. *Ann Surg Oncol* 2008;15:889–899.
12. Jin M, Kawakami K, Fukui Y, et al. Different histological types of non-small cell lung cancer have distinct folate and DNA methylation levels. *Cancer Sci* 2009.
13. Shia J, Klimstra DS, Nitzkorski JR, et al. Immunohistochemical expression of folate receptor alpha in colorectal carcinoma: patterns and biological significance. *Hum Pathol* 2008;39:498–505.
14. Scagliotti GV, Ceppi P, Capelletto E, Novello S. Updated clinical information on multitargeted antifolates in lung cancer. *Clin Lung Cancer* 2009;10 Suppl 1:S35–S40.
15. Taylor EC, Kuhnt D, Shih C, et al. A dideazatetrahydrofolate analogue lacking a chiral center at C-6, N-[4-[2-(2-amino-3,4-dihydro-4-oxo-7H-pyrrolo[2,3-d]pyrimidin-5-yl)ethyl]benzoyl]-L-glutamic acid, is an inhibitor of thymidylate synthase. *J Med Chem* 1992;35:4450–4454.
16. Schultz RM, Patel VF, Worzalla JF, Shih C. Role of thymidylate synthase in the antitumor activity of the multitargeted antifolate, LY231514. *Anticancer Res* 1999;19(1A):437–443.
17. Shih C, Habeck LL, Mendelsohn LG, Chen VJ, Schultz RM. Multiple folate enzyme inhibition: mechanism of a novel pyrrolopyrimidine-based antifolate LY231514 (MTA). *Adv Enzyme Regul* 1998;38:135–152.
18. Ebel W, Routhier EL, Foley B, et al. Preclinical evaluation of MORAb-003, a humanized monoclonal antibody antagonizing folate receptor-alpha. *Cancer Immunol* 2007;7:6.
19. Konner JA, Bell-McGuinn KM, Sabbatini P, et al. Farletuzumab, a humanized monoclonal antibody against folate receptor alpha, in epithelial ovarian cancer: a phase I study. *Clin Cancer Res* 2010;16:5288–5295.
20. Spannuth WA, Sood AK, Coleman RL. Farletuzumab in epithelial ovarian carcinoma. *Expert Opin Biol Ther* 2010;10:431–437.
21. Shigematsu H, Lin L, Takahashi T, et al. Clinical and biological features associated with epidermal growth factor receptor gene mutations in lung cancers. *J Natl Cancer Inst* 2005;97:339–346.
22. Tang X, Shigematsu H, Bekele BN, et al. EGFR tyrosine kinase domain mutations are detected in histologically normal respiratory epithelium in lung cancer patients. *Cancer Res* 2005;65:7568–7572.
23. Rhodes DR, Yu J, Shanker K, et al. ONCOMINE: a cancer microarray database and integrated data-mining platform. *Neoplasia* 2004;6:1–6.
24. Tomida S, Koshikawa K, Yatabe Y, et al. Gene expression-based, individualized outcome prediction for surgically treated lung cancer patients. *Oncogene* 2004;23:5360–5370.
25. Bild AH, Yao G, Chang JT, et al. Oncogenic pathway signatures in human cancers as a guide to targeted therapies. *Nature* 2006;439:353–357.
26. Kim J. Prediction of recurrence-free survival in postoperative NSCLC patients—a useful prospective clinical practice. Available at <http://www.ncbi.nlm.nih.gov/geo/query/acc.cgi?acc=GSE8894>. Accessed August 29, 2007.
27. Chen HY, Yu SL, Chen CH, et al. A five-gene signature and clinical outcome in non-small-cell lung cancer. *N Engl J Med* 2007;356:11–20.
28. Chitale D, Gong Y, Taylor BS, et al. An integrated genomic analysis of lung cancer reveals loss of DUSP4 in EGFR-mutant tumors. *Oncogene* 2009;28:2773–2783.
29. Simon R, Lam A, Li MC, Ngan M, Menendez S, Zhao Y. Analysis of gene expression data using BRB-ArrayTools. *Cancer Inform* 2007;3:11–17.
30. Irizarry RA, Bolstad BM, Collin F, Cope LM, Hobbs B, Speed TP. Summaries of Affymetrix GeneChip probe level data. *Nucleic Acids Res* 2003;31:e15.
31. Sadlish H, Williams FM, Flintoff WF. Cytoplasmic domains of the reduced folate carrier are essential for trafficking, but not function. *Biochem J* 2002;364(Pt 3):777–786.
32. Scagliotti GV, Parikh P, von Pawel J, et al. Phase III study comparing cisplatin plus gemcitabine with cisplatin plus pemetrexed in chemotherapy-naïve patients with advanced-stage non-small-cell lung cancer. *J Clin Oncol* 2008;26:3543–3551.
33. Sun S, Schiller JH, Gazdar AF. Lung cancer in never smokers—a different disease. *Nat Rev Cancer* 2007;7:778–790.
34. Eberhard DA, Johnson BE, Amler LC, et al. Mutations in the epidermal growth factor receptor and in KRAS are predictive and prognostic indicators in patients with non-small-cell lung cancer treated with chemotherapy alone and in combination with erlotinib. *J Clin Oncol* 2005;23:5900–5909.
35. Adjei AA. Pemetrexed (ALIMTA), a novel multitargeted antineoplastic agent. *Clin Cancer Res* 2004;10(12 Pt 2):4276s–4280s.
36. Ceppi P, Volante M, Saviozzi S, et al. Squamous cell carcinoma of the lung compared with other histotypes shows higher messenger RNA and protein levels for thymidylate synthase. *Cancer* 2006;107:1589–1596.
37. Zheng Z, Li X, Schell MJ, et al. Thymidylate synthase in situ protein expression and survival in stage I nonsmall-cell lung cancer. *Cancer* 2008;112:2765–2773.
38. Hanauske AR, Eismann U, Oberschmidt O, et al. In vitro chemosensitivity of freshly explanted tumor cells to pemetrexed is correlated with target gene expression. *Invest New Drugs* 2007;25:417–423.
39. Sun JM, Han J, Ahn JS, Park K, Ahn MJ. Significance of thymidylate synthase and thyroid transcription factor 1 expression in patients with nonsquamous non-small cell lung cancer treated with pemetrexed-based chemotherapy. *J Thorac Oncol* 2011;6:1392–1399.
40. Liu J, Schmitz JC, Lin X, et al. Thymidylate synthase as a translational regulator of cellular gene expression. *Biochim Biophys Acta* 2002;1587:174–182.

Histopathologic Response Criteria Predict Survival of Patients with Resected Lung Cancer After Neoadjuvant Chemotherapy

Apar Pataer, MD, PhD,* Neda Kalhor, MD,† Arlene M. Correa, PhD,* Maria Gabriela Raso, MD,†
 Jeremy J. Erasmus, MD,‡ Edward S. Kim, MD,§ J. Jack Lee, PhD,||
 Jack A. Roth, MD,* David J. Stewart, MD,§ Ara A. Vaporciyan, MD,* Ignacio I. Wistuba, MD,†§
 Stephen G. Swisher, MD,* and The University of Texas M. D. Anderson Lung Cancer Collaborative Research Group

Introduction: We evaluated the ability of histopathologic response criteria to predict overall survival (OS) and disease-free survival (DFS) in patients with surgically resected non-small cell lung cancer (NSCLC) treated with or without neoadjuvant chemotherapy.

Methods: Tissue specimens from 358 patients with NSCLC were evaluated by pathologists blinded to the patient treatment and outcome. The surgical specimens were reviewed for various histopathologic features in the tumor including percentage of residual viable tumor cells, necrosis, and fibrosis. The relationship between the histopathologic findings and OS was assessed.

Results: The percentage of residual viable tumor cells and surgical pathologic stage were associated with OS and DFS in 192 patients with NSCLC receiving neoadjuvant chemotherapy in multivariate analysis ($p = 0.005$ and $p = 0.01$, respectively). There was no association of OS or DFS with percentage of viable tumor cells in 166 patients with NSCLC who did not receive neoadjuvant chemotherapy ($p = 0.31$ and $p = 0.45$, respectively). Long-term OS and DFS were significantly prolonged in patients who had $\leq 10\%$ viable tumor compared with patients with $>10\%$ viable tumor cells (5 years OS, 85% versus 40%, $p < 0.0001$ and 5 years DFS, 78% versus 35%, $p < 0.001$).

Conclusion: The percentages of residual viable tumor cells predict OS and DFS in patients with resected NSCLC after neoadjuvant chemotherapy even when controlled for pathologic stage. Histopathologic assessment of resected specimens after neoadjuvant

chemotherapy could potentially have a role in addition to pathologic stage in assessing prognosis, chemotherapy response, and the need for additional adjuvant therapies.

Key Words: Lung cancer, Neoadjuvant chemotherapy, Histopathology.

(*J Thorac Oncol.* 2012;7: 825–832)

Surgical resection is the treatment of choice in patients with localized non-small cell lung cancer (NSCLC).¹ Neoadjuvant chemotherapy followed by resection has been used in patients with locally advanced NSCLC to address the high rate of local and systemic failure.^{2–5} Histopathologic features in the resected specimen of patients receiving neoadjuvant chemotherapy or chemoradiation have been reported in a small number of studies to be useful in the prediction of survival and assessment of tumor response after neoadjuvant treatment.^{6–17} The purpose of this study was to assess in a larger cohort of patients the ability of histopathologic criteria to predict survival and chemotherapy response in patients with NSCLC treated with neoadjuvant chemotherapy even when controlled for surgical pathologic stage.

PATIENTS AND METHODS

Patients and Tissue Samples

We examined 192 patients with NSCLC treated with neoadjuvant chemotherapy followed by complete surgical resection from 2001 to 2006. We also examined a control group of 166 patients with NSCLC from the same time period who did not receive neoadjuvant chemotherapy. Histologic slides from the files of the Department of Pathology, M. D. Anderson Cancer Center¹⁸ and all cases were reviewed. The study was approved by the University of Texas M. D. Anderson Institutional Review Board.

Histopathologic Evaluation

Hematoxylin and eosin-stained slides of sections of the gross residual tumor were assessed in a total of 358 patients by pathologists blinded to the patient treatment and outcome. In this study, at least 1 section per cm of tumor greatest diameter

Departments of *Thoracic and Cardiovascular Surgery, †Pathology, ‡Diagnostic Radiology, §Thoracic/Head and Neck Medical Oncology, and ||Biostatistics, the University of Texas M. D. Anderson Cancer Center, Houston, Texas.

Members of the M.D. Anderson Lung Cancer Collaborative Research Group: John Heymach, Lauren Byers, Joseph Chang, George Blumenschein, James D. Cox, Wayne Hofstetter, Bingliang Fang, Frank Fossella, Bonnie Glisson, Waun Ki Hong, Kathryn Gold, Faye Johnson, Merrill S. Kies, Zhongxing Liao, Steven Lin, Scott Lippmann, Ritsuko Komaki, Michael O' Reilly, Vali Papadimitrakopoulou, Katherine Pisters, David Rice, Pierre Saintigny, Anne Tsao, Garrett L. Walsh, James Welsh, and William N. William Jr.

Disclosure: The authors declare no conflicts of interest.

Address for correspondence: Apar Pataer, MD, PhD, Department of Thoracic and Cardiovascular Surgery, Unit 445, The University of Texas M. D. Anderson Cancer Center, 1515 Holcombe Blvd., Houston, TX 77030.

E-mail: apataer@mdanderson.org

Copyright © 2012 by the International Association for the Study of Lung Cancer

ISSN: 1556-0864/12/825-832

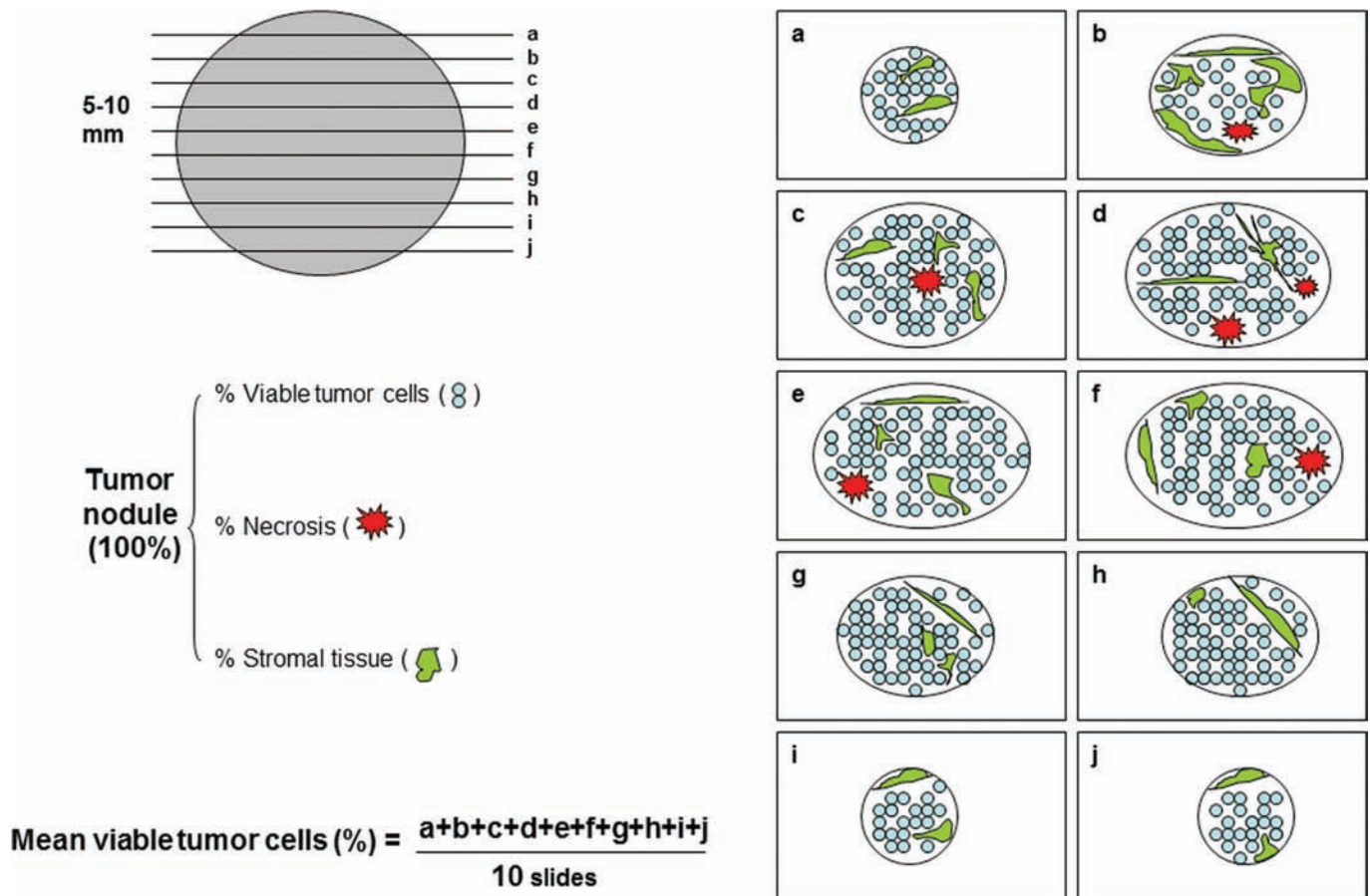


FIGURE 1. Schematic diagram of histologic evaluation of lung cancer tissue resected from patients treated with neoadjuvant chemotherapy.

was obtained. The number of slides examined for each case ranged from 5 to 30. Figure 1 shows the schematic diagram for histopathologic evaluation of NSCLC. The percentage of residual tumor was estimated by comparing the estimated cross-sectional area of the viable tumor foci with estimated cross-sectional areas of necrosis, fibrosis, and inflammation on each slide. Histologic parameters were analyzed including necrosis, fibrosis, foamy macrophages, giant cell reaction, cholesterol cleft granuloma, and inflammation. The results for all slides were averaged together to determine the mean values for each patient. All histopathologic changes were then compared with patients who had not received neoadjuvant chemotherapy.

Statistical Analysis

Overall survival (OS) was defined as the time from date of the surgery until death from any cause. Disease-free survival (DFS) was defined as the time from surgery until time of the tumor recurrence or date of last follow-up. Survival probability as a function of time was computed by the Kaplan-Meier estimator. The log-rank test was used to compare patient survival times between groups. Univariable Cox proportional hazards regression model was used to examine the association between histopathologic features and various clinical factors with OS and DFS. The variables found significant on

univariate analysis (p value < 0.25) were evaluated by multivariable analysis using the Cox proportional hazards model after backward stepwise Wald elimination. A p value of less than 0.05 on multivariate analysis was taken to be significant. The statistical analyses were performed using SPSS Software (version 15; SPSS, Inc., Chicago, IL).

RESULTS

Patient Demographics and Treatment Characteristics

Table 1 presents the patient demographics of the patients with NSCLC treated with and without neoadjuvant chemotherapy. Patients treated with neoadjuvant chemotherapy tended to have a higher clinical and pathologic stage. There was some evidence of clinical downstaging in the resected specimens of the neoadjuvant-treated patients (clinical stage IIIA/B 41%, pathologic stage IIIA/B 30%, $p < 0.05$), which was not seen in patients treated with surgery alone. Neoadjuvant-treated patients also tended to have more patients classified as “other” on histology (NSCLC-not otherwise specified, adenosquamous, and neuroendocrine carcinoma). No difference was noted between groups in the type or extent of surgery. The majority of patients with NSCLC treated with neoadjuvant chemotherapy received a platinum and

TABLE 1. Patient Demographics and Treatment Characteristics

Characteristics	Chemotherapy Followed by Surgery (N = 192)	Surgery Alone (N = 166)	p
Age mean (range)	63 (40–85)	66 (40–90)	0.29
Gender, n (%)			0.31
Male	111 (58)	79 (48)	
Female	81 (42)	87 (52)	
Histology, n (%)			<0.0001
Adenocarcinoma	89 (46)	107 (65)	
Squamous cell carcinoma	58 (30)	55 (33)	
Others	45 (24)	4 (2)	
Tumor size (cm), n (%)			0.38
0.0–2.0	47 (25)	24 (15)	
2.1–3.0	49 (25)	46 (28)	
3.1–4.0	32 (17)	39 (23)	
4.1–5.0	21 (11)	28 (17)	
>5.1	43 (22)	29 (17)	
Clinical stage, n (%)			<0.0001
IA/IB	60 (31)	118 (71)	
IIA/IIB	44 (23)	30 (18)	
IIIA/IIIB	79 (41)	14 (9)	
IV	9 (5)	4 (2)	
Pathologic stage, n (%)			<0.0001
0/IA/IB	78 (40)	98 (59)	
IIA/IIB	49 (26)	45 (27)	
IIIA/IIIB	57 (30)	21 (13)	
IV	8 (4)	2 (1)	
Type of resection n (%)			0.69
Wedge or segmentectomy	5 (2)	7 (4)	
Bilobectomy or lobectomy	174 (91)	148 (89)	
Pneumonectomy	13 (7)	11 (7)	
Neoadjuvant chemotherapy, n (%)			
T + C	171 (89)		
Carboplatin	134 (70)		
Cisplatin	58 (30)		
Taxol	98 (51)		
Taxotere	75 (39)		
Gemcitabine	17 (9)		
Etoposide	3 (1)		
Treatment cycle mean (range)	3 (2–7)		

Others of chemotherapy group (39 patients with NSCLC-NOS, 5 with adenocarcinoma, and 1 with neuroendocrine carcinoma) and surgery alone group (4 patients with NSCLC-not otherwise specified).

T, taxol or taxotere; C, carboplatin or cisplatin; AJCC7, American Joint Committee on Cancer 7.

taxane-based regimen (171 patients, 89%, Table 1). The median number of treatment cycles was three cycles (range: 2–7 cycles).

Histopathologic Features in Patients Treated with and without Neoadjuvant Chemotherapy

Histopathologic patterns observed with treatment-induced tumor regression included necrosis, fibrosis, foamy

macrophages, cholesterol cleft granuloma, giant cell reaction, and inflammation. Figure 2 shows typical examples of the histopathologic features of tumors associated with extensive (A and C) or no (B and D) response to neoadjuvant chemotherapy.

We compared the percentage of viable tumor cells in patients treated with or without neoadjuvant chemotherapy. In patients treated with neoadjuvant chemotherapy, 36 (19%) of 192 patients had $\leq 10\%$ viable tumor cells (Table 2). All patients who underwent surgery alone had $>10\%$ viable tumor cells (Table 2). The percentage of viable tumor cells was a significant predictor of the survival only in the patients with NSCLC who received neoadjuvant chemotherapy (Table 2, $p < 0.003$). There was no relationship with survival in patients with NSCLC who did not receive neoadjuvant chemotherapy (Table 2). Compared with patients with $\leq 10\%$ viable tumor cells, the hazard ratio for neoadjuvant-treated patients with NSCLC with $>70\%$ viable tumor cells was 4.78 with a 95% confidence interval of 2.06–11.11.

Histopathologic Criteria of Chemotherapy Response and Pathologic Stage are Associated with Long-Term Survival

We analyzed the relationship between pathologic stage and survival in patients with neoadjuvant-treated NSCLC and found that even after chemotherapy the pathologic stage was a significant predictor of long-term survival (Figure 3). The percentage of viable tumor cells in the resected specimens was also a significant predictor of long-term survival after neoadjuvant chemotherapy when assessed in a categorical (Figure 3) or continuous fashion (Table 3). Multivariable analysis (Table 3) suggests that the significant predictors of OS and DFS after neoadjuvant chemotherapy include pathologic stage and percentage of viable tumor cells. In multivariable analysis, for every 1% increase in viable tumor, hazard ratio increased by 0.01.

DISCUSSION

Although the survival benefits of neoadjuvant chemotherapy remain controversial,^{2–7} it has been observed that pathologic response after neoadjuvant therapy in patients with resected stage IIIA NSCLC is associated with improved OS.⁸ In a multicenter, phase II trial evaluating pN2 patients treated with three cycles of neoadjuvant docetaxel-cisplatin, Betticher et al.⁸ noted that the 60% of patients who downstaged from pN2 at mediastinoscopy to pN0–N1 at surgery had improved 3 years OS (60% versus 10%, $p < 0.0001$). Several authors have also noted that histopathologic response criteria may be a prognostic factor in clinical N2 (cN2) patients treated with neoadjuvant chemotherapy or chemoradiotherapy.^{9,10} Because of these preliminary observations, we wanted to see whether reproducible histopathologic response criteria could be developed that would predict long-term survival in a larger cohort of patients with stages I to III NSCLC treated with neoadjuvant chemotherapy even when controlled for pathologic stage. We also wanted to see whether these criteria might provide a surrogate end point for long-term survival and chemotherapy response in biomarker-driven translational clinical trials.

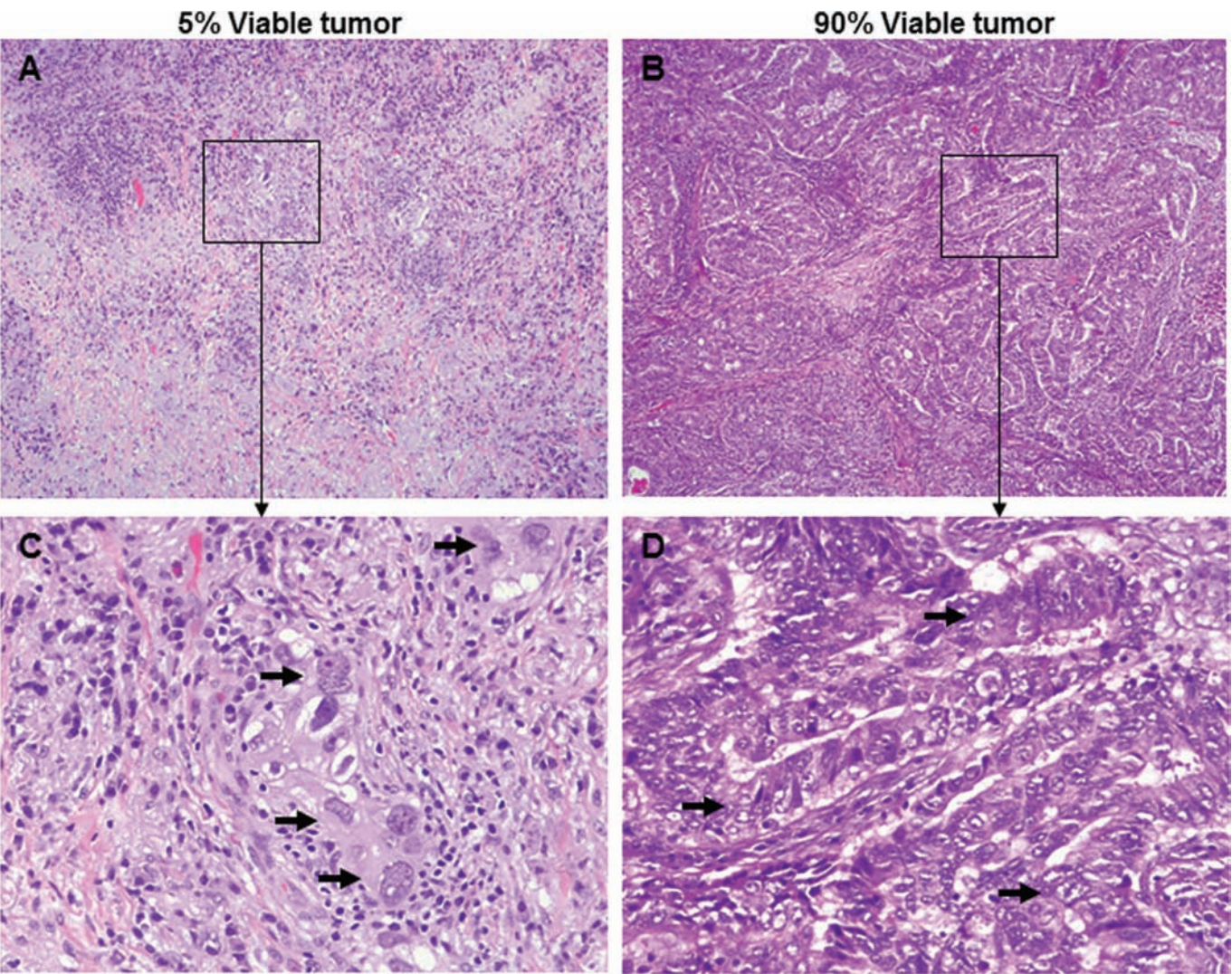


FIGURE 2. Pathologic response to neoadjuvant chemotherapy for lung cancer. Representative examples of the histopathology of tumors associated with extensive response to treatment (A, C) or no response to treatment (B, D). Arrows indicate viable tumor cells (C, D). Original magnification: $\times 40$ (pictures) and $\times 200$ (insets).

TABLE 2. Association of Survival with Percentage of Viable Tumor Cells in Patients with NSCLC with or without Neoadjuvant Chemotherapy						
Percentage of Viable Tumor Cells	Neoadjuvant Treatment (N = 192)			Surgery Alone (N = 166)		
	No. of Patients (%)	HR (95% CI)	p	No. of Patients (%)	HR (95% CI)	p
0–10%	36 (19)	1.00	0.003	0 (0)		0.51
11–30%	19 (10)	2.51 (0.91–6.96)		6 (4)	1.00	
31–50%	35 (18)	3.39 (1.40–8.22)		27 (16)	1.02 (0.31–3.33)	
51–70%	56 (29)	4.57 (1.98–10.52)		64 (38)	0.62 (0.19–1.96)	
71–100%	46 (24)	4.78 (2.06–11.11)		69 (42)	0.76 (0.25–2.41)	

HR, hazard ratio; CI, confidence interval.

Neoadjuvant chemotherapy is a therapeutic option that is used in patients with locally advanced resectable NSCLC. The response to neoadjuvant chemotherapy in these patients is typically assessed by radiologic measurements of tumor size before and after therapy. Unfortunately, this change in tumor size is not always reliable in the prediction of long-term survival because of the difficulty in differentiating fibrosis from viable tumor radiographically. Attempts to improve the

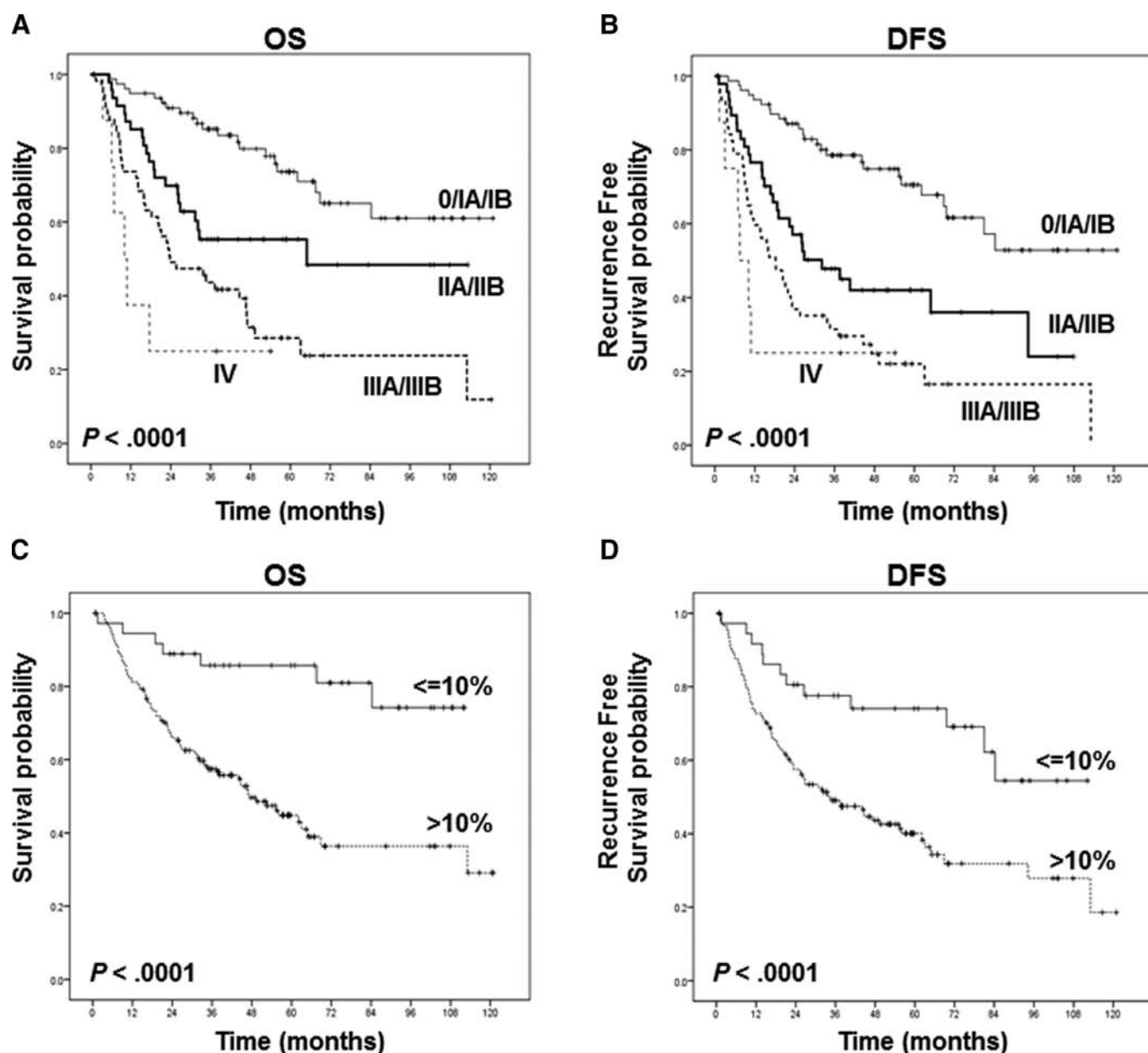


FIGURE 3. Kaplan-Meier estimates of overall survival (A, C) and disease-free survival (B, D) based on pathologic stages (A, B) and percentage of viable tumor cells (C, D). A, The overall survival was significantly longer in patients with stages 0, IA, and IB than in patients with pathologic stage II, III, or IV. B, The disease-free survival was significantly longer in patients with stages 0, IA, and IB than in patients with pathologic stage II, III, or IV. C, The overall survival was significantly longer in patients with $\leq 10\%$ viable tumor cells than in patients with $>10\%$ viable tumor cells. D, The disease-free survival was significantly longer in patients with $\leq 10\%$ viable tumor cells than in patients with $>10\%$ viable tumor cells.

prediction of chemotherapy response with positron emission tomography/computed tomography findings have also been confounded by false-positive F-fluorodeoxyglucose avidity due to macrophage infiltration.¹¹ Several small studies have suggested that the degree of tumor regression after neoadjuvant therapy as determined by histopathologic findings in the resected tumor may be a more objective criterion of chemotherapy response (Table 4).^{12–15} Our data on 192 patients with NSCLC treated with neoadjuvant chemotherapy suggest

that the percentage of viable tumor cells does indeed predict OS even when controlled for pathologic stage. Importantly, in patients who are not treated with neoadjuvant chemotherapy (Table 2), the percentage of viable tumor cells is not predictive of OS. The prognostic effect of the percentage of viable tumor cells is significant when looked at in a continuous ($p < 0.003$) or categorical ($>10\%$ versus $\leq 10\%$ viable tumor, $p < 0.001$) fashion and when controlled for pathologic stage (Table 3). Several other authors have observed a relationship

TABLE 3. Univariate and Multivariate Analyses for Survival on Patients with NSCLC Treated with Neoadjuvant Chemotherapy

Characteristics	No. of Patients	OS		DFS	
		HR (95% CI)	<i>p</i>	HR (95% CI)	<i>p</i>
Univariate Cox model					
Age (continuous)	192	1.01 (0.98–1.03)	0.59	1.00 (0.98–1.03)	0.8
Gender			0.45		0.11
Female (reference)	81	1.00		1.00	
Male	111	0.85 (0.56–1.3)		0.71 (0.49–1.04)	
Histology			0.26		0.29
Adenocarcinoma (reference)	89	1.00		1.00	
Squamous cell carcinoma	58	0.64 (0.38–1.09)		0.71 (0.45–1.14)	
Other	45	0.89 (0.54–1.47)		0.76 (0.47–1.22)	
Pathologic stage			<0.001		<0.001
0/IA/IB (reference)	78	1.00		1.00	
IIA/IIB	49	2.24 (1.22–4.11)		2.66 (1.55–4.58)	
IIA/IIB	57	4.23 (2.48–7.22)		4.54 (2.76–7.47)	
IV	8	7.69 (3.07–19.33)		6.73 (2.73–16.61)	
Viable tumor cells (continuous)	192	1.02 (1.01–1.03)	<0.001	1.01 (1.01–1.02)	<0.001
Multivariate Cox model					
Pathologic stage			<0.001		<0.001
0/IA/IB (reference)	78	1.00		1.00	
IIA/IIB	49	1.85 (1.00–3.43)		2.36 (1.36–4.09)	
IIA/IIB	57	3.16 (1.80–5.52)		3.72 (2.19–6.31)	
IV	8	7.25 (2.88–18.29)		6.60 (2.66–16.33)	
Viable tumor cells (continuous)	192	1.01 (1.00–1.02)	0.005	1.01 (1.00–1.02)	0.01

OS, overall survival; DFS, disease-free survival; HR, hazard ratio; CI, confidence interval; AJCC7, American Joint Committee on Cancer 7.

TABLE 4. Summary of Previous Histology Analysis on Patients with NSCLC Treated with Neoadjuvant therapy

Authors	No. of Patients	Stages	Treatment	Histologic Criteria	Prognostic Data
Junker et al. ¹²	40	IIIA and IIIB	Combined chemotherapy and radiotherapy	% Viable tumor (≤10% vs. >10%)	<i>p</i> = 0.02
Liu-Jarin et al. ¹⁴	30	IIB, IIIA, IIIB, and IV	Combined chemotherapy and radiotherapy	% Viable tumor	None
Yamane et al. ¹⁵	53	I–IV	40 chemotherapy, 11 chemoradiotherapy, and 1 radiotherapy	Area of residual tumor (≤400 vs. >400 mm ²)	<i>p</i> = 0.01

with histopathologic response and survival in patients with NSCLC, but these studies have been limited by small numbers, variable types of induction therapy (chemotherapy and chemoradiation), and have not controlled for pathologic stage or included a control group of patients with NSCLC treated with surgery alone (Table 4).^{12–15} These studies evaluated only one slide for each tumor. Nevertheless, we evaluated multiple slides for each tumor on a large number of patients with NSCLC who only received neoadjuvant chemotherapy. Assessment of histopathologic response in the tumor was performed in a continuous (i.e., percent viable tumor) and categorical fashion (10%, 20%, 30%, 40%, or 50%, data not

shown) with a modification of the regression grading system introduced by Junker et al.,¹⁵ nonresponder = morphologic evidence of therapy-induced changes but >10% viable tumor cells and responder = extensive response with ≤10% viable tumor cells. Our study clearly demonstrates that the percentage of viable tumor cells is a significant predictor of OS and DFS in patients with neoadjuvant-treated NSCLC but not in those patients who undergo surgery alone. Although necrosis was present in patients with resected NSCLC who did not receive neoadjuvant therapy (Table 2), it was not predictive of OS or DFS. Although not statistically significant, there is a suggestion in the surgery-only patients (Table 2)

that increased tumor necrosis is associated with reduced OS perhaps because larger tumors outgrow their native blood supply and are associated with a worse prognosis and less viable tumor.

Numerous histopathologic criteria were reviewed, and the only significant factors when controlled for pathologic stage were the percentage of viable tumor and stromal tissue noted on the resected specimens. The percentage of necrosis did not correlate with OS or DFS (data not shown). This may have been due to the fact that a certain amount of necrosis is present in all tumors even those which are not treated with neoadjuvant chemotherapy. Several other histopathologic features such as cholesterol clefts, foreign body reactive giant cells, stromal hyalinosis, granulation tissue, and peripheral scar formation were associated with receiving neoadjuvant chemotherapy. Nevertheless, these histologic features had no significant correlation with clinical response and prognosis. Additionally, several other histologic features, such as coagulation necrosis, foam cell infiltration, and inflammatory cell infiltration, were present in the resected specimens from both those patients who received neoadjuvant chemotherapy and those who underwent surgical resection alone. Similar to the histologic features related to neoadjuvant chemotherapy, there was no significant correlation of these unrelated histopathologic features to response and prognosis.

A potential limitation in our study is that variations of histologic features can occur in any grading system. In an attempt to decrease interobserver variability, all surgical specimens were histologically evaluated by two pathologists. It is important to note that histopathologic criteria depend on complete sampling of the resected specimen, especially when no gross residual tumor is appreciable. As incomplete evaluation of the treated tumor site in cases with only rare microscopic foci of viable tumor could result in misclassification, examination of multiple tissue slices obtained from the tumor site is important for accurate and reproducible classification of histopathologic features. The variation between slides was as much as 5 to 10% in the same specimen. Because of this variability, we believe that it is important to assess numerous slides and take the mean of all the slides characterized (minimum of 1 slide per cm of resected tumor).

Chemotherapy resistance may be a significant contributor to treatment failure in some patients with NSCLC who receive neoadjuvant chemotherapy. A personalized approach to treatment selection could potentially improve survival in patients with NSCLC who receive neoadjuvant therapy. In this regard, chemotherapeutic agents selected on the basis of molecular determinants of the tumor may augment response rates and survival. Clinical studies suggest that epidermal growth factor receptor mutations (particularly exon 19 deletions) have increased sensitivity to some chemotherapeutic agents.¹⁶⁻¹⁷ It has also been reported that high expression levels of excision repair crosscomplementation group 1 protein and ribonucleotide reductase predict resistance to platinum or gemcitabine chemotherapy.^{18,19} The histopathologic response reported in this article may form a surrogate end point for survival in phase II clinical trials. Such a surrogate end point would help

accelerate biomarker-driven questions of response in translational clinical trials. The ability to separate biomarkers of response from biomarkers of prognosis may also be helped by assessment of pathologic response. The surrogate end point of pathologic response may ultimately be a better and faster correlate for chemotherapy response than OS or DFS.

In summary, our results indicate that the percentage of viable tumor cells in the resected specimen correlates with OS and DFS in patients with NSCLC treated with neoadjuvant chemotherapy even when controlled for pathologic stage. The routine histologic assessment of the resected specimen could potentially have a role in the subsequent therapeutic management of patients who undergo surgery after neoadjuvant therapy. The percentage of viable tumor cells in the resected specimen may also serve as a surrogate end point for survival and may provide a more accurate and rapid comparison between different neoadjuvant treatment regimens, shortening the period needed to evaluate novel chemotherapeutic and biologic therapies in clinical trials.

ACKNOWLEDGMENTS

Supported, in part, by Department of Defense W81XWH-07-1-0306 and the National Institutes of Health through M. D. Anderson's Cancer Center Support Grant CA 016672—Lung Program and by the Homer Flower Research Fund, the Charles Rogers Gene Therapy Fund, the Margaret Wiess Elkins Endowed Research Fund, the Flora and Stuart Mason Lung Cancer Research Fund, and the Phalan Thoracic Gene Therapy Fund.

The authors thank Lakshmi Kakarala for her technical assistance.

REFERENCES

1. American Cancer Society. Cancer Facts and Figures. Atlanta, GA: American Cancer Society, 2008. Available at: <http://www.cancer.org/downloads/STT/2008CAFFfinalsecured.pdf>. Accessed April 1, 2011.
2. Roth JA, Atkinson EN, Fossella F, et al. Long-term follow-up of patients enrolled in a randomized trial comparing perioperative chemotherapy and surgery with surgery alone in resectable stage IIIA non-small-cell lung cancer. *Lung Cancer* 1998;21:1-6.
3. Rosell R, Gomez-Codina J, Camps C, et al. Preresectional chemotherapy in stage IIIA non-small-cell lung cancer: a 7-year assessment of a randomized clinical trial. *Lung Cancer* 1999;26:7-14.
4. Pisters KM, Ginsberg RJ, Giroux DJ, et al. Induction chemotherapy before surgery for early-stage lung cancer: a novel approach. Bimodality Lung Oncology Team. *J Thorac Cardiovasc Surg* 2000;119:429-439.
5. Depierre A, Milleron B, Moro-Sibilot D, et al. Preoperative chemotherapy followed by surgery compared with primary surgery in resectable stage I (except T1N0), II, and IIIa non-small-cell lung cancer. *J Clin Oncol* 2002;20:247-253.
6. Dettterbeck FC, Boffa DJ, Tanoue LT. The new lung cancer staging system. *Chest* 2009;36:260-271.
7. Song W-A, Zhou N-K, Wang W, et al. Survival benefit of neoadjuvant chemotherapy in non-small cell lung cancer. An updated meta-analysis of 13 randomized control trials. *J Thorac Oncol* 2010;5:510-516.
8. Betticher DC, Schmitz S-F, Totsch M, et al. Mediastinal lymph node clearance after docetaxel-cisplatin neoadjuvant chemotherapy is prognostic of survival in patients with stage IIIA pN2 non-small cell lung cancer: a multicenter phase II trial. *J Clin Oncol* 2003;21:1752-1759.
9. Stefani A, Alifano M, Bobbio A, et al. Which patients should be operated on after induction chemotherapy for N2 non-small cell lung cancer?

- Analysis of a 7-year experience in 175 patients. *J Thorac Cardiovasc Surg* 2010;55:1–8.
10. Betticher DC, Schmitz S-F, Totsch M, et al. Prognostic factors affecting long-term outcomes in patients with resected stage IIIA p N2 non-small-cell lung cancer: 5 year follow-up of a phase II study. *Br J Cancer* 2006;94:1099–1106.
 11. Poetten C, Theegarten D, Eberhardt W, et al. Correlation of PET/CT findings and histopathology after neoadjuvant therapy in non-small cell lung cancer. *Oncology* 2007;73:316–323.
 12. Junker K, Thomas M, Schulmann K, et al. Tumour regression in non-small-cell lung cancer following neoadjuvant therapy. Histological assessment. *J Cancer Res Clin Oncol* 1997;123:469–477.
 13. Junker K, Langner K, Klinker F, et al. Grading of tumor regression in non-small cell lung cancer: morphology and prognosis. *Chest* 2001;120:1584–1591.
 14. Liu-Jarin X, Stoopler MB, Raftopoulos H, et al. Histologic assessment of non-small cell lung carcinoma after neoadjuvant therapy. *Mod Pathol* 2003;16:1102–1108.
 15. Yamane Y, Ishii G, Goto K, et al. A novel histopathological evaluation method predicting the outcome of non-small cell lung cancer treated by neoadjuvant therapy: the prognostic importance of the area of residual tumor. *J Thorac Oncol* 2010;5:49–55.
 16. Herbst RS, Giaccone G, Schiller JH, et al. Gefitinib in combination with paclitaxel and carboplatin in advanced non-small-cell lung cancer: a phase III trial-INTACT 2. *J Clin Oncol* 2004;22:785–794.
 17. Gatzemeier U, Pluzanska A, Szczesna A, et al. Phase III study of erlotinib in combination with cisplatin and gemcitabine in advanced non-small-cell lung cancer: the Tarceva Lung Cancer Investigation Trial. *J Clin Oncol* 2007;25:1545–1552.
 18. Bepler G, Kusmartseva I, Sharma S, et al. RRM1 modulated in vitro and in vivo efficacy of gemcitabine and platinum in non-small-cell lung cancer. *J Clin Oncol* 2006;24:4731–4737.
 19. Ceppi P, Volante M, Novello S, et al. ERCC1 and RRM1 gene expressions but not EGFR are predictive of shorter survival in advanced non-small-cell lung cancer treated with cisplatin and gemcitabine. *Ann Oncol* 2006;17:1818–1825.

Published in final edited form as:

Cancer. 2012 June 1; 118(11): 2889–2899. doi:10.1002/cncr.26584.

Histologic Patterns and Molecular Characteristics of Lung Adenocarcinoma Associated With Clinical Outcome

Luisa M. Solis, MD¹, Carmen Behrens, MD², M. Gabriela Raso, MD¹, Heather Y. Lin, MD, PhD³, Humam Kadara, PhD², Ping Yuan, MD¹, Hector Galindo, MD¹, Ximing Tang, MD, PhD², J. Jack Lee, PhD³, Neda Kalhor, MD¹, Ignacio I. Wistuba, MD^{1,2}, and Cesar A. Moran, MD¹

¹Department of Pathology, The University of Texas M. D. Anderson Cancer Center, Houston, Texas

²Department of Thoracic/Head and Neck Medical Oncology, The University of Texas M. D. Anderson Cancer Center, Houston, Texas

³Department of Biostatistics, The University of Texas M. D. Anderson Cancer Center, Houston, Texas

⁴Department of Thoracic Surgery, The University of Texas M. D. Anderson Cancer Center, Houston, Texas

Abstract

BACKGROUND—Lung adenocarcinoma is histologically heterogeneous and has 5 distinct histologic growth patterns: lepidic, acinar, papillary, micropapillary, and solid. To date, there is no consensus regarding the clinical utility of these patterns.

METHODS—The authors performed a detailed semiquantitative assessment of histologic patterns of 240 lung adenocarcinomas and determined the association with patients' clinicopathologic features, including recurrence-free survival (RFS) and overall survival (OS) rates. In a subset of tumors, expression levels of 2 prognostic molecular markers were evaluated: thyroid transcription factor-1 (TTF-1) (n = 218) and a panel of 5 proteins (referred as the FILM signature index) (n = 185).

RESULTS—Four mutually exclusive tumor histology pattern groups were identified: 1) any solid (38%), 2) any papillary but no solid (14%), 3) lepidic and acinar but no solid or papillary (30%), and 4) acinar only (18%). Patients in group 3 had a higher RFS rate than patients in group 1 (hazard ratio [HR], 0.4510; *P* = .0165) and group 2 (HR, 0.4253; *P* = .0425). Solid pattern tumors (group 1) were associated with a lower OS rate than nonsolid pattern tumors (all stages: HR, 1.665; *P* = .0144; stages I and II: HR, 2.157; *P* = .008). In the patients who had tumors with a nonsolid pattern, high TTF-1 expression was associated significantly with higher RFS (HR, 0.994; *P* = .0017) and OS (HR, 0.996; *P* = .0276) rates in all stages, and a high FILM signature index score was associated with lower RFS and OS rates in all stages (RFS: HR, 1.343; *P* = .0192; OS:

© 2011 American Cancer Society.

Corresponding author: Cesar Moran, MD, Department of Pathology, Unit 85, The University of Texas M. D. Anderson Cancer Center, 1515 Holcombe Boulevard, Houston, TX 77030; Fax: (713) 745-3740; cesarmoran@mdanderson.org; Ignacio I. Wistuba, MD, Department of Pathology and Thoracic/Head and Neck Medical Oncology, Unit 85, The University of Texas M. D. Anderson Cancer Center, 1515 Holcombe Boulevard, Houston, TX 77030; Fax: (713)-792-0309; iiwistuba@mdanderson.org. The last 2 authors contributed equally to this article.

CONFLICT OF INTEREST DISCLOSURES

The authors made no disclosures.

HR, 1.371; $P = .0156$) and in stages I and II (RFS: HR, 1.419; $P = .0095$; OS: HR, 1.315; $P = .0422$).

CONCLUSIONS—The presence of a solid histologic pattern was identified as a marker of unfavorable prognosis in patients with primary lung adenocarcinoma. High TTF-1 expression and low FILM signature index scores were associated with a better prognosis for patients who had tumors with a nonsolid pattern.

Keywords

histologic patterns; lung adenocarcinoma; thyroid transcription factor 1; prognostic signature

INTRODUCTION

Lung adenocarcinoma is the most common histologic lung cancer type in the United States.¹ It has a wide spectrum of clinical, radiologic, molecular, and morphologic features.² The 2004 World Health Organization classification of lung tumors includes 4 architectural growth patterns: bronchioloalveolar (also known as lepidic), acinar, papillary, and solid.^{2,3} More recently, a micropapillary pattern was described.^{4–7} Most invasive lung adenocarcinomas (>80%) include 2 or more of these patterns^{2,8}; therefore, histologic classification systems of this tumor type and potential clinical applications must account for its histologic heterogeneity.

To date, several studies have attempted to determine the clinical importance of histologic subtypes of lung adenocarcinoma by assessing the presence and extent of histologic growth patterns.^{9–24} It has been demonstrated that the lepidic growth pattern is associated with a better survival rate in patients with lung adenocarcinoma.^{9,13,14,19,20,23} In contrast, a solid pattern has been associated with a poor outcome.^{10,11,17,18,21,22,24} However, most of those studies had had small sample sizes or no rigorous histologic tumor sampling. At present, no consensus exists on the clinical utility of growth patterns in lung adenocarcinoma.

Currently, the use of molecular markers to predict recurrence and survival rates in patients with lung cancer who undergo surgery represents an area of very active investigation.^{25,26} Recently, our group reported that, in patients with stages I, II, and III lung adenocarcinoma who undergo surgery the immunohistochemical expression of thyroid transcription factor-1 (TTF-1)²⁷ and of a panel of 5 proteins (referred as the FILM signature)^{28,29} in tumors was correlated with clinical outcome. TTF-1 is a homeodomain-containing transcription factor that is essential for morphogenesis and differentiation of the lungs.³⁰ It has been used commonly as a marker for the diagnosis of primary and metastatic lung adenocarcinomas.³¹ The results from recent studies suggest that it is a lineage-specific proto-oncogene for lung cancer, and high TTF-1 expression has been associated with better survival by us²⁷ and others.^{32–36} We recently developed the FILM signature using a risk model based on the protein expression of certain genes (ubiquitin-conjugating enzyme E2C [*UBE2C*], minichromosome maintenance 2 [*MCM2*] and 6 [*MCM6*], flap structure-specific endonuclease 1 [*FEN1*], and targeting protein for Xklp2 [*TPX2*]) that were expressed differentially in an in vitro model of lung carcinogenesis.²⁹ We recently reported that an index accounting for the immunohistochemical expression of the proteins included in the FILM signature in archival tumor tissues predicted survival in all stages or stage I only lung adenocarcinomas.²⁸

In the current study, we determined the clinical relevance of histologic growth patterns in primary lung adenocarcinoma by performing a detailed semiquantitative assessment of pattern distribution (lepidic, acinar, papillary, micropapillary, and solid) in 240 surgically resected tumors that were selected by using strict criteria for tumor sampling. We studied the

association between tumor growth pattern distribution and clinicopathologic features, including age, sex, stage, and recurrence-free survival (RFS) and overall survival (OS) rates. In addition, we tested whether the use of prognostic molecular markers like TTF-1 and the FILM signature index improved our ability to determine the outcome of patients beyond the histologic subtype assessment.

MATERIALS AND METHODS

Patient Selection

We retrospectively collected surgically resected primary lung adenocarcinoma tissue samples from patients who underwent surgical resection with curative intent between 1997 and 2005 at The University of Texas M. D. Anderson Cancer Center (Houston, Tex). Clinicopathologic information was retrieved from the electronic clinical records for all patients and included age, sex, smoking history and status (current, former, or never), tumor size, tumor stage (according to the Mountain³⁷ and International Association for the Study of Lung Cancer [IASLC]³⁸ classification systems), the number of nodules (single or multiple), receipt of neoadjuvant and adjuvant treatment, and follow-up information for RFS and OS rates. This study was approved by The University of Texas M. D. Anderson Cancer Center institutional review board.

We selected 240 patients with a single-nodule, first primary lung adenocarcinoma who had not received neo-adjuvant therapy and had a minimum of 1 hematoxylin and eosin (H&E)-stained histologic slide per centimeter of the greatest tumor dimension available for histologic analysis. In addition, in most patients, formalin-fixed, paraffin-embedded tumor tissue blocks were retrieved for immunohistochemical analysis of molecular prognostic markers. Patients' clinicopathologic characteristics are listed in Table 1.

Histopathologic Analysis

All H&E-stained histologic tumor sections were examined by 3 pathologists (C.A.M., M.G.R., and L.M.S.) for the presence and extent of 5 histologic growth patterns: lepidic, acinar, papillary, micropapillary, and solid. The extent of each pattern was annotated using the percentage present in the entire set of tumor slides per patient in 5% increments. The patterns were defined histologically according to the 2004 World Health Organization classification system² with slight modifications^{39,40} and the criteria defined by Amin et al⁴ for micropapillary growth. Histologic growth patterns were defined as follows: 1) lepidic (mucinous and nonmucinous tumor cells with lepidic growth along alveolar walls and with no evidence of stromal, vascular, or pleural invasion)² (Fig. 1A,B); 2) acinar (invasive tumor arranged in *acini* and tubules and composed of cuboidal or columnar cells that resemble bronchial gland or bronchial-lining epithelial cells, including Clara cells)² (Fig. 1C); 3) papillary (invasive tumor composed of papillae structures with a fibrovascular core and complicated secondary and tertiary branches)^{2,39,40} (Fig. 1D); 4) micropapillary (small papillary tufts composed of tumor cells with peripheral nuclei and no fibrovascular core)^{2,4,7,41} (Fig. 1E); and 5) solid (invasive tumor composed of nests or sheets of tumor cells that lack acini, tubules, and papillae with mucin production) (Fig. 1F).² Tumors with 1 pattern are referred to as pure tumors, and tumors with 2 or more patterns are referred to as mixed tumors. In addition, we also analyzed the presence of lymphovascular invasion and tumor necrosis.

Immunohistochemical Analysis

To determine the immunohistochemical expression of TTF-1 and the 5 proteins (UBE2C, MCM2, MCM6, FEN1, and TPX2) of the FILM signature in lung adenocarcinomas, we used formalin-fixed, paraffin-embedded tumor tissues placed in tissue microarray (TMAs)

from a subset of patients who were included in this study (TTF-1, n = 218; FILM signature, n = 185). Immunohistochemical staining for TTF-1 was performed using 5- μ M-thick sections from TMAs as reported previously²⁷ with slight modifications. For analysis of the FILM signature, we used previously published immunohistochemical data available on the expression of the 5 FILM proteins.²⁸ All staining in malignant cells was nuclear and was quantified by 2 pathologists using a 4-value intensity score (0, 1+, 2+, and 3+) and the percentage (0%-100%) of the extent of reactivity in each core. The final score was then obtained by multiplying the intensity and reactivity extension values (range, 0–300) as reported previously.^{28,42} To determine the FILM signature index, we used a combined immunoreactivity score for each patient that was computed by simple addition of the individual final scores for each of the 5 biomarkers analyzed as published previously.²⁸

Statistical Analysis

To determine the association between histologic growth pattern and clinicopathologic covariates and time-to-event outcomes (RFS and OS), we classified patients into 4 mutually exclusive groups on the basis of the distribution of histologic growth patterns (Table 2). Chi-square tests or Fisher exact tests were used to determine differences in categorical variables, and the Wilcoxon rank-sum test or the Kruskal-Wallis test was used to detect differences in continuous variables between groups. RFS and OS distributions were estimated using the Kaplan-Meier method. The log-rank test⁴³ was used to determine survival differences between groups. Regression analyses of survival data based on the Cox proportional hazards model⁴³ were conducted for the RFS and OS rates. RFS was calculated from the date of surgery to the date of either recurrence or last contact, and OS was calculated from the date of surgery to the date of either death or last contact. Both RFS and OS were censored at 5 years. Associations between nuclear TTF-1 expression, the FILM signature index, and clinicopathologic variables and tumor growth pattern were calculated using continuous variables and a cutoff value of 160 for TTF-1 and 113.3 for the FILM signature index, which represent the median expression level for adenocarcinomas evaluated using TMAs. The statistical software packages SAS (version 9.1; SAS Institute, Inc., Cary, NC), R (2.80; R Foundation for Statistical Computing, Austria, Vienna), and S-Plus (version 8.0; TIBCO Software, Inc., Palo Alto, Calif) were used to perform the computations for all analyses.

RESULTS

Growth Pattern Distribution

Most adenocarcinomas that we evaluated (n = 191; 80%) had 2 growth patterns (mixed tumors), as expected. Of the 49 adenocarcinomas (20%) that had a single growth pattern (pure tumors), acinar was the most common pattern (n = 42; 18%) followed by solid (n = 6; 3%), and papillary (n = 1; 0.4%). No pure lepidic or micropapillary growth patterns were identified. In all tumors, the most common pattern was acinar (n = 232; 97%), followed by lepidic (n = 116; 48%; 8 mucinous and 108 nonmucinous), solid (n = 92; 38%), papillary (n = 44; 18%), and micropapillary (n = 15; 6%).

To determine the potential clinical implications of histologic pattern distribution in lung adenocarcinomas, we clustered the 240 tumors according to growth pattern distribution (single and combined) (Table 2). We identified 4 mutually exclusive histologic groups: 1) tumors with any solid pattern (n = 92; 38%), 2) tumors with any papillary pattern but no solid pattern (n = 34; 14%); 3) tumors with acinar and lepidic patterns but no solid or papillary pattern (n = 72; 30%); and 4) tumors with an acinar pattern only (n = 42, 18%).

We determined the associations among the 4 pattern groups and patients' clinical and pathologic characteristics. Table 1 indicates that the histologic pattern groups differed

significantly in a comparison according to the presence of tumor necrosis ($P < .0001$), age (median, 66.8 years; $P = .00079$), smoking status ($P = .0001$), and tumor classification (IASLC, $P = .01377$; Mountain et al, $P = .00164$). It is noteworthy that the tumors with solid growth patterns (group 1) had more tumor necrosis and were more common in younger patients (aged ≤ 66.8 years), current smokers, and patients with stage II through IV disease (according to Mountain et al and IASLC). Tumors with nonsolid or papillary patterns but with acinar and lepidic growth patterns (group 3) had less tumor necrosis and were more common in older patients (aged >66.8 years), never smokers, and patients with stage I disease (Table 1).

Association Between Growth Patterns and Outcome

We determined the association between histologic growth pattern and RFS and OS rates. The median follow-up was 4.21 years. In multivariate survival analysis, as expected, patients with stage III and IV disease (IASLC staging) had lower RFS and OS rates than patients with stage I and II disease. In addition, patients who were older than the median age (>66.8 years) and men had lower OS rates than younger patients and women, respectively (Table 3). Adjuvant chemotherapy was not associated significantly with RFS or OS when all tumor stages were examined.

Overall, on multivariate analysis, we observed that lung adenocarcinoma pattern groups were associated significantly with RFS ($P = .0418$). Specifically, patients in group 3 had significantly higher RFS rates than patients in group 1 (hazard ratio [HR], 0.4510; 95% confidence interval [CI], 0.235–0.865; $P = .0165$) and group 2 (HR, 0.4253; 95% CI, 0.1862–0.9713; $P = .0425$) after adjusting for IASLC stage and adjuvant treatment. Although multivariate analysis revealed no significant association between all histologic groups and OS ($P = .0738$), patients in group 3 had significantly higher OS rates (HR, 0.437; 95% CI, 0.225–0.847; $P = .0143$) than patients in group 1 after adjusting for IASLC stage, adjuvant treatment, age, and sex. No other differences in the RFS or OS rates were observed between the 4 groups.

In patients with stage I or II disease, lung adenocarcinoma pattern groups were correlated significantly with OS ($P = .0278$) in multivariate analysis. Specifically, patients in group 3 had significantly higher OS rates than patients in group 1 (HR, 0.317; 95% CI, 0.148–0.679; $P = .0031$) after adjusting for IASLC stage, adjuvant treatment, age, and sex. Although we did not observe a significant association between pattern groups and RFS in multivariate analysis ($P = .1149$), patients in group 3 had significantly higher RFS rates than patients in group 1 (HR, 0.400; 95% CI, 0.183–0.875; $P = .0217$) after adjusting for IASLC stage and adjuvant treatment. In addition, we determined the survival rates of all patients according to the presence of a lepidic (vs nonlepidic), papillary (vs nonpapillary), and micropapillary (vs nonmicropapillary) growth pattern component and observed no statistically significant association among these patterns and RFS or OS (data not shown).

Association Between Solid Growth Pattern and Outcome

Because patients who had tumors with solid patterns (group 1) had a trend toward lower RFS and OS rates than patients who had tumors with other patterns, we performed a survival analysis of patients with solid tumors (group 1) versus nonsolid tumors (groups 2–4). Patients who had tumors with a solid pattern had lower OS and RFS rates than patients who had tumors with nonsolid patterns at all stages (Fig. 2A,C). These associations were statistically significant on univariate and multivariate analyses for both RFS (HR, 1.722; 95% CI, 1.060–2.796; $P = .0280$) and OS (HR, 1.665; 95% CI, 1.036–2.675; $P = .0144$) after adjusting for stage and adjuvant therapy for RFS and additionally for age and sex for OS (Table 3). In patients with stage I or II disease, tumors with a solid pattern were associated

with a lower OS rate on univariate and multivariate analyses (HR, 2.157; 95% CI, 1.222–3.808; $P = .008$) after adjusting for stage (I vs II) and adjuvant therapy. The presence of a solid pattern was associated with a lower RFS rate on univariate analysis (HR, 1.820; 95% CI, 1.050–3.152; $P = .0327$), but this association was not significant on multivariate analysis after adjusting for stage (II vs I) and adjuvant therapy (HR, 1.543; 95% CI, 0.872–2.733; $P = .1367$) (Fig. 2B,D).

Prognostic Value of TTF-1 Expression and FILM Signature Index In Tumors With Nonsolid Patterns

To test whether the use of prognostic molecular markers improves our ability to determine the outcome of patients who have tumors with nonsolid patterns, we compared tumor immunohistochemical expression of TTF-1 and the FILM signature index with RFS and OS rates in all patients and in patients with stage I and II tumors. First, we determined that both TTF-1 and the FILM signature index correlated significantly with tumor histology patterns. TTF-1 expression was significantly lower ($P = .015$) in solid pattern tumors (group 1) compared the other groups; in contrast, the FILM signature index was significantly higher ($P < .001$) in solid pattern tumors compared with nonsolid pattern tumors.

In all tumor stages, in tumors with nonsolid patterns, higher TTF-1 expression (as a continuous variable) was correlated significantly with higher RFS and OS rates (RFS: HR, 0.994; $P = .0017$; OS: HR, 0.996; $P = .0276$) on multivariate analysis (Table 4, Fig. 3A,C). We did not observe any significant association between TTF-1 expression and outcome in patients with stage I and II disease. Conversely, we observed that, in all patients and in patients with stage I and II disease only, a higher FILM signature index (as a continuous variable) was with lower RFS and OS rates at all stages (RFS: HR, 1.343; $P = .0192$; OS: HR, 1.371; $P = .0156$;) and for stages I and II only (RFS: HR, 1.419; $P = .0095$; OS: HR, 1.315; $P = .0422$) on multivariate analysis (Table 4, Fig. 3B,D). It is noteworthy that, in tumors with a solid pattern, TTF-1 expression and the FILM signature index were not associated with RFS or OS rates in all patients (TTF1: RFS; $P = .6838$; OS; $P = .4088$; FILM index: RFS; $P = .5127$; OS; $P = .6560$) or in patients with stage I and II disease only (TTF1: RFS; $P = .9776$; OS; $P = .6752$; FILM index: RFS; $P = .3906$; OS; $P = .5231$).

DISCUSSION

In this study, we determined the clinical relevance of growth pattern quantification in 240 primary lung adenocarcinomas that had been surgically resected with curative intent. The patients were selected using strict tumor-sampling inclusion criteria and were subjected to a detailed semiquantitative histologic assessment. Most adenocarcinomas (80%) had mixed patterns. By analyzing the pattern distributions, we identified 4 mutually exclusive groups of tumors, including 1 in which any solid pattern was present (38%). On multivariate analysis, we observed that patients who had tumors with any solid pattern had lower OS rates than patients from all other histologic groups combined (nonsolid), both for all tumor stages and for stages I and II. To improve our ability to determine the outcome of patients who had tumors with nonsolid patterns, we compared tumor immunohistochemical expression of TTF-1 and the FILM signature index with RFS and OS rates. In these patients, higher TTF-1 expression and a lower FILM signature index were correlated significantly with higher RFS and OS rates on multivariate analysis at all stages. In addition, a lower FILM signature index correlated with higher RFS and OS rates in patients with stage I and II disease. It is noteworthy that these associations were not detected in patients who had solid pattern tumors. We demonstrated that a histologic solid pattern is a marker of a poor prognosis in surgically resected lung adenocarcinomas and that high immunohistochemical TTF-1 expression and a low FILM signature index are associated with a better prognosis in patients with nonsolid histologic patterns.

We observed a correlation between the presence of a solid histologic pattern and poor outcome in surgically resected lung adenocarcinoma, which highlights the clinical importance of a detailed histologic assessment of this tumor type by pathologists examining at least 1 slide per centimeter of the tumor's greatest dimension. The association between a solid histologic component and patient prognosis using a multivariate analysis in stages I through III lung adenocarcinoma has been reported previously in 7 studies.^{10,11,17,18,21,24,44} However, only 1 study provided complete outcome data for patients at all stages and those with stage I and II disease,¹⁷ and only 2 reported RFS or disease-free survival data.^{21,24}

To our knowledge, the current study, which was based on a large patient series, is the first to report the use of rigorous selection criteria for histologic examination and detailed semiquantitative assessment of histologic growth patterns. We also assessed RFS and OS and reported outcome data both for all stages and for stages I and II. Therefore, we believe our results provide important and novel insights into the clinical relevance of detailed histologic assessments of lung adenocarcinoma growth patterns as suggested by the International Association for the Study of Lung Cancer/American Thoracic Society/European Respiratory Society for the Classification of Lung Adenocarcinoma.⁴⁵ Our results indicate that a simple semiquantitative assessment to determine the presence of a solid pattern is sufficient to predict RFS and OS in patients with lung adenocarcinoma who undergo curative surgery.

In this study we have improved our ability to determine the outcome of patients who have tumors with non-solid patterns by comparing tumor immunohistochemical expression of TTF-1 and the FILM signature index with RFS and OS rates in patients with disease in all stages and with stage I and II disease. We observed that high TTF-1 immunohistochemical expression levels were associated significantly with prognosis in patients with lung adenocarcinoma. Although we examined TTF-1 expression in TMA specimens, our findings are in agreement with previously published data using either TMAs^{33,46} or whole-section samples.^{32,35} However, to our knowledge, ours is the first study to demonstrate that this marker is predictive of prognosis in patients who have tumors with nonsolid patterns. We also observed that the FILM signature index was able to predict RFS and OS outcomes in our patients with adenocarcinoma who had nonsolid histologic patterns at all stages and at stages I and II. The robustness of the gene-derived and protein-derived protein signature has been tested before and was predictive of a poor outcome in patients with lung adenocarcinoma rather than in patients with squamous cell carcinoma.²⁸ It is noteworthy that in this study, we also demonstrated that the expression of TTF-1 and the FILM signature index were not predictive of outcome for patients who had tumors with any solid growth pattern.

In conclusion, our findings demonstrate that the presence of a histologic solid pattern in primary, single-nodule lung adenocarcinoma is a marker of unfavorable prognosis and that high immunohistochemical TTF-1 expression and a low FILM signature index are associated with a better prognosis in patients who have tumors non-solid patterns. Here, we demonstrate that the integration of molecular markers and the semiquantitative assessment of histologic growth patterns improve the prognostic stratification of patients with lung adenocarcinomas.

Acknowledgments

FUNDING SOURCES

This study was supported in part by grants from the Department of Defense (W81XWH-04-1-0142), Uniting Against Lung Cancer, Specialized Program of Research Excellence in Lung Cancer Grant P50CA70907, and Cancer Center Support Grant CA-16672 from the National Cancer Institute.

References

1. Devesa SS, Bray F, Vizcaino AP, Parkin DM. International lung cancer trends by histologic type: male:female differences diminishing and adenocarcinoma rates rising. *Int J Cancer*. 2005; 117:294–299. [PubMed: 15900604]
2. Travis, WD.; Brambilla, E. World Health Organization Classification of Tumours. Pathology and Genetics of Tumours of the Lung, Pleura, Thymus and Heart. Muller–Hemelink, HK.; Harris, CC., editors. Lyon, France: IARC Press; 2004.
3. Travis WD, Garg K, Franklin WA, et al. Bronchioloalveolar carcinoma and lung adenocarcinoma: the clinical importance and research relevance of the. 2004 World Health Organization pathologic criteria. *J Thorac Oncol*. 2006; 1(9 suppl):S13–S19. [PubMed: 17409995]
4. Amin MB, Tamboli P, Merchant SH, et al. Micropapillary component in lung adenocarcinoma: a distinctive histologic feature with possible prognostic significance. *Am J Surg Pathol*. 2002; 26:358–364. [PubMed: 11859208]
5. Makimoto Y, Nabeshima K, Iwasaki H, et al. Micropapillary pattern: a distinct pathological marker to subclassify tumours with a significantly poor prognosis within small peripheral lung adenocarcinoma (< 20 mm) with mixed bronchioloalveolar and invasive subtypes (Noguchi's type C tumours). *Histopathology*. 2005; 46:677–684. [PubMed: 15910599]
6. Miyoshi T, Satoh Y, Okumura S, et al. Early stage lung adenocarcinomas with a micropapillary pattern, a distinct pathologic marker for a significantly poor prognosis. *Am J Surg Pathol*. 2003; 27:101–109. [PubMed: 12502932]
7. Sanchez-Mora N, Presmanes MC, Monroy V, et al. Micropapillary lung adenocarcinoma: a distinctive histologic subtype with prognostic significance. Case series. *Hum Pathol*. 2008; 39:324–330. [PubMed: 18261622]
8. Motoi N, Szoke J, Riely GJ, et al. Lung adenocarcinoma: modification of the 2004 WHO mixed subtype to include the major histologic subtype suggests correlations between papillary and micropapillary adenocarcinoma subtypes, EGFR mutations and gene expression analysis. *Am J Surg Pathol*. 2008; 32:810–827. [PubMed: 18391747]
9. Anami Y, Iijima T, Suzuki K, et al. Bronchioloalveolar carcinoma (lepidic growth) component is a more useful prognostic factor than lymph node metastasis. *J Thorac Oncol*. 2009; 4:951–958. [PubMed: 19543119]
10. Barletta JA, Yeap BY, Chirieac LR. Prognostic significance of grading in lung adenocarcinoma. *Cancer*. 2010; 116:659–669. [PubMed: 20014400]
11. Bryant CM, Albertus DL, Kim S, et al. Clinically relevant characterization of lung adenocarcinoma subtypes based on cellular pathways: an international validation study [serial online]. *PLoS One*. 2010; 5:e11712. [PubMed: 20661423]
12. Kurokawa T, Matsuno Y, Noguchi M, Mizuno S, Shimosato Y. Surgically curable “early” adenocarcinoma in the periphery of the lung. *Am J Surg Pathol*. 1994; 18:431–438. [PubMed: 8172319]
13. Maeshima AM, Tochigi N, Yoshida A, Asamura H, Tsuta K, Tsuda H. Histological scoring for small lung adenocarcinomas 2 cm or less in diameter: a reliable prognostic indicator. *J Thorac Oncol*. 2010; 5:333–339. [PubMed: 20125041]
14. Noguchi M, Morikawa A, Kawasaki M, et al. Small adenocarcinoma of the lung. Histologic characteristics and prognosis. *Cancer*. 1995; 75:2844–2852. [PubMed: 7773933]
15. Okudela K, Woo T, Mitsui H, et al. Proposal of an improved histological subtyping system for lung adenocarcinoma—significant prognostic values for stage I disease. *Int J Clin Exp Pathol*. 2010; 3:348–366. [PubMed: 20490327]
16. Petersen I, Kotb WF, Friedrich KH, Schluns K, Bocking A, Dietel M. Core classification of lung cancer: correlating nuclear size and mitoses with ploidy and clinicopathological parameters. *Lung Cancer*. 2009; 65:312–318. [PubMed: 19168259]
17. Riquet M, Foucault C, Berna P, Assouad J, Dujon A, Danel C. Prognostic value of histology in resected lung cancer with emphasis on the relevance of the adenocarcinoma subtyping. *Ann Thorac Surg*. 2006; 81:1988–1995. [PubMed: 16731118]

18. Russell PA, Wainer Z, Wright GM, Daniels M, Conron M, Williams RA. Does lung adenocarcinoma subtype predict patient survival? A clinicopathologic study based on the new International Association for the Study of Lung Cancer/ American Thoracic Society/European Respiratory Society international multidisciplinary lung adenocarcinoma classification. *J Thorac Oncol.* 2011; 6:1496–1504. [PubMed: 21642859]
19. Sakurai H, Dobashi Y, Mizutani E, et al. Bronchioloalveolar carcinoma of the lung 3 centimeters or less in diameter: a prognostic assessment. *Ann Thorac Surg.* 2004; 78:1728–1733. [PubMed: 15511463]
20. Sakurai H, Maeshima A, Watanabe S, et al. Grade of stromal invasion in small adenocarcinoma of the lung: histopathological minimal invasion and prognosis. *Am J Surg Pathol.* 2004; 28:198–206. [PubMed: 15043309]
21. Sica G, Yoshizawa A, Sima CS, et al. A grading system of lung adenocarcinomas based on histologic pattern is predictive of disease recurrence in stage I tumors. *Am J Surg Pathol.* 2010; 34:1155–1162. [PubMed: 20551825]
22. Sorensen JB, Hirsch FR, Olsen J. The prognostic implication of histopathologic subtyping of pulmonary adenocarcinoma according to the classification of the World Health Organization. An analysis of 259 consecutive patients with advanced disease. *Cancer.* 1988; 62:361–367. [PubMed: 3383137]
23. Terasaki H, Niki T, Matsuno Y, et al. Lung adenocarcinoma with mixed bronchioloalveolar and invasive components: clinicopathological features, subclassification by extent of invasive foci, and immunohistochemical characterization. *Am J Surg Pathol.* 2003; 27:937–951. [PubMed: 12826886]
24. Yoshizawa A, Motoi N, Riely GJ, et al. Impact of proposed IASLC/ATS/ERS classification of lung adenocarcinoma: prognostic subgroups and implications for further revision of staging based on analysis of 514 stage I cases. *Mod Pathol.* 2011; 24:653–664. [PubMed: 21252858]
25. Herbst RS, Heymach JV, Lippman SM. Lung cancer. *N Engl J Med.* 2008; 359:1367–1380. [PubMed: 18815398]
26. Sudhindra A, Ochoa R, Santos ES. Biomarkers, prediction, and prognosis in nonsmall-cell lung cancer: a platform for personalized treatment [published online ahead of print May 8, 2011]. *Clin Lung Cancer.* 2011
27. Tang X, Kadara H, Behrens C, et al. Abnormalities of the TTF-1 lineage-specific oncogene in NSCLC: implications in lung cancer pathogenesis and prognosis. *Clin Cancer Res.* 2011; 17:2434–2443. [PubMed: 21257719]
28. Kadara H, Behrens C, Yuan P, et al. A 5-gene and corresponding protein signature for stage-I lung adenocarcinoma prognosis. *Clin Cancer Res.* 2010; 17:1490–1501. [PubMed: 21163870]
29. Kadara H, Lacroix L, Behrens C, et al. Identification of gene signatures and molecular markers for human lung cancer prognosis using an in vitro lung carcinogenesis system. *Cancer Prev Res (Phila).* 2009; 2:702–711. [PubMed: 19638491]
30. Bingle CD. Thyroid transcription factor-1. *Int J Biochem Cell Biol.* 1997; 29:1471–1473. [PubMed: 9570141]
31. Moldvay J, Jackel M, Bogos K, et al. The role of TTF-1 in differentiating primary and metastatic lung adenocarcinomas. *Pathol Oncol Res.* 2004; 10:85–88. [PubMed: 15188024]
32. Barlesi F, Pinot D, Legoffic A, et al. Positive thyroid transcription factor 1 staining strongly correlates with survival of patients with adenocarcinoma of the lung. *Br J Cancer.* 2005; 93:450–452. [PubMed: 16052216]
33. Barletta JA, Perner S, Iafrate AJ, et al. Clinical significance of TTF-1 protein expression and TTF-1 gene amplification in lung adenocarcinoma. *J Cell Mol Med.* 2009; 13(8B):1977–1986. [PubMed: 19040416]
34. Berghmans T, Mascaux C, Haller A, Meert AP, Van Houtte P, Sculier JP. EGFR, TTF-1 and Mdm2 expression in stage III nonsmall cell lung cancer: a positive association. *Lung Cancer.* 2008; 62:35–44. [PubMed: 18355939]
35. Berghmans T, Mascaux C, Martin B, Ninane V, Sculier JP. Prognostic role of thyroid transcription factor-1 in stage III nonsmall cell lung cancer. *Lung Cancer.* 2006; 52:219–224. [PubMed: 16545887]

36. Kwei KA, Kim YH, Girard L, et al. Genomic profiling identifies TTF1 as a lineage-specific oncogene amplified in lung cancer. *Oncogene*. 2008; 27:3635–3640. [PubMed: 18212743]
37. Mountain CF. The international system for staging lung cancer. *Semin Surg Oncol*. 2000; 18:106–115. [PubMed: 10657912]
38. Detterbeck FC, Boffa DJ, Tanoue LT. The new lung cancer staging system. *Chest*. 2009; 136:260–271. [PubMed: 19584208]
39. Silver SA, Askin FB. True papillary carcinoma of the lung: a distinct clinicopathologic entity. *Am J Surg Pathol*. 1997; 21:43–51. [PubMed: 8990140]
40. Moran CA. Pulmonary adenocarcinoma: the expanding spectrum of histologic variants. *Arch Pathol Lab Med*. 2006; 130:958–962. [PubMed: 16831050]
41. Borczuk AC. Micropapillary histology: a frequent morphology of mutation-associated lung adenocarcinoma? *Am J Clin Pathol*. 2009; 131:615–617. [PubMed: 19369618]
42. Solis LM, Behrens C, Dong W, et al. Nrf2 and Keap1 abnormalities in nonsmall cell lung carcinoma and association with clinicopathologic features. *Clin Cancer Res*. 2010; 16:3743–3753. [PubMed: 20534738]
43. Kalbfleisch, JD.; Prentice, RL. *The Statistical Analysis of Failure Time Data* (Wiley Series in Probability and Statistics). 2. New York: John Wiley & Sons, Inc; 2002.
44. Haruki T, Shomori K, Shiomi T, Taniguchi Y, Nakamura H, Ito H. The morphological diversity of small lung adenocarcinoma with mixed subtypes is associated with local invasiveness and prognosis. *Eur J Cardiothorac Surg*. 2011; 39:763–768. [PubMed: 20864350]
45. Travis WD, Brambilla E, Noguchi M, et al. International Association for the Study of Lung Cancer/American Thoracic Society/European Respiratory Society international multidisciplinary classification of lung adenocarcinoma. *J Thorac Oncol*. 2011; 6:244–285. [PubMed: 21252716]
46. Anagnostou VK, Syrigos KN, Bepler G, Homer RJ, Rimm DL. Thyroid transcription factor 1 is an independent prognostic factor for patients with stage I lung adenocarcinoma. *J Clin Oncol*. 2009; 27:271–278. [PubMed: 19064983]

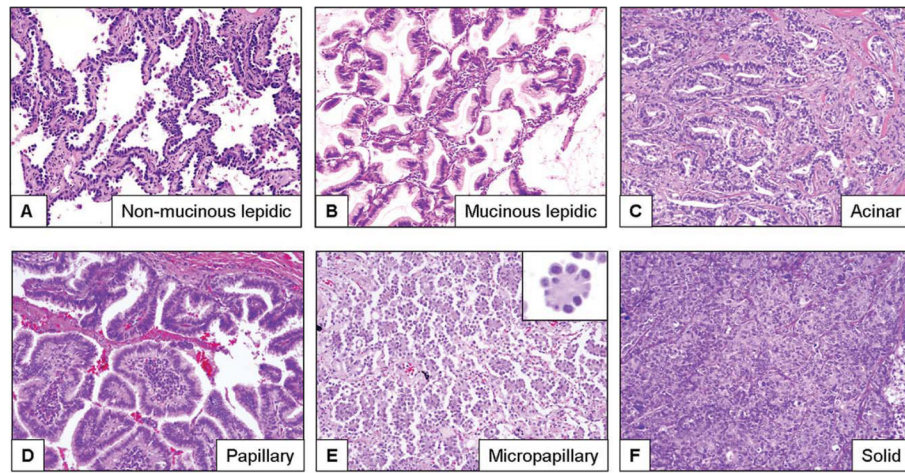
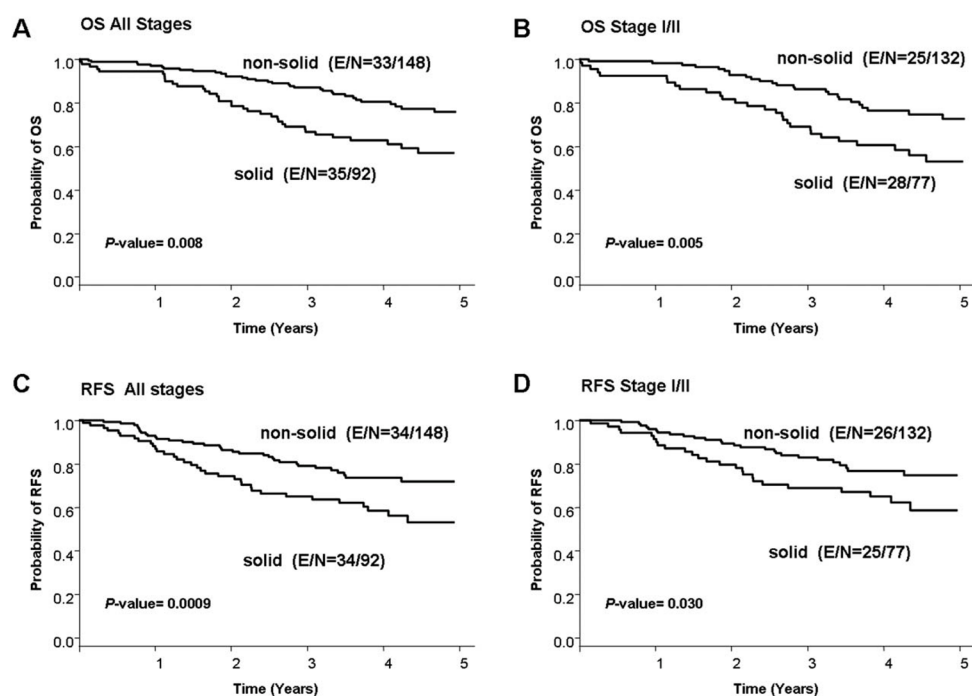


Figure 1.

These are photomicrographs of hematoxylin and eosin-stained sections of lung adenocarcinoma tumors with different growth patterns, including (A) lepidic (nonmucinous), (B) lepidic (mucinous), (C) acinar, (D) papillary, (E) micropapillary, and (F) solid (original magnification, $\times 100$).

**Figure 2.**

The rates of (A,B) 5-year overall survival (OS) and (C,D) 5-year recurrence-free survival (RFS) are illustrated in patients with lung adenocarcinoma according to tumor growth pattern (solid vs nonsolid) both (A,C) for all stages and (B,D) for stages I and II only. E indicates events; N, total number of patients.

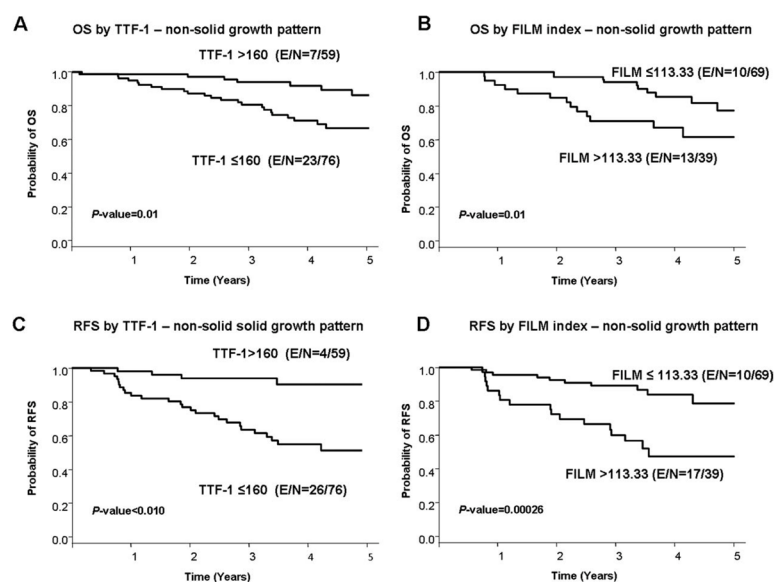


Figure 3.

The rates of (A,B) 5-year overall survival (OS) and (C,D) 5-year recurrence-free survival (RFS) are illustrated in patients with lung adenocarcinoma who had nonsolid tumor growth patterns according to (A,C) thyroid transcription factor 1 (TTF-1) expression and (B,D) scores on a panel of 5 proteins (referred as the FILM signature index). E indicates events; N, total number of patients.

Clinical and Pathologic Characteristics of All 240 Primary Lung Adenocarcinoma Tumors Studied and Their Association With 4 Histologic Pattern Groups

Table 1

Characteristic	All Tumors, N = 240	Histologic Pattern Group: No. of Patients (%) ^a			P
		Group 1, N = 92	Group 2, N = 34	Group 3, N = 72	Group 4, N = 42
Age, y^b					.00079
66.8	118	53 (45)	20 (17)	21 (18)	24 (20)
>66.8	122	39 (32)	14 (11)	51 (42)	18 (15)
Sex					.09314
Women	137	47 (34)	16 (12)	49 (36)	25 (18)
Men	103	45 (44)	18 (17)	23 (22)	17 (17)
Smoking status					.00010
Current	97	54 (56)	13 (13)	15 (15)	15 (15)
Former	102	30 (29)	15 (15)	37 (36)	20 (20)
Never	41	8 (20)	6 (15)	20 (49)	7 (17)
IASLC stage^c					.01377
I	167	54 (32)	23 (14)	60 (36)	30 (18)
II	42	23 (55)	8 (19)	7 (17)	4 (10)
III or IV	31	15 (48)	3 (10)	5 (16)	8 (26)
TNM stage^d					.00164
I	173	55 (32)	24 (14)	63 (36)	31 (18)
II	36	22 (61)	7 (19)	4 (11)	3 (8)
III or IV	31	15 (48)	3 (10)	5 (16)	8 (26)
Adjuvant therapy^e					.27792
No	163	57 (35)	26 (16)	53 (33)	27 (17)
Yes	71	33 (47)	7 (10)	18 (25)	13 (18)
Necrosis					<.0001
No	114	26 (23)	19 (17)	48 (42)	21 (18)
Yes	126	66 (52)	15 (12)	24 (19)	21 (17)
Lymphovascular invasion					.1398
No	200	74 (37)	26 (13)	66 (33)	34 (17)

Characteristic	Histologic Pattern Group: No. of Patients (%) ^a			
	All Tumors, N = 240	Group 1, N = 92	Group 2, N = 34	Group 3, N = 72
Yes	40	18 (45)	8 (20)	6 (15)

Abbreviations: IASLC, International Association for the Study of Lung Cancer; TNM, tumor, lymph node, metastasis.

^aHistologic pattern groups were defined as follows: group 1, tumors with any solid pattern; group 2, any papillary pattern but no solid pattern; group 3, acinar and lepidic patterns but no solid or papillary patterns; and group 4, acinar pattern only.

^bThe median age of the entire population is indicated.

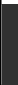






















































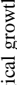




^cSee Dettterbeck FC, Boffa DJ, Tanoue LT. The new lung cancer staging system. *Chest*. 2009;136:260–271.³⁸

^dSee Mountain CF. The international system for staging lung cancer. *Semin Surg Oncol*. 2000;18:106–115.³⁷

^eAdjuvant treatment information was not available for 6 patients.

Lung Adenocarcinoma Histologic Groups Identified by Histologic Growth pattern Distributions

Table 2

Group	HISTOLOGIC GROWTH PATTERN					Frequency, N (%)
	Solid ^a	Papillary ^b	Lepidic ^a	Micro-papillary ^a	Actinar ^d	
Group 1, n=92 (38%)						56 (23.3)
						17 (7.1)
						7 (2.9)
						6 (2.5)
						2 (0.8)
						2 (0.8)
						1 (0.4)
						1 (0.4)
						
						
Group 2, n= 34 (14%)						19 (7.9)
						7 (2.9)
						3 (1.3)
						1 (0.4)
						1 (0.4)
						1 (0.4)
						1 (0.4)
						1 (0.4)
						1 (0.4)
						1 (0.4)
Group 3, n= 72 (30%)						68 (28.3)
						4(1.6)
Group 4, n= 42 (18%)						42 (17.5)

^aThe shaded boxes represent the presence of histological growth patterns in the tumors analyzed.

Table 3

Multivariate Cox Model of 5-Year Recurrence-Free and Overall Survival in All Patients (n = 240) According to Solid (Group 1) Versus Nonsolid (Groups 2–4) Growth Patterns

Variable	RFS		OS	
	HR (95% CI)	P	HR (95% CI)	P
Solid growth pattern: Solid vs nonsolid	1.722 (1.060–2.796)	.0280	1.665 (1.036–2.675)	.0144
Final IASLC stage: III or IV vs I or II ^a	4.087 (2.179–7.665)	<.0001	2.791 (1.404–5.549)	.0034
Adjuvant treatment: yes vs no	0.945 (0.536–1.667)	.8459	0.551 (0.289–1.051)	.0705
Age: >66.8 y vs 66.8 y ^b	—	—	1.769 (1.064–2.943)	.0280
Sex: Men vs women	—	—	1.974 (1.192–3.271)	.0083

Abbreviations: CI, confidence interval; HR, hazard ratio; IASLC, International Association for the Study of Lung Cancer; OS, overall survival; RFS, recurrence-free survival.

^aSee Detterbeck FC, Boffa DJ, Tanoue LT. The new lung cancer staging system. *Chest*. 2009;136:260–271.³⁸

^bThe median age of the entire population is indicated.

Table 4

Multivariate Cox Model of 5-Year Recurrence-Free and Overall Survival Only in Patients With Nonsolid Growth Patterns According to Thyroid Transcription Factor 1 Expression and FILM Signature Index

Variable	RFS		OS	
	HR (95% CI)	P	HR (95% CI)	P
Nonsolid tumors according to TTF-1 expression, n = 135				
Nuclear TTF-1 expression: per unit increase	0.994 (0.992–0.998)	.0017	0.996 (0.992–1.000)	.0276
Final IASLC stage: III and IV vs I and II ^a	4.555 (1.934–10.729)	.0005	4.959 (2.092–11.752)	.0003
Adjuvant treatment: Yes vs no	1.205 (0.550–2.638)	.6409	0.558 (0.206–1.513)	.2514
Age: >66.8 y vs 66.8 y ^b	—	—	1.620 (0.703–3.735)	.2574
Sex: Men vs women	—	—	1.510 (0.715–3.187)	.2810
Nonsolid tumors by FILM signature index, n = 108^c				
FILM signature index: 1-Fold increase	1.343 (1.049–1.719)	.0192	1.371 (1.062–1.770)	.0156
Final IASLC stage: III and IV vs I and II ^a	2.290 (0.775–6.765)	.1338	-	—
Adjuvant treatment: Yes vs no	1.124 (0.455–2.776)	.8008	0.733 (0.286–1.878)	.5176
Age: >66.8 y vs 66.8 y ^b	—	—	—	—
Sex: Men vs women	—	—	1.810 (0.771–4.247)	.1730

Abbreviations: CI, confidence interval; HR, hazard ratio; IASLC, International Association for the Study of Lung Cancer; OS, overall survival; RFS, recurrence-free survival; TTF-1, thyroid transcription factor 1.

^aSee Detterbeck FC, Boffa DJ, Tanoue LT. The new lung cancer staging system. *Chest*. 2009;136:260–271.³⁸

^bThe median age of the entire population is indicated.

^cThe FILM signature index is a panel of 5 proteins that was developed using a risk model based on the protein expression of certain genes.



Histologic features of low- and intermediate-grade neuroendocrine carcinoma (typical and atypical carcinoid tumors) of the lung

Koji Tsuta^{a,d}, Maria G. Raso^b, Neda Kalhor^a, Diane D. Liu^c, Ignacio I. Wistuba^{a,b}, Cesar A. Moran^{a,*}

^a Department of Pathology, The University of Texas M. D. Anderson Cancer Center, Houston, TX, USA

^b Department of Thoracic/Head and Neck Medical Oncology, The University of Texas M. D. Anderson Cancer Center, Houston, TX, USA

^c Department of Biostatistics, The University of Texas M. D. Anderson Cancer Center, Houston, TX, USA

^d Division of Clinical Laboratory, National Cancer Center Hospital, Tokyo, Japan

ARTICLE INFO

Article history:

Received 10 November 2009

Received in revised form 5 February 2010

Accepted 1 April 2010

Keywords:

Typical carcinoid

Atypical carcinoid

Mitosis

Necrosis

Recurrence-free survival

Neuroendocrine carcinoma

ABSTRACT

Background: Determining the differential diagnosis between typical (TCs) and atypical carcinoid tumors (ACs) is imperative, as the distinction between TCs and ACs is currently based on histologic criteria that are not always correlated with the unfavorable clinical outcomes.

Patients and methods: We conducted a retrospective study of patients who were diagnosed with carcinoid tumors between 1990 and 2005 at M. D. Anderson Cancer Center. We reviewed the slides for the following pathologic features: infiltrative growth; pleural, blood, or lymphatic vessel invasion; tumor stroma; presence of active fibroblastic proliferation; chromatin pattern; presence of nucleolus; and nuclear pleomorphism. We also evaluated the necrotic patterns. Finally, we evaluated three methods for calculating the number of mitoses: randomly selected, the most mitotically active in 10 high-power fields (HPFs), or overall mean mitotic count.

Results: Our cohort consisted of 80 patients (68 with TCs and 12 with ACs). Older age ($P=0.002$), pathologic stage III or IV disease ($P=0.04$), active fibroblastic proliferation ($P=0.041$), and comedo-like necrosis ($P=0.001$) were significantly associated with tumor recurrence or patient's death. Among the three mitotic counting methods, the overall mean number of mitoses was significantly correlated with recurrence-free survival ($P<0.0001$). Our criteria for distinguishing AC from TC included the presence of comedo-like necrosis and/or an overall mean number of mitoses ≥ 0.2 /HPF.

Conclusions: Using an overall mean number in counting mitoses and detecting comedo-like necrosis is important for classifying lung carcinoid tumors.

© 2010 Published by Elsevier Ireland Ltd.

1. Introduction

Bronchopulmonary neuroendocrine tumors comprise about 20% of all lung carcinomas and represent a spectrum of tumors arising from neuroendocrine cells. The different types of bronchopulmonary neuroendocrine carcinomas share structural, morphologic, immunohistochemical, and ultrastructural features, and they are separated into four subgroups in increasing order of biologic aggressiveness: low-grade (typical carcinoids; TCs), intermediate-grade (atypical carcinoids; ACs), and high-grade (large-cell neuroendocrine carcinomas; LCNECs), or (small-cell lung carcinomas). TCs and ACs account for approximately 1–2% of all primary lung carcinomas [1,2].

Although TCs are generally regarded as low-grade carcinomas, approximately 10–23% [3] of cases metastasize to the regional lymph nodes at presentation, with the 5-year overall survival rates ranging from 82% to 100% for patients with TCs [4,5]. In contrast, approximately 40–50% of ACs metastasize to the regional lymph nodes at presentation, with the 5-year overall survival rates ranging from 25% to 78% for patients with ACs [2,5–9].

Conventional carcinoid tumors are composed of homogeneous cellular proliferation with an organoid and trabecular structure. Tumor cells are composed of small- to medium-sized, round to polygonal cells with a scant to moderate amount of eosinophilic cytoplasm and centrally located round to oval nuclei with fine granular chromatin. Histologic atypia, such as nuclear atypia, prominent nucleoli, and pleomorphism, is more common in AC than TC, but these features are sometimes observed in TC [6,7,10]. Therefore, the unfavorable clinical outcomes and atypical histologic features associated with these lung carcinoid tumors are unreliable for distinguishing TCs from ACs.

* Corresponding author at: Department of Pathology, Unit 85, The University of Texas M. D. Anderson Cancer Center, 1515 Holcombe Boulevard, Houston, TX 77030, USA. Tel.: +1 713 792 8134; fax: +1 713 745 3740.

E-mail address: CesarMoran@mdanderson.org (C.A. Moran).

Arrigoni et al. [11] first defined ACs as carcinoid tumors with (1) 1 mitosis/1–2 high-power fields (HPFs) or 5–10 mitoses/10 HPF; (2) necrosis; (3) pleomorphism, hyperchromasia, or an abnormal nuclear/cytoplasmic ratio; and (4) areas of increased cellularity with disorganization. In 1998, Travis et al. [6] proposed that LCNECs be classified in a separate category from ACs, as this poorly differentiated high-grade carcinoma was characterized by a neuroendocrine appearance under light microscopy. These criteria have been applied to the latest World Health Organization classification [10]. With the establishment of diagnostic criteria for LCNEC, the definition of AC was then restricted to tumors with a mitotic rate of 2–10 mitoses per 2 mm² (10 HPF) or the presence of necrosis.

Differentiating ACs from TCs or LCNECs is clinically important because the treatment modalities and prognoses for these types of tumors are different. However, the distinction between ACs and TCs is currently based only on the histologic evaluation of mitotic count and necrosis. In this study, we sought to retrospectively evaluate the various histologic features of ACs and TCs and relate these to their outcomes (i.e., tumor recurrence, patient death, or lymph node metastasis). Furthermore, we revised the relevance of the patterns of necrosis and mitotic counting methods.

2. Materials and methods

2.1. Case selection

We retrospectively reviewed the tumor specimens from patients who were surgically resected and diagnosed with TC or AC between 1990 and 2005. We obtained the tumor specimens from cases deposited in the files of the University of Texas M. D. Anderson Cancer Center (Houston, TX, USA) Lung SPORE Tissue Bank, which was approved by the institutional review board. We reviewed the pathologic records of the specimens and all available hematoxylin and eosin (HE)-stained slides, some special stains, and the immunohistochemical and/or ultrastructural analyses available. We collected the patients' clinical information, including age, gender, smoking history, presenting symptoms, treatment modalities, site of any tumor recurrence, duration of recurrence or survival, tumor location (which lobe and whether central or not), maximum tumor size (in cm), and pathologic disease stage (p-stage).

2.2. Histologic examination

All available HE-stained slides for each case were examined by two pathologists (K.T. and C.A.M.); each pathologist was blinded to the clinical details of each patient. We evaluated the pathologic features of tumor invasiveness, including the infiltrative growth of the adjacent normal architecture, presence of pleural invasion, and presence of blood or lymphatic vessel invasion. The stroma between the tumor nests was mainly composed of capillary or fibrous tissue. We also observed active fibroblastic proliferation [12]. We then evaluated the histologic features of the tumor cells, including the chromatin pattern (i.e., fine granular or coarse) and the presence or absence of nucleolus and nuclear pleomorphism (i.e., whether there was more than a 3-fold variation in nuclear size that did not include the presence of giant cells).

We then evaluated the necrotic pattern, such as the presence or absence of comedo-like necrosis (necrosis present within the center of tumor nest) and coagulative necrosis (necrosis involving one or more whole tumor nests and/or forming bridging necrosis) (Fig. 1A). We also evaluated the histologic features suggesting tumor damage, such as pyknotic cells (i.e., foci of dyscohesive cells) with somewhat pyknotic nuclei and condensed, shrunken-appearing cytoplasm without karyorrhexis, eosinophilic debris, or apoptosis (Fig. 1B), cholesterol cleft, stromal hemorrhage, and psammoma bodies.

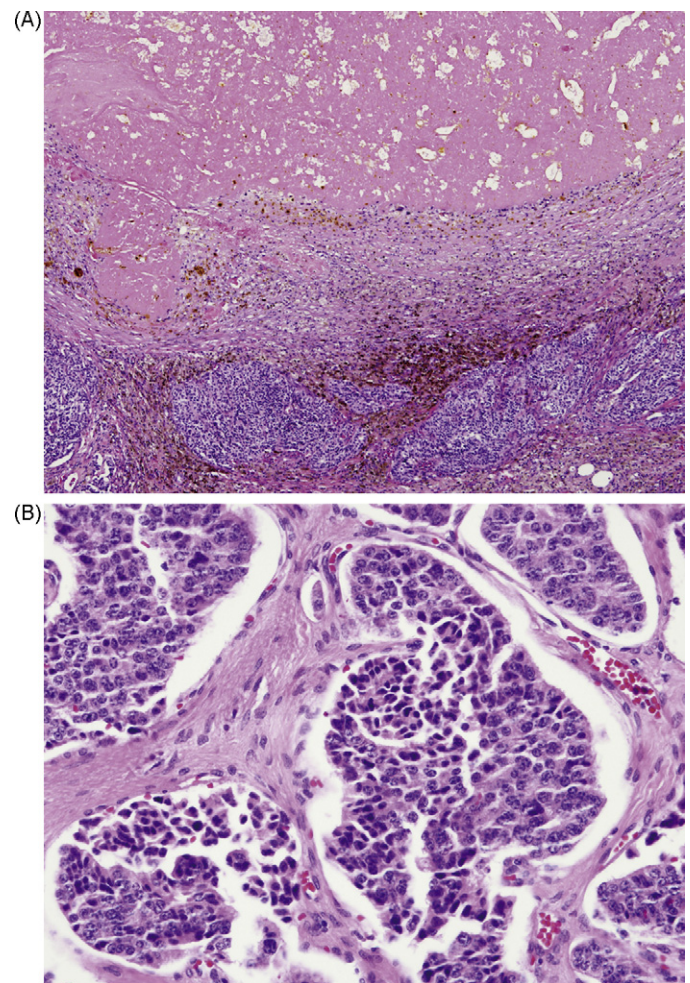


Fig. 1. (A) Massive coagulative necrosis surrounded by thick fibrous tissue with a hemosiderin deposition. The outermost portion of the necrosis consisted of tumor cells. (B) Foci of dyscohesive cells with somewhat pyknotic nuclei and condensed, shrunken-appearing cytoplasm without karyorrhexis, eosinophilic debris, or apoptosis observed in tumor nests.

or apoptosis (Fig. 1B), cholesterol cleft, stromal hemorrhage, and psammoma bodies.

2.3. The mitotic counting method

After all slides were reviewed on an Olympus CX31 microscope (Olympus; Tokyo, Japan), the mitoses were counted on one representative slide. This microscope's standard field of view number is 20 (0.2 mm²); therefore, an HPF magnification of 400× equals to 0.2 mm². To determine the most suitable mitotic counting method, we studied three methods: (1) the number of mitoses in a randomly selected 10-HPF area counted; (2) the number of mitoses in the most mitotically active 10-HPF areas (so called hot spots) counted; or (3) the mean number of mitoses in the whole section calculated (the number of mitoses divided by the number of HPFs in the whole section). To avoid overcounting the number of mitoses at the telophase, two adjoining mitotic figures were counted as one mitosis.

2.4. Statistical analysis

We performed all statistical analyses using SPSS version 12.0 software for Windows (SPSS; Chicago, IL). We used the Wilcoxon rank-sum test to analyze the continuous variables and Fisher's

exact test to analyze lymph node metastasis. We calculated the recurrence-free survival (RFS) curves using the Kaplan–Meier method, and we compared the curves using the log-rank test. We considered a P -value of ≤ 0.05 to be significant in two tailed analysis.

3. Results

3.1. Clinical features

We reviewed the tumor specimens from 88 patients with an original diagnosis of lung carcinoid tumors. We excluded 5 patients who received therapy preoperatively (4 who received neoadjuvant chemotherapy and 1 who received YAG laser ablation). Furthermore, we excluded 3 patients who had high mitotic activity and massive necrosis; their diagnosis was then changed to LCNEC based on the latest World Health Organization criteria [10]. Therefore, our final cohort consisted of 80 patients with lung carcinoid tumors, including 68 patients with TCs and 12 with ACs. The patients' mean age (at the time of diagnosis) was 54.3 years (range, 19–80 years). The presenting symptoms were documented in 27 out of 77 patients. Smoking history was documented in 76 cases; 32 patients were never smokers, 32 were former smokers, and 12 were present smokers. The tumor was located in the right-upper lobe in 11 patients, the middle lobe in 10, the right-lower lobe in 26, the left-upper lobe in 13, and the left-lower lobe in 19, and 1 patient had a hilar lesion. The tumor was located in the central portion of the lung in 49 patients or in the intermediate or peripheral portion in 31 patients. A preoperative biopsy and/or cytologic diagnostic procedure were carried out in 69 patients, including the diagnoses were not tumorous lesions.

The tumor sizes ranged from 1.0 to 13.0 cm (mean, 2.96 cm). Lymph node status was recorded in 79 patients, and metastasis was observed in 17. Sixty-one cases had p-stage I disease, 6 had p-stage II disease, 11 had p-stage III disease, 1 had p-stage IV disease, and 1 case was unstaged.

Tumor recurrence was observed in 6 of 80 patients (2 cases of liver recurrence and 1 case each of kidney, brain, chest wall, and subclavicular lymph node recurrence). The mean follow-up time for all 80 patients was 68 months (range, 1–197 months), with 74 still alive at the time of this report. Only 1 patient died of a tumor progression, and 5 died of other causes.

3.2. Histologic factors

We reviewed an average of 4.7 (range, 1–16) HE-stained slides for each case. Infiltrative growth was observed in 47 cases. Blood-vessel, lymph-vessel, and pleural invasion were observed in 34 cases, 29 cases, and 1 case, respectively. Capillary rich stroma was observed in 57 cases, and fibrous rich stroma was observed in 23 cases. Active fibroblastic proliferation was observed in 38 cases (Fig. 2A). We found a fine chromatin pattern in 47 cases and a coarse chromatin pattern in 33 cases. We also observed a conspicuous nucleolus in 15 cases and nuclear pleomorphism in 13 cases. We found other unusual histologic features of the tumors, such as bone formation in 16 cases and granulomatous inflammation in 2 cases.

We found comedo-like necrosis in 5 cases and coagulative necrosis in 10 cases (Fig. 2B), and we found both comedo-like and coagulative necrosis in 2 cases. All but 1 patient with coagulative necrosis had undergone preoperative biopsy. Pyknotic cells, cholesterol cleft, hemorrhage, and psammoma bodies were observed in 54 cases, 4 cases, 29 cases, and 13 cases, respectively.

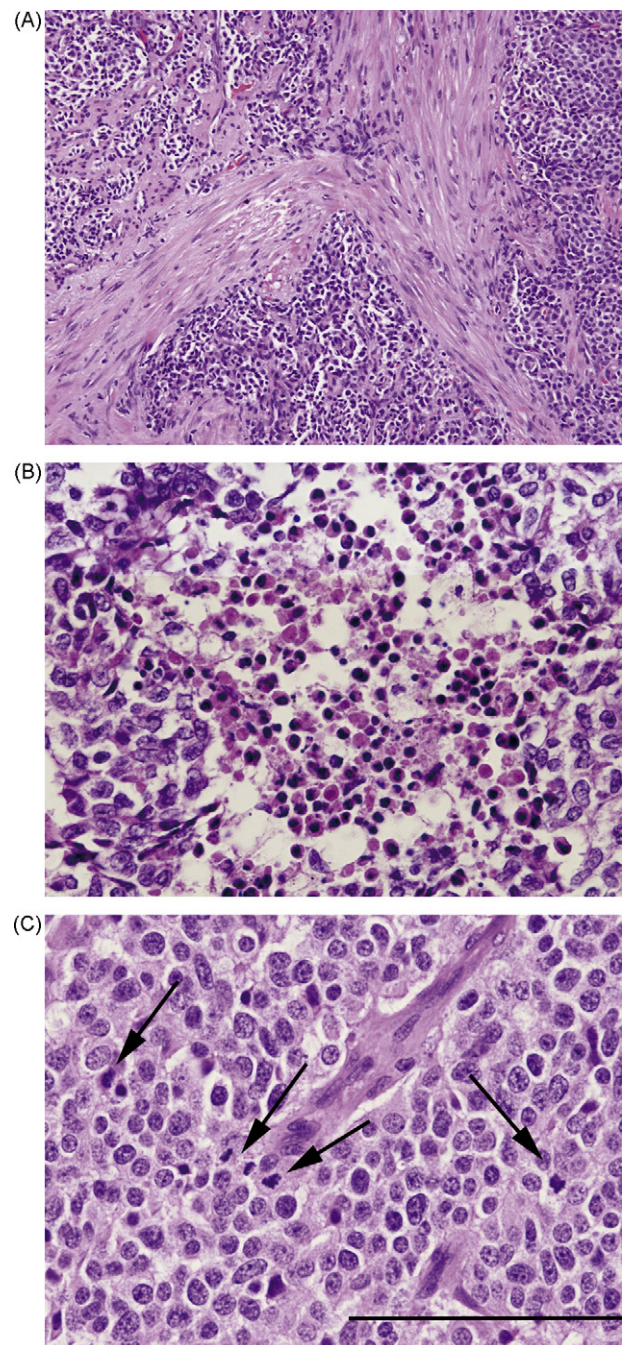


Fig. 2. (A) Bundles of spindle-shaped fibroblasts are shown between tumor nests (magnification, $10\times$). (B) The tumor had a large solid nest with comedo-like necrosis (magnification, $20\times$). (C) Although this case showed 5 mitoses in 1 high-power field (HPF), this photomicrograph area is smaller than 1 HPF (0.2 mm^2) and corresponded to a 0.134 mm^2 area. Because this image was captured using the Olympus DP-70 system (Tokyo, Japan), this photomicrograph showed 4 mitotic figures, indicated by the arrows (2 in prophase, 1 in metaphase, and 1 in telophase). This case's mitotic count in the most mitotically active area was 15 mitoses/10 HPF, but the average mitosis was 0.18 mitoses/HPF. This patient was alive at 45 months with no evidence of tumor recurrence (bar = $200\text{ }\mu\text{m}$).

3.3. Mitotic count

We reviewed a mean of 341.6 HPF (range, 44–762 HPF) per case. The number of mitoses ranged from 0 to 115, with a mean of 10.9 per case. The number of mitoses in 1 HPF exceeded 2 in 26 cases, and the highest recorded mitotic count in 1 HPF was 5 (Fig. 2C). The mean number of mitoses in the randomly selected 10-HPF

areas was 0.45 mitoses/10 HPF (range, 0–6 mitoses/10 HPF), and the mean number of mitoses in the most mitotically active 10-HPF areas was 5.73 mitoses/10 HPF (range, 0–25 mitoses/10 HPF). The overall mean number of mitoses was 0.04 mitoses/1 HPF (range, 0–0.32 mitoses/1 HPF).

Both the presence of comedo-like necrosis and an overall mean number of mitoses of ≥ 0.2 mitoses/1 HPF were observed in 3 cases. These cases corresponded to 60% of cases bearing comedo-like necrosis and 60% of cases having an overall mean number of mitoses ≥ 0.2 mitoses/1 HPF.

3.4. Clinicopathologic features based on unfavorable outcomes

We next evaluated whether there was an association between the patients' clinicopathologic factors and tumor recurrence, patient death, and/or lymph node metastasis (Table 1). An older age ($P=0.002$), p-stage III or IV disease ($P=0.0029$), pleural invasion ($P<0.0001$), and the presence of active fibroblasts ($P=0.0184$) were significantly associated with tumor recurrence or patient death. All patients with tumor specimens that exhibited an active fibroblastic proliferation had undergone a preoperative biopsy and/or cytologic diagnostic procedure. Blood-vessel invasion ($P=0.0417$), lymph-vessel invasion ($P=0.0017$), coarse chromatin pattern ($P=0.0304$), conspicuous nucleolus ($P=0.0085$), and nuclear pleomorphism ($P=0.0019$) were significantly associated with lymph node metastasis.

3.5. Evaluation of necrotic patterns based on the patients' unfavorable outcomes and RFS

We then sought to determine if there was a correlation between the tumor specimens' necrotic patterns and histologic features suggesting tumor damage and the patients' unfavorable outcomes (Table 2). Only the presence of comedo-like necrosis was significantly associated with tumor recurrence or patient death ($P<0.0001$).

3.6. Evaluation of mitotic count based on the patients' unfavorable outcomes, RFS, and OS

We investigated whether there was a correlation between the results of three mitotic counting methods and the patients' unfavorable outcomes and RFS (Table 3). For specimens in which the number of mitoses in a randomly selected 10-HPF area was counted, the presence of 2–10 mitoses/10 HPF appeared to be significantly associated with tumor recurrence or patient death ($P=0.003$). In addition, the 5-year RFS rates for the specimens with 0–1 mitoses/10 HPF and 2–10 mitoses/10 HPF were 94.2% and 58.3%, respectively (Fig. 3A). However, when we individualized each case and correlated the number of mitotic figures with the 5-year RFS rates, we obtained the following information: 0 mitoses = 95.1%; 1 mitotic figure = 87.5%; 2 mitotic figures = 75.0%; 3 mitotic figures = 100%. Based on these data, we analyzed changing the cut off number of mitosis from 0–3 to 4–10. The 5-year RFS rates for the specimens with 0–3 mitoses/10 HPF and 4–10 mitoses/10 HPF were 93.1% and 0%, respectively ($P=0.002$).

For specimens in which the number of mitoses in the most mitotically active 10-HPF area was counted, this method showed tendency with tumor recurrence or patient death ($P=0.0575$). The 5-year RFS rates for specimens with 0–1 mitoses/10 HPF, 2–10 mitoses/10 HPF, and more than 11 mitoses/10 HPF were 95.5%, 94.6%, and 75.2%, respectively ($P=0.0575$; Fig. 3B). Once again, when we individualized each case and correlated the number of mitotic figures with the 5-year RFS rates, we obtained the following information: 0 mitoses = 100%; 1 mitotic figure = 90.0%; 2 mitotic figures = 100%; and 3 mitotic figures = 100%. Based on these

data, we analyzed changing the cut off number of mitosis from 0–3 to 4 or more. The 5-year RFS rates for the specimens with 0–3 mitoses/10 HPF and 4 or more mitoses/10 HPF were 97.4% and 83.4%, respectively ($P=0.024$).

For specimens in which the overall mean number of mitoses was calculated, the value of ≥ 0.2 mitoses per 1 HPF was significantly associated with tumor recurrence or patient death ($P<0.0001$). The 5-year RFS rates for specimens with an overall mean mitosis <0.2 and a mean mitosis ≥ 0.2 were 95.9% and 0%, respectively (Fig. 3C). Multivariate analysis was not performed because of the small number of events (recurrence and death) in our patient population. Based on the 5-year RFS rates, we considered that the overall mean mitotic counting method was the most useful. Furthermore, we also found that the criteria on the number of mitosis should be selected based on the counting methods (0–3 and 4–10 in randomly selected areas and 0–3 and ≥ 4 in the most mitotically active areas).

Although there were few deaths, we analyzed 5-year OS rates. For specimens in which the number of mitoses was counted in a randomly selected 10-HPF area, the 5-year OS rates with 0–1 mitoses/10 HPF and 2–10 mitoses/10 HPF were 100% and 96.6%, respectively ($P=0.0033$; Fig. 3D). For specimens in which the number of mitoses in the most mitotically active 10-HPF area was counted, the 5-year OS rates for specimens with 0–1 mitoses/10 HPF, 2–10 mitoses/10 HPF, and >11 mitoses/10 HPF were 100%, 95.5%, and 82.1%, respectively ($P=0.1471$; Fig. 3E). For specimens in which the overall mean number of mitoses was calculated, the 5-year OS rates for specimens with an overall mean mitosis <0.2 and a mean mitosis ≥ 0.2 were 98.7% and 0%, respectively ($P<0.0001$; Fig. 3F).

3.7. New recommended definition for AC

Based on these results, we recommend that the definition for AC include comedo-like necrosis and/or an overall mean number of mitosis of ≥ 0.2 . Based on this definition, we observed AC in 7 cases rather than the 12 cases specified in the records. The 5-year RFS rates for patients with TC and AC by this new definition were 97.2% and 0%, respectively ($P<0.0001$; Fig. 4). We observed lymph node metastasis in 14 patients with TC and 3 patients with AC; however, there was no significant difference between these two rates ($P=0.166$).

4. Discussion

Our results favor a new histological definition for AC. In this study, we found that the overall mean number of mitoses was superior to calculate the number of mitoses in a randomly selected 10-HPF area or in the most mitotically active 10-HPF area. Furthermore, the presence of comedo-like necrosis was significantly associated with tumor recurrence and patient death when compared to the presence of coagulative necrosis.

A high mitotic count is generally reported as an unfavorable factor in patients with tumors. In general, selecting the most mitotically active 10-HPF area is the preferred method for calculating mitotic counts [13–15]. Most of the articles on pulmonary neuroendocrine tumors, including the first publication on the definition of LCNEC, counted the mitoses in the most mitotically active areas [7,16,17]. Our results indicated that the mitotic counts in both ACs and TCs were distributed heterogeneously. Surprisingly, 21 of 26 cases with a mitotic count exceeding 2 mitoses in only 1 HPF showed no tumor recurrence or patient death. When compared with a randomly selected 10-HPF area or the most mitotically active 10-HPF area, ≥ 2 mitoses in only 1 HPF had the least selection bias to go beyond the diagnostic criteria for TC. Furthermore, when we selected the most mitotically active areas, 20 cases went

Table 1
Correlation between clinicopathological factors and unfavorable outcomes.

	Recurrence/death		P-value ^a	Lymph node metastasis		P-value ^b
	(–)	(+)		(–)	(+)	
Original diagnosis						
Typical	63	5	<0.0001	55	12	0.1192
Atypical	7	5		7	5	
Age (years)	52.5	67.1	0.002	54.1	54.4	1.00
Gender						
Female	45	4	0.1944	38	10	0.8536
Male	25	6		24	7	
Symptom						
None	43	7	0.8271	38	11	0.5524
Present	24	3		23	4	
Smoking						
Never	31	1	0.0767	27	4	0.5267
Former	25	7		24	8	
Present	10	2		10	2	
Location						
Central	44	5	0.3645	38	11	0.7971
Non-central	26	5		24	6	
Tumor size (cm)	2.92	3.23	0.936	3.05	2.69	0.9952
Lymph node metastasis						
Absent	55	7	0.4563	–	–	–
Present	14	3		–	–	
Pathologic stage						
I and II	61	6	0.0029	–	–	–
III and IV	8	4		–	–	
Infiltrative growth						
Absent	29	4	0.4805	27	5	0.4051
Present	41	6		35	12	
Blood-vessel invasion						
Absent	46	3	0.088	39	6	0.0417
Present	27	7		23	11	
Lymph-vessel invasion						
Absent	46	5	0.2246	45	5	0.0017
Present	24	5		17	12	
Pleural invasion						
Absent	70	9	<0.0001	61	17	1.00
Present	0	1		1	0	
Stroma						
Capillary rich	52	5	0.1467	43	13	0.7649
Fibrous rich	18	5		19	4	
Active fibroblastic proliferation						
Absent	40	2	0.0184	34	7	0.3179
Present	30	8		28	10	
Chromatin pattern						
Fine	40	7	0.5614	40	6	0.0304
Coarse	30	3		22	11	
Nucleolus						
Inconspicuous	57	8	0.7714	54	10	0.0085
Conspicuous	13	2		8	7	
Nuclear pleomorphism						
Absent	59	8	0.5684	56	10	0.0019
Present	11	2		6	7	

^a Log-rank test.

^b Fisher's exact test.

beyond the diagnostic criteria for AC. These results indicated that the latest WHO criteria for diagnosing ACs is strict only evaluating in 10 HPFs.

We also attempted to determine if there was a pattern to the distribution of mitoses (such as within the tumor's center or in the periphery); however, we did not see a uniform tendency (unpublished results). Travis et al. counted the number of mitoses in

pulmonary neuroendocrine tumors in three sets of 10 HPF and calculated the mean [6,16]. Their results indicated that one set of 10 HPFs is not enough to evaluate the mitotic activity because of the mitotic heterogeneity in carcinoid tumors. Tiny material, such as biopsy specimens may not be suitable for a final diagnosis of TC or AC, because there may not be enough HPFs. The results of our study are based on surgically resected materials,

Table 2

Correlation between necrosis and unfavorable outcomes.

	Recurrence/death		<i>P</i> -value ^a	Lymph node metastasis		<i>P</i> -value ^b
	(–)	(+)		(–)	(+)	
Comedo-like necrosis						
Absent	69	6	<0.0001	60	14	0.0639
Present	1	4		2	3	
Coagulative necrosis						
Absent	62	8	0.3143	55	14	0.4414
Present	8	2		7	3	
Pyknotic change						
Absent	25	1	0.0954	22	3	0.2405
Present	45	9		40	14	
Cholesterol cleft						
Absent	67	9	0.4762	59	16	1.00
Present	3	1		3	1	
Hemorrhage						
Absent	47	4	0.102	41	9	0.3176
Present	23	6		21	8	
Psammomatous body						
Absent	61	6	0.0559	53	13	0.4611
Present	9	4		9	4	

^a Log-rank test.^b Fisher's exact test.

and it is unclear whether calculating the overall mean number of mitoses would be applicable for materials acquired from a biopsy.

The presence of necrosis is another criterion for differentiating TC from AC. In the current study, we analyzed the necrosis separating comedo-like and coagulative necrosis. We found that comedo-like necrosis was significantly associated with tumor recurrence and patient death when compared to coagulative necrosis. In fact, we did not see tumor recurrence or patient death in the cases with only coagulative necrosis. This may be because coagulative necrosis is not related to the tumor's malignant behavior but rather it may be related to preoperative biopsy or erosion. Travis et al. also pointed out that the large zone of infarct-like necrosis (corresponding to current coagulative necrosis) was not seen in ACs but was seen in high-grade neuroendocrine carcinomas [16].

It has been reported that hemorrhage, psammoma bodies, and/or cholesterol cleft form after the degeneration and disappear-

ance of tumor cells [18–20]. However, we found that these factors were not associated with the patients' clinical outcomes in our study. We observed pyknotic cells, which can sometimes be confused with incipient necrosis, in 69% of patients with both ACs and TCs. Similar to previous reports, our results demonstrated that the presence of pyknotic cells was not associated with the patients' clinical outcomes [7,8].

The presence of an active fibroblastic proliferation is one of the known unfavorable clinical outcomes in patients with pulmonary adenocarcinomas [12]. In our study, we observed active fibroblastic proliferation in 48% of the cases, which was significantly associated with tumor recurrence or patient death ($P=0.0184$). All patients who had tumor specimens with active fibroblastic proliferation had undergone a preoperative biopsy and/or cytologic diagnostic procedure. However, these results did not exclude the possibility of the active fibroblastic proliferation induced by preoperative diagnostic procedures. Therefore, it will be necessary to study a larger number of patients who have not undergone

Table 3

Correlation between three mitotic count methods and unfavorable outcomes.

	Recurrence/death		<i>P</i> -value ^a	Lymph node metastasis		<i>P</i> -value ^b
	(–)	(+)		(–)	(+)	
Randomly selected 10 HPF						
<2	65	6	0.003	56	14	0.3957
≥2	5	4		6	3	
<2	69	8	0.002	60	16	0.522
≥2	1	2		2	1	
Highest 10 area						
<2	21	1	0.0575	21	1	0.0641
2–10	35	4		28	11	
>11	14	5	0.0238	13	5	0.180
0–3	37	2		28	11	
≥4	33	8		34	6	
Mean mitosis						
<0.2	69	6	<0.0001	60	14	0.0639
≥0.2	1	4		2	3	

^a Log-rank test.^b Fisher's exact test.

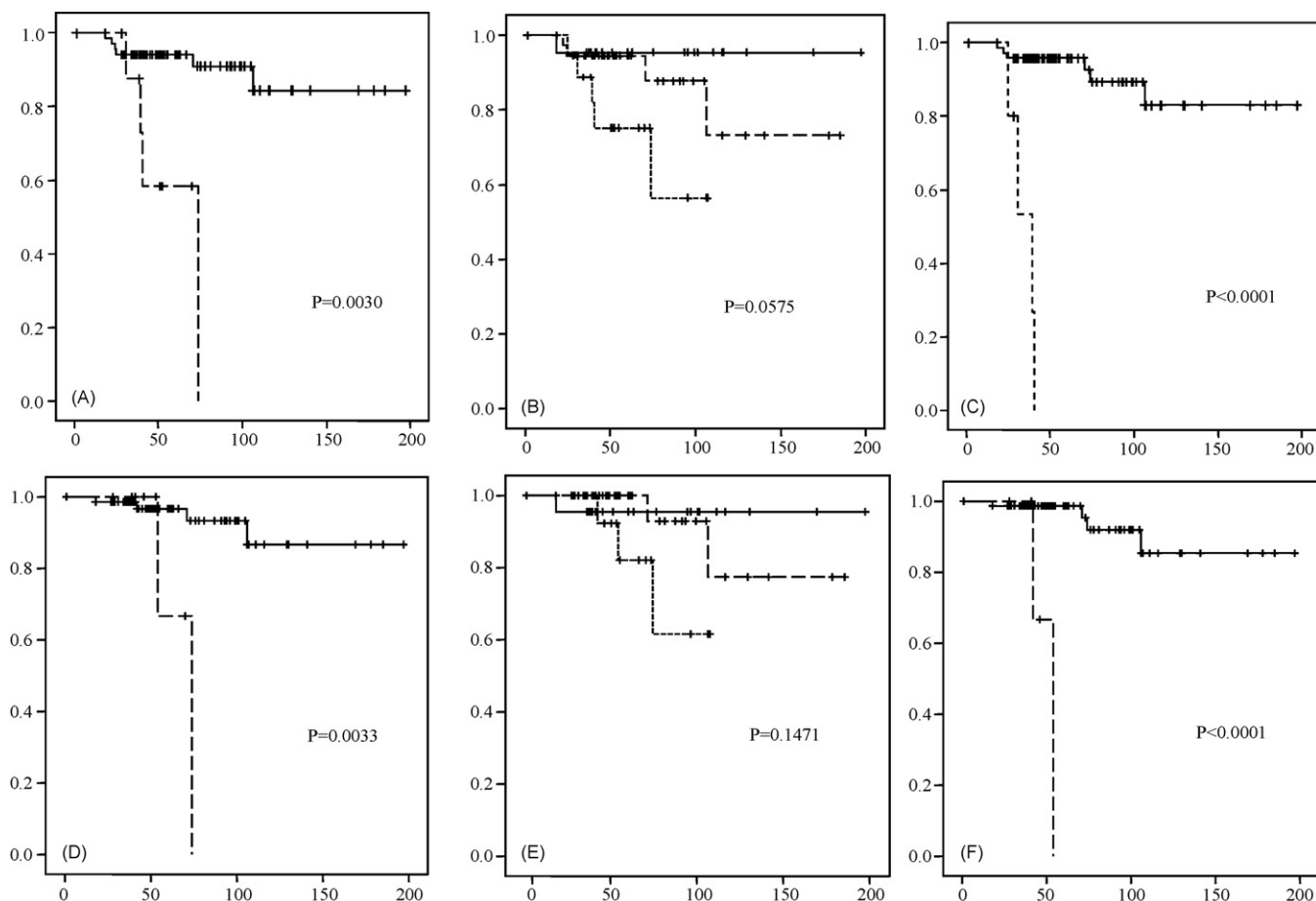


Fig. 3. The recurrence-free survival (RFS) rates for patients with ACs. (A) For cases where the number of mitoses was calculated in randomly selected 10-high-power field (HPF) areas, the 5-year RFS rates for cases with 0–1 mitoses/10 HPF (solid line) and 2–10 mitoses/10 HPF (dashed line) were 94.2% and 58.3%, respectively. (B) For cases where the number of mitoses was calculated in the most mitotically active 10-HPF area, the 5-year RFS rates for cases with 0–1 mitoses/10 HPF (solid line), 2–10 mitoses/10 HPF (dashed line), and ≥ 11 mitoses/10 HPF (square-dot line) were 95.5%, 94.6% and 75.2%, respectively. (C) For cases where the average mitotic count was calculated, the 5-year RFS rates for cases with <0.2 mitoses/10 HPF (solid line) and ≥ 0.2 mitoses/10 HPF (dashed line) were 95.9% and 0%, respectively. (D) specimens with randomly selected 10-HPF are, the 5-year OS rates with 0–1 mitoses/10 HPF and 2–10 mitoses/10 HPF were 100% and 96% respectively. (E) Specimens with more mitotically active 10 HPF area, 5-year OS rates with 0–1 mitoses/10 HPF, 2–10 mitoses/10 HPF, and >11 mitoses/10 HPF were 100%, 95%, and 82% respectively. (F) Specimens with overall mean of mitoses, the 5-year OS rates with mean <0.2 and a mean mitosis >0.2 were 98.7% and 0% respectively.

preoperative diagnostic procedures to determine the significance of active fibroblastic proliferation in patients with carcinoid tumors.

Although our cohort was not large enough to analyze each pathologic disease stage, patients with p-stage III or IV disease were more likely to experience a tumor recurrence or death than patients with p-stage I or II disease ($P=0.00294$). Adapting the TNM classification scheme for patients with lung carcinoid tumors is an important factor for predicting survival [21]. However, one of the important factors of TNM classification – lymph node metastasis – was not correlated with tumor recurrence or patient death in our study. Currently, there are conflicting reports about the effect of lymph node metastasis for survival in patients with carcinoid tumors. Some studies have found that in patients with TC, lymph node metastasis did not affect survival [8,22]. However, if some histologic factors can predict the risk of lymph node metastasis, they may be useful for determining the extent of the regional lymph node dissection for surgeons. In our study, the presence of blood-vessel invasion, lymph-vessel invasion, coarse chromatin pattern, nucleolus prominence, and nuclear pleomorphism were correlated with lymph node metastasis, but mitotic activity and/or the presence of necrosis were not. Based on these factors, the presence of a coarse chromatin pattern,

nucleolus prominence, and nuclear pleomorphism can be diagnostic features for lymph node metastasis in preoperative biopsy materials.

We found that counting the overall mean number of mitoses was superior to the other methods for determining the specimens' mitotic counts. However, counting the number of mitoses in all fields in each case at a high magnification may be unsuitable for daily practice because of the substantial time involved. Therefore, based on our results, we made a flow chart (Fig. 5) to aid in the diagnosis of low- and intermediate-grade neuroendocrine carcinomas.

In short, we concluded that the mitotic figures of carcinoid tumors have a heterogeneous distribution. To reduce the selection biases of fields and observer variation, we recommended calculating the overall mean number of mitoses. We also pointed out the potential for overdiagnosing carcinoid tumors using the method for counting mitoses in the most mitotically active 10-HPF. Furthermore, we concluded that comedo-like necrosis was a more important pattern to look for than coagulative necrosis for predicting tumor recurrence or patient death. The combination of calculating the mean number of mitoses and the presence of comedo-like necrosis should be added to the current criteria for diagnosing ACs.

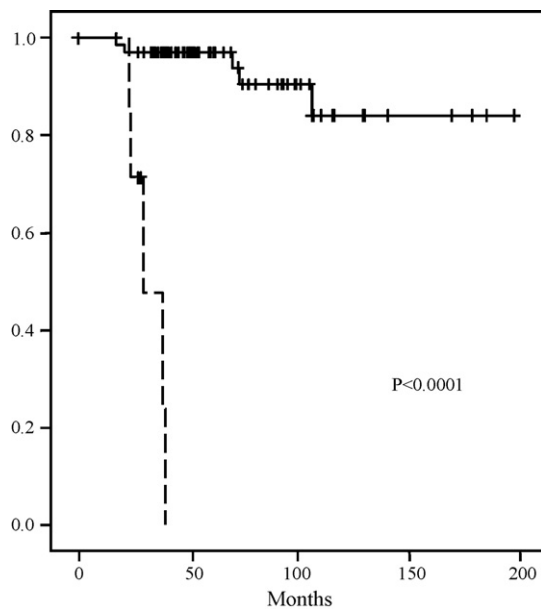


Fig. 4. Based on our recommended criteria for atypical carcinoids, the 5-year disease-free survival rates for patients with typical carcinoids (solid line) and atypical carcinoids (comedo-like necrosis and/or an average mitosis ≥ 0.2 mitoses/10 HPF; dashed line) were 97.2% and 0%, respectively.

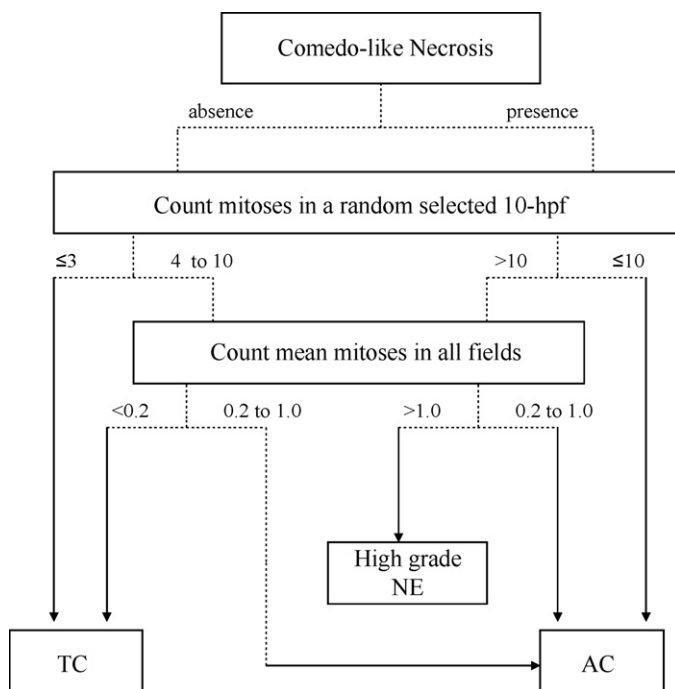


Fig. 5. A dichotomous tree for diagnosing neuroendocrine tumors of the lung, according to our results. Abbreviations: TC, typical carcinoid; AC, atypical carcinoid; NE, neuroendocrine tumor; HPF, high-power field.

Conflict of interest statement

There is no conflict of interest with regard to this manuscript.

Acknowledgements

We would like to thank Susan Cweren for her skillful technical assistance and Alyson Todd for her skillful English editing.

This work was supported in part by the grant from the US Department of Defense PROSPECT W81XWH-07-1-0306.

References

- [1] Fink G, Krelbaum T, Yellin A, Bendayan D, Saute M, Glazer M, et al. Pulmonary carcinoid: presentation, diagnosis, and outcome in 142 cases in Israel and review of 640 cases from the literature. *Chest* 2001;119:1647–51.
- [2] Hage R, de la Riviere AB, Seldenrijk CA, van den Bosch JM. Update in pulmonary carcinoid tumors: a review article. *Ann Surg Oncol* 2003;10:697–704.
- [3] Granberg D, Wilander E, Oberg K, Skogseid B. Prognostic markers in patients with typical bronchial carcinoid tumors. *J Clin Endocrinol Metab* 2000;85:3425–30.
- [4] Cooper WA, Thourani VH, Gal AA, Lee RB, Mansour KA, Miller JL. The surgical spectrum of pulmonary neuroendocrine neoplasms. *Chest* 2001;119:14–8.
- [5] Garcia-Yuste M, Matilla JM, Cueto A, Paniagua JM, Ramos G, Cañizares MA. Typical and atypical carcinoid tumours: analysis of the experience of the Spanish Multi-centric Study of Neuroendocrine Tumours of the Lung. *Eur J Cardiothorac Surg* 2007;31:192–7.
- [6] Travis WD, Rush W, Flieder DB, Falk R, Fleming MV, Gal AA. Survival analysis of 200 pulmonary neuroendocrine tumors with clarification of criteria for atypical carcinoid and its separation from typical carcinoid. *Am J Surg Pathol* 1998;22:934–44.
- [7] Beasley MB, Thunnissen FB, Brambilla E, Hasleton P, Steele R, Hammar SP, et al. Pulmonary atypical carcinoid: predictors of survival in 106 cases. *Hum Pathol* 2000;31:1255–65.
- [8] Thomas Jr CF, Tazelaar HD, Jett JR. Typical and atypical pulmonary carcinoids: outcome in patients presenting with regional lymph node involvement. *Chest* 2001;119:1143–50.
- [9] Asamura H, Kameya T, Matsuno Y, Noguchi M, Tada H, Ishikawa Y, et al. Neuroendocrine neoplasms of the lung: a prognostic spectrum. *J Clin Oncol* 2006;24:70–6.
- [10] Beasley MB, Thunnissen FB, Hasleton PhS, Barbareschi M, Pugatch B. Carcinoid tumour. In: Travis WD, Brambilla E, Muller-Hermelink HK, Harris CC, editors. *Pathology and genetics: tumors of the lung, pleura, thymus and heart*. Lyon, France: IARC; 2004. p. 59–62.
- [11] Arrigoni MG, Woolner LB, Bernatz PE. Atypical carcinoid tumors of the lung. *J Thorac Cardiovasc Surg* 1972;64:413–21.
- [12] Noguchi M, Morikawa A, Kawasaki M, Matsuno Y, Yamada T, Hirohashi S, et al. Small adenocarcinoma of the lung. Histologic characteristics and prognosis. *Cancer* 1995;75:2844–52.
- [13] Kempson RL. Mitosis counting-II (editorial). *Hum Pathol* 1976;7:482–3.
- [14] Baak JPA. Mitosis counting in tumors. *Hum Pathol* 1990;21:683–5.
- [15] van Diest PJ, Baak JP, Matze-Cok P, Wisse-Brekelmans EC, van Galen CM, Kurver PH, et al. Reproducibility of mitosis counting in 2,469 breast cancer specimens: results from the Multicenter Morphometric Mammary Carcinoma Project. *Hum Pathol* 1992;23:603–7.
- [16] Travis WD, Linnoila RI, Tsokos MG, Hitchcock CL, Cutler Jr GB, Nieman L, et al. Neuroendocrine tumors of the lung with proposed criteria for large-cell neuroendocrine carcinoma: an ultrastructural, immunohistochemical, and flow cytometric study of 35 cases. *Am J Surg Pathol* 1991;15:529–53.
- [17] Rugge M, Fassan M, Clemente R, Rizzardi G, Giacomelli L, Pennelli G, et al. Bronchopulmonary carcinoid: phenotype and long-term outcome in a single-institution series of Italian patients. *Clin Cancer Res* 2008;14:149–54.
- [18] Shimosato Y, Suzuki A, Hashimoto T, Nishiwaki Y, Kodama T, Yoneyama T, et al. Prognostic implications of fibrotic focus (scar) in small peripheral lung cancers. *Am J Surg Pathol* 1980;4:365–73.
- [19] McCluggage WG, Lyness RW, Atkinson RJ, Dobbs SP, Harley I, McClelland HR, et al. Morphological effects of chemotherapy on ovarian carcinoma. *J Clin Pathol* 2002;55:27–31.
- [20] Liu-Jarin X, Stoopler MB, Raftopoulos H, Ginsburg M, Gorenstein L, Borczuk AC. Histologic assessment of non-small cell lung carcinoma after neoadjuvant therapy. *Mod Pathol* 2003;160:1102–8.
- [21] Travis WD, Giroux DJ, Chansky K, Crowley J, Asamura H, Brambilla E, et al. The IASLC Lung Cancer Staging Project: proposals for the inclusion of bronchopulmonary carcinoid tumors in the forthcoming (seventh) edition of the TNM Classification for Lung Cancer. *J Thorac Oncol* 2008;3:1213–23.
- [22] Schreurs AJ, Westermann CJ, van den Bosch JM, Vanderschueren RG, Brutel de la Riviere A, Knaepen PJ. A twenty-five-year follow-up of ninety-three resected typical carcinoid tumors of the lung. *Thorac Cardiovasc Surg* 1992;104:1470–5.

Clinical Cancer Research



Robust Gene Expression Signature from Formalin-Fixed Paraffin-Embedded Samples Predicts Prognosis of Non – Small-Cell Lung Cancer Patients

Yang Xie, Guanghua Xiao, Kevin R. Coombes, et al.

Clin Cancer Res 2011;17:5705-5714. Published OnlineFirst July 8, 2011.

Updated Version

Access the most recent version of this article at:
doi:[10.1158/1078-0432.CCR-11-0196](https://doi.org/10.1158/1078-0432.CCR-11-0196)

Supplementary Material

Access the most recent supplemental material at:
<http://clincancerres.aacrjournals.org/content/suppl/2011/08/23/1078-0432.CCR-11-0196.DC1.html>

Cited Articles

This article cites 41 articles, 14 of which you can access for free at:
<http://clincancerres.aacrjournals.org/content/17/17/5705.full.html#ref-list-1>

Citing Articles

This article has been cited by 4 HighWire-hosted articles. Access the articles at:
<http://clincancerres.aacrjournals.org/content/17/17/5705.full.html#related-urls>

E-mail alerts

[Sign up to receive free email-alerts](#) related to this article or journal.

Reprints and Subscriptions

To order reprints of this article or to subscribe to the journal, contact the AACR Publications Department at pubs@aacr.org.

Permissions

To request permission to re-use all or part of this article, contact the AACR Publications Department at permissions@aacr.org.

Robust Gene Expression Signature from Formalin-Fixed Paraffin-Embedded Samples Predicts Prognosis of Non-Small-Cell Lung Cancer Patients

Yang Xie^{1,2}, Guanghua Xiao¹, Kevin R. Coombes⁶, Carmen Behrens⁷, Luisa M. Solis⁸, Gabriela Raso⁸, Luc Girard^{4,5}, Heidi S. Erickson⁷, Jack Roth⁹, John V. Heymach⁷, Cesar Moran⁸, Kathy Danenberg¹⁰, John D. Minna^{2,3,4,5}, and Ignacio I. Wistuba^{7,8}

Abstract

Purpose: The requirement of frozen tissues for microarray experiments limits the clinical usage of genome-wide expression profiling by using microarray technology. The goal of this study is to test the feasibility of developing lung cancer prognosis gene signatures by using genome-wide expression profiling of formalin-fixed paraffin-embedded (FFPE) samples, which are widely available and provide a valuable rich source for studying the association of molecular changes in cancer and associated clinical outcomes.

Experimental Design: We randomly selected 100 Non-Small-Cell lung cancer (NSCLC) FFPE samples with annotated clinical information from the UT-Lung SPORE Tissue Bank. We microdissected tumor area from FFPE specimens and used Affymetrix U133 plus 2.0 arrays to attain gene expression data. After strict quality control and analysis procedures, a supervised principal component analysis was used to develop a robust prognosis signature for NSCLC. Three independent published microarray datasets were used to validate the prognosis model.

Results: This study showed that the robust gene signature derived from genome-wide expression profiling of FFPE samples is strongly associated with lung cancer clinical outcomes and can be used to refine the prognosis for stage I lung cancer patients, and the prognostic signature is independent of clinical variables. This signature was validated in several independent studies and was refined to a 59-gene lung cancer prognosis signature.

Conclusions: We conclude that genome-wide profiling of FFPE lung cancer samples can identify a set of genes whose expression level provides prognostic information across different platforms and studies, which will allow its application in clinical settings. *Clin Cancer Res*; 17(17); 5705–14. ©2011 AACR.

Introduction

Lung cancer is the leading cause of death from cancer for both men and women in the United States and in most parts of the world, with a 5-year survival rate of 15% (1). Non-small-cell lung cancer (NSCLC) is the most

common cause of lung cancer death, accounting for up to 85% of such deaths (2). Clinicopathologic staging is the standard prognosis factor for lung cancer used in clinical practice but does not capture the complexity of the disease so that heterogeneous clinical outcomes within the same stage are commonly seen. Several randomized clinical trials showed that adjuvant chemotherapy improves survival in resected NSCLC (3–7). The effect of adjuvant chemotherapy on prolonging survival is modest—only 4% to 15% improvement in 5-year survival—although such treatment is associated with serious adverse effects (6, 8). Therefore, it is of considerable clinical importance to have a robust and accurate prognostic signature for lung cancer, especially in early stage lung cancer to improve the current clinical decisions on whether an individual lung cancer patient should receive adjuvant chemotherapy or not.

Genome-wide expression profiles have been used to identify gene signatures to classify lung cancer patients with different survival outcomes (9–16). However, the requirement of frozen tissues for microarray experiments limits the clinical usage of these gene signatures.

Authors' Affiliations: Departments of ¹Clinical Sciences, ²Simmons Cancer Center, ³Internal Medicine, ⁴Pharmacology, and ⁵Hamon Center for Therapeutic Oncology Research, The University of Texas Southwestern Medical Center, Dallas; Departments of ⁶Bioinformatics and Computational Biology, ⁷Thoracic/Head and Neck Medical Oncology, ⁸Pathology and ⁹Thoracic and Cardiovascular Surgery, The University of Texas MD Anderson Cancer Center, Houston, Texas; and ¹⁰Response Genetics, Inc., Los Angeles, California

Note: Supplementary data for this article are available at Clinical Cancer Research Online (<http://clincancerres.aacrjournals.org/>).

Corresponding Author: Ignacio I. Wistuba, Departments of Pathology and Thoracic/Head and Neck Medical Oncology, Unit 85, The University of Texas MD Anderson Cancer Center, 1515 Holcombe Boulevard, Houston, TX 77030. Phone: 713-563-9184; Fax: 713-792-0309; E-mail: iiwistuba@mdanderson.org

doi: 10.1158/1078-0432.CCR-11-0196

©2011 American Association for Cancer Research.

Translational Relevance

This article is the first study to develop a robust prognosis signature for non-small cell lung cancer (NSCLC) on the basis of genome-wide expression profiling of clinically available formalin-fixed and paraffin-embedded (FFPE) samples. Although clinical FFPE tumor samples are widely available, the genome-wide expression profiling of FFPE samples has been hampered because of the degradation of RNAs extracted from them. In this article, we show that NSCLC FFPE-derived signature is strongly associated with clinical outcome of the patients, is independent of clinical prognostic variables, and can be validated in several independent studies. We showed that, after strict quality control and analysis procedures, genome-wide profiling of FFPE samples can actually provide a unique opportunity to identify a set of genes whose expression level is less sensitive to the environmental changes. This gene signature is more robust across different platforms and studies, which is critical for the successful application of gene signatures in real clinical settings.

Furthermore, prognostic gene signatures for NSCLC developed by different groups show minimal overlap and are often difficult to reproduce by independent groups (17, 18). To address the problem of requirement for frozen issues, we designed this study to test the feasibility of developing lung cancer prognosis gene signatures by using genome-wide expression profiling of formalin-fixed paraffin-embedded (FFPE) samples, which are widely available and provide a valuable rich source for studying the association of molecular changes in cancer and associated clinical outcomes. We derived a prognosis signature for NSCLC from FFPE samples and validated it in several independent studies. To facilitate other researchers to reproduce all results in this study, we have provided a literate programming R package.

Materials and Methods

Tissue specimens

The overall study design and the flow chart of the derivation and validation of the robust gene signature are described in Figure 1. We randomly selected 100 NSCLC FFPE samples with annotated clinical information from the UT-Lung SPORC Tissue Bank from 2001 to 2005. From these samples, 75 samples passed the mRNA quality control criteria (Supplementary Methods). Among these 75 samples, 48 samples are adenocarcinomas and 27 are squamous cell carcinomas. The median follow-up time is 2.8 years and the maximum follow-up time is 6.9 years; the characteristics of these patients are summarized in Supplementary Table S1. The samples were obtained under approval of the Institutional Review Boards at MD Anderson Cancer Center.

Sample microdissection and RNA extraction

FFPE tumor specimens were cut into serial sections with a thickness of 10 μm . For the pathologic diagnosis, one slide was stained with H&E and evaluated by a pathologist. Other sections were stained with nuclear fast red (NFR; American MasterTech Scientific Inc.) to enable visualization of histology. Tumor tissue was isolated by using manual macrodissection when the tumor area was more than $0.5 \times 0.5 \text{ mm}^2$ or laser capture microdissection (P.A.L.M. Microlaser Technologies AG) in cases of smaller tumor areas. At least 50 mm^2 of tumor tissue was collected from each FFPE block. The extraction of RNA from tissue samples was done by a proprietary procedure of Response Genetics, Inc. (United States Patent Application 20090092979) designed to optimize the yield of higher molecular weight RNA fragments from FFPE specimens.

Microarray data preprocessing and quality control

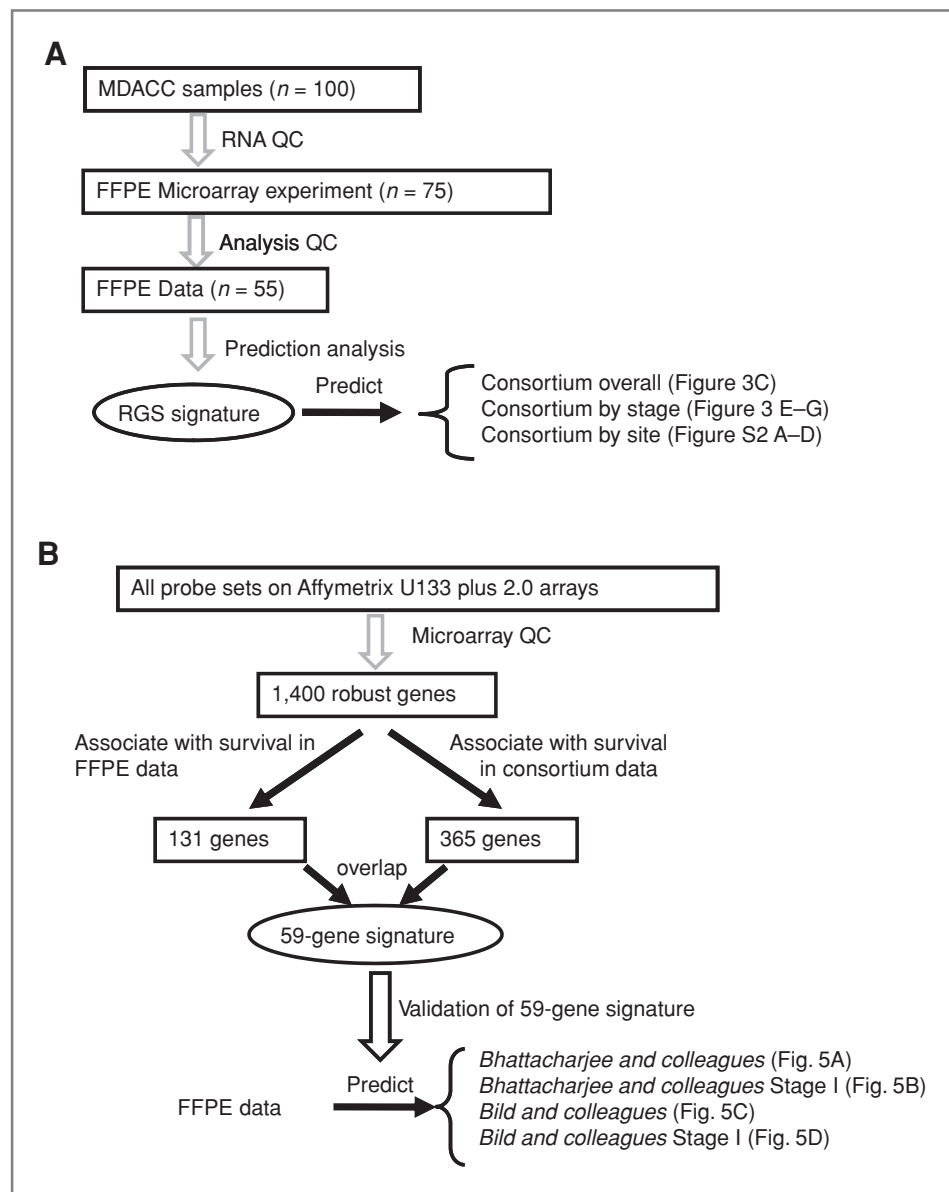
Total RNA was processed for analysis on the Affymetrix U133 plus 2.0 arrays according to Affymetrix protocols for first- and second-strand synthesis, biotin labeling, and fragmentation. The quality control procedure for microarray data analysis was based on the percentage of present calls calculated by the MAS5 package. We selected arrays with at least 15% of probe sets present; 55 of 75 arrays passed this quality control criterion and will be used for the analysis. We selected probe sets that are present on all 55 arrays; 1,400 genes passed this criterion. These 1,400 genes were referred as the robust gene set (RGS), because the mRNA expression of these genes is robust to FFPE processing. The 55 samples and the 1,400 genes were used to develop gene signatures.

After microarray analysis QC, we used the RMA background correction algorithm (19) to remove nonspecific background noise. A robust regression model (20) was fitted to the probe level data, and the fitted expression values for the probes at the 3' end were used to summarize the probe set expression values. Quantile-quantile normalization was used to normalize all the arrays. Consortium microarray raw data (13) was downloaded from caArray database of the National Cancer Institute (NCI) and preprocessed by RMA background correction and quantile-quantile normalization. All gene expression values were log transformed (on a base 2 scale).

Supervised classification by using supervised principal component analysis

Classification was done by using supervised principal component analysis (21, 22), a widely used classification method in biomedical research (23–26). As a supervised classification method, each prediction model was trained in a training dataset and then the performance was tested in an independent test dataset. We used an R package (version 2.81), Superpc (version 1.05), to implement the prediction algorithm, and the default parameters were used. The implementation details can be found in the Supplementary Swebate Report. The training and testing sets for each

Figure 1. A, flow chart of the derivation and validation of the robust gene signature from FFPE samples collected from MD Anderson UT-Lung Cancer SPORE tissue bank (MDACC). B, flow chart of the derivation and validation of 59-gene prognosis signature.



prediction model are summarized in Supplementary Table S2.

Survival analysis

Overall survival time was calculated from the date of surgery until death or the last follow-up contact. Survival curves were estimated by using the product-limit method of Kaplan–Meier (27) and were compared by using the log-rank test. The maximum follow-up time for the FFPE patient cohort is less than 7 years, whereas some patients in the consortium cohort have been followed for up to 17 years. To avoid the extrapolation of the prediction model, the comparison of survival time between predicted groups are truncated at 7 years. The analysis results without truncation can be seen in Supplementary Sweave Report. Uni-

variate and multivariate Cox proportional hazards analysis (28) were also done, with survival as the dependent variable.

Results

The robust gene set defines two tumor groups

The expression of these 1,400 genes divided the 55 patients into 2 groups on the basis of unsupervised clustering analysis (with Euclidean distance and complete linkage for the hierarchical clustering algorithm; Fig. 2). Interestingly, group 1 has significantly shorter survival time compared with group 2 (Fig. 2B; HR = 3.6, $P = 0.017$), and multivariate Cox proportional hazards analysis showed that the association between RGS groups

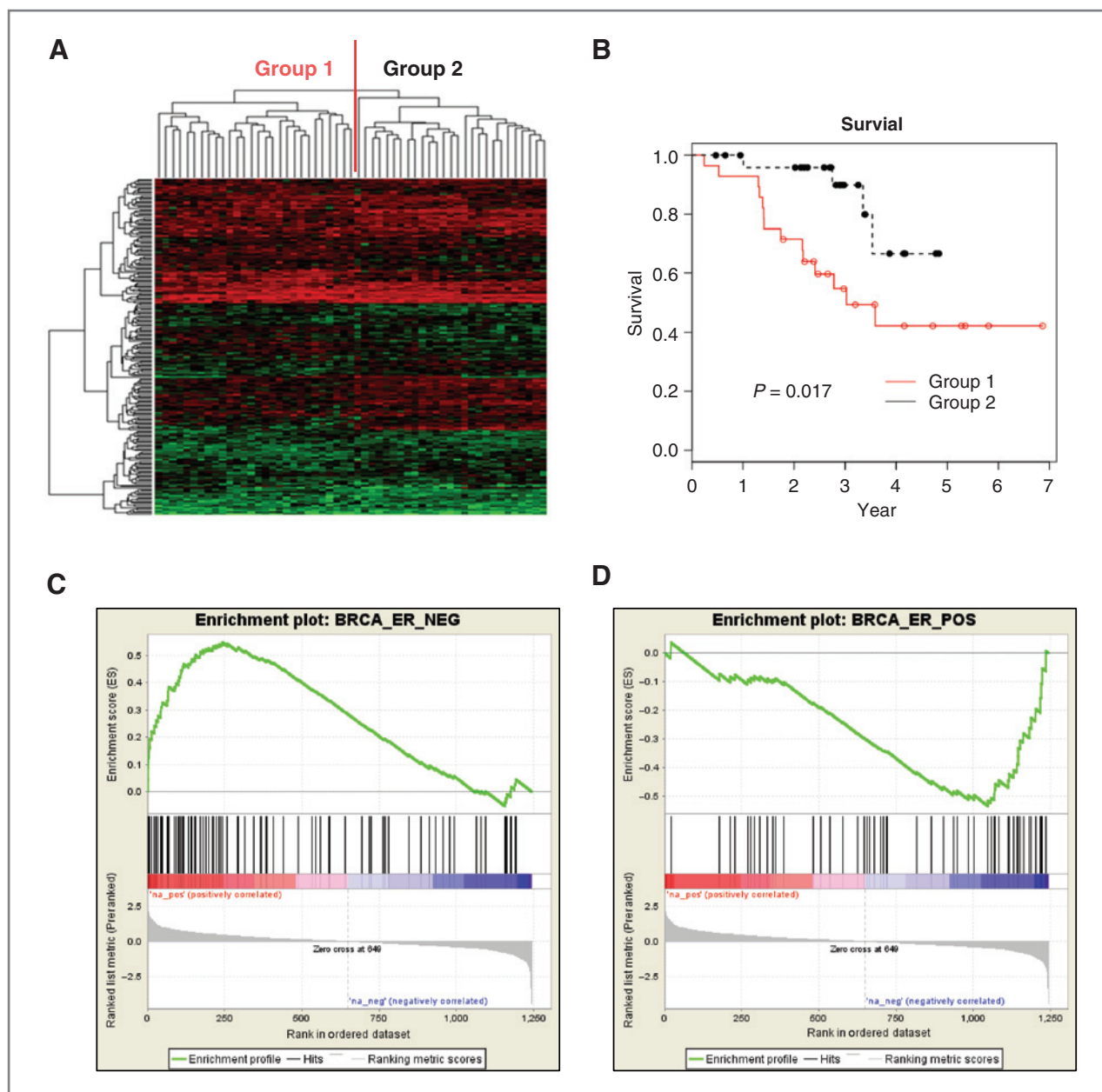
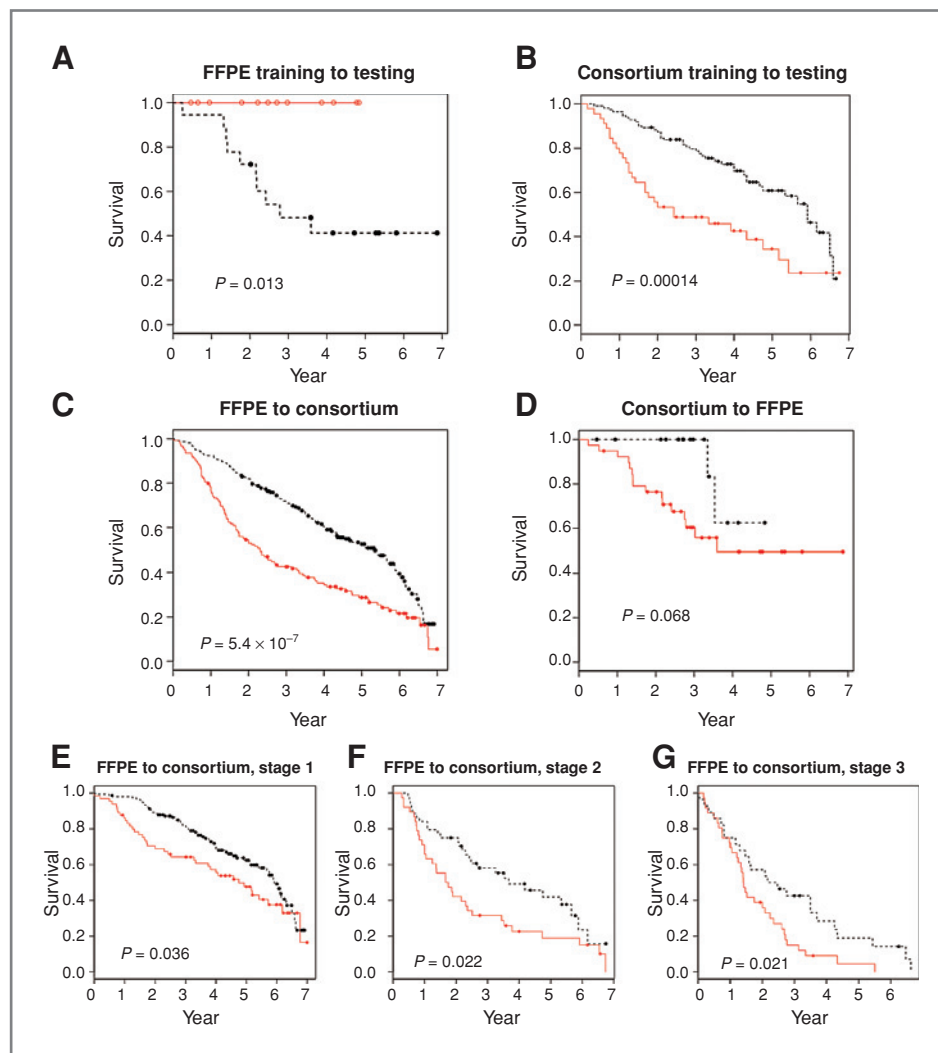


Figure 2. Microarray analysis of the gene expression profiles from FFPE lung tumor samples. A, unsupervised cluster analysis of the 55 FFPE lung cancer patient cohort by using the expression profile of 1,400 robust genes that pass the microarray quality control criterion. Vertical and horizontal axes represent robust genes and lung cancer patient clusters, respectively. B, Kaplan–Meier plot showing the association of the expression of robust genes with patient survival P values were obtained by using the log-rank test. Red color represents sample cluster I and black color represents sample cluster II defined by unsupervised clustering algorithm by using robust gene profiling data. • indicates censored samples. Gene set enrichment analysis found that the ER-negative signature derived from breast cancer patients is enriched in group 1 defined by RGS expression (C), and the ER-positive signature derived from breast cancer patients is enriched in group 2 defined by RGS expression (D). The y-axis shows running enrichment scores for the specific gene set on the 1,400 preranked genes. The x-axis shows the rank in the ordered dataset. The vertical lines represent the locations of the genes that are in the specific gene set.

and survival ($P = 0.012$) is independent of stage. Notably, group 1 was dominated by squamous cell carcinoma (23/28), whereas group 2 was dominated by adenocarcinomas (25/27; $P < 0.0001$; Supplementary Table S3). The other clinical characteristics including gender, age, and

smoking status were not significantly different between the 2 groups. To explore whether the association between RGS groups and survival is due to the histologic difference between two groups, we drew Kaplan–Meier curves by both histology and RGS groups (Supplementary Fig. S1),

Figure 3. Kaplan–Meier plots showing the predictive power of the robust gene signatures. Fifty-five FFPE tumor samples from MD Anderson Cancer Center were randomly divided into training (25 samples) and testing (30 samples) sets (A). Independent validation of the robust gene signature in the 442 frozen sample cohort from multi-institute consortium. The microarray datasets were divided into 2 groups, one for the training and the other for the testing cohort according to the original paper (B). The training data were 55 FFPE tumor samples and the testing dataset were 442 frozen sample cohort from multi-institute consortium. The testing was done for all patients (C), stage I patients (E), stage II patients (F) and stage III patients (G) separately. The training data were the consortium dataset with 442 frozen samples and the testing data were 55 FFPE samples from MD Anderson Cancer Center (D). *P* values were obtained by the log-rank test. Red and black lines represent predicted high- and low-risk groups, respectively. ● indicates censored samples.



and it shows clearly that RGS can distinguish high- and low-risk groups within both adenocarcinoma and squamous groups, indicating the association of RGS groups and survival is independent of histology groups.

We used gene set enrichment analysis to identify the enriched gene sets in both RGS groups. Interestingly, an estrogen receptor (ER)-negative signature in breast cancer (29) is enriched in RGS group 1, meanwhile, an ER-positive signature in breast cancer (29) is enriched in RGS group 2 (Fig. 2C and D), indicating the relationship between the ER signatures and the RGS groups. The other enriched gene sets are summarized in Supplementary Table S4; notably, genes enriched in group 1 are also enriched in mouse neural stem cells and embryonic stem cells.

Construct and validate RGS prognosis signatures

FFPE samples training to testing. The strong associations between RGS groups and survival outcomes motivated us to explore whether RGS expression profile can be

used to construct prognosis signature. We randomly divided 55 patients into training (25 samples) and testing (30 samples) sets and constructed a prediction model by using 1,400 robust gene expression values in the training set through a supervised principle component approach (21). Figure 3A shows that the predicted low-risk group has significant longer survival time than the predicted high-risk group ($P = 0.013$) in the testing set. To test whether this association was not random, we randomly split the data into training and testing sets 200 times, repeated the same prediction and testing procedures for each set, and found that the prognosis performance of RGS signature is significantly better than random ($P = 0.02$).

Frozen samples training to testing. We then tested whether this robust gene set can be used to construct prognosis signature in frozen samples. The largest independent public available lung cancer microarray dataset is the recently published NCI Director's Consortium for study of lung cancer involving 442 resected adenocarcinomas

(13). From that study, Affymetrix U133A microarray data for the 1,012 robust genes were excerpted with 388 less genes than our FFPE data because of the microarray platform difference. We used the same training and testing strategy as in the original analyses of these data (13) for constructing and validating prognosis signature through supervised principal component approach. The training set included samples from University of Michigan Cancer Center (UM) and Moffitt Cancer Center (HLM), and the testing set included the Memorial Sloan-Kettering Cancer Center (MSKCC) and Dana-Farber Cancer Institute (DFCI) samples. This analysis revealed that the predicted low-risk group has significant longer survival time than the predicted high-risk group (HR = 2.44, $P = 0.00014$) in the testing dataset (Fig. 3B).

FFPE to frozen samples and vice versa. Next, we used our FFPE and the consortium datasets as frozen samples to investigate whether the predication model built from one type of sample can be validated in another type of sample. Again, the same supervised principal component method was used to construct the prediction model. The prediction model built from FFPE samples can significantly distinguish the high- and low-risk groups in frozen samples (Fig. 3C; HR = 1.95, $P = 5.4 \times 10^{-7}$), and the prediction model built from frozen samples can also distinguish the high- and low-risk groups in FFPE samples but with marginal significance (Fig. 3D; HR = 3.59, $P = 0.068$). We also tested the performance of FFPE prediction model on 4 individual datasets in consortium study and found that the predicted low-risk groups have longer survival time compared with the predicted high-risk groups for all sets: MSKCC dataset (median survival time 6.5 vs. 3.3 years; HR = 2.31, $P = 0.0093$), DFCI dataset (median survival time 5.9 vs. 0.9 years; HR = 2.62, $P = 0.0076$), HLM dataset (median survival time 3.4 vs. 2.2 years; HR = 1.25, $P = 0.4$) and UM dataset (median survival time 5.4 vs. 2.2 years; HR = 1.98, $P = 0.0011$; Supplementary Fig. S2). Next, we compared the performance of RGS signature with previous published lung cancer prognosis signatures by using the same consortium dataset as testing set. Shedden and colleagues (13) showed that the HRs for Method A signature (the best signature in their study) and Chen and colleagues (11) signatures range from 1.10 to 1.83 for the MSKCC test set, whereas the HR for our RGS signature is 2.89 on the same MSKCC test set. For the DFCI test set, the HRs range from 1.76 to 2.30 by using the published signatures, whereas the HR for our RGS signature on the same DFCI test set is 2.39. Therefore, the prognosis performance of RGS prognosis is at least as good as other published signatures in the microarray dataset.

The RGS prognosis signature is independent of clinical variables

To test whether RGS is an independent prognosis signature, we fitted a multivariate Cox regression model including RGS risk scores, age, gender, stage, smoking status, adjuvant chemotherapy usage, and clinical sites as covariables for the consortium dataset. The RGS risk scores

Table 1. The association between characteristics of patients and RGS risk scores and survival time for consortium patients on the basis of multivariate Cox regression model

Variables	HR (95% CI)	P
RGS risk scores	1.300 (1.074–1.574)	0.0070
Gender (female vs. male)	0.803 (0.576–1.119)	0.19
Age (continuous in unit of 10 y)	1.571 (1.321–1.868)	<0.0001
Smoking (current/former vs. never)	1.356 (0.791–2.322)	0.27
Stage		
Stage II vs. stage I	2.116 (1.433–3.126)	0.0002
Stage III vs. stage I	4.855 (3.164–7.449)	<0.0001
Adjuvant chemotherapy (yes vs. no)	1.688 (1.172–2.431)	0.0049
Study sites		
DFCI vs. UM	1.295 (0.741–2.264)	0.36
HLM vs. UM	1.632 (1.094–2.434)	0.016
MSKCC vs. UM	0.657 (0.419–1.031)	0.068

NOTE: RGS scores were calculated from the prediction model built from MD Anderson Cancer Center FFPE samples.

were calculated from the prediction model built from the FFPE samples set. Table 1 shows that the RGS signature is significantly associated with the survival time after adjusting for other clinical variables (HR = 1.3, $P = 0.007$). Pathologic stages based on international staging system is the most widely used and important prognosis variable for lung cancer patients (30); here we tested whether RGS signature can further refine the prognosis within each stage. The RGS prognosis signature from FFPE samples was tested within each stage of the consortium dataset. The results show clearly that the RGS signature is significantly associated with survival outcome within each stage (Fig. 3E–G; HR = 1.54, $P = 0.036$ for stage I, HR = 1.81, $P = 0.022$ for stage II and HR = 1.90, $P = 0.021$ for stage III), indicating that the RGS signature can refine the prognosis for lung cancer patients. The RGS prognosis signature from FFPE samples was further tested for patients with or without adjuvant chemotherapy separately, and the results show that the RGS signature is significantly associated with survival for both groups (Supplementary Fig. S3A and B; HR = 1.95, $P = 0.015$ for patients with chemotherapy, HR = 1.99, $P = 0.00062$ for patients without chemotherapy).

Refine to 59-gene prognosis signature

Among all the RGS genes, 131 genes are associated with survival ($P < 0.05$) in the FFPE dataset, and 365 genes are associated with overall survival ($P < 0.05$) in the consortium dataset by univariate Cox regression analysis. There is significant overlap between these two gene lists (Fig. 4A; 59 common genes; $P = 0.0008$, hypergeometric test). More significant genes were found in the consortium data

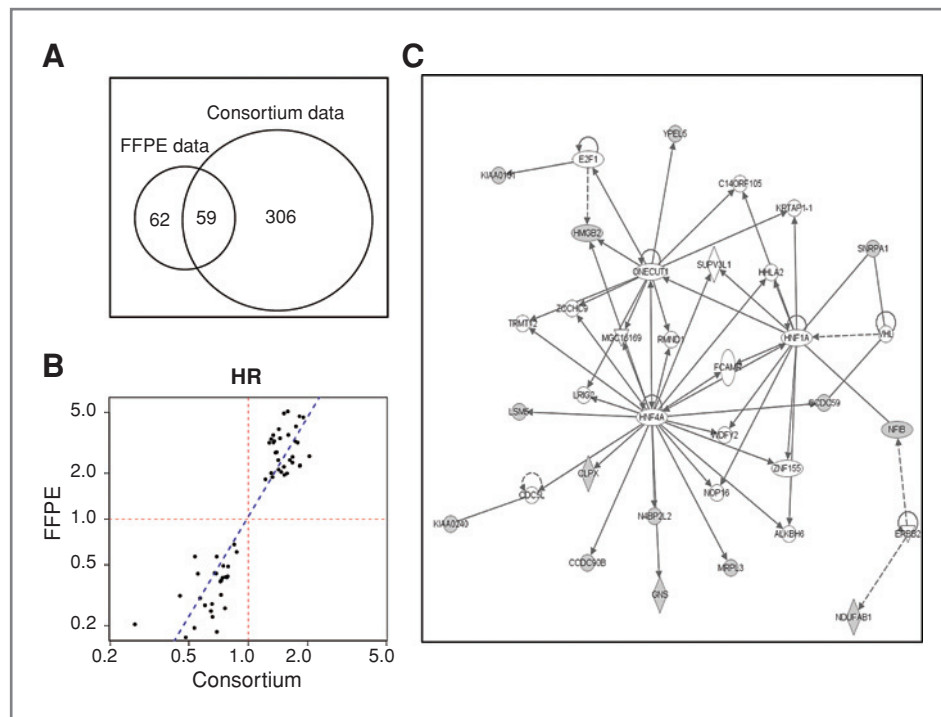


Figure 4. Comparison of individual gene effect across FFPE samples from MD Anderson Cancer Center and 442 frozen samples from consortium. **A**, Venn diagram of genes associated with overall survival ($P < 0.05$ in univariate Cox regression models). It shows 59 genes are significantly associated with survival in both FFPE data and consortium data. **B**, the HRs from univariate Cox regression models for the 59 genes common in both sets are consistent between FFPE set and consortium set. **C**, regulatory gene and protein interaction networks defined by the 59 predictors. Computational molecular interaction network prediction on the basis of genes and proteins associated with the significant pathways in the Ingenuity Pathways Knowledge Base (IPKB) by IPA. Interactions between the different nodes are given as solid (direct interaction) and dashed (indirect interaction) lines (edges). This network received the highest score by IPA and is mostly centered on the transcription factors *HNF4A* and *HNF1A*, and *ONECUT1*. The shaded genes are the genes belonging to 59-gene signature.

compared with the FFPE data, which is likely due to the larger sample size ($n = 442$) of the consortium dataset compared with the FFPE dataset sample size ($n = 55$). Surprisingly, HRs from the two datasets are very consistent with each other. All 59 genes have the same direction of effects (positive or negative) on the survival between the 2 datasets and the HRs from 2 datasets are highly correlated (Pearson's correlation = 0.86; Fig. 4B), indicating the high consistency of expressions of these genes across datasets. These results motivated us to hypothesize that these 59 genes (Supplementary Table S5) alone can be used for lung cancer prognosis. To test this hypothesis, we applied supervised principal component analysis to these 59 genes by using the FFPE dataset to construct a 59-gene prognosis signature. Because the selection of these 59 genes used information from both FFPE and consortium datasets, we used another 2 independent lung cancer datasets, including the Bild and colleagues ($n = 111$; ref. 9) dataset and the Bhattacharjee and colleagues dataset ($n = 117$; ref. 31) downloaded from the literature to validate our 59-gene signature. The 59-gene prediction model built from FFPE samples can significantly distinguish the high- and low-risk groups for both the Bhattacharjee and colleagues and Bild and colleagues datasets (Fig. 5A; HR = 1.81, $P = 0.016$ and

Fig. 5C; HR = 2.10, $P = 0.02$, respectively). Furthermore, this signature can also significantly distinguish the high- and low-risk groups within stage I patients for both datasets (Fig. 5B and D), indicating that this 59-gene signature can refine the prognosis for lung cancer patients within stage I patients. Because of the small sample size for stage II and stage III patients in Bild and colleagues and Bhattacharjee and colleagues studies, the 59-gene prognosis signature was not tested for stage II and stage III patients. We also found that 59-gene prediction model built from the consortium dataset can also distinguish the high- and low-risk groups for the Bild and colleagues and Bhattacharjee and colleagues datasets (Supplementary Fig. S4A–D).

To understand the potential biological relevance of these 59 genes significantly associated with survival in the FFPE and consortium datasets, we used Ingenuity Pathway Analysis (IPA) to explore which known regulatory networks are enriched in this 59-gene set. IPA analysis revealed the most significant molecular networks to be cancer, tumor morphology, and respiratory disease. This network (Fig. 4C) includes 14 genes of the 59-gene set and is centered on transcription factors *HNF4A*, *HNF1A*, and *ONECUT1* (*HNF6A*). This hepatocellular network has been implicated in hepatocellular carcinoma as determined by *in vitro* study

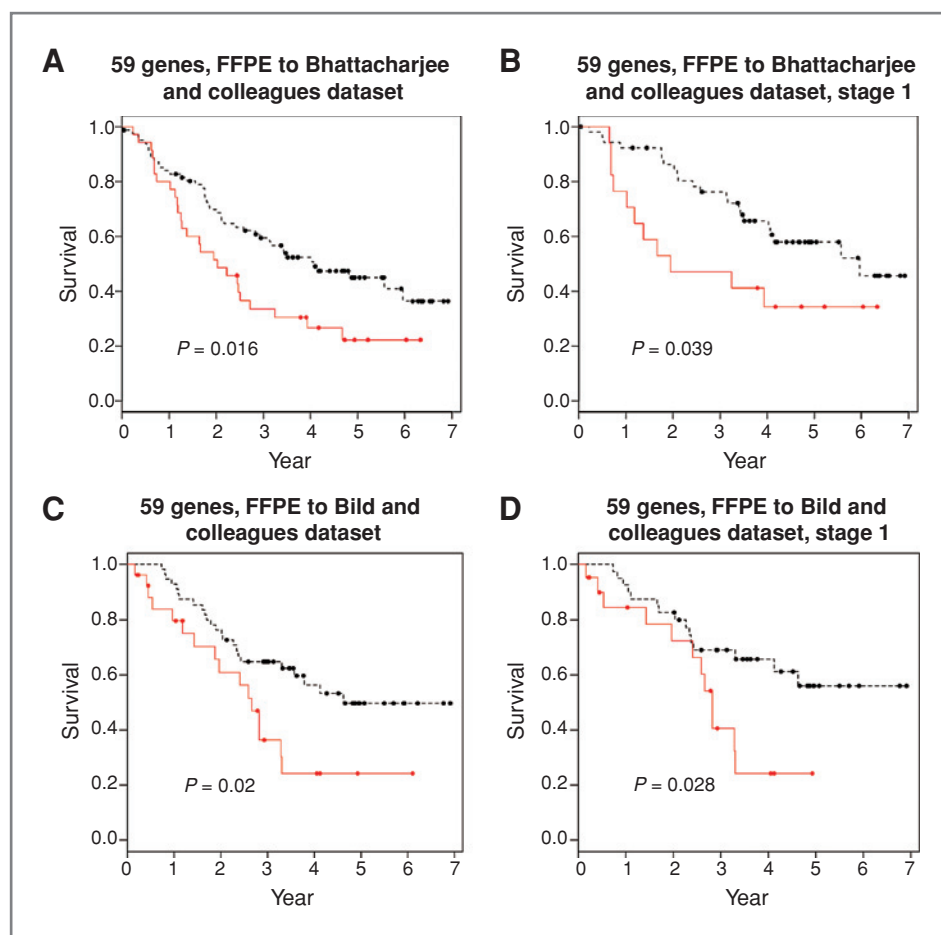


Figure 5. Kaplan-Meier plots showing the predictive power of the 59-gene signature for 2 independent validation sets. The training data were 55 FFPE tumor samples from MD Anderson Cancer Center and the testing dataset was frozen samples from lung cancer patients from Bhattacharjee and colleagues (31) dataset (A), the stage I patients from Bhattacharjee and colleagues dataset (B), frozen samples from lung cancer patients from Bild and colleagues (9) dataset (C), and the stage I patients from Bild and colleagues dataset (D). *P* values were obtained by the log-rank test. Red and black lines represent predicted high- and low-risk groups, respectively. • indicates censored samples.

(32) and molecular interactions in this network are putatively involved in lung cancer survival.

Discussion

In this study, we tested the feasibility of deriving a lung cancer prognosis gene signature from FFPE tumor samples on the basis of genome-wide mRNA expression profiling. Although reverse transcriptase PCR methods have been used to measure gene expression level from FFPE samples (33–35), the selection of genes for testing are limited to the current knowledge base which is incomplete and inconsistent (36). Because of degradation and chemical alteration of RNA extracted from FFPE samples, the use of microarray analysis of gene expression from FFPE samples has been hampered (36). New technology and methodologies developed to extract RNA from FFPE samples coupled with new array platforms have made it possible to measure gene expression from FFPE samples (33, 37–40). A recent study showed the feasibility of using DNA-mediated annealing, selection, extension, and ligation arrays with 6,100 preselected genes to profile mRNA expression from hepatocellular carcinoma tissue (41). No prognosis signature for other types of cancer has been developed by using

microarray analysis of gene expression from FFPE extracted RNA. In this study, we built a robust gene signature for NSCLC on the basis of microarray analysis of FFPE samples. We claim that this is a robust gene signature because it has been validated in 6 independent published datasets, including 4 sets from the consortium study and 2 additional studies from DFCI and Duke. We also built a prediction model by using the same set of robust genes from frozen samples and validated the model in both frozen and FFPE samples.

Most published gene signatures identified from different studies are usually very different and with little overlap. However, we found that there is significant overlap among the robust genes associated with survival outcomes between the FFPE dataset and the consortium dataset ($P = 0.008$). More impressively, the HRs, indicating the strength of the association of genes expression and survival time, are highly consistent between 2 independent datasets. Our interpretation for this consistency across studies is that the gene expression variation across studies is a major contribution to signature differences across studies. In this study, we used strict quality steps to exclude genes that were not expressed in our FFPE samples. This allowed for analysis of the remaining genes

which had more stable expression patterns and were more robust to environment changes. Validation of our novel 59-gene signature prognostic for NSCLC survival in 2 additional independent datasets further confirmed the robustness of these genes.

By grouping our RGS of 1,400 genes by gene expression, we found that the group expression levels correlated with survival. Interestingly, group 1 had a shorter survival and contained an ER-negative breast cancer signature. Group 2 had a longer survival and contained an ER-positive breast cancer signature. This correlation with ER status and survival has been shown previously in breast cancer and shown to have predictive power for prognosis (29). In addition to ER status, the RGS groups were separated by the presence of stem cell signatures (embryonic stem cell signature and neural stem cell signature), with group 1 (shorter survival) having 2 stem cell signatures, whereas group 2 (longer survival) did not. The embryonic stem cell signature has previously been shown to be associated with poor prognosis of NSCLC (42). In addition, in mouse models, a hematopoietic and neural stem cell-like signature in primary tumors has been shown to be a predictor of poor prognosis in 11 types of cancer, including lung (43). These ER status and stem cell signature data support our RGS expression groupings and their correlation with survival prognosis.

Besides the prognostic signature, the predictive signatures to determine the optimal chemotherapy regimen for

individual patients also have tremendous clinical benefit. Tumor samples from clinical trials data are important to develop predictive signatures to reduce the selection bias for evaluating treatment efficacy within signature groups. However, very limited frozen tumor samples are available from completed clinical trials. Our study showed the feasibility of using FFPE samples for genome-wide mRNA profiling. Therefore, this study provides an important step to construct and validate predictive signatures for chemotherapy response by using the available FFPE samples from clinical trials in the future.

Disclosure of Potential Conflicts of Interest

No potential conflicts of interest were disclosed.

Grant Support

This study was supported in part by grants from the Department of Defense (W81XWH-07-1-0306 03 to J.D. Minna and I.I. Wistuba), the Specialized Program of Research Excellence in Lung Cancer Grant (P50CA70907 to J.D. Minna, J. Roth, and I.I. Wistuba), the NCI (1R01CA152301-01 to Y. Xie and I.I. Wistuba, Cancer Center Support Grant CA-16672), the NIH (5R21DA027592 to G. Xiao), and the NSF (DMS0907562 to G. Xiao).

The costs of publication of this article were defrayed in part by the payment of page charges. This article must therefore be hereby marked *advertisement* in accordance with 18 U.S.C. Section 1734 solely to indicate this fact.

Received January 26, 2011; revised June 10, 2011; accepted June 29, 2011; published OnlineFirst July 8, 2011.

References

- Jemal A, Siegel R, Ward E, Hao Y, Xu J, Thun MJ. Cancer statistics, 2009. *CA Cancer J Clin* 2009;59:225-49.
- Tsuboi M, Ohira T, Saji H, Miyajima K, Kajiura N, Uchida O, et al. The present status of postoperative adjuvant chemotherapy for completely resected non-small cell lung cancer. *Ann Thorac Cardiovasc Surg* 2007;13:73-7.
- Douillard JY, Rosell R, De Lena M, Carpagnano F, Ramlau R, Gonzales-Larriba JL, et al. Adjuvant vinorelbine plus cisplatin versus observation in patients with completely resected stage IB-IIIA non-small-cell lung cancer (Adjuvant Navelbine International Trialist Association [ANITA]): a randomised controlled trial. *Lancet Oncol* 2006;7:19-27.
- Kato H, Ichinose Y, Ohta M, Hata E, Tsubota N, Tada H, et al. A randomized trial of adjuvant chemotherapy with uracil-tegafur for adenocarcinoma of the lung. *N Engl J Med* 2004;350:1713-21.
- Arriagada R, Bergman B, Dunant A, Le Chevalier T, Pignon JP, Vansteenkiste J. Cisplatin-based adjuvant chemotherapy in patients with completely resected non-small-cell lung cancer. *N Engl J Med* 2004;350:351-60.
- Winton T, Livingston R, Johnson D, Rigas J, Johnston M, Butts C, et al. Vinorelbine plus cisplatin vs. observation in resected non-small-cell lung cancer. *N Engl J Med* 2005;352:2589-97.
- Strauss GM, Herndon JE 2nd, Maddaus MA, Johnstone DW, Johnson EA, Harpole DH, et al. Adjuvant paclitaxel plus carboplatin compared with observation in stage IB non-small-cell lung cancer: CALGB 9633 with the Cancer and Leukemia Group B, Radiation Therapy Oncology Group, and North Central Cancer Treatment Group Study Groups. *J Clin Oncol* 2008;26:5043-51.
- Olaussen KA, Mountzios G, Soria JC. ERCC1 as a risk stratifier in platinum-based chemotherapy for nonsmall-cell lung cancer. *Curr Opin Pulm Med* 2007;13:284-9.
- Bild AH, Yao G, Chang JT, Wang Q, Potti A, Chasse D, et al. Oncogenic pathway signatures in human cancers as a guide to targeted therapies. *Nature* 2006;439:353-7.
- Boutros PC, Lau SK, Pintilie M, Liu N, Shepherd FA, Der SD, et al. Prognostic gene signatures for non-small-cell lung cancer. *Proc Natl Acad Sci U S A* 2009;106:2824-8.
- Chen HY, Yu SL, Chen CH, Chang GC, Chen CY, Yuan A, et al. A five-gene signature and clinical outcome in non-small-cell lung cancer. *N Engl J Med* 2007;356:11-20.
- Lu Y, Lemon W, Liu PY, Yi Y, Morrison C, Yang P, et al. A gene expression signature predicts survival of patients with stage I non-small cell lung cancer. *PLoS Med* 2006;3:e467.
- Shedden K, Taylor JM, Enkemann SA, Tsao MS, Yeatman TJ, Gerald WL, et al. Gene expression-based survival prediction in lung adenocarcinoma: a multi-site, blinded validation study. *Nat Med* 2008;14:822-7.
- Sun Z, Wigle DA, Yang P. Non-overlapping and non-cell-type-specific gene expression signatures predict lung cancer survival. *J Clin Oncol* 2008;26:877-83.
- Hsu DS, Balakumaran BS, Acharya CR, Vlahovic V, Walters KS, Garman K, et al. Pharmacogenomic strategies provide a rational approach to the treatment of cisplatin-resistant patients with advanced cancer. *J Clin Oncol* 2007;25:4350-7.
- Hayes DN, Monti S, Parmigiani G, Gilks CB, Naoki K, Bhattacharjee A, et al. Gene expression profiling reveals reproducible human lung adenocarcinoma subtypes in multiple independent patient cohorts. *J Clin Oncol* 2006;24:5079-90.
- Coombes KR, Wang J, Baggerly KA. Microarrays: retracing steps. *Nat Med* 2007;13:1276-7; author reply 7-8.
- Ioannidis JP, Allison DB, Ball CA, Coulibaly I, Cui X, Culhane AC, et al. Repeatability of published microarray gene expression analyses. *Nat Genet* 2009;41:149-55.

19. Bolstad BM, Irizarry RA, Astrand M, Speed TP. A comparison of normalization methods for high density oligonucleotide array data based on variance and bias. *Bioinformatics* 2003;19:185–93.
20. Huber PJ. 1972 Wald Lecture - Robust Statistics - Review. *Ann Math Stat* 1972;43:1041–67.
21. Bair E, Tibshirani R. Semi-supervised methods to predict patient survival from gene expression data. *PLoS Biol* 2004;2:E108.
22. Breiman L, Friedman J, Stone JC, Olshen RA. *Classification and regression trees*. New York: Chapman & Hall/CRC; 1984.
23. Garzotto M, Beer TM, Hudson RG, Peters L, Hsieh YC, Barrera E, et al. Improved detection of prostate cancer using classification and regression tree analysis. *J Clin Oncol* 2005;23:4322–9.
24. Hess KR, Abbruzzese MC, Lenzi R, Raber MN, Abbruzzese JL. Classification and regression tree analysis of 1000 consecutive patients with unknown primary carcinoma. *Clin Cancer Res* 1999;5:3403–10.
25. Koziol JA, Zhang JY, Casiano CA, Peng XX, Shi FD, Feng AC, et al. Recursive partitioning as an approach to selection of immune markers for tumor diagnosis. *Clin Cancer Res* 2003;9:5120–6.
26. Valera VA, Walter BA, Yokoyama N, Koyama Y, Iiai T, Okamoto H, et al. Prognostic groups in colorectal carcinoma patients based on tumor cell proliferation and classification and regression tree (CART) survival analysis. *Ann Surg Oncol* 2007;14:34–40.
27. Kaplan ELM P. Nonparametric estimation from incomplete observations. *J Am Stat Assoc* 1958;53:457–81.
28. Collett D. *Modelling survival data in medical research*. Boca Raton: Chapman & Hall/CRC; 2003.
29. van 't Veer LJ, Dai H, van de Vijver MJ, He YD, Hart AA, Mao M, et al. Gene expression profiling predicts clinical outcome of breast cancer. *Nature* 2002;415:530–6.
30. Mountain CF. The new International Staging System for Lung Cancer. *Surg Clin North Am* 1987;67:925–35.
31. Bhattacharjee A, Richards WG, Staunton J, Li C, Monti S, Vasa P, et al. Classification of human lung carcinomas by mRNA expression profiling reveals distinct adenocarcinoma subclasses. *Proc Natl Acad Sci U S A* 2001;98:13790–5.
32. Hatzis P, Talianidis I. Regulatory mechanisms controlling human hepatocyte nuclear factor 4alpha gene expression. *Mol Cell Biol* 2001;21:7320–30.
33. Farragher SM, Tanney A, Kennedy RD, Paul Harkin D. RNA expression analysis from formalin fixed paraffin embedded tissues. *Histochem Cell Biol* 2008;130:435–45.
34. Cronin M, Pho M, Dutta D, Stephans JC, Shak S, Kiefer MC, et al. Measurement of gene expression in archival paraffin-embedded tissues: development and performance of a 92-gene reverse transcriptase-polymerase chain reaction assay. *Am J Pathol* 2004;164:35–42.
35. Gianni L, Zambetti M, Clark K, Baker J, Cronin M, Wu J, et al. Gene expression profiles in paraffin-embedded core biopsy tissue predict response to chemotherapy in women with locally advanced breast cancer. *J Clin Oncol* 2005;23:7265–77.
36. van't Veer LJ, Bernards R. Enabling personalized cancer medicine through analysis of gene-expression patterns. *Nature* 2008;452:564–70.
37. Loudig O, Milova E, Brandwein-Gensler M, Massimi A, Belbin TJ, Childs G, et al. Molecular restoration of archived transcriptional profiles by complementary-template reverse-transcription (CT-RT). *Nucleic Acids Res* 2007;35:e94.
38. Penland SK, Keku TO, Torrice C, He X, Krishnamurthy J, Hoadley KA, et al. RNA expression analysis of formalin-fixed paraffin-embedded tumors. *Lab Invest* 2007;87:383–91.
39. Ravo M, Mutarelli M, Ferraro L, Grober OM, Paris O, Tarallo R, et al. Quantitative expression profiling of highly degraded RNA from formalin-fixed, paraffin-embedded breast tumor biopsies by oligonucleotide microarrays. *Lab Invest* 2008;88:430–40.
40. Roberts RA, Sabalos CM, LeBlanc ML, Martel RR, Frutiger YM, Unger JM, et al. Quantitative nuclease protection assay in paraffin-embedded tissue replicates prognostic microarray gene expression in diffuse large-B-cell lymphoma. *Lab Invest* 2007;87:979–97.
41. Hoshida Y, Villanueva A, Kobayashi M, Peix J, Chiang DY, Camargo A, et al. Gene expression in fixed tissues and outcome in hepatocellular carcinoma. *N Engl J Med* 2008;359:1995–2004.
42. Hassan KA, Chen G, Kalemkerian GP, Wicha MS, Beer DG. An embryonic stem cell-like signature identifies poorly differentiated lung adenocarcinoma but not squamous cell carcinoma. *Clin Cancer Res* 2009;15:6386–90.
43. Glinisky GV, Berezovska O, Gliniskii AB. Microarray analysis identifies a death-from-cancer signature predicting therapy failure in patients with multiple types of cancer. *J Clin Invest* 2005;115:1503–21.



Cancer Research

Increased VEGFR-2 Gene Copy Is Associated with Chemoresistance and Shorter Survival in Patients with Non – Small-Cell Lung Carcinoma Who Receive Adjuvant Chemotherapy

Fei Yang, Ximing Tang, Erick Riquelme, et al.

Cancer Res 2011;71:5512-5521. Published OnlineFirst July 1, 2011.

Updated Version

Access the most recent version of this article at:
doi:[10.1158/0008-5472.CAN-10-2614](https://doi.org/10.1158/0008-5472.CAN-10-2614)

Supplementary Material

Access the most recent supplemental material at:
<http://cancerres.aacrjournals.org/content/suppl/2011/07/01/0008-5472.CAN-10-2614.DC1.html>

Cited Articles

This article cites 32 articles, 10 of which you can access for free at:
<http://cancerres.aacrjournals.org/content/71/16/5512.full.html#ref-list-1>

E-mail alerts

[Sign up to receive free email-alerts](#) related to this article or journal.

Reprints and Subscriptions

To order reprints of this article or to subscribe to the journal, contact the AACR Publications Department at pubs@aacr.org.

Permissions

To request permission to re-use all or part of this article, contact the AACR Publications Department at permissions@aacr.org.

Increased VEGFR-2 Gene Copy Is Associated with Chemoresistance and Shorter Survival in Patients with Non-Small-Cell Lung Carcinoma Who Receive Adjuvant Chemotherapy

Fei Yang^{1,9}, Ximing Tang², Erick Riquelme¹, Carmen Behrens², Monique B. Nilsson², Uma Giri², Marileila Varella-Garcia⁸, Lauren A. Byers², Heather Y. Lin³, Jing Wang⁴, Maria G. Raso¹, Luc Girard⁵, Kevin Coombes⁴, J. Jack Lee³, Roy S. Herbst², John D. Minna^{5,6,7}, John V. Heymach², and Ignacio I. Wistuba^{1,2}

Abstract

VEGF receptor-2 (VEGFR-2 or kinase insert domain receptor; KDR) is a known endothelial target also expressed in NSCLC tumor cells. We investigated the association between alterations in the *KDR* gene and clinical outcome in patients with resected non-small-cell lung carcinoma (NSCLC; $n = 248$). *KDR* copy number gains (CNG), measured by quantitative PCR and fluorescence *in situ* hybridization, were detected in 32% of tumors and associated with significantly higher *KDR* protein and higher microvessel density than tumors without CNGs. *KDR* CNGs were also associated with significantly increased risk of death ($HR = 5.16$; $P = 0.003$) in patients receiving adjuvant platinum-based chemotherapy, but no differences were observed in patients not receiving adjuvant therapy. To investigate potential mechanisms for these associations, we assessed NSCLC cell lines and found that *KDR* CNGs were significantly associated with *in vitro* resistance to platinum chemotherapy as well as increased levels of nuclear hypoxia inducible factor-1 α (HIF-1 α) in both NSCLC tumor specimens and cell lines. Furthermore, *KDR* knockdown experiments using small interfering RNA reduced platinum resistance, cell migration, and HIF-1 α levels in cells bearing *KDR* CNGs, providing evidence for direct involvement of *KDR*. No *KDR* mutations were detected in exons 7, 11, and 21 by PCR-based sequencing; however, two variant single nucleotide polymorphism genotypes were associated with favorable overall survival in adenocarcinoma patients. Our findings suggest that tumor cell *KDR* CNGs may promote a more malignant phenotype including increased chemoresistance, angiogenesis, and HIF-1 α levels, and that *KDR* CNGs may be a useful biomarker for identifying patients at high risk for recurrence after adjuvant therapy, a group that may benefit from VEGFR-2 blockade. *Cancer Res*; 71(16); 5512–21. ©2011 AACR.

Authors' Affiliations: Departments of ¹Pathology, ²Thoracic/Head and Neck Medical Oncology, ³Biostatistics, and ⁴Bioinformatics and Computational Biology, The University of Texas MD Anderson Cancer Center, Houston; ⁵Hamon Center for Therapeutic Oncology; Departments of ⁶Internal Medicine and ⁷Pharmacology, The University of Texas Southwestern Medical Center, Dallas, Texas; ⁸Department of Medicine/Medical Oncology and Pathology, University of Colorado Cancer Center, Aurora, Colorado; and ⁹Department of Pathology, Shanghai Cancer Hospital, Fudan University, Shanghai, People's Republic of China

Note: Supplementary data for this article are available at Cancer Research Online (<http://cancerres.aacrjournals.org/>).

F. Yang, X. Tang, and E. Riquelme contributed equally to the work. J. V. Heymach and I. I. Wistuba are co-senior authors of this article.

Corresponding Author: Ignacio I. Wistuba, Department of Pathology (Unit 085), The University of Texas MD Anderson Cancer Center, 1515 Holcombe Blvd, Houston, TX 77030. Phone: 713-563-9184; Fax: 713-563-1848; E-mail: iiwistuba@mdanderson.org

doi: 10.1158/0008-5472.CAN-10-2614

©2011 American Association for Cancer Research.

Introduction

Tumor growth is critically dependent on neovascularization (1). The ligand VEGF is an endothelial cell-specific mitogen known to be a highly potent and specific mediator of angiogenesis, and has 2 identified tyrosine kinase receptors, VEGF receptor-1 (VEGFR-1) and VEGF receptor-2 (VEGFR-2 or kinase insert domain receptor; KDR; refs. 2–5). The VEGFR-2 coded by the gene *KDR* (located in 4q12) is the predominant mediator of VEGF-stimulated endothelial cell functions, including cell migration, proliferation, survival, and enhancement of vascular permeability (6, 7). VEGFR-2 exhibits robust protein tyrosine kinase activity in response to the VEGF ligand (3).

In human epithelial tumors, including lung, VEGFR-2 has shown to be expressed in malignant cells as well as in the endothelial cell of tumor vasculature (8–11). In non-small-cell lung carcinoma (NSCLC), VEGFR-2 has been found to be overexpressed in malignant cells of tumor tissues, and

associated with a poor outcome (8–12). The mechanism and biological impact of VEGFR-2 overexpression of NSCLC cells, however, is not known. Recent work from our group and others has shown that tumor cell expression of VEGFR-1 may drive tumor cell invasiveness (13, 14) and promote hypoxia-independent upregulation of hypoxia inducible factor-1 α (HIF-1 α), but it is not known whether VEGFR-2 signaling directly impacts the tumor cell phenotype in NSCLC.

Recently, a relatively high frequency (9%) of mutation and amplification of *KDR* has been detected in lung adenocarcinoma histology (15); however, the presence of these abnormalities in squamous cell carcinomas of the lung is unknown. In addition, there is no data available on the correlation of *KDR* abnormalities with tumor and patients' characteristics in lung cancer, including outcome and response to therapy.

The objective of this study was to characterize the molecular abnormalities of VEGFR-2 in epithelial malignant cells of NSCLC major histology types, adenocarcinoma and squamous cell carcinoma, and correlate with patients' clinical characteristics. We studied *KDR* copy number gain (CNG), mutation, and genetic variations in malignant cells of surgically resected NSCLC tumor tissues and correlated results with pathologic features in NSCLC patients' tumors and with their platinum adjuvant treatments and outcomes. In addition, using a series of NSCLC cell lines and tissue specimens, we investigated molecular mechanisms associated with *KDR* CNG in resistance to platinum, particularly the potential role of HIF-1 α , a key regulator of angiogenesis in malignant tumors (16).

Materials and Methods

NSCLC tumor specimens

We obtained archived frozen and formalin-fixed and paraffin-embedded (FFPE) tissues from NSCLC patients who were surgically resected with curative intent from the Lung Cancer Specialized Program of Research Excellence (SPORE) tissue bank at The University of Texas MD Anderson Cancer Center (Houston, Texas). The tissue banking and the study were approved by the Institutional Review Board. We randomly selected 248 NSCLC specimens (159 adenocarcinomas and 89 squamous cell carcinomas) to test *KDR* abnormalities. Detailed clinical and pathologic information of the cases is presented in Supplementary Table S1.

KDR copy number analysis in tumor specimens

We utilized 2 methodologies to test *KDR* CNG in NSCLC tumor specimens: real-time quantitative PCR (qPCR) and fluorescence *in situ* hybridization (FISH). To enrich for malignant cell content for qPCR analysis, tumor tissues were manually microdissected from optimal cutting temperature compound-embedded frozen tissue sections for subsequent DNA extraction. Tumor DNA was extracted using Pico Pure DNA Extraction Kit (Arcturus) according to the manufacturer's instructions. DNA samples with proportions of microdissected tumor cell greater than 70% were qualified for qPCR analysis. *KDR* gene copy number was detected by qPCR using the ABI 7300 real time PCR system (Applied

Biosystems). The primers used to amplify *KDR* were KF-GACACACCCTCAGGCTCTTG and KR-ACTTTTCACCGCCT-GTTCTC. Each PCR was carried out using Power SYBR Green PCR Master Mix (Applied Biosystems) at 50°C for 2 minutes and 95°C for 10 minutes followed by 40 cycles at 95°C for 15 seconds and 60°C for 1 minute. β -Actin was introduced as the endogenous reference gene, and TaqMan Control Human Genomic DNA (Applied Biosystems) was amplified as a standard control for calibration. All sample and standard DNA reactions were set in triplicate to gauge reaction accuracy. The target gene copy number was quantified using the comparative C_t method. Gene copy number of greater than 4 was considered as CNG, as previously reported (17).

KDR copy number analysis in NSCLC malignant tumor cells was also carried out using a dual-color FISH assay developed by 1 of the coauthors (M.V.-G.). The *KDR* probe was prepared from the BAC clone RP11-21A18 obtained from CHORI. The FISH assay was conducted as we have previously published (18). Copy number analysis was done in approximately 50 nuclei per tumor in at least 4 areas. Greater than 2 gene copies per cell on average were considered as CNG.

KDR copy number and VEGFR-2 and HIF-1 α expression analyses in cell lines

All NSCLC cell lines were authenticated by DNA fingerprinting. Whole genome single nucleotide polymorphism (SNP) array profiling was carried out in 75 NSCLC cell lines using the Illumina Human1M-Duo DNA Analysis BeadChip (Illumina, Inc.). Prior to analysis, SNP data were normalized to the regional baseline copy number to account for aneuploidy. For VEGFR-2 reverse phase protein array (RPPA) analysis conducted in 63 NSCLC cell lines, protein lysate was collected from subconfluent cultures after 24 hours growth in media with 10% FBS and assayed by RPPA as previously described (19, 20). Cisplatin and carboplatin sensitivity was determined in triplicate by MTS (inner salt) assay for each cell line, and the concentration required for 50% growth inhibition (IC₅₀) was determined. For HIF-1 α expression analysis, the cells were serum starved for 24 hours and stimulated with 50 ng/mL VEGF-A (R&D Systems). Cells were incubated in normoxia, and protein lysates were collected after 8 hours. HIF-1 α ELISA (R&D Systems) was carried out according to the manufacturer's instructions (13).

Microvascular density, VEGFR-2, and HIF-1 α expression analyses in tumors

Histology sections were incubated with primary antibodies against VEGFR-2 (dilution 1:50; Abcam) for 90 minutes, CD34 (dilution 1:100; Lab Vision) for 35 minutes, and HIF-1 α (dilution 1:100; Novus Biologicals) for 65 minutes. Tissue sections were then incubated with the secondary antibody (EnVision Dual Link+; DAKO) for 30 minutes, after which diaminobenzidine chromogen was applied for 5 minutes.

Protein expression was quantified by immunohistochemistry using light microscopy with a 200 \times magnification by 2 observers (F.Y. and I.W.). Tissue samples were analyzed for VEGFR-2 expression in the cytoplasm and membrane of malignant cells and for HIF-1 α in the nucleus. We used a

4-value intensity score (0, 1+, 2+, and 3+) and the percentage (0% to 100%) of the extent of reactivity. The final score was obtained by multiplying the intensity and extent-of-reactivity values (range, 0–300). Microvascular density (MVD) was assessed by Ariol 2.0 Image System (Ariol, Genetix) using the criteria of Weidner and colleagues (21).

siRNA transfection, platinum cytotoxicity, and cell migration assays in cell lines

We transfected NSCLC cells with 3 *KDR* gene-specific siRNA duplexes and control siRNA (OriGene Technology), at a final concentration of 10 nmol/L using Lipofectamine RNAiMAX (Invitrogen) according to the manufacturer's instructions. To verify the knockdown efficiency, mRNA and protein of transfected cells were collected for real-time reverse transcriptase PCR (RT-PCR) and Western blot analyses. The assessment of *in vitro* resistance to cisplatin and carboplatin was determined by the MTS assay. NSCLC cell lines were seeded in octuplicate at a density of 2,000 per well in 96-well plates. The following day, cells were treated with cisplatin and carboplatin at various concentrations ranging from 0 to 120 μ mol/L for cisplatin and 0 to 200 μ mol/L for carboplatin. After 72 hours of drugs exposure, 20 μ L of MTS solution were added per well. Cells were incubated for 1 to 4 hours at 37°C and read at a wavelength of 490 nm. The cell migration assay using NSCLC cell lines was carried out as previously reported (13).

KDR mutation and SNPs genotyping analyses

For *KDR* mutation and SNP genotyping analysis in NSCLC cell lines, we examined exons 7, 11, 21, 26, 27, and 30, using PCR-based sequencing and intron-based PCR primers as detailed in the Supplementary Table S2.

Statistical analysis

Demographic and clinical information were compared by using the χ^2 or Fisher exact tests for category variables, and Wilcoxon rank-sum or Kruskal-Wallis tests for continuous variables. The distributions of overall survival (OS) and recurrence-free survival (RFS) were estimated by the Kaplan–Meier method and compared between groups using the log-rank test. Cox proportional hazard models were used for regression analyses of survival data and conducted on OS defined as time from surgery to death or last contact, and on RFS defined as time from surgery to recurrence or last contact. Follow-up time was censored at 5 years. For the correlation analysis of *KDR* CNG in NSCLC cell lines using the whole genome SNP arrays data with cisplatin sensitivity, we used the Wilcoxon rank sum test. The NSCLC cell lines RPPA data were quantified using the SuperCurve method which detects changes in protein level as previously reported (22).

Results

KDR gene CNG analysis

In epithelial malignant NSCLC cells microdissected from tumor tissues, *KDR* CNG was detected in 45 (32%) of 139 tumors examined. Similar frequency of *KDR* CNG was found in adenocarcinoma (26/85, 31%) and squamous cell carcinoma

(19/54, 35%) histologies ($P = 0.572$). The range of increased *KDR* copy numbers was from 4 to 11 gene copies. None of 15 normal tissue samples adjacent to the NSCLC tested showed *KDR* CNG. To confirm *KDR* CNG results by qPCR, 20 tumor specimens with *KDR* CNG by qPCR were examined by FISH. *KDR* copy gains in the malignant cells were confirmed by FISH in all 20 NSCLC specimens detected by qPCR (Fig. 1A).

Correlation between KDR CNG and VEGFR-2 protein expression and MVD

To assess the immunohistochemical (IHC) expression of VEGFR-2 in NSCLC malignant cells and the MVD (CD34) in lung tumor tissue stroma, we selected 52 lung tumor specimens with whole histologic sections from FFPE tissues. Of these, 26 cases had *KDR* CNG and 26 cases did not. VEGFR-2 protein expression was present both in the cytoplasm and membrane of malignant cells as well as in vessel endothelial cells (Fig. 1B).

Levels of VEGFR-2 expression in cytoplasm and in membrane were associated with *KDR* CNG in malignant cells of NSCLC. Tumors with *KDR* CNG showed significantly higher cytoplasmic ($P = 0.013$) and membrane ($P = 0.009$) VEGFR-2 protein expression in the malignant cells (Fig. 1C), and higher MVD ($P = 0.018$) and larger vessel areas ($P = 0.033$) in the tumor stroma than cases without *KDR* CNG (Fig. 2A and B).

Association between tumor KDR CNG, clinicopathologic features, and clinical outcome

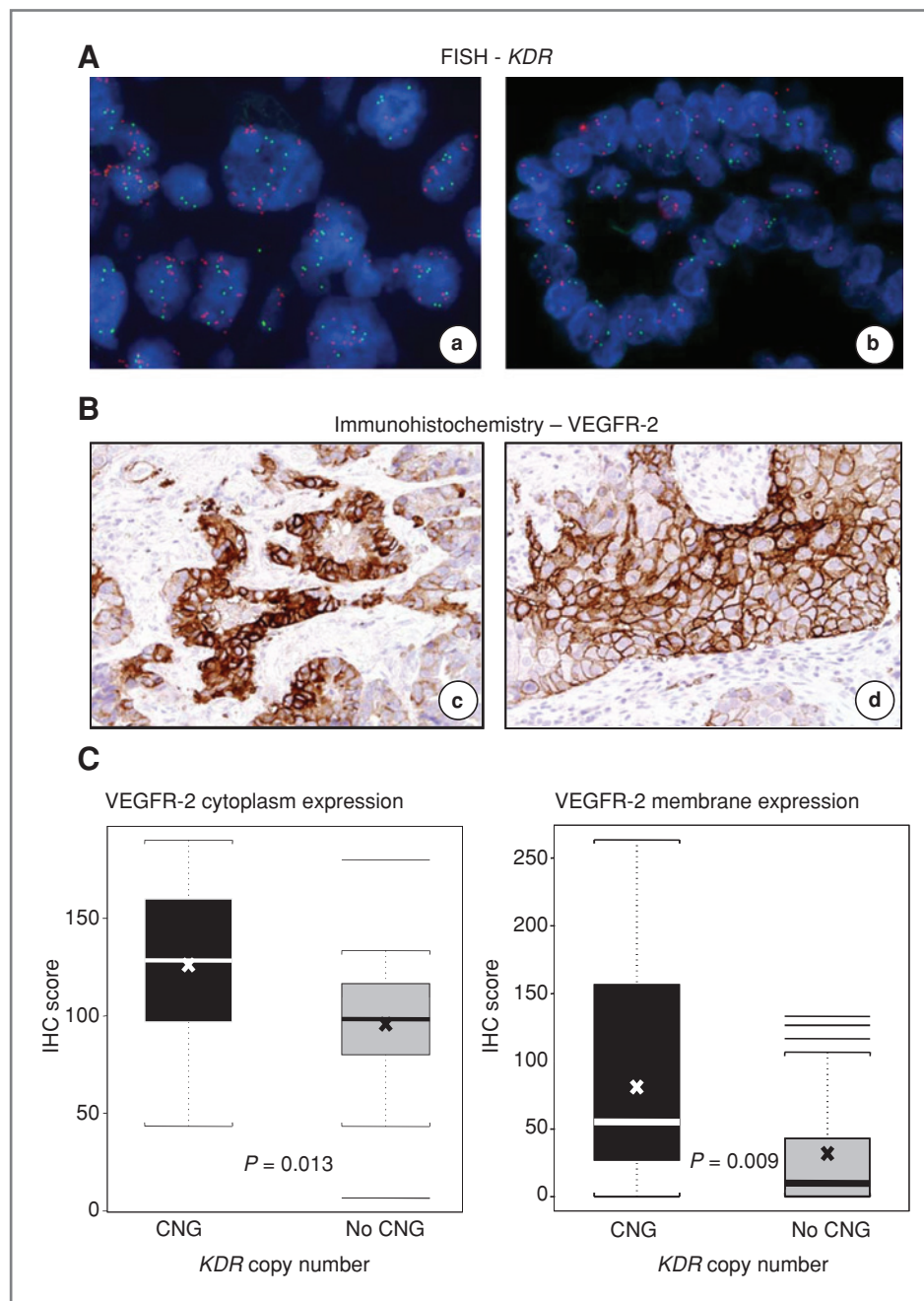
When we correlated *KDR* CNG with patients' clinicopathologic features, we did not find correlation with tumor histology, smoking status, and tumor stage. In the multivariate analysis after adjusting for stage and adjuvant therapy, *KDR* CNG was associated with poor OS (HR = 4.0; 95% CI: 1.76–9.07; $P = 0.001$) and shortened RFS (HR = 1.83, 95% CI: 1.02–3.29; $P = 0.044$) in 115 NSCLC patients who underwent surgical resection. Strikingly, *KDR* CNG was associated with a significantly worse OS (HR = 5.16, 95% CI: 1.75–15.2; $P = 0.003$) in NSCLC patients receiving platinum adjuvant therapy, but not in patients without adjuvant therapy ($P = 0.349$; Fig. 3 and Table 1). These data suggest that *KDR* CNG in malignant cells may represent a predictive marker of worse outcome in patients with surgically resected NSCLC treated with platinum-based adjuvant chemotherapy.

We also investigated and examined the impact of neoadjuvant chemotherapy on *KDR* CNGs. The platinum neoadjuvant-treated tumors (33%, 8/24) had similar frequency of *KDR* CNGs than cases without neoadjuvant therapy (32%, 37/115).

KDR CNG and VEGFR-2 protein levels and correlation with platinum resistance in cell lines

The association detected between *KDR* CNG and worse outcome in patients treated with platinum adjuvant therapy prompted us to examine the correlation between *KDR* gain and VEGFR-2 protein levels in NSCLC cell lines with *in vitro* resistance to platinum drugs. *KDR* CNG was assessed by SNP array analysis in 75 NSCLC cell lines. Cell lines with *KDR* copy gains of 6 to 9 copies or 10 or more copies above the regional baseline copy number were identified. Nineteen (25%) cell

Figure 1. *KDR* CNG correlated with VEGFR-2 protein expression in NSCLC tumors. **A**, representative examples of *KDR* copy number examined by FISH in NSCLC tissue specimens. **a**, CNG; **b**, no CNG. Red signals represent the *KDR* gene probe, and green signals the internal control probe (magnification 1,000 \times). **B**, representative example of IHC expression of VEGFR-2 in NSCLC tissue specimens. VEGFR-2 protein expression was present both in the cytoplasm and membrane of tumor cells in **(c)** adenocarcinoma and **(d)** squamous cell carcinoma (magnification 200 \times). **C**, expression of VEGFR-2 in tumors with *KDR* CNG compared with lung cancers without CNG. The box plots depict scores of IHC expression of VEGFR-2 cytoplasm and VEGFR-2 membrane comparing 26 lung cancers having *KDR* CNG with 26 lung cancers without CNG. In the box plots, bars indicate median score, \times indicates mean scores, and dashed line SD.



lines showed *KDR* CNG defined as 6 or more copies. Of these, 3 (4%) cell lines contained high-level gains (≥ 10 copies), and 16 (21%) had CNG between 6 to 9. Of interest, cisplatin sensitivity in cell lines with 6 or more *KDR* copies showed significantly more resistance to cisplatin ($P = 0.0179$; Fig. 4A).

Then, we correlated the expression of VEGFR-2 protein in a panel of 63 untreated NSCLC cell lines by RPPA with each cell line's sensitivity to cisplatin or carboplatin. We found that higher VEGFR-2 expression levels were significantly associated with resistance to both cisplatin (Fig. 4B) and carbo-

platin (data not shown) by Pearson correlation. The correlation coefficient (r) between VEGFR-2 expression and the concentration of cisplatin and carboplatin required to inhibit cell growth by 50% (IC_{50}) were 0.346 ($P = 0.005$) and 0.319 ($P = 0.011$), respectively.

Effect of *KDR* knockdown on platinum sensitivity and cell migration in cell lines

To investigate the role of *KDR* CNG and VEGFR-2 overexpression in resistance to both cisplatin and carboplatin, we

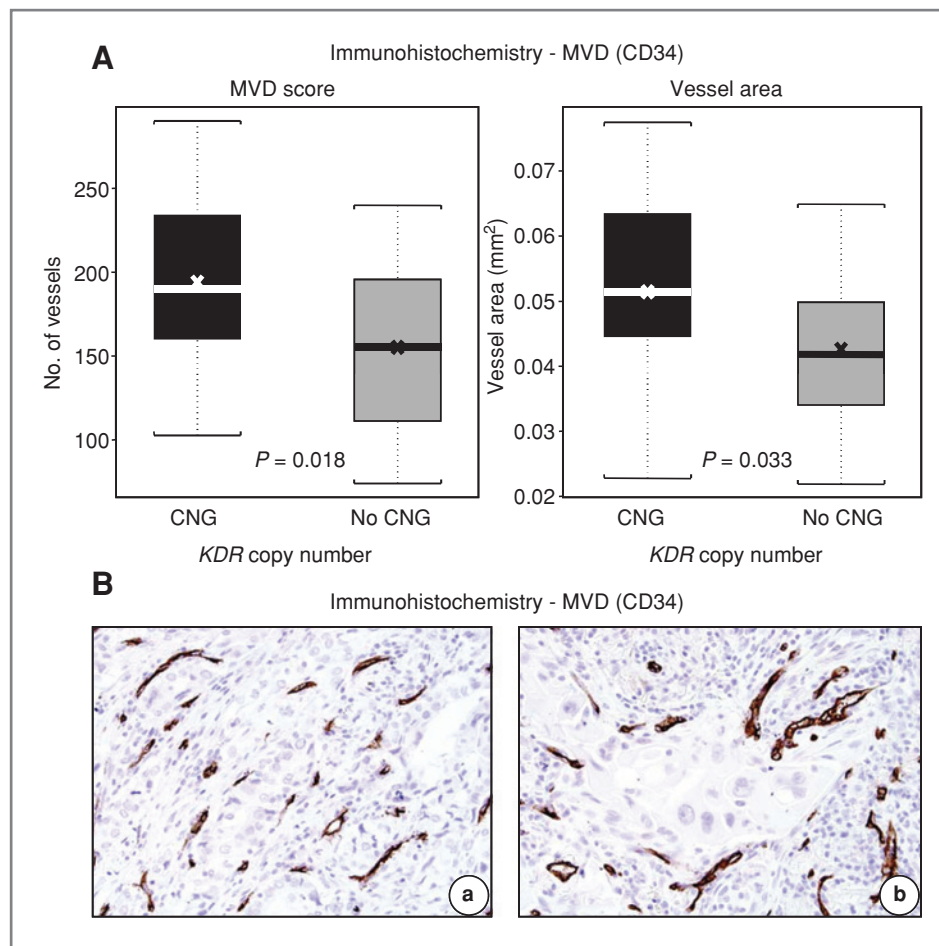


Figure 2. *KDR* CNG correlated with MVD in NSCLC tumors. **A**, expression of MVD in tumors with *KDR* CNG compared with lung cancers without CNG. The box plots depict scores of IHC assessment of MVD and vessel area (mm²) comparing tumors with and without *KDR* CNG. In the box plots, bars indicate median score, x indicates mean scores, and dashed line SD. **B**, representative example of IHC expression of CD34-positive vessels (MVD) in (a) adenocarcinoma and (b) squamous cell carcinoma (magnification 200 \times).

utilized siRNA to knock down *KDR* expression in H23 and H461 NSCLC cell lines, which contain 6 to 9 *KDR* gene copies, and as control A549 NSCLC cell line with normal *KDR* copy number. In both cell lines, siRNA targeting *KDR* significantly decreased *KDR* mRNA expression by real-time RT-PCR, and VEGFR-2 expression by Western blot, compared with control cells transfected with scrambled siRNA and nontransfected cells ($P < 0.05$; Fig. 4C). The *in vitro* sensitivity of H23 and H461 cells to cisplatin (Fig. 4D) or carboplatin (data not shown) treatment was increased in si*KDR* transfected cells compared with control siRNA-transfected or untransfected cells, suggesting that VEGFR-2 is contributing to chemoresistance in this model. This phenomenon was not observed in cell A549 with normal *KDR* copy number.

In addition, we found that knockdown of reduction of VEGFR-2 expression induced by si*KDR* transfection significantly inhibited the migration of H23 and H461 cells compared with siRNA control-transfected or untransfected cells (Fig. 4E and F).

Correlation between *KDR* CNG and HIF-1 α expression in cell lines and tumors

The observations that *KDR* CNGs were associated with increased angiogenesis, chemoresistance, and migration sug-

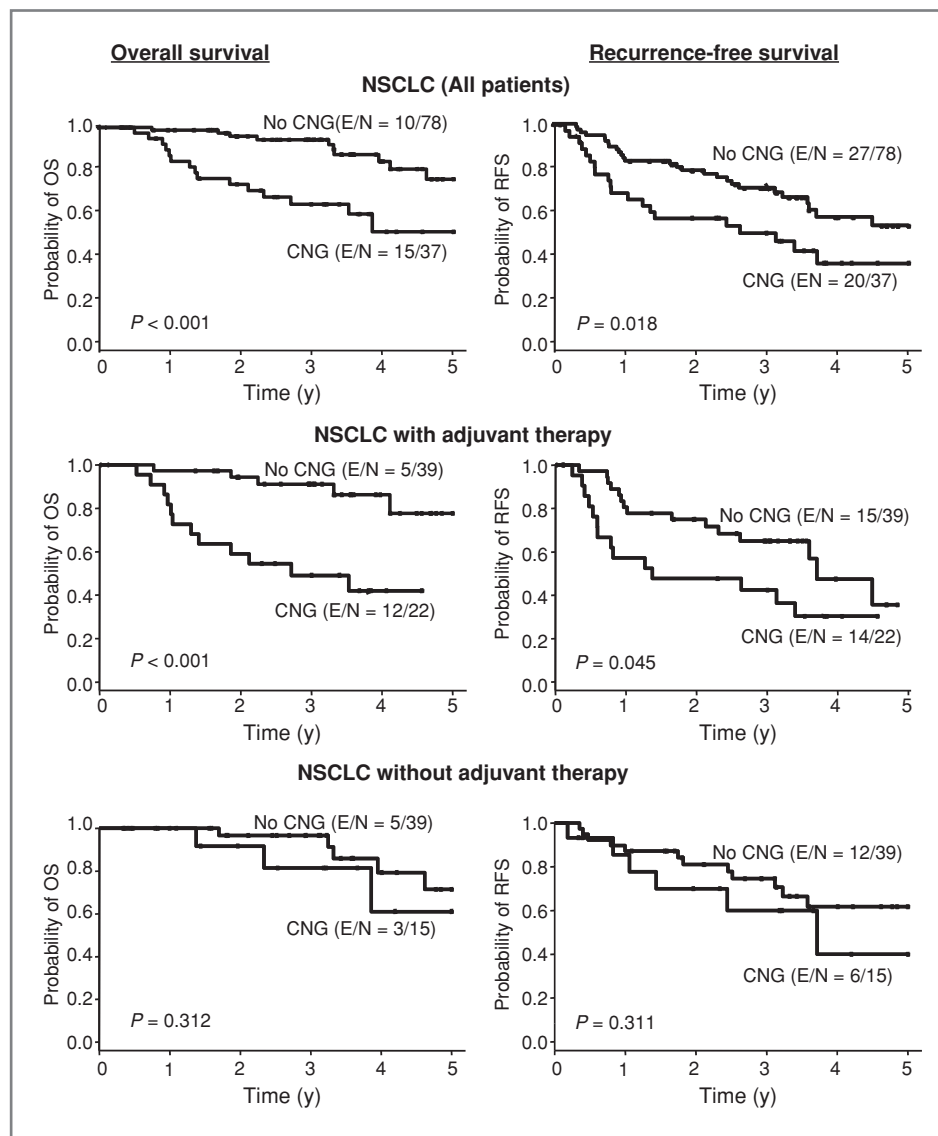
gested that VEGFR-2 may be impacting the HIF-1 α pathway, which is known to impact each of these cellular properties (13, 14). To investigate this further, we evaluated HIF-1 α levels by ELISA in a panel of NSCLC cell lines with a range of *KDR* copy numbers and expression of VEGFR-2. HIF-1 α levels were higher in cell lines with *KDR* CNG, and significantly ($P = 0.02$) higher in cells with 6 to 9 gene copies, compared with cells with no CNG (Fig. 5A). In H23 cells which have *KDR* CNG, stimulation with 50 ng/mL VEGF-A for 8 hours induced a rise in HIF-1 α expression. Furthermore, knockdown of *KDR* with siRNA significantly ($P = 0.01$) reduced HIF-1 α levels (Fig. 5B). This phenomenon was not detected in cell lines A549 with normal *KDR* copy number. These data indicated that VEGFR-2 can regulate HIF-1 α in a ligand-dependent, but hypoxia-independent, manner in NSCLC cells.

We next investigated the potential association between *KDR* CNG and HIF-1 α in NSCLC clinical specimens. Similar to the results in the NSCLC cell lines, tumor tissue specimens with *KDR* CNG ($n = 25$) showed a significantly ($P = 0.037$) higher expression of nuclear HIF-1 α expression by immunohistochemistry than tumors without CNG ($n = 22$; Fig. 5C and D).

KDR mutation and SNP analyses

To investigate whether alterations in the *KDR* gene other than CNGs may impact NSCLC tumors, we assessed the *KDR*

Figure 3. *KDR* CNG associated with outcome in NSCLC patients treated with adjuvant chemotherapy. Kaplan–Meier curve for OS and RFS by *KDR* CNG in NSCLC patients and 2 subgroups of platinum adjuvant therapy and without adjuvant therapy (E, event; N, total number of cases).



gene for mutations and SNPs. For *KDR* mutation analysis in NSCLC cell lines, we examined 6 *KDR* exons (7, 11, 21, 26, 27 and 30) they showed to be mutant in adenocarcinoma tumors

in a study published by Ding and colleagues (15). In 37 tested NSCLC cell lines, we found only 2 mutations in the *KDR* gene, an intronic T + 2A exon 11 mutation in HCC2450 and a

Table 1. Multivariate analysis for outcome by *KDR* copy gain in NSCLC patients by adjuvant chemotherapy

Cases	N	Comparison	Outcome	Adjusted HR ^a (95% CI)	P
All patients	115	Gain vs. no gain	OS	4.00 (1.76–9.07)	0.001
			RFS	1.83 (1.02–3.29)	0.044
Adjuvant therapy	61	Gain vs. no gain	OS	5.16 (1.75–15.2)	0.003
			RFS	1.87 (0.9–3.92)	0.1
No adjuvant therapy	54	Gain vs. no gain	OS	1.99 (0.47–8.4)	0.349
			RFS	1.83 (0.66–5.05)	0.243

^aAdjusting for tumor stage; follow-up is censored at 5 years.

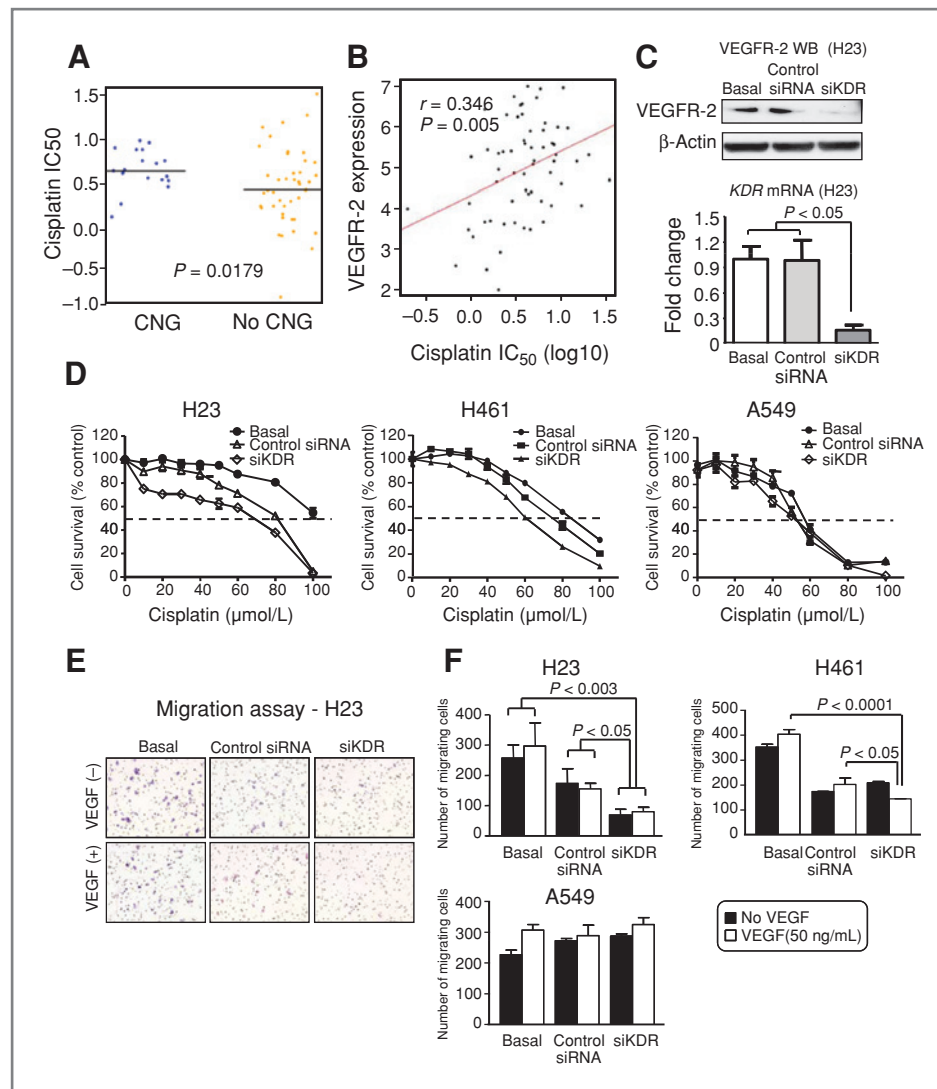


Figure 4. *KDR* CNG and VEGFR-2 expression associated with resistance to cisplatin. A, correlation of *KDR* CNG with *in vitro* resistance to cisplatin. NSCLC cell lines showing CNG (≥ 6 copies) showed significantly higher IC_{50} compared with cell lines without CNG. B, correlation between the concentrations of cisplatin required to inhibit NSCLC cell growth (IC_{50}) and VEGFR-2 protein expression levels by RPPA. C, siKDR in NSCLC cell line H23 inhibited significantly the expression of VEGFR-2 by Western blot (WB) and *KDR* mRNA by qRT-PCR compared with basal and scrambled control siRNA (bars, SD). D, knocking down *KDR* using siRNA decreased the viability of NSCLC cell lines H23 and H461 (6–9 copies) exposed to cisplatin by MTS assay (data are graphed as mean percent increase \pm percent SD). Knockdown of *KDR* in H23 cells caused 1.9-fold decrease in the cisplatin IC_{50} ($P < 0.05$) and 3.5-fold decrease in the carboplatin IC_{50} ($P < 0.05$). Knockdown of *KDR* in H461 cells caused 1.3-fold decrease in the cisplatin IC_{50} ($P < 0.05$). Knockdown of *KDR* in A549 cells did not decrease cisplatin or carboplatin IC_{50} . E, migration of NSCLC cell line H23 by Boyden chamber assay was inhibited by siKDR in cells with and without stimulation with VEGF. F, quantification of the migration assay of NSCLC cell lines before and after knocking down *KDR* using siKDR in cells with and without stimulation with VEGF showed decreased migration in H23 and H461 cells (6–9 *KDR* copies), but not in A549 cells (*KDR* no CNG; bars, SD).

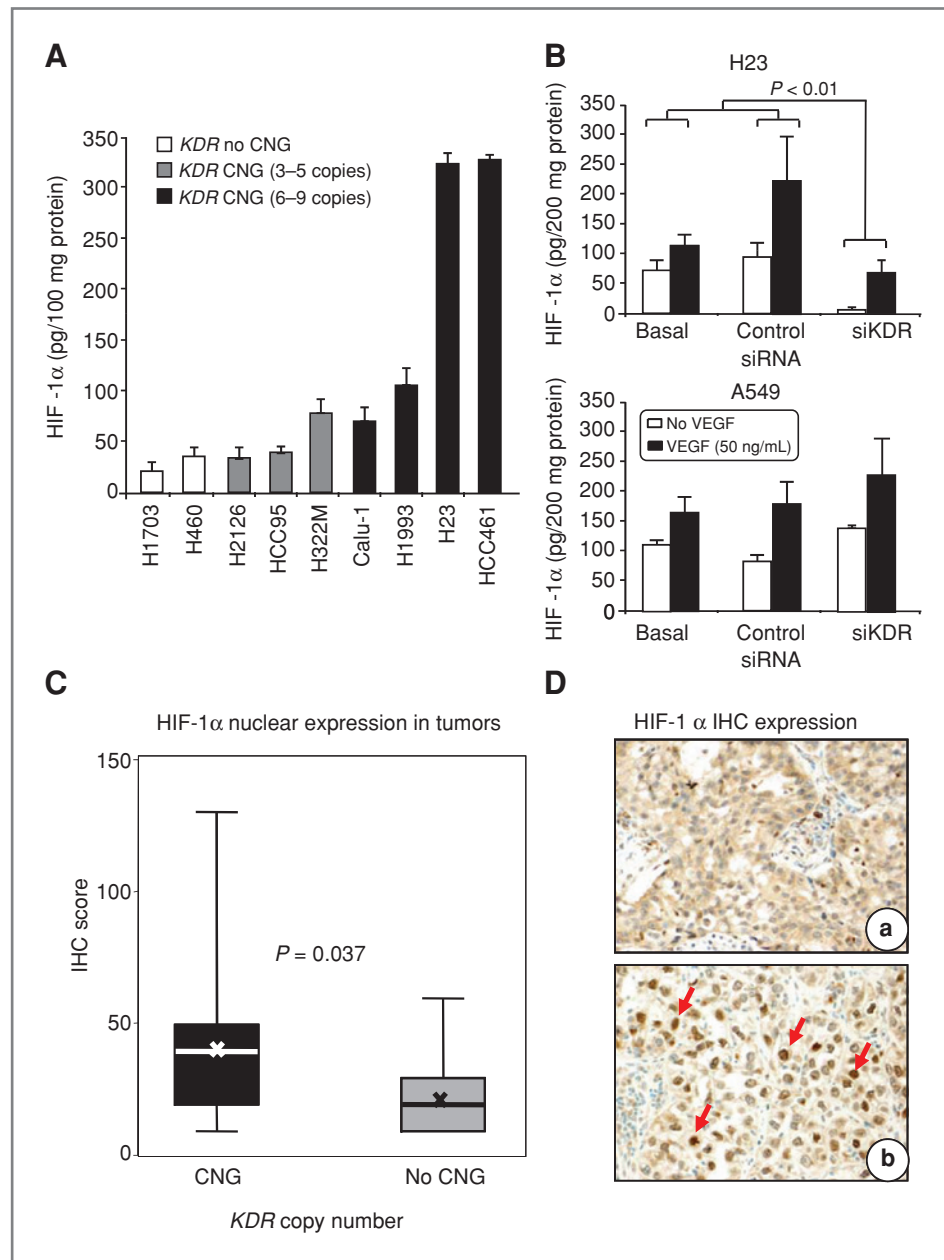
CGT946CAT point mutation in exon 21 in HCC2279. No mutation affecting exons 11 and 21 was detected in 200 NSCLC tissues specimens examined.

In addition, 3 *KDR* SNPs (889G/A, 1416A/T, and -37A/G) were genotyped in DNA extracted from 200 NSCLC tumors (Supplementary Table S3), and correlated with patients clinicopathologic features, including outcome. We did not find correlation between the SNP genotypes distribution and OS or RFS of all NSCLC patients examined. In adenocarcinoma patients both *KDR* 1416 AT/TT (HR = 0.45, 95% CI: 0.2–

0.99; $P = 0.048$) and -37AG/GG (HR = 0.43, 95% CI: 0.2–0.92; $P = 0.031$) variant genotypes were associated with a favorable OS in the multivariate analysis after adjusting for tumor stage and neoadjuvant therapy (Supplementary Fig. S1, and Supplementary Table S4).

Furthermore, among NSCLC patients with the *KDR* 889 GA/AA variant genotypes, those who received platinum neoadjuvant and/or adjuvant chemotherapy showed a significantly better OS (HR = 0.22, 95% CI: 0.05–0.94; $P = 0.041$) than patients who did not receive chemotherapy in the multivariate

Figure 5. *KDR* CNG correlated with HIF-1 α expression in NSCLC cell lines and tumor tissue specimens. **A**, HIF-1 α protein expression determined by ELISA correlated with *KDR* CNG in a series of NSCLC cell lines (bars, SD; cell lines with CNG 6–9 copies versus 3–5 copies and no CNG, $P < 0.02$). **B**, HIF-1 α expression by ELISA was markedly inhibited by knocking down using si*KDR* in NSCLC H23 cell line, with and without stimulation with VEGF (bars, SD). **C**, expression of nuclear HIF-1 α in tumors with *KDR* CNG compared with lung cancers without CNG. The box plots depict scores of IHC expression of nuclear HIF-1 α comparing 22 lung cancers having *KDR* CNG with 25 lung cancers without CNG. In the box plots, bars indicate median score, x indicates mean scores, and dashed line standard deviation. **D**, representative example of low (a, adenocarcinoma) and high (b, squamous cell carcinoma) IHC expression of HIF-1 α in NSCLC tissue specimens (magnification 200 \times). Red arrows, positive nuclear HIF-1 α immunostaining.



analysis after adjusting for histology and tumor stage. However, no survival benefit was found in NSCLC patients with *KDR* 889 GG wild genotype (HR = 1.23, 95% CI: 0.64–2.35; $P = 0.538$).

Discussion

Our study represents the first report in lung cancer showing a high frequency of *KDR* CNG (32%) in both major histology types of NSCLC, adenocarcinoma, and squamous cell carcinoma, by qPCR and confirmed in a subset of cases by FISH. Notably, *KDR* CNG predicted worse OS in patients who received platinum adjuvant therapy but not in untreated patients. In NSCLC cell

lines, we found that *KDR* CNGs were significantly associated with *in vitro* resistance to platinum chemotherapy, as well as increased levels of nuclear HIF-1 α . Furthermore, *KDR* knock-down experiments using siRNA reduced platinum resistance, cell migration, and HIF-1 α levels in cells bearing *KDR* CNGs, providing evidence for direct involvement of *KDR*. Our findings suggest that tumor cell *KDR* CNGs may promote a more malignant phenotype including increased chemoresistance, angiogenesis, and HIF-1 α levels.

In our study, tumors with *KDR* CNG in the malignant cells showed significantly higher VEGFR-2 protein expression in the cytoplasm and membrane of those cells, as well as higher MVD and larger vessel areas in the tumor stroma, compared

with tumors lacking the *KDR* CNG. One possible explanation for this association is that tumor cell VEGFR-2 binds circulating VEGF, increasing local concentrations of the ligand which in turn increases angiogenesis through effects on tumor endothelium. Another possible explanation is that VEGFR-2 overexpressing lung cancer cells may express increased levels of VEGF and other proangiogenic factors via upregulation of HIF-1 α , which in turn could promote autocrine or paracrine signaling that further increases expression. These mechanisms are not mutually exclusive and merit further investigation. Our finding of correlations between *KDR* CNG and higher expression of HIF-1 α in NSCLC cell lines and tumor specimens support the latter hypothesis. It has been showed that activation of several receptor tyrosine kinases (RTK; RET, VEGFR-1, epidermal growth factor receptor, and platelet-derived growth factor receptor) increases HIF-1 α levels in a cell-specific manner in tumors (13, 23, 24); therefore, our data represent the first evidence suggesting that VEGFR-2 may be another RTK that plays a role in increasing the levels of HIF-1 α expression in cancer.

A provocative finding of this study is this first report that *KDR* CNG in malignant cells predicted a worse outcome of NSCLC patients receiving platinum adjuvant chemotherapy after surgical resection with curative intent, but was not predictive in patients without adjuvant therapy. These findings suggest that *KDR* CNG may represent a potential biomarker for predicting resistance to adjuvant platinum-based chemotherapy in NSCLC patients. It is also noteworthy that VEGFR-2 knockdown reduced chemoresistance and cell migration, and lowered HIF-1 α levels, using *in vitro* NSCLC models. One potential implication of these findings is that VEGFR-2 blockade may sensitize tumors bearing *KDR* CNGs to chemotherapy directly through effects of the tumor cells themselves, in addition to its effect on tumor endothelial cells. *KDR* CNGs may therefore identify a group of NSCLC patients that would receive greater relative benefit from combinations of VEGF pathway inhibitors with chemotherapy than patients lacking *KDR* CNGs. Further prospective studies with larger patient cohorts are needed to assess the role of *KDR* CNG in NSCLC tumors and outcome of NSCLC patients treated with platinum-based chemotherapy in both surgically resected and advanced metastatic tumor settings, and to determine whether *KDR* CNGs are predictive of either chemoresistance or benefit for VEGF inhibitor benefit/chemotherapy combinations compared with chemotherapy alone.

Our finding that *KDR* CNG by SNP array and higher levels of VEGFR-2 expression by RPPA in a large series of NSCLC cell lines correlated significantly with *in vitro* resistance to platinum drugs (cisplatin for *KDR* CNG, and cisplatin and carboplatin for VEGFR-2 expression) provides support to our clinical observation. The increased sensitivity of the NSCLC

cell lines having *KDR* CNG to *in vitro* treatment with cisplatin or carboplatin after inhibition of *KDR* mRNA and protein expressions further supports the concept that *KDR* CNG may promote platinum resistance in NSCLC. Although the exact mechanism needs to be elucidated, we postulate that the increased expression of HIF-1 α induced by *KDR* CNG, and subsequent VEGFR-2 expression, in malignant NSCLC cells may explain increased platinum resistance in NSCLC. Interestingly, HIF-1 α has been previously associated to chemoresistance in NSCLC (25, 26) and other solid tumor types (27, 28).

The finding that inhibition of *KDR* and VEGFR-2 expression resulted in decreased NSCLC cell migration points out another new interesting role of VEGFR-2 in NSCLC malignant cells. It has been established that, among other functions, VEGFR-2 is an important mediator of VEGF-stimulated endothelial cell migration (29, 30). We have also observed that that HIF-1 α mediates migration driven by another RTK, EGFR, in NSCLC, independent of hypoxia (31).

In our study, the variant genotypes of *KDR* SNPs 1416 (AT/TT) and -37(AG/GG) associated with a favorable OS in the multivariate analysis. Ours is the first report showing association between *KDR* SNP genotypes and prognosis in lung cancer. In breast cancer patients, the *KDR* SNP 1416 A/T genotypic variant was associated with the expression of progesterone receptors, and its presence suggested a better prognosis for carriers of the T allele (32). Questions remain about the functional roles of the *KDR* SNPs responsible for the associations with outcome of NSCLC patients, particularly in adenocarcinoma patients, found in our study.

In summary, our findings indicate that *KDR* CNG was frequently detected in NSCLC tumors and associated with platinum resistance *in vivo* and *in vitro*, and may be a useful biomarker for identifying patients at high risk for recurrence after adjuvant therapy, a group that may benefit from VEGFR-2 blockade.

Disclosure of Potential Conflicts of Interest

No potential conflicts of interest were disclosed.

Grant Support

This study was supported by grants from the Department of Defense (W81XWH-07-1-0306 to J.D. Minna, J.V. Heymach, and I.I. Wistuba), the Specialized Program of Research Excellence in Lung Cancer (P50CA70907 to J.D. Minna, J.V. Heymach, and I.I. Wistuba; P50CA58187 to M. Varella-Garcia), and the National Cancer Institute (Cancer Center Support Grant CA-16672).

The costs of publication of this article were defrayed in part by the payment of page charges. This article must therefore be hereby marked *advertisement* in accordance with 18 U.S.C. Section 1734 solely to indicate this fact.

Received July 18, 2010; revised June 2, 2011; accepted June 26, 2011; published OnlineFirst July 1, 2011.

References

1. Folkman J. Tumor angiogenesis: therapeutic implications. *N Engl J Med* 1971;285:1182-6.
2. Fidler IJ, Ellis LM. The implications of angiogenesis for the biology and therapy of cancer metastasis. *Cell* 1994;79:185-8.
3. Waltenberger J, Claesson-Welsh L, Siegbahn A, Shibuya M, Heldin CH. Different signal transduction properties of KDR and Flt1, two receptors for vascular endothelial growth factor. *J Biol Chem* 1994;269:26988-95.

4. Ferrara N, Davis-Smyth T. The biology of vascular endothelial growth factor. *Endocr Rev* 1997;18:4–25.
5. Hanahan D, Weinberg RA. Hallmarks of cancer: the next generation. *Cell* 2011;144:646–74.
6. Terman BI, Carrion ME, Kovacs E, Rasmussen BA, Eddy RL, Shows TB. Identification of a new endothelial cell growth factor receptor tyrosine kinase. *Oncogene* 1991;6:1677–83.
7. Bernatchez PN, Soker S, Sirois MG. Vascular endothelial growth factor effect on endothelial cell proliferation, migration, and platelet-activating factor synthesis is Flk-1-dependent. *J Biol Chem* 1999;274:31047–54.
8. Ishii H, Yazawa T, Sato H, Suzuki T, Ikeda M, Hayashi Y, et al. Enhancement of pleural dissemination and lymph node metastasis of intrathoracic lung cancer cells by vascular endothelial growth factors (VEGFs). *Lung Cancer* 2004;45:325–37.
9. Ludovini V, Gregorc V, Pistola L, Mihaylova Z, Floriani I, Darwish S, et al. Vascular endothelial growth factor, p53, Rb, Bcl-2 expression and response to chemotherapy in advanced non-small cell lung cancer. *Lung Cancer* 2004;46:77–85.
10. Seto T, Higashiyama M, Funai H, Imamura F, Uematsu K, Seki N, et al. Prognostic value of expression of vascular endothelial growth factor and its flt-1 and KDR receptors in stage I non-small-cell lung cancer. *Lung Cancer* 2006;53:91–6.
11. Carrillo de Santa Pau E, Arias FC, Caso Pelaez E, Munoz Molina GM, Sanchez Hernandez I, Muguruza Trueba I, et al. Prognostic significance of the expression of vascular endothelial growth factors A, B, C, and D and their receptors R1, R2, and R3 in patients with nonsmall cell lung cancer. *Cancer* 2009;115:1701–12.
12. Donnem T, Al-Saad S, Al-Shibli K, Delghandi MP, Persson M, Nilsen MN, et al. Inverse prognostic impact of angiogenic marker expression in tumor cells versus stromal cells in non small cell lung cancer. *Clin Cancer Res* 2007;13:6649–57.
13. Nilsson MB, Zage PE, Zeng L, Xu L, Cascone T, Wu HK, et al. Multiple receptor tyrosine kinases regulate HIF-1alpha and HIF-2alpha in normoxia and hypoxia in neuroblastoma: implications for antiangiogenic mechanisms of multikinase inhibitors. *Oncogene* 2010;29:2938–49.
14. Roybal JD, Zang Y, Ahn YH, Yang Y, Gibbons DL, Baird BN, et al. miR-200 Inhibits lung adenocarcinoma cell invasion and metastasis by targeting Flt1/VEGFR1. *Mol Cancer Res* 2010;9:25–35.
15. Ding L, Getz G, Wheeler DA, Mardis ER, McLellan MD, Cibulskis K, et al. Somatic mutations affect key pathways in lung adenocarcinoma. *Nature* 2008;455:1069–75.
16. Du R, Lu KV, Petritsch C, Liu P, Ganss R, Passegue E, et al. HIF1alpha induces the recruitment of bone marrow-derived vascular modulatory cells to regulate tumor angiogenesis and invasion. *Cancer Cell* 2008;13:206–20.
17. Yamamoto H, Shigematsu H, Nomura M, Lockwood WW, Sato M, Okumura N, et al. PIK3CA mutations and copy number gains in human lung cancers. *Cancer Res* 2008;68:6913–21.
18. Tang X, Kadara H, Behrens C, Liu DD, Xiao Y, Rice D, et al. Abnormalities of the TITF-1 lineage-specific oncogenes in NSCLC: implications in lung cancer pathogenesis and prognosis. *Clin Cancer Res* 2011;17:2434–43.
19. Cheng KW, Lu Y, Mills GB. Assay of Rab25 function in ovarian and breast cancers. *Methods Enzymol* 2005;403:202–15.
20. Byers LA, Sen B, Saigal B, Diao L, Wang J, Nanjundan M, et al. Reciprocal regulation of c-Src and STAT3 in non-small cell lung cancer. *Clin Cancer Res* 2009;15:6852–61.
21. Weidner N, Semple JP, Welch WR, Folkman J. Tumor angiogenesis and metastasis—correlation in invasive breast carcinoma. *N Engl J Med* 1991;324:1–8.
22. Hu J, He X, Baggerly KA, Coombes KR, Hennessy BT, Mills GB. Non-parametric quantification of protein lysate arrays. *Bioinformatics* 2007;23:1986–94.
23. Hiram Y, Aoe M, Tsukuda K, Hara F, Otani Y, Koshimune R, et al. Relation of epidermal growth factor receptor, phosphorylated-Akt, and hypoxia-inducible factor-1alpha in non-small cell lung cancers. *Cancer Lett* 2004;214:157–64.
24. Phillips RJ, Mestas J, Gharaee-Kermani M, Burdick MD, Sica A, Belperio JA, et al. Epidermal growth factor and hypoxia-induced expression of CXCR4 chemokine receptor 4 on non-small cell lung cancer cells is regulated by the phosphatidylinositol 3-kinase/PTEN/AKT/mammalian target of rapamycin signaling pathway and activation of hypoxia inducible factor-1alpha. *J Biol Chem* 2005;280:22473–81.
25. Mi J, Zhang X, Rabbani ZN, Liu Y, Reddy SK, Su Z, et al. RNA aptamer-targeted inhibition of NF-kappa B suppresses non-small cell lung cancer resistance to doxorubicin. *Mol Ther* 2008;16:66–73.
26. Wen W, Ding J, Sun W, Wu K, Ning B, Gong W, et al. Suppression of cyclin D1 by hypoxia-inducible factor-1 via direct mechanism inhibits the proliferation and 5-fluorouracil-induced apoptosis of A549 cells. *Cancer Res* 2010;70:2010–9.
27. Koukourakis MI, Giatromanolaki A, Sivridis E, Simopoulos C, Turley H, Talks K, et al. Hypoxia-inducible factor (HIF1A and HIF2A), angiogenesis, and chemoradiotherapy outcome of squamous cell head-and-neck cancer. *Int J Radiat Oncol Biol Phys* 2002;53:1192–202.
28. Tan EY, Yan M, Campo L, Han C, Takano E, Turley H, et al. The key hypoxia regulated gene CAIX is upregulated in basal-like breast tumours and is associated with resistance to chemotherapy. *Br J Cancer* 2009;100:405–11.
29. Rousseau S, Houle F, Landry J, Huot J. p38 MAP kinase activation by vascular endothelial growth factor mediates actin reorganization and cell migration in human endothelial cells. *Oncogene* 1997;15:2169–77.
30. Qi JH, Claesson-Welsh L. VEGF-induced activation of phosphoinositide 3-kinase is dependent on focal adhesion kinase. *Exp Cell Res* 2001;263:173–82.
31. Xu L, Nilsson MB, Saintigny P, Cascone T, Herynk MH, Du Z, et al. Epidermal growth factor receptor regulates MET levels and invasiveness through hypoxia-inducible factor-1alpha in non-small cell lung cancer cells. *Oncogene* 2010;29:2616–27.
32. Forsti A, Jin Q, Altieri A, Johansson R, Wagner K, Enquist K, et al. Polymorphisms in the KDR and POSTN genes: association with breast cancer susceptibility and prognosis. *Breast Cancer Res Treat* 2007;101:83–93.

[Print this Page](#)

Presentation Abstract

Abstract
Number: 3685

Presentation
Title: Analysis of EZH2 and TTF-1 protein expression identifies a subset of lung adenocarcinomas with better prognosis

Presentation
Time: Tuesday, Apr 03, 2012, 8:00 AM -12:00 PM

Location: McCormick Place West (Hall F), Poster Section 25

Poster
Section: 25

Poster
Board
Number: 27

Author
Block: Carmen Behrens, Luisa Solis, Heather Lin, Ximing Tang, Ping Yuan, Humam Kadara, Erick Riquelme, Hector Galindp, Waun Ki Hong, J.Jack Lee, Ignacio I. Wistuba. UT MD Anderson Cancer Ctr., Houston, TX

Abstract
Body: Lung adenocarcinoma is a heterogeneous tumor with multiple phenotypes that have been associated with prognosis. Recently, we reported that in surgically resected adenocarcinomas, the presence of a solid histologic pattern is associated with poor prognosis. To characterize molecular targets and identify novel prognostic markers in lung adenocarcinoma, we examined by immunohistochemistry (IHC) and tissue microarrays (TMAs) the expression of 75 proteins in archival tumor tissues obtained from 204 surgically resected tumors. We selected two top markers, EZH2 (enhancer of zeste homolog 2) and TTF-1 (thyroid transcription factor-1) that had significant correlation with solid and bronchioloalveolar patterns, respectively, for more detailed clinico-pathologic analyses, including patients' outcome. EZH2 is part of a protein complex that promotes cancer development by epigenetically silencing tumor suppressor genes. TTF-1 is a transcription factor considered a potential lineage-survival oncogene in lung cancer. For EZH2 and TTF-1 IHC expression analysis, we examined 320 surgically resected lung adenocarcinomas, stages I-III, with median follow-up of 6.7 years. *EGFR* and *KRAS* mutation data were available in most cases. High nuclear EZH2 expression in tumor cells correlated with younger patient age ($P<0.0001$), smoking history ($P<0.0001$), higher TNM stage ($P=0.02$), and lack of *EGFR* mutation ($P=0.001$). High nuclear TTF-1 expression correlated with female sex ($P=0.002$), smaller tumor size ($P=0.001$), lower TNM stage ($P=0.02$), and *EGFR* mutation ($P=0.007$). EZH2 and TTF-1 expression did not correlate with *KRAS* mutation status; however, we found that their expression levels were significantly higher ($P=0.022$ and $P=0.005$, respectively) in tumors with *KRAS* CYS substitution compared with other amino acid changes. Univariate and multivariate (adjusting by other clinical prognostic factors) analyses were used to correlate EZH2 and TTF-1 expression with recurrence-free survival (RFS) and overall survival (OS). In the multivariate analysis, high EZH2 expression (≤ 42 , median score) was associated with worse RFS ($P=0.028$ HR 1.53) and OS ($P=0.0002$; HR 1.94), and high TTF-1 expression (>120 score) correlated with better OS ($P=0.004$; HR 0.62). We identified a subset (32%) of tumors with low-EZH2/high-TTF-1 that demonstrated better outcome in multivariate analysis, compared with other tumors, including RFS ($P=0.004$; HR 0.51) and OS ($P=0.0007$; HR 0.49). These tumors were more frequent in patients with female sex ($P=0.003$), never-smoking history ($P=0.004$), smaller tumor size ($P=0.018$), lower TNM stage ($P=0.024$), and *EGFR* mutation ($P=0.0001$). Our findings indicate that the combined analysis of the EZH2 and TTF-1 expression identifies a subset of lung adenocarcinoma patients with better outcome after surgical resection with curative intent. Supported by DoD grant W81XWH-07-1-0306

[American Association for Cancer Research](#)
615 Chestnut St. 17th Floor
Philadelphia, PA 19106

[Print this Page](#)

Presentation Abstract

Abstract
Number: 3454

Presentation
Title: Establishing role of KRAS mutation on NSCLC radio-sensitivity.

Presentation
Time: Tuesday, Apr 03, 2012, 8:00 AM -12:00 PM

Location: McCormick Place West (Hall F), Poster Section 17

Poster
Section: 17

Poster Board
Number: 9

Author
Block: Vikas Bhardwaj¹, Anna Likhacheva¹, Lauren A. Byers A. Byers¹, Lixia Diao¹, Pamela K. Allen¹, John D. Minna², Nathan T. Ihle¹, Garth Powis¹, Amit K. Das², Luc Girard², Michael Peyton², John Yordy², Zhongxing Liao¹, Kian K. Ang¹, Michael Story², Neda Kalhor¹, Ritsuko Komaki¹, Edward S. Kim¹, John V. Heymach¹, James Welsh¹. ¹MD Anderson Cancer Center, Houston, TX; ²UT Southwestern Medical Center, Dallas, TX

Abstract
Body: Lung cancer is the leading cause of cancer related mortality in the US of which more than 75% cases are that of non-small cell lung carcinoma (NSCLC). Mutations in the proto-oncogene KRAS have been linked with poor prognosis for NSCLC patients. In this study, we aimed at analyzing the relationship between specific KRAS mutations and NSCLC cell radiosensitivity and protein expression patterns. We analyzed 22 NSCLC cell lines and stratified them according to their KRAS status. Our results show that NSCLC cells harbouring G12C mutations are more sensitive to radiation compared to cells with other KRAS status ($SF2 = 0.35 \pm 0.16$ for G12C vs. 0.63 ± 0.17 for other KRAS mutants vs 0.54 ± 0.15 for wt KRAS). Our protein expression data suggests that G12C mutants have reduced expression of DNA-repair proteins such as ATM, Rad 50, Ku 80 and XRCC1 ($p < 0.05$) which may be responsible for their radiosensitive nature. Further we found that G12C mutant NSCLC cell lines have reduced expression of pAkt compared to cells with other KRAS status ($p = 0.009$). This suggests that NSCLC cells harboring G12C mutation would be less susceptible to PI3K inhibition induced radio-sensitization. Our clonogenic assay results confirm our finding when 1-hour pretreatment with 5 μ M LY294002 (PI3K inhibitor) sensitized H460 and A549 (non-G12C mutated NSCLC cells) but not H1792 and H23 (G12C mutant NSCLC). Our results strongly suggests that G12C KRAS mutant cells are radio-sensitive compared to NSCLC cells of other KRAS status and PI3K inhibitor therapy along with radiation could be beneficial for patients harboring non-G12C mutational KRAS status.

[American Association for Cancer Research](#)

615 Chestnut St. 17th Floor
Philadelphia, PA 19106

Investigation of poly (ADP-ribose) polymerase 1 (PARP1) as a novel therapeutic target in small cell lung cancer (SCLC)

Byers LA, Nilsson M, Fujimoto J, Saintigny P, Wang J, Diao L, Peyton M, Fan Y-H, Giri U, Weber S, Duchemann B, Girard L, Coombes K, Weinstein J, Minna JD, Wistuba I, Heymach JV

Background: Small cell lung cancer (SCLC) is an aggressive disease characterized by initial sensitivity to chemotherapy and radiation followed by the invariable development of treatment resistance. New therapies are needed to improve clinical outcomes for these patients. Using high-throughput protein array profiling, we previously demonstrated overexpression of poly (ADP-ribose) polymerase 1 (PARP1) in a panel of 35 SCLC cell lines. Here we investigated PARP1 expression in patient tumors and as a potential new therapeutic target.

Methods: PARP1 mRNA levels were assessed in publically available databases. At the protein level, total PARP1 was measured by immunohistochemistry (IHC) in a tissue microarray of archival tumor specimens. IHC scores were calculated based on the percentage of tumor cells staining positive times the staining intensity (0-3+) (possible scores 0-300). For the in vitro studies, cells were treated with a commercially available PARP inhibitor for 14 days +/- 7 days of chemotherapy and relative cell viability assessed by cell count.

Results: PARP1 mRNA was overexpressed in SCLC tumors relative to non-small cell lung cancer (NSCLC) ($p=0.005$) and normal lung tissue ($p=9.7 \times 10^{-8}$) when compared by t-test. In neuroendocrine lung tumors, total PARP1 protein levels correlated with the degree of differentiation. Highest levels were seen in SCLC ($n=12$, mean IHC score 262/300) and large cell neuroendocrine ($n=20$, mean 237/300), while intermediate levels were seen in atypical carcinoid ($n=9$, mean 230/300) and typical carcinoid ($n=55$, mean 197/300). In contrast, PARP1 expression was significantly lower in NSCLC with squamous ($n=15$, mean 120/300) and adenocarcinoma ($n=24$, mean 104/300) histologies. Preliminary in vitro testing showed sensitivity of SCLC and LCNEC cell lines to PARP inhibition, but resistance in NSCLC lines. When combined with cisplatin and etoposide in a SCLC line, cell viability was further decreased beyond that of chemotherapy or PARP inhibitor alone.

Conclusions: PARP1 is highly expressed in high-grade neuroendocrine lung tumors at the mRNA and protein level. PARP1 inhibition alone and in combination with chemotherapy showed activity in SCLC and LCNEC lines. These findings support further investigation of PARP1 as a potential novel therapeutic target in high-grade neuroendocrine lung cancers.

An epithelial to mesenchymal transition (EMT) gene expression signature predicts resistance to PI3K/Akt pathway inhibitors in non-small cell lung cancer

Lauren Averett Byers¹, Jing Wang¹, Lixia Diao¹, Luc Girard², Michael Peyton², Kevin R. Coombes¹, John N. Weinstein¹, Varsha Gandhi¹, Nancy Krett³, Steven T. Rosen³, John D. Minna², John V. Heymach¹. ¹UT MD Anderson Cancer Ctr., Houston, TX; ²Hamon Center for Therapeutic Oncology Research, UT Southwestern Medical Center, Dallas, TX; ³Robert H. Lurie Comprehensive Cancer Center, Northwestern University, Chicago, IL

Background: Epithelial/mesenchymal transition (EMT) is associated with loss of cell adhesion molecules such as E-cadherin and increased invasion, migration, and proliferation in epithelial cancers. In non-small cell lung cancer (NSCLC), EMT is associated with greater resistance to EGFR inhibitors. However, its potential to predict response to other targeted drugs or chemotherapy has not been well characterized. Using a previously-derived EMT gene signature, we tested the association between EMT and drug response in a panel of >50 NSCLC cell lines.

Materials/Methods: NSCLC cell lines were classified as epithelial or mesenchymal by a previously described 76-gene EMT gene expression signature. IC50s for more than 30 drugs or drug combinations were determined by MTS assay. Differences in IC50 between epithelial and mesenchymal lines were assessed by t-test (p-values ≤ 0.05 were considered significant).

Results: As expected, EGFR mutated cell lines were classified by the EMT signature as epithelial and were highly sensitive to EGFR inhibition by erlotinib. Among wild-type EGFR cell lines, those that had undergone EMT were significantly more resistance to erlotinib (p=0.029). NSCLC cell lines with mesenchymal signatures were also more resistant to drugs targeting the PI3K/Akt pathway such as GDC0941 (p=0.037) and 8-amino-adenosine (p=0.009). A trend towards greater resistance was also seen in mesenchymal cells treated with the Akt inhibitor MK2206 (p=0.12). There was no association between EMT and response to cytotoxic chemotherapies, including cisplatin, carboplatin, gemcitabine, pemetrexed, docetaxel, paclitaxel, and platinum-doublets (p-values ≥ 0.2).

Conclusion: EMT is associated with greater resistance to PI3K/Akt pathway inhibitors and may be a useful predictive marker for patients treated with these drugs. The EMT signature is being investigated prospectively in patients treated with an Akt inhibitor in an ongoing clinical trial.

[Print this Page](#)

Presentation Abstract

Abstract
Number: 5605

Presentation
Title: ***LKB1* and *KRAS* mutations predict resistance to PI3K/Akt inhibitors in non-small cell lung cancer**

Presentation
Time: Wednesday, Apr 04, 2012, 8:00 AM -12:00 PM

Location: McCormick Place West (Hall F), Poster Section 29

Poster
Section: 29

Poster Board
Number: 14

Author
Block: Lauren Averett Byers¹, Lixia Diao¹, Jing Wang¹, Luc Girard², Michael Peyton², Adi Gazdar², Philip Groth³, Julianne Paul³, Ningshu Liu³, Edward S. Kim¹, David Mauro⁴, Roy S. Herbst⁵, Vali Papadimitrakopoulou¹, Kevin R. Coombes¹, John N. Weinstein¹, John D. Minna², John V. Heymach¹. ¹UT MD Anderson Cancer Ctr., Houston, TX; ²UT Southwestern, Houston, TX; ³Bayer Schering Pharma AG, Berlin, Germany; ⁴Merck, Whitehouse Station, NJ; ⁵Yale Comprehensive Cancer Center, New Haven, CT

Abstract
Body: **Background:** *LKB1* and *KRAS* are the most commonly mutated genes in non-small cell lung cancer (NSCLC), each present in up to 35% of patient tumors. *KRAS* mutations have been associated with resistance to EGFR tyrosine kinase inhibitors, but it is not established to what extent *KRAS* or *LKB1* mutations may predict response to other systemic treatments, including PI3K/Akt and MEK inhibitors. **Methods:** IC₅₀s for cytotoxic chemotherapies and targeted drugs were determined by MTS assay in a large panel of NSCLC cell lines with known mutational status. Cells lines with and without mutations were compared by t-test and linear mixed model to determine the effect of single and double mutations. Protein expression in cell lines was measured by reverse phase protein array. **Results:** *LKB1* mutations strongly predicted resistance to Akt inhibition by MK2206 (p=0.004), but not to PI3K inhibitors BAY80-6949, GDC0941, or 8-amino-adenosine (p>0.24). In contrast, *KRAS* mutations were strongly associated with resistance to PI3K inhibitors BAY80-6949 (p≤0.0001) and GDC0941 (p=0.034) and to Akt inhibition by MK2206 (p=0.047). Conversely, there was a trend towards greater sensitivity in the *KRAS* mutated cells to the MEK inhibitor BAY86-9766. Resistance to PI3K inhibition in *KRAS* mutated lines was largely abrogated by the combination of BAY80-6949 and BAY86-9766. Co-existing *LKB1* and *KRAS* mutations were present in 18% of cell lines, but were not significantly more resistant to PI3K/Akt inhibitors, nor did they predict greater MEK inhibitor sensitivity. There was no association between *KRAS* or *LKB1* mutations and response to cytotoxic chemotherapies, including docetaxel, pemetrexed, or platinum doublets. At the protein level, *LKB1* mutant cell lines had significantly higher expression of IGF1R (p<0.0001 by t-test), compared to wild type cell lines, which may represent an alternative signaling pathway contributing to resistance in mutant cell lines. **Conclusions:** *KRAS* and *LKB1* mutations are associated with greater resistance to PI3K/Akt inhibitors, although there are some differences in resistance with specific drugs. These findings suggest that these mutations may have potential as predictive biomarkers and warrant further investigation prospectively in clinical trials of PI3K, Akt, and MEK inhibitors. In addition, the observation of increased protein expression of IGF1R in *LKB1* mutated lines supports a rationale for combining PI3K/Akt and IGF1R inhibitors as a strategy to overcome resistance.

[American Association for Cancer Research](#)
615 Chestnut St. 17th Floor
Philadelphia, PA 19106

[Print this Page](#)

Presentation Abstract

Abstract
Number: LB-347

Presentation
Title: **Identify signaling responses to MEK inhibitor AZD6244 in lung cancer cells with proteomics reverse phase protein array**

Presentation
Time: Tuesday, Apr 03, 2012, 1:00 PM - 5:00 PM

Location: McCormick Place West (Hall F), Poster Section 39

Author *Bingbing Dai, Wenbin Liu, John V. Heymach, Lauren A. Byers, Jing Wang, Kevin R. Coombes, Bingliang Fang, Jack A. Roth.* UT MD
Block: Anderson Cancer Ctr., Houston, TX

Abstract
Body: AZD6244 is small-molecule inhibitor that targets the MAPK pathway, and is currently in phase I/II clinical evaluation. While some efficacy of these agents has been observed in phase I/II clinical trials, one of the hurdles of targeted therapy is the intrinsic and acquired resistance mediated by complex feedback pathways. Identifying downstream effectors required for cellular response to MEK inhibitors will help us understand the mechanism of resistance, possibly leading to the development of direct therapeutic targets. Explore the signaling responses after treatment with MEK inhibitors will also allow us to identify signaling feedback loops and cross talks. We used reverse phase protein array (RPPA) technology to determine which downstream effectors of MEK/ERK pathways critical for cell growth inhibition or apoptosis induced by MEK inhibitors, and to identify which signaling pathways are inhibited or activated when the pathways is blocked. RPPA is a antibody-based quantitative assay used to analyze nanoliter amounts of sample for 200 proteins to determine expression levels and protein modifications such as phosphorylation or cleavage. Experiments were carried out in 5 resistant and 5 sensitive cell lines with the MEK inhibitor, AZD6244. Cells were treated at different time points (0, 6, 12, 24, 48, and 72 hours) and with various dosages (0, 0.3, 1, 3 and 10 μ M). Cell lysates were collected and quantified for RPPA assays. The data was analyzed for the presence of clusters based on differential protein expression by using available methods with a statistical software package (StatSoft, Tulsa, OK). Significantly changed proteins were analyzed with Ingenuity Pathway Analysis (IPA). Proteins Data from RPPA was further validated by using Western blotting with the same antibody used in the RPPA assay. The results showed that inhibition of MEK/ERK could activate multiple signaling pathways including AKT, SRC, STAT3 and IGF1R. Activation of those signaling pathway through signaling cross talk and feedbacks may involved in the intrinsic and acquitted resistance to MEK inhibitor. We also indentified a penal of molecules, such as BIM, P27, p53 and JNK were specifically induced only in the sensitive cells. Those molecules might be the mediators of MEK inhibitor induced cell apoptosis. The results will be helpful in understanding of the signaling cross talks and feedbacks and in the exploration of mechanisms of sensitivity and resistance to the treatment with MEK inhibitors in lung cancer.

[American Association for Cancer Research](#)
615 Chestnut St. 17th Floor
Philadelphia, PA 19106

[Print this Page](#)

Presentation Abstract

Abstract
Number: 821

Presentation
Title: Developing a molecular understanding of non small cell lung cancer (NSCLC) resistance to platin-taxane chemotherapy

Presentation
Time: Sunday, Apr 01, 2012, 1:00 PM - 5:00 PM

Location: McCormick Place West (Hall F), Poster Section 31

Poster
Section: 31

Poster Board
Number: 8

Author
Block: Maithili P. Dalvi¹, Carmen Behrens², Milind Suraokar², Luc Girard¹, Yang Xie¹, Ignacio Wistuba², John D. Minna¹. ¹UT Southwestern Medical Center, Dallas, TX; ²The University of Texas MD Anderson Cancer Center, Houston, TX

Abstract Body: **Purpose:** While chemotherapy has improved lung cancer patient survival, relapse rates after neoadjuvant or adjuvant chemotherapy (minimal residual disease settings) are high. This could be due to cancer cells acquiring resistance to therapy or selective survival of pre-existing resistant cells. The molecular basis for primary or acquired resistance to standard platinum doublet chemotherapies are unknown and their elucidation is necessary for developing curative therapy that can be personalized for each patient. **Methods:** 3 complementary approaches were used to explore mechanisms underlying NSCLC resistance to platin-taxane chemotherapy: A) NSCLC lines were exposed *in vitro* to cycles of paclitaxel + carboplatin to mimic clinical treatment and resistance validated with cell viability and colony formation assays. Genome wide mRNA expression profiles of resistant and parental lines were compared using Illumina arrays and qRT-PCR. B) A large dataset of clinically and molecularly annotated NSCLC tumor specimens obtained after no chemotherapy or neoadjuvant platin-taxane chemotherapy were subjected to mRNA microarray analysis. C) Lung cancer xenografts were treated with chemotherapy *in vivo* in mice and profiled for mRNA expression. Biostatistical and bioinformatics approaches were used to identify genes that are differentially expressed in resistant cells in these three settings, and their function studied using over-expression or shRNA mediated knockdown. **Results:** NSCLC lines H1299 and H1355 were treated *in vitro* with paclitaxel + carboplatin and showed progressive increases in resistance to chemotherapy (after 5 to 15 cycles) ultimately achieving 30 (H1299) or 60 fold (H1355) differences compared to parental cells. In addition, multiple single cell clones also demonstrated chemotherapy resistance. Resistant NSCLC strains were also resistant to platin+docetaxel and platin+pemetrexed combinations. Expression profiles revealed upregulation of *ABCB1/MDR1*, down regulation of epithelial-specific genes suggesting EMT, differences in expression of epigenetic modulators as well as cancer testis family of GAGE genes and many of these genes had expression correlated with recurrence after neoadjuvant chemotherapy and with poor survival. Resistance was only partially reversed by verapamil indicating that it can be only partly explained by MDR mechanisms. Mechanistic studies of genes identified by these three approaches provide opportunities for overcoming chemotherapy resistance and developing novel therapies for NSCLC. **Grant support:** UT-Lung SPORE (5 P50 CA70907-11) and DoD PROSPECT (W81XWH-07-1-0306)

[American Association for Cancer Research](#)
615 Chestnut St. 17th Floor
Philadelphia, PA 19106

[Print this Page](#)

Presentation Abstract

Abstract
Number: 140

Presentation
Title: microRNA regulation of cell viability and drug response in cancer

Presentation
Time: Sunday, Apr 01, 2012, 1:00 PM - 5:00 PM

Location: McCormick Place West (Hall F), Poster Section 5

Poster
Section: 5

Poster Board
Number: 22

Author
Block: Liqin Du¹, Christopher DeSevo², Robert Borkowski², Michael Baker², Ignacio Wistuba³, John Minna², Alexander Pertsemlidis¹. ¹UT Health Science Center at San Antonio, San Antonio, TX; ²UT Southwestern Medical Center, Dallas, TX; ³UT MD Anderson Cancer Center, Houston, TX

Abstract
Body: Lung cancer is the leading cause of cancer-related deaths, with the majority of deaths due to failed therapy from tumor drug resistance. Third-generation chemotherapeutic agents represent the standard first-line treatment for advanced small cell (SCLC) and non-small cell (NSCLC) lung cancer patients. Response rates are poor (20-40%) with a median survival of 8-10 months. In an unbiased and comprehensive approach, we have combined a high-throughput screening platform with a library of chemically synthesized microRNA mimics and inhibitors. We have used this platform to identify mimics and inhibitors that reduce cell viability in general, and those that specifically sensitize cells to taxanes. We have identified several miRNAs for which over-expression or inhibition has a dramatic and selective effect on cell viability or drug response. We have demonstrated that miR-337-3p mimic sensitizes NSCLC cells to taxanes. By combining in vitro and in silico approaches, we identified STAT3 and RAP1A as direct targets that mediate the effect of miR-337-3p by enhancing taxane-induced arrest in the G2 phase of the cell cycle. We have identified an inhibitor of miR-139-5p as a potent and selective regulator of SCLC cell viability. Inhibiting miR-139-5p decreases SCLC cell viability by over 80%, but has a minimal cytotoxic effect on that of NSCLCs or immortalized human bronchial epithelial cells. We are currently investigating the targets of miR-139-5p that mediate its effect on SCLC cell viability. We also identified miR-10a inhibitor as increasing cell viability, with the converse observed for miR-10a mimic, suggesting that miR-10a acts as a tumor suppressor gene by directly decreasing expression of gene(s) that promote cell survival and growth. Manipulation of miR-10a levels also resulted in significant changes in both mRNA and protein levels of its predicted target, the catalytic subunit of phosphatidylinositol 3-kinase (PI3K), which has been shown to play a major role in proliferation and survival in a number of human cancers and is a significant therapeutic target. We have identified miR-337-3p as a regulator of taxane sensitivity, and miR-10a and miR-139-5p as modulators of cell viability. Increasing levels of miR-337-3p and inhibiting miR-10a and miR-139-5p may therefore provide novel therapeutic tools for the treatment of NSCLC and SCLC.

[American Association for Cancer Research](#)

615 Chestnut St. 17th Floor
Philadelphia, PA 19106

[Print this Page](#)

Presentation Abstract

Abstract
Number: 272

Presentation
Title: Nanoscale high-throughput quantitative RT-PCR for the characterization of targeted-therapy related molecular biomarkers from recurrent and non-recurrent NSCLC tissues

Presentation
Time: Sunday, Apr 01, 2012, 1:00 PM - 5:00 PM

Location: McCormick Place West (Hall F), Poster Section 10

Poster
Section: 10

Poster Board
Number: 6

Author
Block: Heidi S. Erickson¹, Katherine Hale¹, Lixia Diao¹, Angela Silvestro², Christina McDowell¹, M. Gabriela Raso¹, M. Carmen Behrens¹, Elen Ortenberg², Doug Roberts², Joe Heath³, Brian T. Hennessy¹, Gordon Mills¹, Jing Wang¹, Ignacio Wistuba¹. ¹UT MD Anderson Cancer Center, Houston, TX; ²Life Technologies, Carlsbad, CA; ³NuGEN Technologies, Inc, San Carlos, CA

Abstract
Body: Currently, there are no good biomarkers to predict targeted therapy outcomes for patients whose cancers recur vs. those that do not. Technology limitations have prevented extensive qRT-PCR biomarker analysis on small tumor tissue samples obtained in our unique lung cancer MD Anderson BATTLE clinical trials. Clinical sample size limitations are inherent due to the extremely small core needle biopsies (CNB) and fine needle aspirates (FNA). Identifying technology that can reliably analyze, in a quantitative manner, molecular biomarker signatures of 200-300 genes from CNB and FNA, will allow for comparative analysis of patients' untreated tumor with treated follow-up tissue samples. We hypothesize RNA amplification coupled with nanoscale high-throughput (HT) qRT-PCR, will allow analysis of 320 gene expression patterns from 10ng RNA from frozen NSCLC tissues. We believe primary NSCLC tumors that recur have a different pattern of molecular abnormalities than NSCLCs from non-recurrent tumors (≤ 5 years), possibly accounting for lack of response to targeted therapy in some patients.

RNA from 40 frozen adenocarcinoma (ADC) NSCLC tumor and matched normal cases with annotated clinicopathologic data was extracted/isolated and quantity/quality measured. 10ng from each sample was pre-amplified by WT-Ovation Pico protocol (NuGEN). Nanoscale high-throughput OpenArray quantitative RT-PCR (Life Technologies) with SYBR chemistry and DLD platform TaqMan chemistry was used to analyze 206 and 94 genes of interest, respectively, and 18 endogenous controls (EC). EC geometric mean was used for data normalization. Two-sample t-test was applied as test statistic for identifying differentially expressed genes in respect to recurrence, clinical stage, race and gender. Statistical significant level was set as $p \leq 0.05$. Statistical analysis was conducted using R packages.

WT-Ovation Pico protocol successfully amplified all 10ng samples (mean = 235.2ng/ul, 1.94 260/280). OpenArray qRT-PCR successfully produced quantitative gene expression measurements as assessed by technical replicates (SD, median = 0.14; range = 0.00 to 12.70; $R=0.931$) and sample to sample correlation from chip to chip for each gene (Spearman Rho median = 0.3; range = -0.44 to 0.82). 14 genes included in the SYBR subset (KDR↓, SLCO4A1↓, ESR1↓, TIE1↓, EZH2↓, VEGFA↓, ADM↓, CYP1A1↓, NEO1↓, CXCL5↓, FGFR2↓, HMBS↓, ID1↑, NRP2↓) and 3 genes included in the TaqMan subset (DDX20↑, CIDEA↓, PERP↓) were significantly dysregulated in recurrent vs. non-recurrent ADC NSCLCs.

Amplification coupled with nanoscale HT qRT-PCR allowed for 320 quantitative gene expression measurements from 10ng RNA from NSCLC tissue. Data identified 17 genes with significantly dysregulated expression in recurrent vs. non-recurrent ADC NSCLCs. Supported in part by DoD PROSPECT grant W81XWH-07-1-0306.

[American Association for Cancer Research](#)
615 Chestnut St. 17th Floor
Philadelphia, PA 19106

[Print this Page](#)

Presentation Abstract

Abstract
Number: 1711

Presentation
Title: Expression patterns of the G protein-coupled receptor, GPRC5A, in human malignant pleural mesothelioma

Presentation
Time: Monday, Apr 02, 2012, 8:00 AM -12:00 PM

Location: McCormick Place West (Hall F), Poster Section 26

Poster
Section: 26

Poster
Board
Number: 1

Author
Block: Junya Fujimoto¹, Humam Kadara¹, Junya Fukuoka², Keisuke Aoe³, Nobukazu Fujimoto⁴, Takumi Kishimoto⁴, Kouki Inai⁵, Kenzo Hiroshima⁶, Milind Suraokar¹, Anne Tsao¹, Reza Mehran¹. ¹UT MD Anderson Cancer Ctr., Houston, TX; ²Toyama University Hospital, Toyama, Japan; ³NHO Yamaguchi-Ube Medical Center, Ube, Japan; ⁴Okayama Rosai Hospital, Okayama, Japan; ⁵Hiroshima University Graduate School of Biomedical Sciences, Hiroshima, Japan; ⁶Tokyo Women's Medical University, Yachiyo Medical Center, Yachiyo, Japan

Abstract
Body: The G protein-coupled receptor family C group 5 member A (hGPRC5A, mGprc5a) was previously shown to function as a lung-specific tumor suppressor gene evidenced by the development of lung adenomas and adenocarcinomas in mice with knockout of the gene. Moreover, we have demonstrated that the immunohistochemical expression of GPRC5A protein was significantly lower in non-small cell lung cancer (NSCLC) resected specimens compared to normal bronchial epithelia from healthy individuals. The latter findings prompted us to examine the expression patterns of GPRC5A in malignant pleural mesothelioma (MPM) because, like NSCLC, this malignancy develops in the thoracic cavity. Analysis of two publicly available MPM microarray datasets revealed that GPRC5A mRNA expression is significantly higher in MPMs compared to matched normal pleura (5.5 fold higher, $p=0.002$; 6.57 fold higher, $p=0.04$). GPRC5A immunohistochemical protein expression was semi-quantitatively assessed in formalin-fixed paraffin embedded (FFPE) MPM surgical specimens ($n=73$) comprised of 41 epitheloid, 14 biphasic and 18 sarcomatoid type MPMs. GPRC5A protein expression was also assessed in a subset of the MPM specimens ($n=51$) that were reconstructed as high-density spiral tissue microarrays (TMA) developed by J. Fukuoka and colleagues (Sakura-Finetek, Tokyo, Japan) comprised of 35 epitheloid, 9 biphasic and 7 sarcomatoid type MPMs. ANOVA analysis demonstrated significant differences in GPRC5A immunohistochemical expression among MPMs based on the histological subtype ($p<10^{-6}$) with relative highest expression in the epitheloid tumors (mean, 98.04 ± 54.55 ; min, 0; max, 200), intermediate expression in biphasic-type tumors (mean, 53.57 ± 38.55 ; min, 0, max, 140) and lowest expression in sarcomatoid-type MPMs (mean, 24.44 ± 21.48 ; min, 0; max, 70). The patterns of GPRC5A expression based on histological type of surgical MPM specimens were corroborated using the spiral TMA technology with relative highest expression in the epitheloid tumors lowest expression in sarcomatoid-type MPMs. Importantly, GPRC5A immunohistochemical protein expression was positively significantly correlated between the surgical and spiral TMA specimens ($R=0.71$, $p<10^{-6}$). We then sought to examine the association of GPRC5A expression with overall survival in MPM. GPRC5A expression was not associated with overall survival when all histological-type MPMs were included. Interestingly, patients with non-epitheloid type MPMs with relatively higher GPRC5A expression exhibited significantly worse overall survival compared to MPM patients with similar histology and lower expression ($p=0.02$ of the log-rank test). These findings suggest that GPRC5A may function as an oncogene in MPMs and warrant further studies to probe the function of this receptor in mesotheliomas. Supported by DoD PROSPECT grant W81XWH-07-1-0306.

[American Association for Cancer Research](#)

615 Chestnut St. 17th Floor
Philadelphia, PA 19106

epithelial and stromal CD4+, CD8+, and CD20+ lymphocytes.

Results: In univariate analyses, increasing numbers of epithelial CD8+ ($P = 0.023$), stromal CD8+ ($P = 0.002$), epithelial CD20+ ($P = 0.023$), stromal CD20+ ($P < 0.001$), and stromal CD4+ ($P < 0.001$) lymphocytes correlated significantly with an improved disease-specific survival. No such relation was noted for epithelial CD4+ cells. Furthermore, a low level of stromal CD8+ lymphocyte infiltration was associated with an increased incidence of angiolymphatic invasion ($P = 0.032$). In multivariate analyses, a high number of stromal CD8+ ($P = 0.043$) and CD4+ ($P = 0.002$) cells were independent positive prognostic factors for disease-specific survival.

Conclusion: High densities of CD4+ and CD8+ lymphocytes in the stroma are independent positive prognostic indicators for resected NSCLC patients. This may suggest that these cells are mediating a strong antitumor immune response in NSCLC.

Poster Session 2 – Prognostic and Predictive Markers Tuesday, 5 July 2011 12:15-14:00

P2.078 ABERRANT SIGNAL TRANSDUCTION AND DNA DAMAGE RESPONSE PATHWAYS IN PRIMARY LUNG CANCER

Yong He¹, Zhen Zhou², Wayne L. Hofstetter³, Yanbin Zhou³, Wenxian Hu³, Apar Pataer³, Arlene M. Correa³, Yiling Lu³, Jing Wang³, Lixia Diao³, Lauren A. Byers³, Ignacio Wistuba³, Jack A. Roth³, Stephen G. Swisher³, John V. Heymach³, Bingliang Fang⁴

¹Thoracic Surgery, Daping Hospital/China,

²Shanghai Lung Tumor Clinic Medical Center/China,

³MD Anderson Cancer Center/United States Of

America, ⁴Thoracic & Cardiovascular Surgery, MD Anderson Cancer Center/United States Of America

Background: Because cell signaling and cell metabolic pathways are executed through proteins, characterizing protein signatures in tumor tissues is required to identify key nodes in signaling networks whose alteration is associated with malignancy. This study aimed to determine protein profiles in primary lung cancer tissues.

Methods: Case-matched normal and tumor samples from 101 lung cancer patients, mostly non-small cell lung cancer, were analyzed with reverse-phase protein array assay for 127 proteins and/

or protein phosphorylation sites. Differences in signal intensities between normal and tumor tissues and their association with clinical parameters were analyzed with analysis of variance, some of them were validated by Western blot and/or immunohistochemical analyses.

Results: We found that 18 molecules were significantly different ($p < 0.05$) by at least 30% between normal and tumor tissues. Most of those molecules play roles in cell proliferation (cyclin B1), DNA damage response (ATM, CHK2, and Ku80), signal transduction (14-3-3zeta, IGFBP2, p38-pT180, IRS-pS307, Src, PI3K-p85, mTOR, and Stat5), or lipid metabolism (COX2 and ACC-1pS79) or function as cell surface/matrix proteins (caveolin 1, CD31, and collagen type VI). Analysis on association with clinical parameters revealed that Ku80 levels were significantly higher in tumors of nonsmokers than in those of smokers. Cyclin B1 levels were significantly higher in poorly differentiated tumors than in well or moderately differentiated tumors. The levels of five molecules were significantly higher in neuroendocrinal tumors than in other types of tumors. A comparison with a separate RPPA profiling on another set of patient samples showed that the results were highly repeatable.

Conclusion: Molecules involved in DNA damage response, signal transductions (in the PI3K/AKT/mTOR, Src/Stat, and MAP kinase pathways), lipid metabolism, and cell proliferation were drastically aberrant in lung cancer tissues and some of those could be useful for molecular diagnosis of lung cancers.

Keywords: DNA damage, primary tumor, Biomarkers, signal transduction

Poster Session 2 – Prognostic and Predictive Markers Tuesday, 5 July 2011 12:15-14:00

P2.079 HE4 EXPRESSION IS ASSOCIATED WITH WORSE PROGNOSIS IN PULMONARY ADENOCARCINOMA

Shin-Ichi Yamashita¹, Keita Tokuishi¹, Toshihiko Moroga¹, Takafumi Hashimoto¹, Mirei Kamei¹, Shuji Suehiro¹, Kiyoshi Ono¹, Satoshi Yamamoto¹, Masao Chujo¹, Kazuyuki Ohbo², Katsunobu Kawahara¹

¹Surgery Ii, Oita University/Japan, ²Histology And Cell Biology, Advanced Medical Research Center, Yokohama City University, School Of Medicine/Japan

[Print this Page](#)

Presentation Abstract

Abstract
Number: 2177

Presentation
Title: Tumor suppressor effects of ETS2 transcriptional factor in human non-small cell lung cancer

Presentation
Time: Monday, Apr 02, 2012, 1:00 PM - 5:00 PM

Location: McCormick Place West (Hall F), Poster Section 7

Poster
Section: 7

Poster
Board
Number: 11

Author
Block: Mohamed Kabbout, Melinda M. Garcia, Junya Fujimoto, Chi-Wan Chow, Denise Woods, Patricia Koch, Amin Momin, Brian P. James, Luisa M. Solis, Carmen Behrens, Ignacio I. Wistuba, Humam Kadara. MD Anderson Cancer Center, Houston, TX

Abstract
Body: Advances in prevention and treatment of non-small cell lung cancer (NSCLC) are dependent in part on the characterization of tumor suppressor genes and oncogenes and the roles they elicit in the pathogenesis of this malignancy. Although v-ets erythroblastosis virus E26 oncogene homolog 2 (ETS2) is a canonical transcription factor that regulates various cancer-associated cellular and developmental processes including proliferation and migration, its function in lung carcinogenesis is still unknown. In this study we sought to examine the role of ETS2 in NSCLC pathogenesis. We first examined *ETS2* mRNA expression in lung adenocarcinomas (n=80) and normal lung (n=30) which we profiled using microarrays, and in seven matched adenocarcinoma and normal lung pairs analyzed using next-generation sequencing technology. Both array and sequencing datasets revealed that *ETS2* mRNA was significantly lower in lung adenocarcinomas relative to normal lung ($p<0.001$) which was confirmed by quantitative PCR analysis. Moreover and in the microarray dataset, *ETS2* mRNA expression was significantly anti-correlated with that of the proliferation marker *KI67* ($R=-0.59$, $p<0.001$). In addition, *in silico* analysis of publicly available datasets demonstrated that *ETS2* mRNA was lower in NSCLC compared to normal lung (all $p<0.001$), and interestingly, was also lower in airways of healthy smokers relative to non-smokers ($p<0.001$). We next assessed ETS2 immunohistochemical protein expression using tissue microarrays comprised of 342 formalin-fixed paraffin-embedded NSCLC (adenocarcinoma, n=226; SCC, n=116) tissue specimens. There were no statistically significant differences in ETS2 expression by histology, stage or age. We then assessed the association of ETS2 protein expression with clinical outcome. Non-treated all stage (n=206) or stage-I (n=157) patients with relatively lower ETS2 protein expression exhibited significantly shortened disease-free survival compared to patients with higher expression ($p=0.008$ and $p=0.004$ of the log-rank test, respectively). In addition, patients with relatively lower ETS2 expression exhibited significantly poorer response to adjuvant therapy compared to patients with higher ETS2 expression ($p=0.01$). We then probed the effect of modulating ETS2 expression in NSCLC cells. Knockdown of *ETS2* expression by RNA interference significantly increased anchorage-dependent colony formation ($p=0.004$) as well as augmented cellular migration ($p=0.01$) and invasion through matrigel ($p=0.02$) compared to cells transfected with control siRNA. Our findings provide evidence that ETS2 may function as a tumor suppressor gene in NSCLC that can aid clinically in identification of aggressive tumors and biologically in increasing our understanding of the pathogenesis of this malignancy (Supported by DoD PROSPECT W81XWH-07-1-0306 and Lung Cancer Research Foundation grants).

[American Association for Cancer Research](#)
615 Chestnut St. 17th Floor
Philadelphia, PA 19106

Correlation Between Tissue Platinum Concentration and Tumor Response in Non-small Cell Lung Cancer

Eric S. Kim, Guangan He, Chi-Wan Chow, Junya Fujimoto, Neda Kalhor, Stephen G. Swisher, Ignacio I. Wistuba, David J. Stewart, Zahid H. Siddik

From the Departments of Thoracic and Cardiovascular Surgery, Pathology, Thoracic/Head and Neck Medical Oncology, and Experimental Therapeutics, the University of Texas M. D. Anderson Cancer Center, Houston, Texas

Background: Platinum-based chemotherapy is the mainstay of treatment for advanced non-small cell lung cancer (NSCLC). Despite initial sensitivity, most tumors develop resistance. Reduced intracellular drug accumulation is one of the most consistently identified features of platinum-resistant cell lines, but clinical data are limited. We assessed correlations between tissue platinum concentrations and response in NSCLC.

Methods: We measured total platinum concentrations in 17 archived fresh frozen NSCLC specimens from patients who received neoadjuvant platinum-based chemotherapy. Approximately 30 mg of tumor was homogenized in benzethonium hydroxide. After acidification, samples were analyzed by flameless atomic absorption spectrophotometry (FAAS) to assess absorbance reading associated with platinum content. Two specimens from patients who underwent surgery only were analyzed as negative controls. Absorbance value per mg of tissue was correlated with percent change in tumor diameter on post- vs pre-chemotherapy CT scans.

Results: Platinum absorbance values ranged from 0.00077 to 0.00470 per mg of tissue while two negative controls demonstrated absorbance readings similar to 0.1N HCL (Table 1). Platinum absorbance correlated negatively with percent change in tumor size ($R^2=0.45$, $P=0.003$) (Figure 1).

Conclusion: This is the first tissue-based study to demonstrate a correlation between total platinum concentrations and response in NSCLC. Reduced intracellular platinum accumulation may constitute a significant mechanism of platinum resistance even in clinical specimens. Further studies investigating factors that modulate intracellular platinum concentration are warranted.

Sample	Weight (mg)	Absorbance Unit	Absorbance Unit /mg
0.1N HCL	0.0	0.0196	n/a
Surgery only control #1	31.0	0.0209	0.00067
Surgery only control #2	30.0	0.0121	0.00040
Neoadjuvant case #1	31.0	0.0732	0.00236
Neoadjuvant case #2	31.3	0.0249	0.00080
Neoadjuvant case #3	30.0	0.0361	0.00120
Neoadjuvant case #4	31.0	0.1267	0.00409
Neoadjuvant case #5	30.8	0.0895	0.00291
Neoadjuvant case #6	31.0	0.0630	0.00203
Neoadjuvant case #7	32.0	0.1494	0.00467
Neoadjuvant case #8	29.0	0.0973	0.00336
Neoadjuvant case #9	30.0	0.1411	0.00470
Neoadjuvant case #10	30.5	0.0237	0.00078
Neoadjuvant case #11	30.5	0.0545	0.00179
Neoadjuvant case #12	32.0	0.0485	0.00151
Neoadjuvant case #13	31.0	0.0868	0.00280
Neoadjuvant case #14	30.0	0.0368	0.00123
Neoadjuvant case #15	31.5	0.0816	0.00259
Neoadjuvant case #16	29.5	0.0747	0.00253
Neoadjuvant case #17	30.0	0.0990	0.00330

Table 1. Platinum measurements by FAAS in resected NSCLC specimens from 17 patients who received neoadjuvant platinum and 2 patients who underwent surgery only

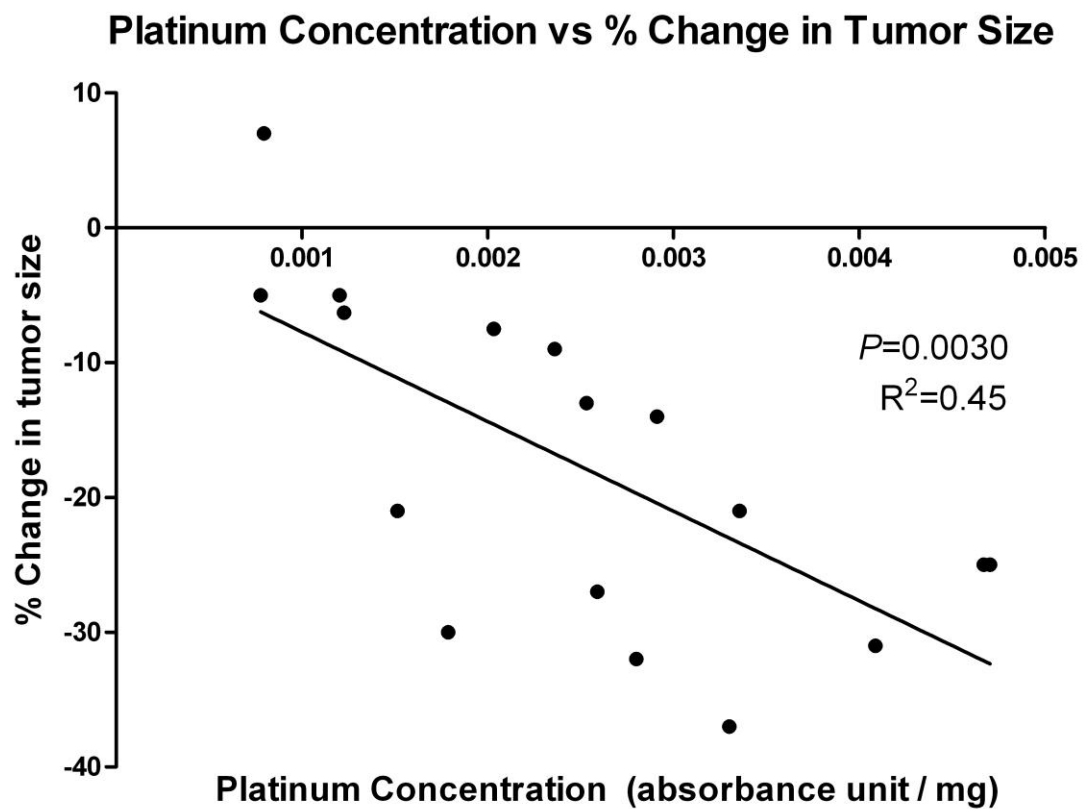


Figure 1. Correlation between tissue platinum concentration and tumor response in 17 NSCLC specimens

[Print this Page](#)

Presentation Abstract

Abstract
Number: 1714

Presentation
Title: *EZH2*^{High} and *miR-101*^{Low} expressions are associated with chemoresistance and shorter survival in patients with lung adenocarcinoma who received adjuvant chemotherapy

Presentation
Time: Monday, Apr 02, 2012, 8:00 AM -12:00 PM

Location: McCormick Place West (Hall F), Poster Section 26

Poster
Section: 26

Poster Board
Number: 4

Author
Block: Erick M. Riquelme¹, Carmen Berhens¹, Milind Suraokar¹, Chi-Wan Chow Chow¹, Humam Kadara¹, Ignacio I. Wistuba¹, Luc Girard², John D. Minna². ¹UT MD Anderson Cancer Ctr., Houston, TX; ²UT Southwestern Medical Center, Dallas, TX

Abstract
Body: **Background.** EZH2 (a histone methyltransferase and part of the polycomb repressive complex-2) has been implicated in neoplastic transformation, tumor progression, and resistance to chemotherapy. Though EZH2 overexpression has been described in non-small cell lung cancer (NSCLC), there have been no functional studies reported. Recently, it has been demonstrated that *miR-101* negatively regulates the expression of *EZH2*. In this study, we investigated the effect of *EZH2* and *miR-101* expression levels on the outcome of lung adenocarcinoma patients treated with surgery and adjuvant chemotherapy, and analyzed in vitro mechanisms associated with the role in chemoresistance and cell migration of lung adenocarcinoma.

Methods. We analyzed *EZH2* and *miR-101* expression in RNA extracted from 151 lung adenocarcinoma tumors obtained from patients treated with surgery with (n=57) or without (n=94) platinum adjuvant therapy, and compared those data with patients' overall survival (median follow-up 5.6 years). *EZH2* and *miR-101* expression levels were tested using Illumina mRNA arrays W6-6 V.3 and Agilent V3 human microRNA, respectively. We knockdown *EZH2* expression in adenocarcinoma cell lines using small interfering RNA (siRNA). Cisplatin sensitivity (IC₅₀) was determined by MTS assay. Cell migration was measured using Boyden chamber.

Results. We found that, high *EZH2* expression ($p=0.007$) and low *miR-101* ($p=0.01$) expression were significantly associated with worse overall survival in lung adenocarcinoma patients who received platinum adjuvant therapy, but not in patients who did not receive such therapy. Similar results ($p=0.008$) were observed when combined *EZH2*^{High}/*miR-101*^{Low} expression was examined. From a panel of 21 adenocarcinoma cell lines with known EZH2 gene/protein expression, we selected 4 cell lines: 2 with high EZH2 (H1993 and HCC1171), and 2 with low EZH2 (HCC461 and HCC193) expression. Knockdown of *EZH2* using siRNA reduced cell migration of H1993 and HCC1171 cells (3.7-fold decrease and 1.7-fold, respectively, $p<0.05$), but not of HCC193 and HCC461 cells. Knockdown of *EZH2* significantly decreased ($p<0.05$) the viability (by MTS assay) of cell lines H1993 and HCC1171 when treated with cisplatin, but not of HCC193 and HCC461 cells.

Conclusion. Our in vitro findings suggest that EZH2 overexpression may promote a more malignant phenotype of lung adenocarcinoma, including increased chemoresistance and cell migration capabilities. Expression of *EZH2* and *miR-101* may represent a predictive marker of worse outcome in lung adenocarcinoma patients treated with surgery and adjuvant platinum chemotherapy. EZH2 is a potential target that regulates the epigenome to overcome drug resistance in lung cancer (Supported in part by grants DoD PROSPECT W81XWH-07-1-0306 and NCI/UT Lung SPORE 5P50CA70907-11, ER, Becas Chile program)

[American Association for Cancer Research](#)
615 Chestnut St. 17th Floor
Philadelphia, PA 19106

[Print this Page](#)

Presentation Abstract

Abstract
Number: 4819

Presentation
Title: Gene-expression profiles predict sorafenib efficacy in wild-type EGFR non-small cell lung cancer (NSCLC)

Presentation
Time: Tuesday, Apr 03, 2012, 3:20 PM - 3:35 PM

Location: McCormick Place West (Level 1), Room W192

Author
Block: Pierre Saintigny¹, George R. Blumenschein, Jr.¹, Lixia Diao¹, Jing Wang¹, Kevin Coombes¹, Suyu Liu¹, Edward Kim¹, Anne Tsao¹, Roy Herbst², Christine Alden¹, Jack J. Lee¹, Ximing Tang¹, David Stewart³, Merrill Kies¹, Frank Fossella¹, Hai Tran¹, Li Mao⁴, Marshall Hicks¹, Jeremy Erasmus¹, Sanjay Gupta¹, Luc Girard⁵, Michael Peyton⁵, Suzanne Davis¹, Scott Lippman¹, Waun Ki Hong¹, John Minna⁵, Ignacio Wistuba¹, John Heymach¹. ¹UT MD Anderson Cancer Ctr., Houston, TX; ²Yale Cancer Center, New Haven, CT; ³University of Ottawa Faculty of Medicine, Canada, ON, Canada; ⁴University of Maryland, Baltimore, MD; ⁵UT Southwestern Medical Ctr., Dallas, TX

Abstract
Body: Background: Results from our Biomarkers-Integrated Approaches of Targeted Therapy for Lung Cancer Elimination (BATTLE) program suggest that patients with chemorefractory wild-type (wt) EGFR NSCLC including those with mutant KRAS may benefit from sorafenib. Using 3 different approaches, we tested the hypothesis that gene expression profiles from wild-type (wt) EGFR tumors may predict sorafenib efficacy by capturing effects on multiple targets. Material and Methods: Baseline tumor biopsies from 37 BATTLE patients (pts) with EGFR wt tumors and treated with sorafenib were profiled (Affymetrix Human Gene 1.5T), as well as 68 EGFR wt NSCLC cell lines with available IC50 to sorafenib (Illumina HumanWG-6 v3.0 expression beadchip). (i) We first developed an In vitro Sorafenib Signature (ISS). Correlation of IC50 with each individual probe expression level was computed. Most significant probes were summarized by the first principal component (PC), and correlated with IC50 of sorafenib. To validate the signature, the first PC was computed in BATTLE samples, and progression-free survival (PFS) of pts with high- vs. low-sensitivity signature was compared based on the median of the first PC. (ii) Alternatively, we developed a Clinical Sorafenib Signature (CSS) using BATTLE samples. We compared 23 (62%) pts who achieved 8-week disease control with 14 (38%) who did not (t-test). Most significant probesets were summarized by the first PC and PFS of pts with a high- vs. low-sensitivity signature were compared. To validate the signature, the first PC was computed in cell lines and correlated with IC50 of sorafenib. (iii) Finally, we tested a previously reported KRAS mutation gene expression signature derived by comparing genes differentially expressed in mutant vs. wt KRAS early stage resected lung adenocarcinomas, in 124 BATTLE samples including 24 mutant KRAS. Results: (i) The ISS included 50 probes. The first PC was correlated with the IC50 of sorafenib ($\rho = -0.71$, $P < 0.0001$). The ISS was then tested in BATTLE and PFS was significantly different in pts with the high- (median PFS 3.61 months) vs. the low-sensitivity signature (median PFS 1.84 months, log-rank $P = 0.0263$). (ii) The CSS developed in BATTLE included 80 probesets summarized using the first PC. PFS was significantly different in pts with the high- vs. the low-sensitivity signature (log-rank $P < 0.0001$). The CSS was then tested in cell lines and the first PC was significantly correlated with IC50 of sorafenib ($\rho = 0.24$, $P = 0.0483$). (iii) Finally, the KRAS signature was significantly associated with KRAS mutation, but no association was observed with outcome in pts treated with sorafenib in BATTLE. Conclusion: We report 2 gene expression signatures, ISS and CSS, that predicted benefit from sorafenib in patients with chemorefractory NSCLC and in vitro sensitivity to sorafenib respectively. Further validation is planned in our ongoing BATTLE-2 program.

[American Association for Cancer Research](#)
615 Chestnut St. 17th Floor
Philadelphia, PA 19106



American Society of Clinical Oncology

www.asco.org

Factors associated with membrane carbonic anhydrase IX (mCAIX) immunohistochemistry (IHC) in non-small cell lung cancer (NSCLC).

Sub-category:

Prognostic Factors

Category:

Tumor Biology

Meeting:

2011 ASCO Annual Meeting

Session Type and Session Title:

This abstract will not be presented at the 2011 ASCO Annual Meeting but has been published in conjunction with the meeting.

Abstract No:

e21125

Citation:

J Clin Oncol 29: 2011 (suppl; abstr e21125)

Author(s):

D. J. Stewart, M. Nunez, C. Behrens, S. Swisher, J. A. Roth, J. Heymach, I. I. Wistuba; University of Texas M. D. Anderson Cancer Center, Houston, TX

Abstracts that were granted an exception in accordance with ASCO's Conflict of Interest Policy are designated with a caret symbol (^) here and in the printed Proceedings.

Abstract Disclosures**Abstract:**

Background: CAIX reduces cell acidity, is upregulated by HIF1a, and correlates with HIF1a and with poor prognosis in some cancers but not others. We found in multivariate analysis that mCAIX but not cytoplasmic (c) CAIX (cCAIX) correlated with relapse in stage I-II NSCLC (Proc AACR, 2010). **Methods:** In 308 resected NSCLCs (stage I, II, III, IV in 188, 61, 46 and 9 patients) we used IHC to assess CAIX and other markers of hypoxia, proliferation, etc. IHC scores (0-300) were calculated by multiplying stain intensity (0-3) by % cells staining. We used nonparametric statistics to assess factors correlating with mCAIX scores. **Results:** Median mCAIX scores were lower in adeno vs squamous NSCLC (5 vs 65, $p < 0.0001$) and correlated inversely with % papillary adeno present ($r = -0.17$, $p = 0.02$). mCAIX correlated with tumor diameter ($r = 0.19$, $p = 0.0008$) but not with node stage (N0 vs N1-2, 30 vs 20, $p = 0.93$). mCAIX correlated with nuclear (n) Ki67 ($r = 0.20$, $p = 0.0005$), mitoses ($r = 0.18$, $p = 0.001$) and necrosis ($r = 0.20$, $p = 0.0006$) but not apoptosis ($r = 0.05$, $p = 0.38$). mCAIX did not correlate with nHIF1a ($r = -0.01$, $p = 0.84$) and paradoxically correlated inversely with cHIF1a ($r = -0.14$, $p = 0.02$) and cVEGF ($r = -0.13$, $p = 0.03$), but did correlate with the hypoxia-induced transcription factor cSHARP2 ($r = 0.18$, $p = 0.002$). cCAIX did correlate with cHIF1a, but only in tumors < 5 cm ($r = 0.14$, $p = 0.04$) and N0 patients ($r = 0.17$, $p = 0.01$). mCAIX was higher with EGFR wild type vs mutant (20 vs 0, $p = 0.006$) and Notch amplified vs not (120 vs 21.25, $p = 0.0006$), and did not vary with KRAS mutation (5 vs 15.83, $p = 0.76$). There was a trend to lower mCAIX in well vs moderately/poorly differentiated tumor (5 vs 30, $p = 0.06$). mCAIX correlated negatively with the tumor suppressors cRB ($r = -0.13$, $p = 0.03$), cP16 ($r = -0.12$, $p = 0.03$), nP16 ($r = -0.13$, $p = 0.03$) and nP14 ($r = -0.12$, $p = 0.04$). **Conclusions:** In NSCLC mCAIX expression correlates with tumor type, subtype, size, proliferation and necrosis, and varies inversely with tumor suppressor genes. mCAIX did not correlate with HIF1a. cCAIX only correlated with cHIF1a in small and N0 tumors. Variable findings between studies with respect to CAIX importance may depend on tumor type, size and stage, and on whether mCAIX is assessed separately from cCAIX. Support: DoD # W81XWH-07-1-0306.

► **Associated Presentation(s):**

No items found.

► **Other Abstracts in this Sub-Category:**

1. A pilot study of tumor-derived exosomes as diagnostic and prognostic markers in breast cancer patients receiving neoadjuvant chemotherapy.

Meeting: [2011 ASCO Annual Meeting](#) Abstract No: TPS248 First Author: R. E. Raab
Category: Tumor Biology - Prognostic Factors

2. ACRIN 6691 monitoring and predicting breast cancer neoadjuvant chemotherapy response using diffuse optical spectroscopic imaging (DOSI).

Meeting: [2011 ASCO Annual Meeting](#) Abstract No: TPS249 First Author: B. J. Tromberg
Category: Tumor Biology - Prognostic Factors

3. Effect of IGF1R protein expression on benefit to adjuvant trastuzumab in early-stage HER2+ breast cancer in NCCTG N9831 trial.

Meeting: [2011 ASCO Annual Meeting](#) Abstract No: 10503 First Author: M. M. Reinholz
Category: Tumor Biology - Prognostic Factors

[More...](#)

► **Abstracts by D. J. Stewart:**

1. Biologic risk model for recurrence in resected early-stage non-small cell lung cancer (ES NSCLC).

Meeting: [2011 ASCO Annual Meeting](#) Abstract No: 7053 First Author: K. A. Gold
Category: Lung Cancer - Local-Regional and Adjuvant Therapy/Small Cell - Adjuvant Therapy

2. Factors associated with membrane carbonic anhydrase IX (mCAIX) immunohistochemistry (IHC) in non-small cell lung cancer (NSCLC).

Meeting: [2011 ASCO Annual Meeting](#) Abstract No: e21125 First Author: D. J. Stewart
Category: Tumor Biology - Prognostic Factors

3. Retrospective review of MRIs in lung cancer patients with brain metastases: An assessment of early response.

Meeting: [2011 ASCO Annual Meeting](#) Abstract No: 7543 First Author: R. Zinner
Category: Lung Cancer - Metastatic/Non-small Cell - Metastatic

[More...](#)

► **Presentations by D. J. Stewart:**

1. Discussion

Meeting: [2010 ASCO Annual Meeting](#)

Discussant: [David J. Stewart, MD](#)

Session: [Developmental Therapeutics - Clinical Pharmacology and Immunotherapy](#)
(Poster Discussion Session)

2. Equipoise lost: Ethics, costs, and the regulation of cancer clinical research.

Meeting: [2010 ASCO Annual Meeting](#)

Presenter: [David J. Stewart, MD](#)

Session: [Health Services Research](#) (General Poster Session)

3. Decitabine effect on human tumor expression of various transporters.

Meeting: [2009 ASCO Annual Meeting](#)

Presenter: [David J Stewart, MD](#)

Session: [Developmental Therapeutics: Cytotoxic Chemotherapy](#) (General Poster Session)

[More...](#)

► ***Educational Book Manuscripts by D. J. Stewart:***

No items found.

[Print this Page](#)

Presentation Abstract

Abstract
Number: 3404

Presentation
Title: Exploring the role of Twist1 in the pathogenesis of malignant pleural mesothelioma (MPM)

Presentation
Time: Tuesday, Apr 03, 2012, 8:00 AM -12:00 PM

Location: McCormick Place West (Hall F), Poster Section 15

Poster
Section: 15

Poster Board
Number: 19

Author
Block: Milind B. Suraokar¹, David Kim¹, Yi Zhang¹, Lixia Diao¹, Erick Riquelme¹, Carmen Behrens¹, Reza Mehran¹, Jing Wang¹, Adi Gazdar², Kevin Coombes¹, Anne Tsao¹, Ignacio Wistuba¹. ¹UT MD Anderson Cancer Ctr., Houston, TX; ²UT Southwestern Medical Center, Houston, TX

Abstract
Body: **Background:** MPM is caused by lethal neoplastic growth of the pleura surrounding lungs. It is resistance to most standard anti-cancer treatment regimens and needs discovery of newer therapeutic approaches. MPM is characterized by massive loco-regional invasion of the malignant pleural cells into the lung parenchyma. Twist1 is a transcription factor, which promotes invasion and metastasis of tumor cells, increases chemotherapeutic resistance and is involved in the pathobiology of many cancers. Also recent studies have highlighted the potential of twist1 as a therapeutic target in cancer. But there is no report investigating its function in mesothelioma.
Methods: We extracted total RNA from 53 frozen resected tumor tissue specimens, comprised of 39 epitheloid, 7 sarcomatoid and 7 biphasic histotypes, along with paired normal tissue. The RNA was labeled and hybridized to Affymetrix U133 plus 2.0 microarray to obtain transcriptomic profiles. Bioinformatic analysis of the microarray data using a 2 sample t-test was applied, on a probe-by-probe basis followed by Beta-uniform Mixture for multiple comparisons, to determine the differences between tumor vs normal specimens. The microarray results were validated by quantitative reverse transcriptase polymerase chain reaction (qRT-PCR) using Taqman assays on the ABI 7300 platform. For all qRT-PCR experiments the twist1 transcript levels were determined relative to endogenous GAPDH as control using $\Delta\Delta CT$ calculation. We performed Western blot analysis on a panel of 16 mesothelioma cell lines including Met-5A (SV-40 immortalized) and HCT-4012 (telomerase immortalized) pleural mesothelial control cell lines.
Results: The bioinformatic analysis of microarray data showed that twist1 transcript level was 8.7 fold higher in tumors ($p = 1.1E-16$) compared to paired normal specimens. Using qRT-PCR, we compared twist1 transcript levels in 12 pairs of tumor vs paired normal tissue specimens and found that twist1 was upregulated to more than 10 fold in MPM tumors ($p < E-4$). Western blot showed that 10 MPM cancer cell lines had higher expression of twist1 protein compared to Met-5A and HCT-4012 cell lines. The highest expression was seen in 2 of the sarcomatoid cell lines - RS5 and DM3, suggesting a correlation with metastatic phenotype since sarcomatoid tumors are highly metastatic in nature.
Conclusion: Our preliminary findings suggest that twist1 is upregulated in MPM tumors and cell lines and may play a role in the development of MPM. Further studies are needed to investigate its role in the process of tumorigenesis and metastasis. Supported by Grants: DoD W81XWH-07-1-0306 (I.I.W and AST), Fleming Foundation, IASLC Young Investigator Award 2011-2013 (MS).

American Association for Cancer Research
615 Chestnut St. 17th Floor
Philadelphia, PA 19106

Use of a gene expression signature related to epithelial-to-mesenchymal transition (EMT) to predict for overall survival (OS) in cohorts of lung and head and neck cancer (HNSCC) patients.

Sub-category:

Local-Regional Therapy

Category:

Lung Cancer - Local-Regional and Adjuvant Therapy/Small Cell

Meeting:

2011 ASCO Annual Meeting

Session Type and Session Title:

Poster Discussion Session, Lung Cancer - Local-regional and Adjuvant Therapy/Small Cell

Abstract No:

7010

Citation:

J Clin Oncol 29: 2011 (suppl; abstr 7010)

Author(s):

J. S. Yordy, L. Shen, L. Diao, J. Wang, K. Coombes, U. Giri, Y. Xie, J. D. Minna, L. Girard, J. Weinstein, J. Heymach, K. K. Ang, M. D. Story, R. Meyn; University of Texas M. D. Anderson Cancer Center, Houston, TX; University of Texas Southwestern Medical Center, Dallas, TX

Abstracts that were granted an exception in accordance with ASCO's Conflict of Interest Policy are designated with a caret symbol (^) here and in the printed Proceedings.

Abstract Disclosures**Abstract:**

Background: Improved predictions for survival and response to therapy will help to refine clinical care and potentially improve outcomes for patients with cancers of the upper aerodigestive tract. **Methods:** Gene expression analysis using three mesenchymal (M) and three epithelial (E) non-small cell lung cancer (NSCLC) cell lines identified 574 differentially expressed probes based on a false discovery rate (FDR) of 30%, which were then used to categorize a panel of 50 cell lines on the Illumina gene expression platform into 30 E-like and 20 M-like cell lines. 46 of these cell lines were analyzed with Affymetrix arrays, corresponding to 27 E-like and 19 M-like cell lines, and the top 4054 differentially expressed probes based on a FDR of 20% were filtered to retain probes with at least 2-fold average difference in expression. Overlap with the Director's Consortium (DC) of mostly early stage lung adenocarcinoma patients treated with surgery and adjuvant therapy as appropriate resulted in 991 probes, which were then ranked using a survival-based Cox regression model with patients combined from the UM and HLM cohorts in the DC. The top 112 probes based on a FDR of 25% were then used in a supervised PCA analysis and two-evenly divided groups of patients were compared using Kaplan-Meier survival analysis. The 112 probe signature was independently tested in the DC MSK cohort and a cohort of surgical-pathologic high-risk HNSCC patients treated with surgery and post-operative radiotherapy. **Results:** Gene expression related to EMT is able to identify two highly different E-like and M-like groups of cell lines. This cell-line derived and clinically refined EMT-related gene expression signature predicted for OS in an independent cohort in the DC ($p = 0.0016$) as well as in HNSCC patients ($p = 0.003$). **Conclusions:** A gene expression signature related to EMT predicts for OS in lung cancer and HNSCC patients. Further prospective validation will be needed to verify these results. In addition, this signature distinguishes between unique biological phenotypes and therefore may also be significant in predicting response to specific therapeutic interventions.

► **Associated Presentation(s):**

1. Use of a gene expression signature related to epithelial-to-mesenchymal transition (EMT) to predict for overall survival (OS) in cohorts of lung and head and neck cancer (HNSCC) patients.

Meeting: [2011 ASCO Annual Meeting](#)

Presenter: [John Stuart Yordy](#)

Session: [Lung Cancer - Local-regional and Adjuvant Therapy/Small Cell \(Poster Discussion Session\)](#)

► **Other Abstracts in this Sub-Category:**

1. [Systematic evaluation of the impact of disease progression \(DP\) date determination on progression-free survival \(PFS\) in advanced lung cancer: A joint North Central Cancer Treatment Group \(NCCTG\) and Southwest Oncology Group \(SWOG\) investigation.](#)

Meeting: [2011 ASCO Annual Meeting](#) Abstract No: 7005 First Author: [S. J. Mandrekar](#)

Category: [Lung Cancer - Local-Regional and Adjuvant Therapy/Small Cell - Local-Regional Therapy](#)

2. [Association between DNA-repair gene and glutathione S-transferase gene polymorphisms and clinical outcome in patients \(pt\) with localized non-small cell lung cancer \(NSCLC\) treated with sequential radiochemotherapy.](#)

Meeting: [2011 ASCO Annual Meeting](#) Abstract No: 7008 First Author: [J. Stoecklmacher-Williams](#)

Category: [Lung Cancer - Local-Regional and Adjuvant Therapy/Small Cell - Local-Regional Therapy](#)

3. [Phase I/II trial of bevacizumab \(B\) and erlotinib \(E\) with induction \(IND\) and concurrent \(CON\) carboplatin \(Cb\)/paclitaxel \(P\) and 74 Gy of thoracic conformal radiotherapy \(TCRT\) in stage III non-small cell lung cancer \(NSCLC\).](#)

Meeting: [2011 ASCO Annual Meeting](#) Abstract No: 7016 First Author: [T. Stinchcombe](#)

Category: [Lung Cancer - Local-Regional and Adjuvant Therapy/Small Cell - Local-Regional Therapy](#)

[More...](#)

► **Abstracts by J. S. Yordy:**

1. [Use of a gene expression signature related to epithelial-to-mesenchymal transition \(EMT\) to predict for overall survival \(OS\) in cohorts of lung and head and neck cancer \(HNSCC\) patients.](#)

Meeting: [2011 ASCO Annual Meeting](#) Abstract No: 7010 First Author: [J. S. Yordy](#)

Category: [Lung Cancer - Local-Regional and Adjuvant Therapy/Small Cell - Local-Regional Therapy](#)

2. [Use of DPC-4 immunostaining of diagnostic cytology specimens to predict the pattern of tumor progression in locally advanced pancreatic cancer patients \(LAPC\).](#)

Meeting: [2011 Gastrointestinal Cancers Symposium](#) Abstract No: 209 First Author: [C. H. Crane](#)

Category: Cancers of the Pancreas, Small Bowel, and Hepatobiliary Tract - [Translational Research](#)

3. [Use of genome-wide transcript profiling to identify genes associated with radiation response in head and neck squamous cell carcinoma cell lines.](#)

Meeting: [2010 Molecular Markers](#) Abstract No: 143 First Author: [J. S. Yordy](#)

Category: [Genetics, Genomics, Epigenetics, Gene Expression](#)

[More...](#)

► **[Presentations by J. S. Yordy:](#)**

1. Use of a gene expression signature related to epithelial-to-mesenchymal transition (EMT) to predict for overall survival (OS) in cohorts of lung and head and neck cancer (HNSCC) patients.

Meeting: [2011 ASCO Annual Meeting](#)

Presenter: [John Stuart Yordy, M.D., Ph.D.](#)

Session: [Lung Cancer - Local-regional and Adjuvant Therapy/Small Cell \(Poster Discussion Session\)](#)

2. Use of protein expression profiling to identify markers of radiation sensitivity and resistance in the NCI 60 cell lines

Meeting: [2008 Molecular Markers](#)

Presenter: [John S Yordy, MD, PhD](#)

Session: [General Poster Session B \(General Poster Session\)](#)

[More...](#)

► **[Educational Book Manuscripts by J. S. Yordy:](#)**

No items found.

[Print this Page](#)

Presentation Abstract

Abstract
Number: 207

Presentation
Title: Casitas B-lineage lymphoma-3 is an epigenetically regulated gene whose knockdown induces mesenchymal to epithelial transition and enhances erlotinib sensitivity in lung cancer cell lines

Presentation
Time: Sunday, Apr 01, 2012, 1:00 PM - 5:00 PM

Location: McCormick Place West (Hall F), Poster Section 8

Poster
Section: 8

Poster Board
Number: 1

Author
Block: Jing Zhang¹, Uma Giri¹, Krystha Cantu², Jing Wang¹, Ilimbek Beketaev¹, Lauren Byers¹, Pierre Saintigny¹, John V. Heymach¹, Steven H. Lin¹. ¹The University of Texas MD Anderson Cancer Center, Houston, TX; ²Rice University, Houston, TX

Abstract
Body: Casitas B-lineage lymphoma (Cbl) proteins are E3 ubiquitin ligases and multifunctional adaptor proteins that are implicated in the regulation of signal transduction in various cell types and in response to different stimuli. Cbl-3 is a distinct member of this family of 3 genes that is specifically expressed in the epithelial lining of organs, particularly the bronchial airways, whose function, especially in cancer cells, is relatively unknown. Here we report that Cbl-3 expression and promoter CpG island DNA methylation differed profoundly in epithelial compared to mesenchymal-like lung cancer cells. 5-azacytidine treatment, as well as DNA methyltransferase-1 (DNMT1) KD (but not DNMT-3a or 3b) enhanced promoter demethylation and Cbl-3 gene expression. Knock down (KD) of Cbl-3 in mesenchymal-like lung cancer cell lines strongly enhanced EGFR expression and activated downstream pathways. As a result, cells that were normally resistant to erlotinib became greatly sensitized to drug treatment by Cbl-3 KD. Additionally, Cbl-3 KD inhibited cellular migration and increased cellular adhesion to the extra cellular matrix (ECM) as well as promoted cell-to-cell interaction through enhanced E-Cadherin and FAK expression. These alterations suggested a mesenchymal to epithelial transition (MET) conferred by Cbl-3 KD. Take together, this data provided new insights into Cbl-3 gene regulation and elucidated a potential role of Cbl-3 in EGFR signaling in the context of EMT in lung cancer cells.

[American Association for Cancer Research](#)
615 Chestnut St. 17th Floor
Philadelphia, PA 19106